

RIJKSUNIVERSITEIT GRONINGEN

A computer simulation study  
**Nanorheology of strongly confined  
molecular fluids**

Proefschrift  
ter verkrijging van het doctoraat in de  
Wiskunde en Natuurwetenschappen  
aan de Rijksuniversiteit Groningen  
op gezag van de  
Rector Magnificus Dr. F. van der Woude  
in het openbaar te verdedigen op  
vrijdag 17 november 1995  
des namiddags te 4.00 uur

door

**Evangelos Manias**

geboren op 9 juni 1969  
te Veroia, Griekenland

**Promotor:** Prof. Dr. Georges Hadzioannou  
**Co-Promotor:** Dr. G. ten Brinke

A computer simulation study

# Nanorheology of strongly confined molecular fluids



by:

**Evangelos Manias**  
son of Dimitrios and Maria

Department of Polymer Science  
Faculty of Mathematics & Natural Sciences  
State University of Groningen  
The Netherlands

**Promotor:** Prof. Dr. Georges Hadzioannou  
**Co-Promotor:** Dr. Gerrit ten Brinke

**leescommissie:** Prof. Dr. H. J. C. Berendsen  
Prof. Dr. A. J. Pennings  
Prof. Dr. D. N. Theodorou

© Evangelos D. Manias, 1995

Published in 1995

Netherlands Royal Library Cataloguing-in-Publication Data  
Manias, Evangelos D.

Nanorheology of strongly confined molecular fluids. A computer simulation study.

Thesis Rijksuniversiteit Groningen –with ref. –with summary in Dutch  
ISBN 90-367-0545-2 (pbk)

Subject headings: Nanorheology / strongly confined molecular fluids / computer simulation

This research was financially supported by the Nederlands Organization of Technology  
(SON-STW) and the Netherlands Organization for Scientific Research (NWO).

Financial support from the IBM Research Division and generous donations of CPU time by  
the Groningen Computer Centre are also gratefully acknowledged.

# Contents

<b>Prolegomenon</b>	<b>vii</b>
<b>1 The simulation model and technique</b>	<b>1</b>
1.1 Molecular Dynamics . . . . .	1
1.2 The simulation geometry and the interactions . . . . .	3
1.3 Simulation details . . . . .	6
1.4 Other bells and whistles . . . . .	7
1.5 Appendix: The systems simulated . . . . .	9
<b>2 Nanoconfined films in equilibrium</b>	<b>11</b>
2.1 Static properties . . . . .	11
2.1.1 The nature of layering across confined films . . . . .	11
2.1.2 Chain conformations . . . . .	16
▷ Bond orientation factor . . . . .	16
▷ Density of chain ends . . . . .	18
▷ Radii of gyration . . . . .	19
▷ Segment distribution around the center of mass . . . . .	22
▷ Conformations of adsorbed chains . . . . .	23
2.1.3 The structure inside the first layer . . . . .	26
2.2 Chain dynamics . . . . .	29
▷ Rotational relaxation of the chains . . . . .	29
▷ Self diffusion of the adsorbed chains . . . . .	33
▷ Self diffusion of the free chains . . . . .	39
2.3 Appendix: Monomers between uncorrugated surfaces . . . . .	41
<b>3 Confined films under shear (I)</b>	<b>45</b>
3.1 Velocity profiles across ultra thin films . . . . .	46
▷ The effect of increasing shear rate . . . . .	50
3.2 Molecular mechanisms of slip in the nm scale . . . . .	53
▷ Neutral surfaces . . . . .	53
▷ Weakly physisorbing surfaces . . . . .	54
▷ Strongly physisorbing surfaces . . . . .	56
▷ Comparison with SFA experiments . . . . .	59
▷ Comparison with other experiments and theory . . . . .	59

3.3 The nature of shear thinning . . . . .	61
<b>4 The phenomenology of sheared <i>nanometer-thin</i> films</b>	<b>69</b>
4.1 Adsorbed chains & density profile under shear . . . . .	70
4.2 The effect of flow on the structure of the adsorbed layer . . . . .	74
4.3 Bond orientation factor . . . . .	77
4.4 Changing the molecular architecture . . . . .	80
4.5 Shape of the confined coils in shear flow . . . . .	82
▷ Radii of gyration across the pores . . . . .	82
▷ Radii of gyration of the adsorbed chains under shear flow . . . . .	85
▷ Radii of gyration of the free chains under shear flow . . . . .	86
4.6 Velocity profile & molecular architecture . . . . .	90
4.7 The influence of flow on pressure . . . . .	92
<b>5 Adsorption-desorption kinetics</b>	<b>95</b>
5.1 Shear enhanced transverse mobility . . . . .	95
5.2 Adsorption-Desorption kinetics under shear . . . . .	100
5.3 Conclusions . . . . .	111
<b>Summary &amp; Conclusions</b>	<b>113</b>
<b>Samenvatting</b>	<b>115</b>
<b>Appendix:</b>	<b>117</b>
<b>A Surface Forces Apparatus (SFA)</b>	<b>117</b>
▷ The experimental device . . . . .	117
▷ More information . . . . .	118
<b>Bibliography</b>	<b>119</b>
<b>Acknowledgements</b>	<b>125</b>
<b>List of publications</b>	<b>126</b>

## Prolegomenon

This dissertation is *not* intended to be a “manual” for the 45-page, one-piece, Fortran source that has been used for nearly all the simulations discussed herein. The design, development, debugging, and optimisation of this code, which allocated most of my two first years in Groningen, do not appear anywhere in the pages of the book in hand.

This dissertation is *not* intended to describe the analysis of the data obtained by the above program either. The struggle to define the relevant quantities and obtain values with good statistics from “representative” systems, which filled up the next two years of my ph. d. student life, is not directly depicted anywhere in this thesis either.

What I really tried to do in the following chapters is to shed some light on the phenomena that take place in nanoscopically confined thin films. As in this case, the intuition built on the understanding of the *bulk* statics, dynamics and rheology does not help us at all to comprehend these systems. More than anything else I tried to present the interesting “exotic” response of these ultra confined systems and unveil the molecular mechanisms that underlie this often striking macroscopic behaviour. This is only a first, very small step in the understanding of these systems and there is still a long way to go. I wish I could have spent a couple of years more before trying to put my thoughts in a book.

Finally, browsing through the pages of this thesis you will (maybe) find some of the topics presented in a *qualitative* style. This is a reaction to the frustration of extracting the physics from gigabytes of numbers produced by the simulation runs and the expression of the satisfaction of comprehending some of the connections between the macroscopic demeanour and the processes taking place at the molecular level.

The whole construction is fragile. But I still hope it can give out a certain feeling about the enthusiasm and the toil, the frustration and the joy of my scientific research during the last four years.

Evangelos D. Manias  
Groningen, August 1995



# Chapter 1

## The simulation model and technique

The confinement of molecules in dimensions comparable to their molecular size gives rise to a novel behaviour, which some times seems striking, as our intuition is usually based on knowledge acquired from bulk systems. In order to study the tribology and rheology of nanoscopically confined molecules the method of *Molecular Dynamics* simulation has been implemented. This method provides in principle the time evolution of a system and moreover many relevant physical properties can be evaluated using statistical mechanics. A brief presentation of the simulation method follows in this chapter.

### 1.1 Molecular Dynamics

Molecular Dynamics (MD) is a well established simulation technique to study molecular systems [1]. In its simplest form, it is the numerical integration of Newton's equations of motion for a system of  $N$  interacting particles:

$$m_i \frac{\partial^2 \mathbf{r}_i}{\partial t^2} = \mathbf{F}_i \quad i = 1 \dots N \quad (1.1)$$

and the forces acting on each particle ( $\mathbf{F}_i$ ) are usually described by some potential  $V$ :

$$\mathbf{F}_i = -\nabla_i V(\mathbf{r}_1, \mathbf{r}_2, \dots, \mathbf{r}_N) \quad (1.2)$$

Although much more elaborate schemes have been developed over the years<sup>1</sup>, throughout this dissertation Newton's equations are used. This means that the MD scheme is *classical* –i.e. classical mechanics are used to describe the motion of particles– and phenomena like tunnelling of particles and high frequency bond vibrations, which are of quantum-mechanical origin, are ignored. Moreover, the potentials used are *conservative*, implying that the atoms are in their ground energy state. Some of the MD simulations are also *Non-Equilibrium*, meaning that there exists an external “field”<sup>2</sup> acting on the system, constantly adding energy to it. A generalized flowchart of the Molecular Dynamics scheme used is shown in figure 1.1 (most of the details will be clarified shortly).

---

<sup>1</sup> ab-initio or from first principles methods, quantumdynamical simulations, configurationally biased MD, stochastic and Brownian simulations and so on

<sup>2</sup> in our case a pair of moving confining walls induces flow

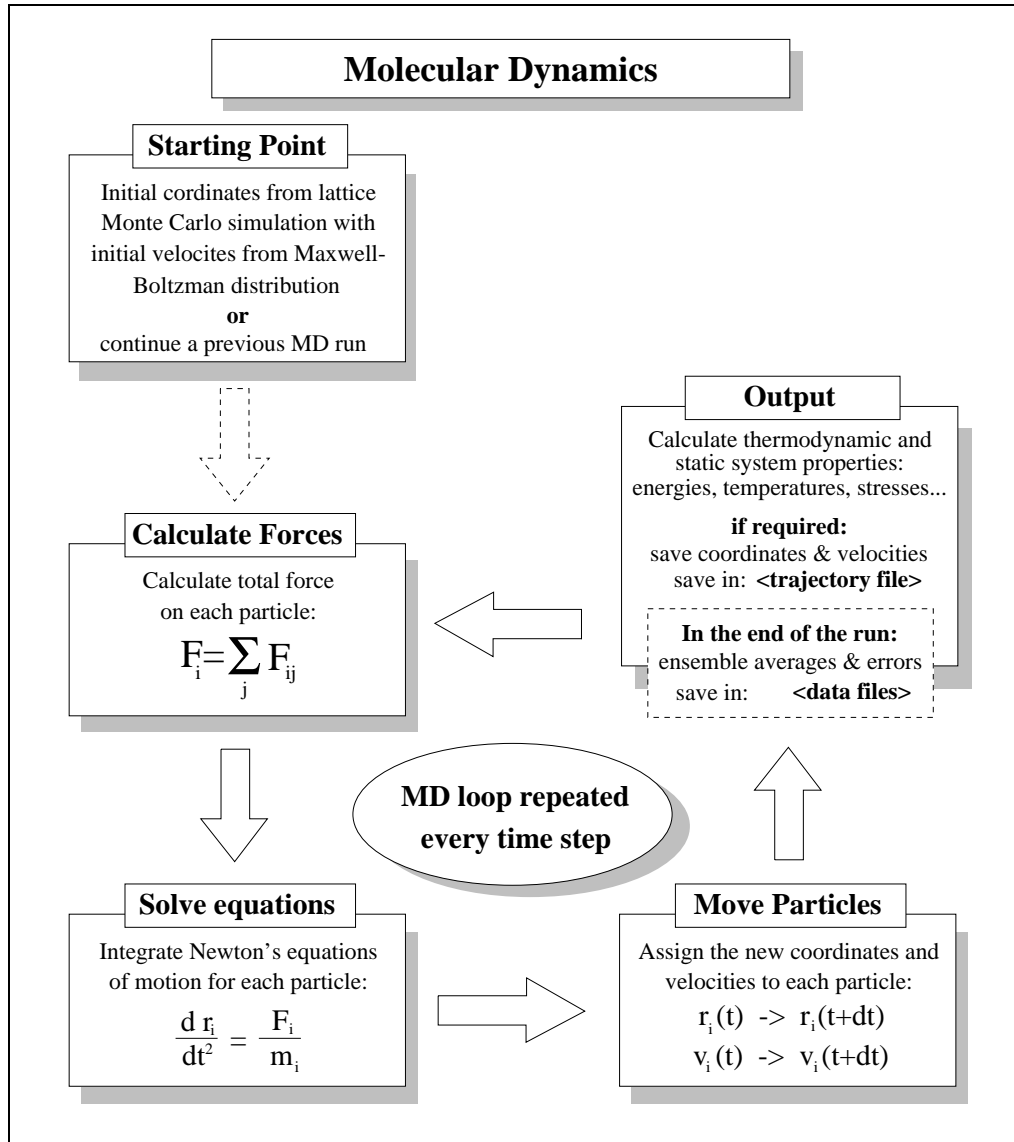


**Figure 1.1:** Generic flow chart of my MD algorithm

Definitions of statistical mechanics relate macroscopic quantities to microscopic properties [2, 3] and thus establish a connection between the macroscopic observable behaviour and the atomic and molecular details of the system<sup>3</sup>. Of course, the use of such definitions in MD simulations implies that the trajectory produced by the MD run is a representative ensemble of the system. Adequately exploring the phase-space requires multiple and long simulations and demands great computational power and time, which is characteristic of the MD method.

<sup>3</sup> for example macroscopic quantities like temperature, density, structural order parameter, diffusion coefficients and so on, can be calculated from the molecular simulations through statistical mechanics definitions by just the knowledge of particle positions and velocities [3]

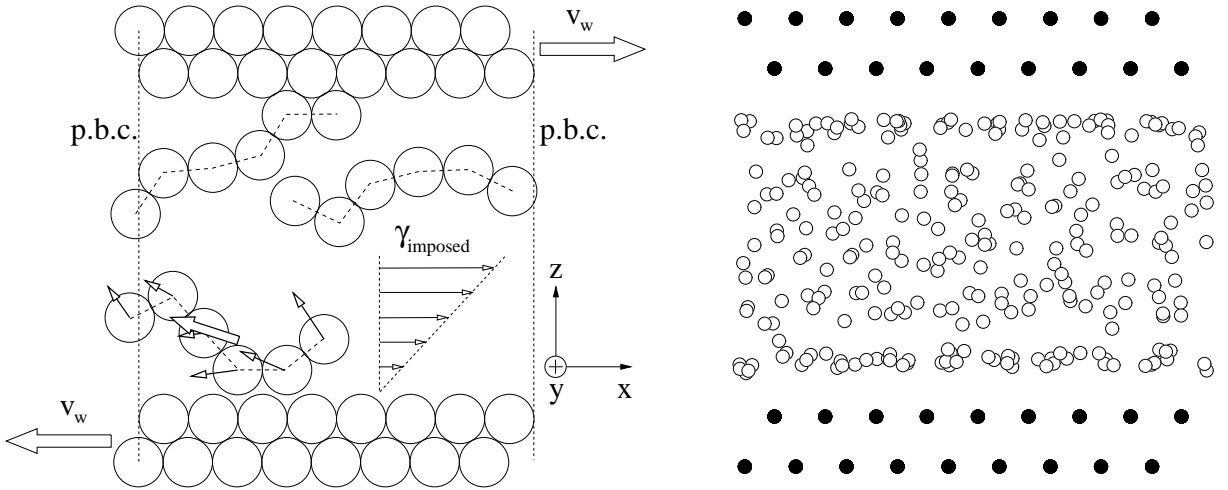


**Figure 1.2:** Schematic representation of the MD simulation geometry and a projection of the particle center of masses on the  $xz$  plane (hexamers,  $h = 6\sigma$ ,  $\epsilon_w = 1.0\epsilon$ , equilibrium).

## 1.2 The simulation geometry and the interactions

The systems studied systematically in this dissertation are confined films of oligomers with mainly 6 (hexamers) or 10 (decamers) segments per chain. Additionally, systems of monomers and oligomers of 5 and 20 segments per chain as well as oligomers with non-linear molecular architectures have also been studied (table 1.3). The chains are modelled by an abstract and generic, though well studied, bead spring model [6] confined between two double layered (111) fcc surfaces normal to  $\vec{z}$  and periodic boundary conditions are imposed in the two other directions (figure 1.2). Shear is imposed by moving the walls with a constant velocity ( $v_w$ ) towards opposite directions ( $\pm \vec{x}$ ). The interactions between the particles are modelled by the pair-additive, central, Lennard-Jones (LJ) potential, usually truncated at a distance  $r_c$  and shifted to a value  $U(r_c) = 0$  to satisfy continuity:

$$U(r) = \begin{cases} 4 \epsilon \left( \left(\frac{\sigma}{r}\right)^{12} - \left(\frac{\sigma}{r}\right)^6 + \left(\frac{\sigma}{r_c}\right)^{12} - \left(\frac{\sigma}{r_c}\right)^6 \right) & r \leq r_c \\ 0 & r \geq r_c \end{cases} \quad (1.3)$$

The potential modelling the interactions between the chain segments is truncated at its minimum ( $r_c = \sqrt[6]{2} \sigma$ ,  $U(\sqrt[6]{2}) = -\epsilon$ ). Thus the chain segments interact with each other via a purely repulsive, shifted and truncated LJ potential:

$$U(r) = \begin{cases} 4 \epsilon \left( \left(\frac{\sigma}{r}\right)^{12} - \left(\frac{\sigma}{r}\right)^6 + \frac{1}{4} \right) & r \leq \sqrt[6]{2} \sigma \\ 0 & r \geq \sqrt[6]{2} \sigma \end{cases} \quad (1.4)$$

where  $\epsilon$  is the LJ energy parameter and  $\sigma$  the LJ length parameter (figure 1.3a). *Connectivity* along the chains is ensured by adding a strongly attractive FENE (Finite Extensi-

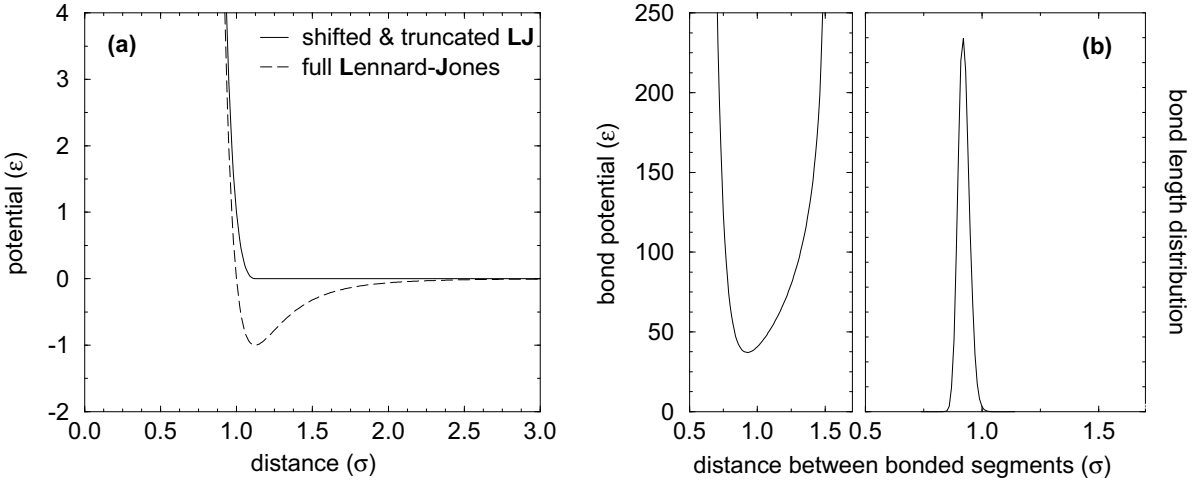


**Figure 1.3:** (a) The shifted and truncated interparticle potential used in the MD simulations. (b) The effective bond potential (superimposed FENE and LJ interactions) and the distribution of bond lengths. Notice the scale difference in the two potential energy graphs.

bility Non Elastic) potential between successive beads along one chain:

$$U_{bond}(r) = -\frac{k}{2}R_0^2 \ln\left(1 - \left(\frac{r}{R_0}\right)^2\right) \quad r < R_0 \quad (1.5)$$

where  $R_0 = 1.5 \sigma$  and  $k = 30.0 \epsilon/\sigma^2$  (figure 1.3b). These potentials have been used before in extensive studies of bulk systems [7], under confinement between walls [8, 9], as well as under shear [10, 11] and reproduce many static and dynamic properties of polymer systems. For our temperature ( $k_B T = 1.0\epsilon$ ) the bond lengths have a very narrow distribution around the mean value ( $0.928 \pm 0.023\sigma$ : figure 1.3b). Furthermore, the choice of parameters for the FENE potential has been proven to prevent bond crossing at temperatures even higher than the one used in our simulation [7]. The interactions between the walls and the segments are modelled by the *full Lennard Jones* potential, which includes an attractive tail (figure 1.3a):

$$U_w(r) = 4\epsilon_w \left( \left(\frac{\sigma_w}{r}\right)^{12} - \left(\frac{\sigma_w}{r}\right)^6 \right) \quad (1.6)$$

In order to reduce the computational effort this potential is truncated at  $r_{wc} = 2.5 \sigma$ . By changing the value of  $\epsilon_w$  the strength of the wall attraction can be varied systematically. For wall attractions  $\epsilon_w \leq 1.0\epsilon$  there is only a slight slowing down of the molecular motions and a very modest increase of the relaxation time characterizing a “weakly physisorbing” surface, whereas for  $\epsilon_w = 2.0\epsilon$  and  $3.0\epsilon$  the surfaces behave as “strongly physisorbing” by inducing a *dramatic* increase in the longest relaxation time of the adsorbed oligomers (by a factor of 70 for  $\epsilon_w = 2.0\epsilon$  and 1500 for  $\epsilon_w = 3.0\epsilon$ ) and an analogous slow down of the molecular motions, which is reflected in a decrease of the diffusion coefficient (by a factor of 40 and 1040 for  $\epsilon_w = 2.0\epsilon$  and  $\epsilon_w = 3.0\epsilon$  respectively, see § 2.2).

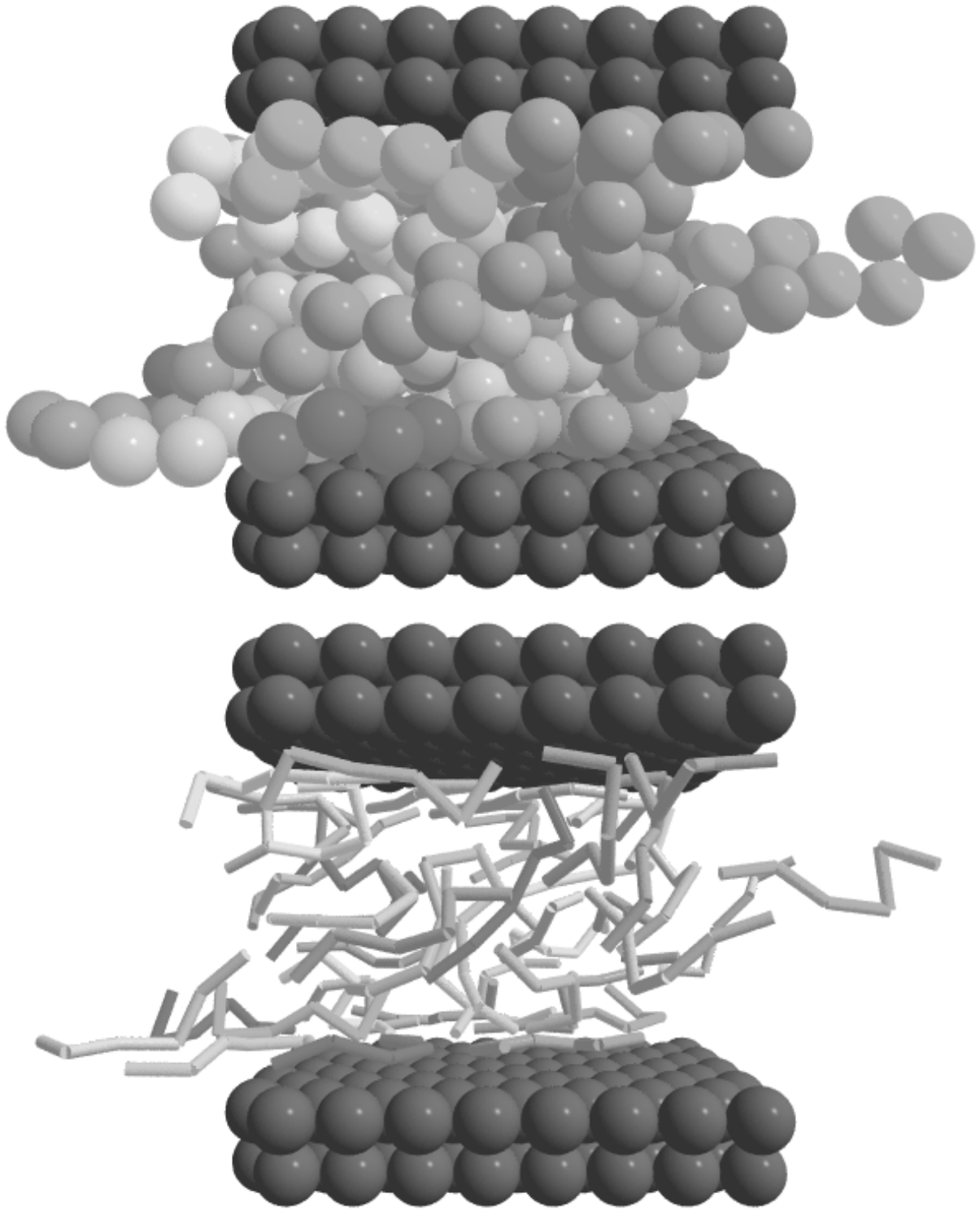


**Figure 1.4:** The beads (top) and the bonds (bottom) of a confined oligomeric systems. A system of hexamers is shown, at equilibrium –no flow– in a  $8\sigma \times 8\sigma$  simulation box, the wall-to-wall distance is  $h = 6\sigma$  and the LJ energy parameter for the walls is  $\epsilon_w = 1.0\epsilon$ .

### 1.3 Simulation details

Temperature is calculated from the principle of equipartition of energy and the definition of the kinetic energy, and for the equilibrium –no flow– case is:

$$\frac{N_{df}}{2} k_B T = \frac{1}{2} \sum_{i=1}^N m_i u_i^2 \quad (1.7)$$

where  $k_B$  is the Boltzmann constant,  $N$  the number of confined segments and  $N_{df}$  the number of degrees of freedom<sup>4</sup> in the system:  $N_{df} = 3N$ . For the Non-Equilibrium systems under shear, the flow velocities must be subtracted from the segment velocities:

$$\frac{N_{df}}{2} k_B T = \frac{1}{2} \sum_{i=1}^N m_i \left( (u_{ix} - u_{flow}(z))^2 + u_{iy}^2 + u_{iz}^2 \right) \quad (1.8)$$

For various reasons –heating due to external and frictional forces, computational and mathematical errors, truncations of potentials, high energy initial lattice configurations– there exist temperature drifts. In order to keep the temperature constant at  $k_B T = 1.0\epsilon$  the system is coupled to an external heat bath. This is achieved by rescaling the velocities [13] in two different ways: (i) scaling only the components of the velocities normal to the direction of the flow ( $u_y$  &  $u_z$ ) and (ii) scaling also the thermal part of the velocity component parallel to flow ( $u_{ix} - u_{flow}(z)$ ). In the second method the film is divided in slices and the flow velocity ( $u_{flow}(z)$ ) is calculated in each slice by averaging and scaling self consistently (eq. 3.2). For all the oligomers and for slices containing on average 15 particles, the two methods give the same results: velocity profiles and local temperatures, within the simulation accuracy. The solid atoms are not allowed to undergo any thermal motion around their equilibrium positions. A more “realistic” thermostat would involve momentum exchange between a thermally stabilized wall and the confined system. But not only is this method far more computationally demanding than the ones used here, but at the same time previous studies show that fixing the substrate atoms does not significantly change the results obtained [14]. Pressure is not coupled to any “pressure bath” and during the simulation it fluctuates around its average value.

A variant of Verlet’s algorithm [12, 1] is used to integrate the differential equations of motion with a time step of  $\Delta t = 0.004620$  MD time units (approximately  $10^{-14}$  seconds or 10 fsec, see table 1.1). This method is the simplest and the most frequently used and can be obtained by keeping from the Taylor expansion of the coordinates  $\mathbf{r}_i(t)$  terms up to  $\Delta t^3$ , thus errors are of order  $\Delta t^4$ :

$$\mathbf{r}_i(t \pm \Delta t) = \mathbf{r}_i(t) \pm \Delta t \frac{d}{dt} \mathbf{r}_i(t) + \frac{\Delta t^2}{2!} \frac{d^2}{dt^2} \mathbf{r}_i(t) \pm \frac{\Delta t^3}{3!} \frac{d^3}{dt^3} \mathbf{r}_i(t) + O(\Delta t^4) \quad (1.9)$$

and by adding  $\mathbf{r}_i(t + \Delta t) + \mathbf{r}_i(t - \Delta t)$  the prediction for the new position is:

$$\mathbf{r}_i(t + \Delta t) = 2\mathbf{r}_i(t) - \mathbf{r}_i(t - \Delta t) + \frac{\mathbf{F}_i}{m_i} \Delta t^2 + O(\Delta t^4) \quad (1.10)$$

---

<sup>4</sup> in our systems the only constraint is the motion of the system’s center of mass which is set to zero; this constraint is holonomic and reduces the  $N_{df}$  by 3, which is small compared to  $3N$  and is ignored

**Table 1.1:** Units of various quantities

Physical quantity	Reduced (MD) units	CGS equivalent
mass	$m$	$6.634 \cdot 10^{-23}$ gr
length	$\sigma$	$3.405 \cdot 10^{-8}$ cm
energy	$\epsilon$	$1.657 \cdot 10^{-14}$ erg
time	$\sqrt{m\sigma^2/\epsilon}$	$2.154 \cdot 10^{-12}$ sec
number density	$\sigma^{-3}$	$4.206 \cdot 10^{-2}$ mole/cm <sup>3</sup>
force	$\epsilon/\sigma$	4.866·10 <sup>-7</sup> dyne
velocity	$\sqrt{\epsilon/m}$	$1.580 \cdot 10^4$ cm/sec
stress	$\epsilon/\sigma^3$	$4.197 \cdot 10^0$ dyne/cm <sup>2</sup>
shear rate	$\sqrt{\epsilon/m\sigma^2}$	$4.463 \cdot 10^{11}$ sec <sup>-1</sup>
viscosity	$\sigma^{-2}\sqrt{\epsilon m}$	$9.043 \cdot 10^{-4}$ poise
diffusivity	$\sigma\sqrt{\epsilon/m}$	$5.381 \cdot 10^{-4}$ cm <sup>2</sup> /sec

although the velocities do not appear in this equation explicitly they can be trivially calculated<sup>5</sup> from the positions.

## 1.4 Other bells and whistles

Lists of neighbours [1] are used to reduce computational costs. There are three different lists of neighbours: two for the solid particles of each wall and one for the interactions between segments. All lists have a spherical *core* of radius  $r_c$  and a *skin* whose width depends on temperature and frequency of list updates [1]:  $r_{list} = r_c + 12 \tau_v \sqrt{T}$  where  $\tau_v$  is the period of list update which is 20 to 5 time steps depending on the shear rate.

Initial conformations are taken from a lattice Monte Carlo algorithm [15] and are assigned random velocities from a Maxwell-Boltzmann distribution of velocities with variance T. These lattice conformations are further equilibrated by a MD run in order to minimize the system energy and subsequently the walls are set in motion until steady state flow is achieved. After all these, extensive productive runs can be performed. The duration of these runs ranges between  $0.4 \times 10^6$  time steps for the systems with  $\epsilon_w = 1.0$  and/or high shear rates, and  $1.0 \times 10^6$  time steps for  $\epsilon_w \geq 3.0$  and/or lower shear rates.

---

<sup>5</sup> equation 1.10 can be rewritten in the form:

$$\mathbf{r}_i(t + \Delta t) = \mathbf{r}_i(t) + \mathbf{u}_i(t)\Delta t + \frac{\mathbf{F}_i}{m_i}\Delta t^2 \Rightarrow \mathbf{u}_i(t) = \frac{\mathbf{r}_i(t) - \mathbf{r}_i(t - \Delta t)}{2 \Delta t}$$

**Table 1.2:** After mapping the computer simulation results onto experimental measurements, one can attain an approximate correspondence between the bead-spring model parameters and the respective quantities for real polymers. The mapping was done for the bulk (K. Kremer and G. Grest *J. Chem. Phys.* **92**, 5057 (1990)) and should only be used as a rough approximation for confined systems. The following data are from this study.

Polymer	T	Monomer mass	M <sub>e</sub>	Monomers per bead	$\sigma$
MD	$1\epsilon/k_B$	1	35	1	
PS	485 K	104	18000	4.95	12.6 Å
PE	448 K	14	1350	2.76	5.1 Å
PDMS	300 K	74	9000	3.47	8.7 Å
PEP	500 K	70	2950	1.20	6.5 Å
PI	307 K	68	4100	1.73	6.7 Å

For the lower shear rates longer runs are necessary since the flow velocities are screened by the thermal motion. For this reason Molecular Dynamics simulations can better study systems under high shear rates, in the range of  $10^8 \text{ sec}^{-1}$  and higher, which are much higher than the shear rates that can be applied in SFA experiments (appendix A: up to  $10^5 \text{ sec}^{-1}$ ), but are of the same order of magnitude as the ones found in magnetic storage devices.

Already from the choice of the model for the chains it becomes evident that the aim of the research described in this thesis is not to study the specific interactions of different polymers and surfaces and/or the calculation of numerical values for physical quantities, but rather to consider the general, *qualitative* features of oligomers confined in ultra-thin films and the effect of wall energetics and shear on these systems. This is the reason behind the distinct *stochastic* character of the MD simulation scheme employed. In this perspective the strong coupling to a heat bath by a sturdy velocity scaling, the simple method for integrating the equations of motion and the simple model for chains and interactions are aiming at creating a representative ensemble of systems with certain thermodynamic properties (temperature, pressure, shear rate) following realistic, though stochastic, dynamics.

One could imagine a coarse-graining where several chemical monomers along the polymer backbone of a chain are combined in one of our segments (beads) and thus the real potentials are lumped into an effective potential, which would not be much different than the shifted and truncated LJ used herein. Keeping this in mind, one could map the results obtained by this model to experimental observations and create some kind of correspondence between the quantities of our model and the real physical quantities of chemically specific systems (table 1.2). This was done by Kremer and Grest [6], whose model is used here without essential modifications. It should be emphasised that such a correspondence is only valid for qualitative comparisons.

## 1.5 Appendix: The systems simulated

**Table 1.3:** Some details of the simulated systems.  $\Delta t$  is the time step used, for all simulations  $\Delta t = 0.00462$  MD units  $\simeq 10fs$ .

Molecule type	pore size ( $\sigma$ )	number of segments	wall velocities ( $\sqrt{\epsilon/m}$ )	simulated time ( $\Delta t$ ) $^\alpha$	wall velocities ( $\sqrt{\epsilon/m}$ )	simulated time ( $\Delta t$ ) $^\alpha$
$\epsilon_w = 0.0\epsilon$						
linear 5mer	10	465	equilibrium	500 000		
	6	270	equilibrium	500 000		
linear 6mer	6	270	equilibrium	500 000	0.3 0.9	750 000
linear 10mer	6	270	equilibrium	1 000 000	0.3 0.9	1 000 000
$\epsilon_w = 1.0\epsilon$						
linear 5mer	10	465	equilibrium	500 000	0.05 0.20	500 000
	6	270	equilibrium	600 000	0.30 0.90	250 000
linear 6mer	10	468	equilibrium	750 000	0.30 0.90	500 000
	7	270	equilibrium	600 000	0.175 0.2 0.30	400 000
	6	270	0.05 0.10 0.15	600 000	0.50 0.70 0.90	400 000
	4	168	equilibrium	800 000	0.175 0.2 0.30	600 000
branched 6mer	7	270	0.05 0.10 0.15	600 000	0.50 0.70 0.90	400 000
	6	270	equilibrium	800 000	0.175 0.2 0.30	600 000
	6	270	0.05 0.10 0.15	600 000	0.50 0.70	600 000
					0.90 1.50	400 000
star 7mer	5.93	266	equilibrium	800 000	0.175 0.2 0.30	600 000
			0.05 0.10 0.15	600 000	0.50 0.70	600 000
					0.90 1.50	400 000
linear 10mer	6	270	equilibrium	600 000	0.30 0.50 0.70	400 000
			0.05 0.10 0.20	400 000	0.90 1.50	400 000

$^\alpha$   $\Delta t$  is the time step equal to 0.00462 reduced units

continuing on the next page ...

Molecule type	pore size	number of segments ( $\sigma$ )	wall velocities ( $\sqrt{\epsilon/m}$ )	simulated time ( $\Delta t$ ) $^\alpha$	wall velocities ( $\sqrt{\epsilon/m}$ )	simulated time ( $\Delta t$ ) $^\alpha$
$\epsilon_w = 2.0\epsilon$						
linear 5mer	10	465	equilibrium	800 000	0.30	0.90
	6	270	equilibrium	500 000	0.30	0.90
linear 6mer	6	270	equilibrium	800 000	0.50	0.90
			0.10 0.20 0.30	600 000	2.00	3.00
branched 6mer	6	270	equilibrium	500 000	0.10	0.90
linear 10mer	6	270	equilibrium	800 000	0.50	0.60
			0.10 0.20 0.40	600 000	0.90	1.50
linear 20mer	$6^\beta$	600	equilibrium	1 000 000	0.10	0.90
$\epsilon_w = 3.0\epsilon$						
linear 5mer	10	465	equilibrium	800 000		
	6	270	equilibrium	800 000	0.30	0.70
linear 6mer	6	270	equilibrium	500 000	0.90	1.50
			0.10 0.20 0.30	600 000	2.00	3.00
branched 6mer	6	270	equilibrium	800 000	0.50	0.90
linear 10mer	6	270	equilibrium	500 000	1.50	2.00
			0.10 0.20 0.40	600 000	3.00	4.00

$\Delta t$  is the time step equal to 0.00462 reduced units

$\beta$  for 20mers a larger  $12 \times 12\sigma$  simulation box is used

Although in the vast majority of the systems simulated the interactions between the fluid segments are modelled by the *truncated* LJ (eq. 1.4), for some systems the *full* LJ potential was used (eq. 1.3,  $r_c = 2.5\sigma$ ). For the monomeric systems this is *essential*:

**Table 1.4:** Details of systems possessing some interparticle cohesion

System:	pore size	wall type	fluid-wall affinity								time
	( $\sigma$ )		( $\epsilon_w$ in $\epsilon$ )								( $\Delta t$ )
monomers (equilibrium)	10	smooth	0.00	0.60	1.00	1.40	1.80	2.00	3.00	4.00	100 000
			1.00	1.74	2.00	2.15	2.22	2.31	3.45	4.62	400 000
	10	fcc $0.80\sigma$			0.00	1.00	1.40	1.80	2.20		100 000
	10	fcc $1.00\sigma$			0.00	1.00	1.40	1.80	2.20		100 000
	10	fcc $1.06\sigma$			0.00	1.00	1.40	1.80	2.20		100 000
	10	fcc $1.12\sigma$	0.0	0.2	0.4	0.6	0.8	1.0	1.4	1.8	2.2
linear 6mer	10	bcc $1.0\sigma$			0.00	0.50	1.00	1.40	1.80	2.00	100 000
	6	fcc $1.00\sigma$			$\epsilon_w = 2.00$		$v_w:$	0.00	0.05		800 000
					$\epsilon_w = 2.00$		$v_w:$	0.50	0.90		600 000

## Chapter 2

### Nanoscopically confined films in equilibrium

The effect of confinement on the equilibrium properties of an oligomer melt is studied in this chapter. Even though the emphasis of this dissertation is on the non-equilibrium properties, the equilibrium case has to be included in this thesis, since only the comparison between the systems in equilibrium and the ones under shear can reveal the way flow influences the confined systems. In this perspective, this chapter contains a presentation of the simulation results on the static and dynamic properties of oligomers confined between two *stationary* walls, aiming to reveal further<sup>1</sup> the molecular origins of the “exotic” behaviour of nanoscopically confined oligomeric systems.

## 2.1 Static properties

### 2.1.1 The nature of layering across confined films

One of the first striking experimental findings obtained with the Surface Forces Apparatus (SFA) was the strongly oscillatory solvation forces. These were first reported for small molecules confined between atomically smooth mica plates, namely OMCTS (octamethylcyclotetrasiloxane) [18, 20], benzene, tetrachloromethane, cyclohexane [20] and simple oligomers like: *iso*-octane [20], *n*-tetradecane and *n*-hexadecane [18]. The existence of such oscillating normal forces, when bringing the two mica surfaces towards each other, suggested that the confined fluids are inhomogeneous near the surfaces –i.e. there exist density fluctuations in the vicinity of the solid surfaces, in the form of layers.

This “wall induced layering” (oscillatory density profile near the confining surfaces) is of the same physical origin as the the oscillations in the radial distribution function of simple liquids [2]. It can be explained fairly easily for the reference system of a hard sphere fluid next to a hard wall; for this system the interparticle interactions are characterized by the complete absence of any attraction<sup>2</sup> but the *effective* hard wall-hard sphere interaction *in the presence of the other hard spheres* is different [21]. When a hard sphere is adjacent to the wall then the collisions with other fluid particles from the side facing the surface

---

<sup>1</sup> some of the physics are well understood and theoretical [16] as well as simulation approaches have been reported [17, 15, 8]

<sup>2</sup> the actual hard wall - hard sphere potential is infinite when a hard sphere penetrates the wall and zero otherwise

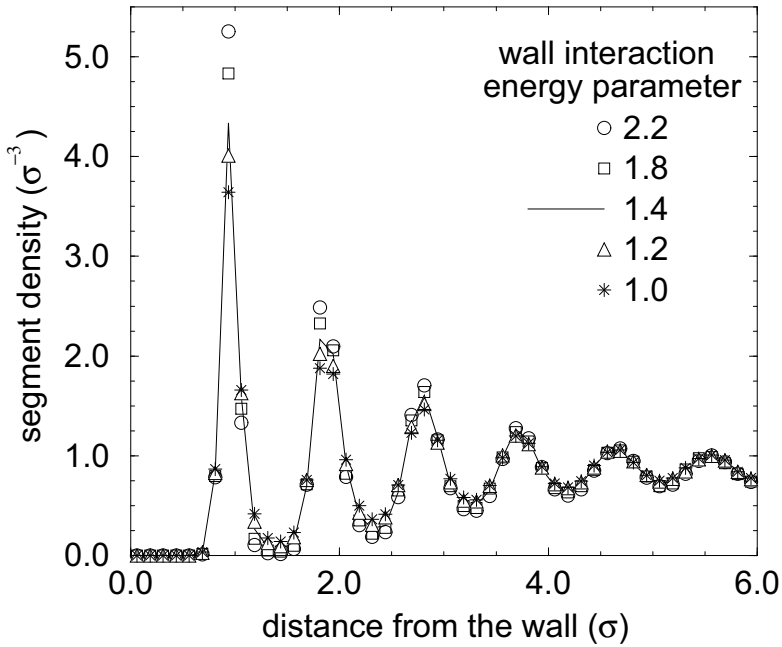


**Figure 2.1:** Number density of segments normal to the confining surfaces. The systems are monomeric Lennard-Jones (LJ) fluids confined in a pore of width  $h = 12\sigma$  between two fcc walls –i.e. only half the pore is shown here with the wall particles having their center of mass at  $z = 0$ . The parameter is the strength of the wall attraction.

are much more frequent than from the side of the wall. In this way, the rest of the fluid particles, acting as a heat bath, give rise to a net force pushing this particle towards the wall. Thus the particles touching the surface are effectively attracted to it due to the *angular asymmetry* of their *collisions* with the other fluid particles. Exactly this idea was exploited to interpret the oscillations of the radial pair correlation function [21] and the “*potential of mean force*” can be defined as the interaction between two particles when the rest of the system is canonically averaged over all configurations. This potential exhibits attractive minima even in the case of hard spheres. Similarly, for attractive surfaces there is an effective mean force potential<sup>3</sup> and moreover the interatomic potential between the wall particles and the fluid particles is added to this effective potential making it even more attractive, thus resulting in an increase of the density oscillations near the wall (fig. 2.1). Unavoidably the high density next to the wall will be followed by a density depletion since the hard core of the fluid particles prevents them to get closer than one diameter. For the same reason this depletion will cause a second density peak and for sufficiently high densities several alternating density minima and maxima will be created across the film. In the case of softer potentials –like the LJ used in our studies– the

<sup>3</sup> defined as the wall particle-fluid particle interaction when the rest of the fluid particles are properly averaged over all possible configurations

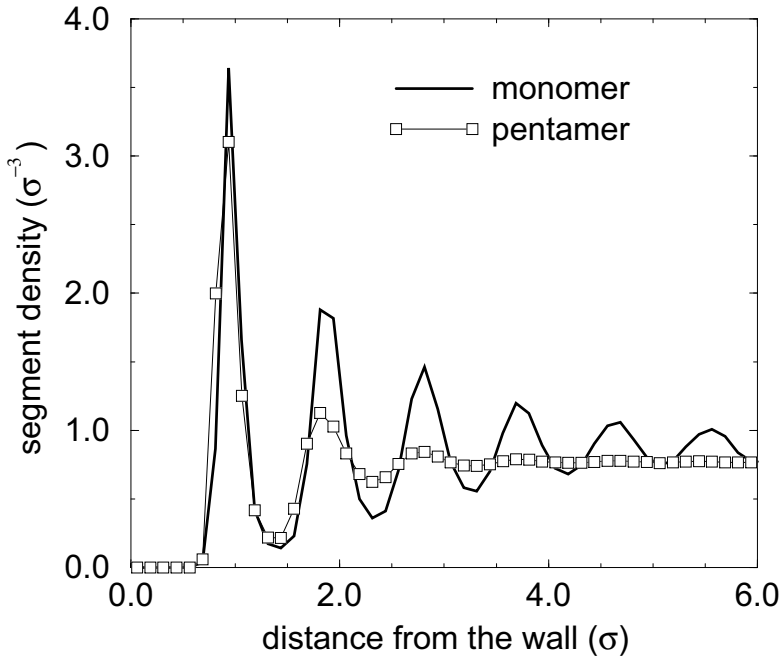


**Figure 2.2:** Number density of segments normal to the confining surfaces. The systems are confined in pores of width  $h = 12\sigma$  between two fcc walls and correspond to a LJ fluid and a pentamer bead-spring melt of the same average density ( $\epsilon_w = 1.0\epsilon$ ).

picture remains qualitatively the same, as for small separations they are steeply repulsive and prevent any significant particle interpenetration [22].

In the pioneering SFA experiments cited, a lot of parameter were investigated providing results that support the above argument for the confinement-induced layering. First, the scenario of a shift in the glass transition temperature near a wall was dropped, after studies with temperatures varying from below the melting point up to values quite higher than it [19, 23], showed only minor temperature effects on the normal forces. Finally, the experimental observation of up to ten fluid layers between the two surfaces clearly indicates that layering occurs much beyond the range of the wall interactions (which extends only to the first layer or two) and has to be attributed to the nature of the fluid. Finally, the use of mica surfaces, which are strongly attractive to most of the fluids studied, gave rise to very pronounced force oscillations when trying to squeeze out of the gap the first layers (i.e. adsorbed molecules) in contrast with less attractive surfaces (CTAB-coated mica [19]).

The comparison of the density profiles of an oligomer melt with a monomeric fluid shows two main differences (figure 2.2):

- the maximum of the first layer is larger (19%) for the monomeric fluid;
- the density oscillations for the oligomer melt are damped much faster than the ones

of the simple liquid. In fact, even for the relatively short chain (pentamer) shown in figure 2.2, only two fluid layers are developed next to the surface, whereas for the monomer layering is quite strong even beyond six fluid layers.

Obviously these differences originate from the *connectivity* between consecutive segments along the chains, since the rest of the interactions are the same in the two systems. Qualitatively it is quite easy to understand both these differences. Both the simple liquid

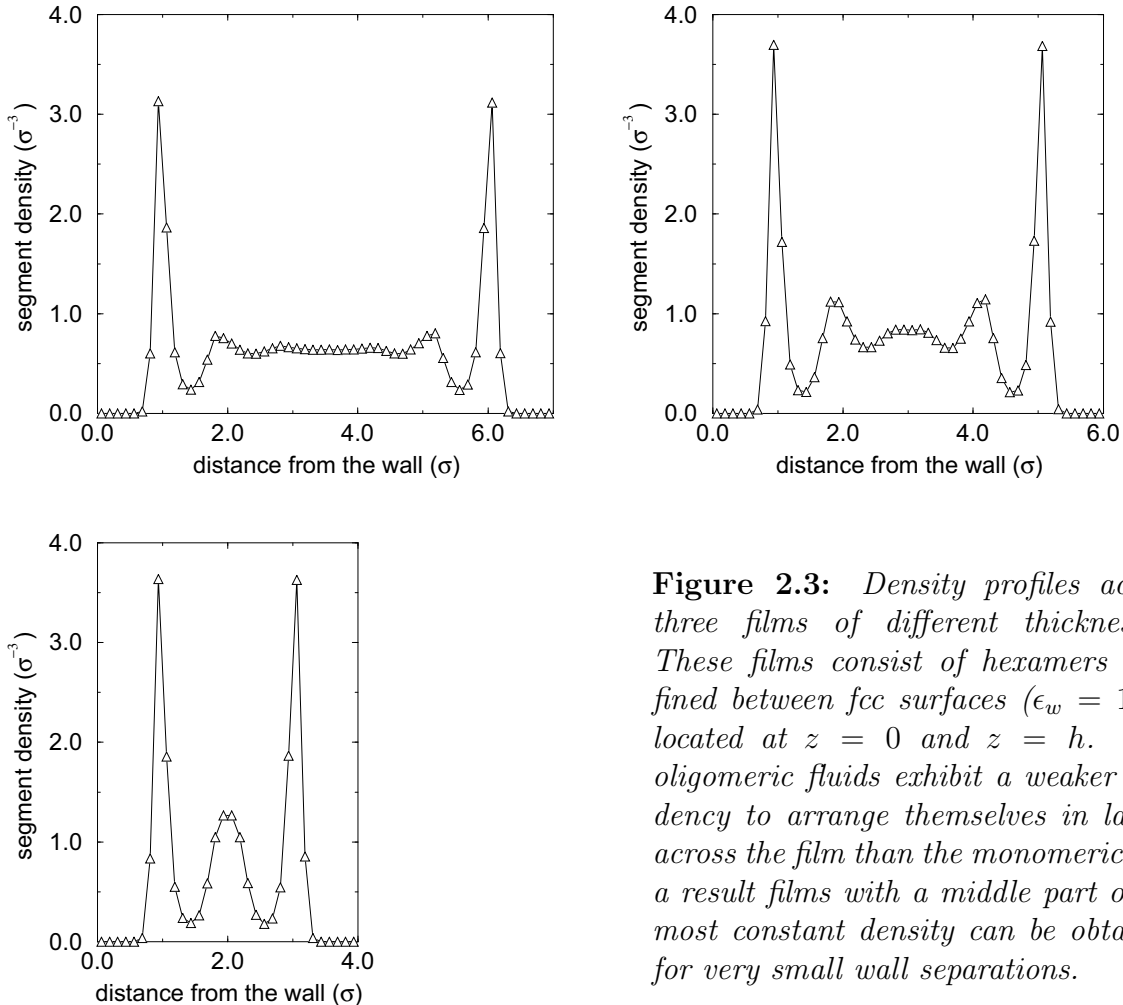


**Figure 2.3:** Density profiles across three films of different thicknesses. These films consist of hexamers confined between fcc surfaces ( $\epsilon_w = 1.0\epsilon$ ) located at  $z = 0$  and  $z = h$ . The oligomeric fluids exhibit a weaker tendency to arrange themselves in layers across the film than the monomeric. As a result films with a middle part of almost constant density can be obtained for very small wall separations.

and the oligomeric fluid exhibit a tendency to develop a layering due to the potential of mean force. But, although the particles are free to occupy the *optimal* positions in the simple liquid, in the oligomeric they have to satisfy the connectivity requirement. So by constraining the segments in chains an extra *entropic* cost is introduced, which makes the layering less perfect. This results both in the decrease of the first layer density, as well as in a fast decay of the density oscillations. The latter has as a direct result for quite narrow oligomer films to develop a constant density middle part. As it can be seen in figure 2.3 the hexamers develop a constant density middle part in the film for separations

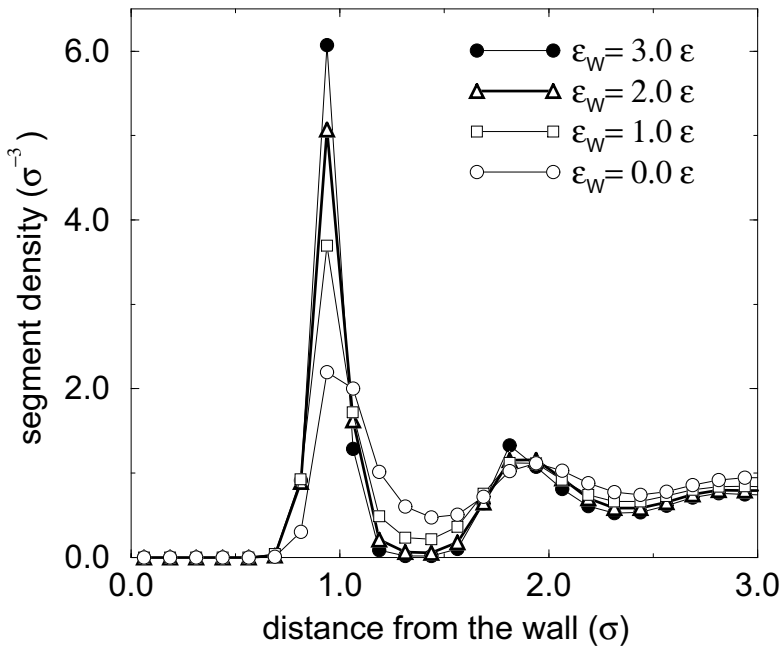


**Figure 2.4:** As with the monomeric fluids, the inhomogeneity of oligomer films increases for stronger wall affinities. Here the number density of segments normal to the surfaces is plotted for three different strengths of the wall attraction  $\epsilon_w$ .

down to seven segment diameters and even for a film thickness of  $h = 6.0\sigma$  –this width accommodates five well developed fluid layers of a monomeric LJ liquid– the middle part of the film is characterized by an almost constant density. This film thickness is the one at which confinement starts to affect measurably the system properties, while there still remains a bulk-like middle part [24, 11, 25].

Another important feature of this confined oligomer films is that when the wall affinity becomes stronger, apart from the inhomogeneity enhancement, constituted by larger variations of the *local* segment density (figure 2.4), there is also an increase of the *average* segment density inside the first layer (table 2.1). These average segment densities per layer have been proven to affect the segment mobility in a much more direct way than the local densities [9, 26, 27, 28] and seem to be the *origin of the “glassy” dynamics in the solid-oligomer interface* [9, 36]. Moreover, this wall induced densification inevitably causes an enhancement of the in-plane ordering in order for more segments to be accommodated inside the first layer.

As the decrease of the layering further away from the walls is of entropic nature, it is expected that with increasing chain length this entropic cost would increase and thus the inhomogeneity would vanish. The important chain length is the one that allows a chain to have always a significant part of it outside the inhomogeneous region. But, since the inhomogeneities are limited to distances only a couple of segment diameters away from

**Table 2.1:** Average segment densities per layer

Layer	$h = 7.0\sigma$		$h = 6.0\sigma$		
	$\epsilon_w = 1.0$	$\epsilon_w = 0.0$	$\epsilon_w = 1.0$	$\epsilon_w = 2.0$	$\epsilon_w = 3.0$
first	1.01	0.95	1.05	1.18	1.26
second	0.74	0.80	0.73	0.74	0.79
third	0.78	0.82	0.80	0.75	0.70

the wall, even quite short chains of five or six segments are long enough to reach this limit and for chains longer than ten segment the density reaches the infinite molecular weight behaviour<sup>4</sup> [8].

### 2.1.2 Chain conformations

The confinement effects on the *static properties* of monomeric films, are mainly the layering normal to the walls and a simultaneous in-plane ordering inside the first layer [29, 30]. On the other hand, the association of segments into chains gives rise to a number of other static properties, which are related to the chain conformations, like the bond orientation, the distribution of segments around the chain center of mass, the radii of gyration and so on. This section focuses on how these static properties are affected by confinement and by the wall energetics and what happens in the vicinity of the surfaces.

**Bond orientation factor:** The arrangement of oligomers next to a surface reduces the freedom of the chains to adopt all the possible conformations. Moreover, the layering of the segments reduces the capability of the bond to orient freely and there is an deviation from an isotropic distribution of bonds in the inhomogeneous part of the film. A quantity that is commonly<sup>5</sup> used to quantify this orientational anisotropy of the bonds is defined by:

$$s(z) = 1.5 * \langle \cos^2 \theta \rangle - 0.5 \quad (2.1)$$

where  $s$  is the bond orientation or bond anisotropy factor and  $\theta$  is the angle between the bond and the reference direction, in our case is the direction normal to the walls ( $z$ -axis), and the average is over all bonds located at distance  $z$  away from the wall and over the simulated time. Obviously  $s(z)$  is the average direction of bonds located at  $z$  and:

$$s(z) = \begin{cases} -0.5 & : \text{bonds are parallel to the wall} \\ 0.0 & : \text{bonds are randomly oriented} \\ 1.0 & : \text{bonds are normal to the solid surfaces} \end{cases}$$

<sup>4</sup> one has to keep in mind that due to the intrinsic high flexibility of this bead-spring model, these short chains correspond to much longer real chains when comparing with experimental systems (table 1.2)

<sup>5</sup>  $s(z)$  as defined by equation 2.1 is the second Legendre polynomial of  $\cos\theta$ :  $P_2(\cos\theta) = \frac{1}{2}\langle 3\cdot\cos^2\theta - 1 \rangle$  which is a very usual choice for an orientation factor

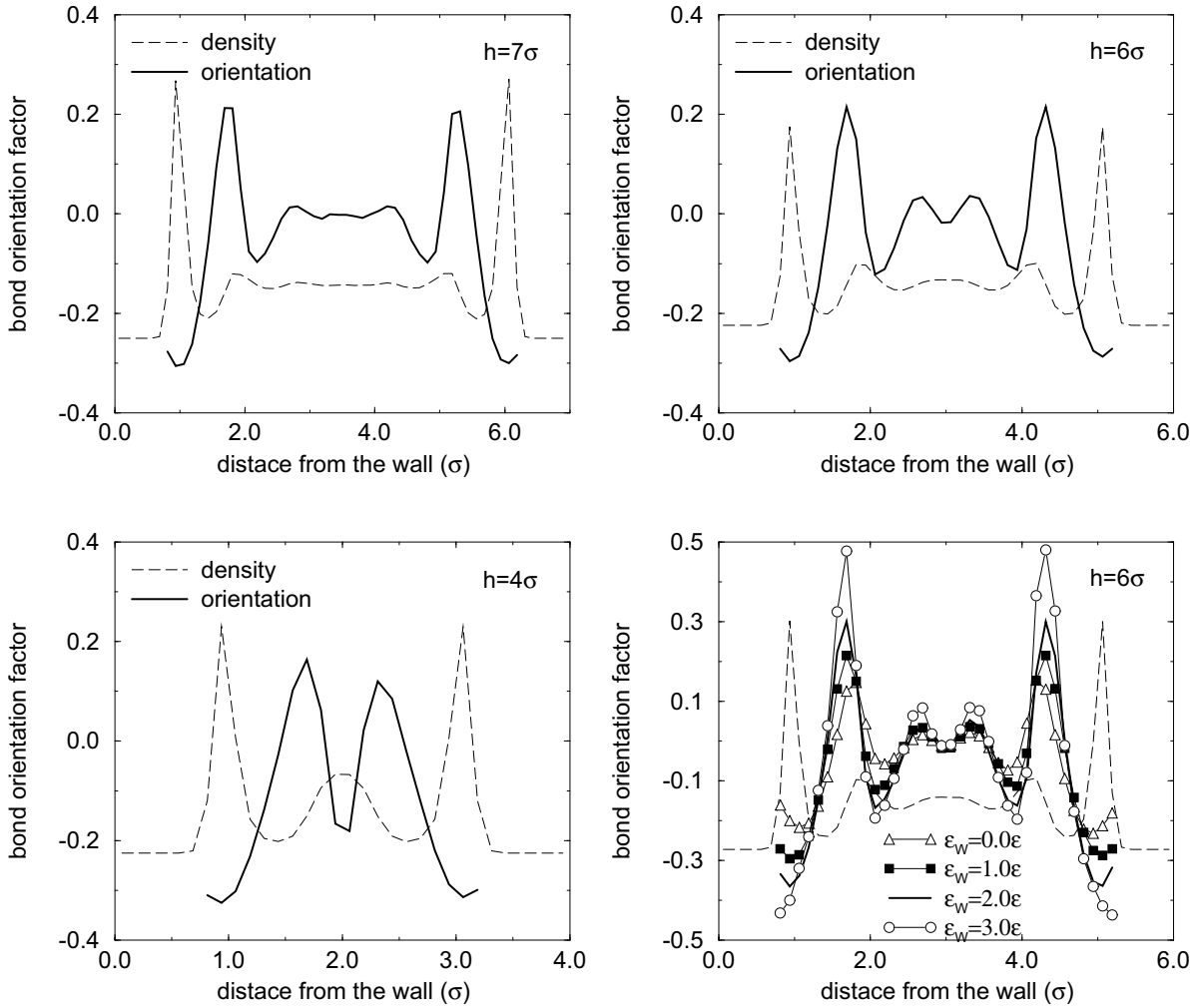


**Figure 2.5:** The bond orientation factors for films of confined hexamers: systems of various thickness ( $h = 4, 6$  and  $7\sigma$ ) confined between moderately attractive fcc surfaces ( $\epsilon_w = 1.0\epsilon$ ); for  $h = 6$  the effect of increasing wall affinity is also shown.

In figure 2.5 the orientation factors are plotted for three film thicknesses ( $h = 4, 6$  and  $7\sigma$ ) for  $\epsilon_w = 1$  walls. Inevitably, the bonds located inside the first fluid layer –connecting two adsorbed segments– are almost parallel to the surfaces, whereas bonds that connect an adsorbed segment with a segment inside the second layer are mostly perpendicular to the walls. Since there is no third density peak, even for these short oligomers, the bond orientation factor levels off to a 0.0 value (random orientation) for sufficiently wide films ( $h = 6$  or  $7\sigma$ ). As far as the bond orientation near the surfaces is concerned it is does not change when reducing the film thickness (even down to  $h = 4!$ ) but bond orientation is systematically enhanced with increasing wall attractions. MD simulations of quite longer chains confined between flat walls [8] and predictions from theoretical lattice models [16] are in quite good agreement with these findings.

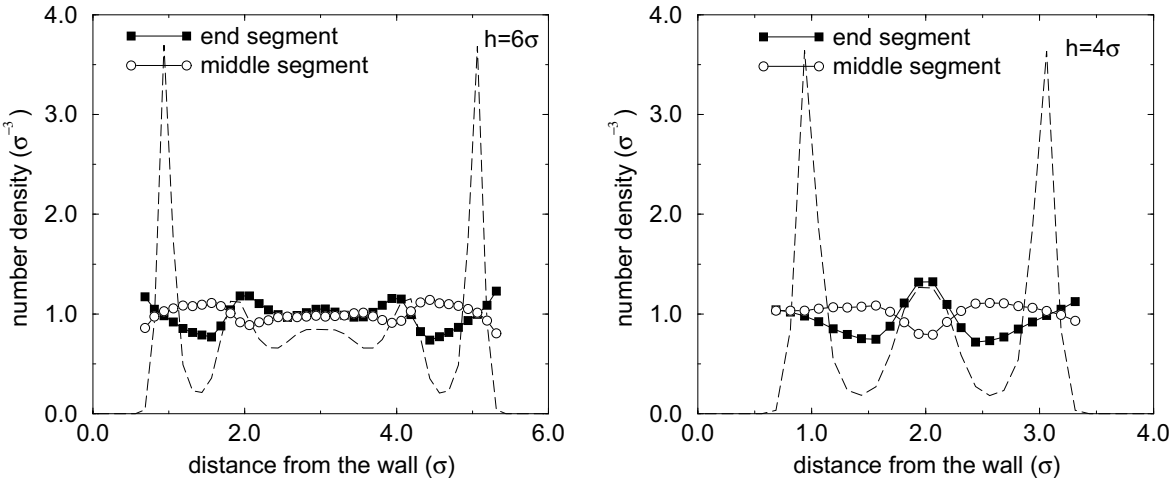


**Figure 2.6:** End and middle segment densities are plotted as a function of their distance from the surfaces; both systems are hexamers confined between walls with  $\epsilon_w = 1.0$ . The data have been decoupled from local density variations and scaled in order to be directly compared with the segment density.

**Density of chain ends:** In a dilute solution, the presence of a surface favours configurations with adsorbed end segments over configurations with a lot of adsorbed middle segments [31]. This has as a direct consequence the end segment density in the vicinity of the walls to be higher than the middle segment density[31]. This preferential adsorption of chain ends on a surface, which causes an enhancement of end segment density, was also observed in simulation studies of dense oligomer and polymer melts on lattice [15] and continuum studies [8, 32]. If one is interested in studying this end density enhancement, one has to decouple the end density profile from the segment density variations and the reduction of chain ends for different chain lengths. This can be done by defining the so-called “end-enhancement factor” or a coarse grain average of this factor over the region of inhomogeneities [8]. Since these have been done and seem to be well understood, in this paragraph only a brief presentation will be made concerning the end-and mid-segment densities across a nanoscopic pore. On the other hand, when shear is imposed across the pore the changes in the conformations of the adsorbed chains are of vital importance to the rheological behaviour of the oligomer film, and from that viewpoint further discussion will be made (for example see §§ 3.2, 3.3, 4.1, 5.1).

In figure 2.6 the end segment and middle segment densities of two hexameric films are plotted. The data have been decoupled from the local segment density variations and scaled taking into account the chain length, e.g. the ratio of end/mid to the total number of segments. Even decoupled from the local density inhomogeneities the end density exhibits similar variations with the segment density profile, while the middle segment density is characterized by smaller oscillations in an almost constant profile across the film. The small enhancement of the end density inside the first fluid layer is in quantitative

agreement with previous studies[8]. This finer structure of end density profile can not be captured by lattice simulations [15].

Perhaps the most interesting observation concerning these findings is the very short range character of the end density variations. In contrast, theoretical predictions for dilute solutions expect these wall-induced end density variations to extend<sup>6</sup> over distances comparable to the chain radius of gyration[31]. Moreover, the end and middle segment density profiles behave in the same way with the total segment density profile when increasing the wall attraction, although the relative differences are considerably smaller (e.g. increasing  $\epsilon_w$  from 1 to 2 results in an increase of the first layer density peak more than 30% (fig. 2.4) whereas for the end density is only 5%; and when  $\epsilon_w = 3$  the same quantities change by 60% and 15% ). This weak effect of  $\epsilon_w$  shows that the enhancement of the end-density near the walls is a geometric effect rather than one that originates from the wall energetics.

**Radii of gyration:** Probably the most interesting static properties in confined oligomer systems concern the shape and size of the chains in the vicinity of the surfaces and how they deviate from the respective bulk shape and sizes. The most appropriate quantities to describe these are the radius of gyration of the chains and the distribution of the segments around the center of mass (CM) vs the distance of the CM from the wall.

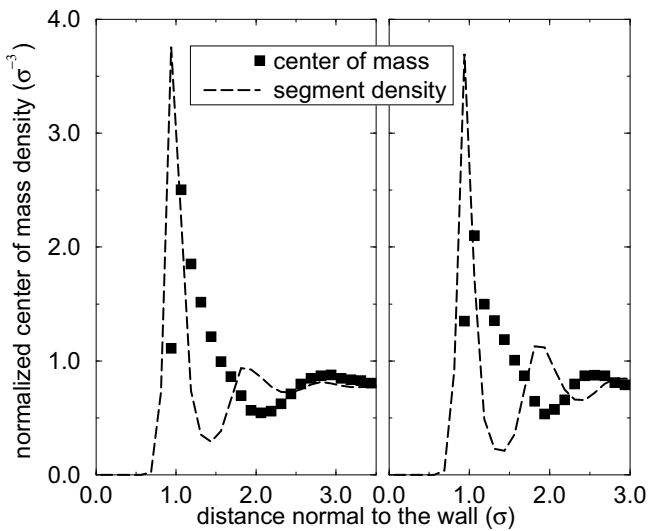


**Figure 2.7:** The center of mass distribution for films of confined hexamers. Both systems are confined between moderately attractive fcc surfaces ( $\epsilon_w = 1.0\epsilon$ ) and only half the pore is shown. The CM density does not follow the segment layering as expected, since the partly adsorbed oligomers have their CM in the region of the depletion zone between the first and second fluid layers.

So, it would be interesting to see how the centers of mass are distributed across this ultra-confined films. In figure 2.7 the distribution of CM across half the film is plotted. In order to be compared with the segment density profile, the CM density was multiplied by the number of segments per chain. Although the segments of the chains exhibit strong layering in the vicinity of the walls, the centers of mass, being mathematical points without any physical existence in the form of a particle, are not expected to layer in the same way like the monomers. On the contrary, they are expected to have significant values inside the segment depletion zone, between the first and second fluid layers, as the centers of

<sup>6</sup> the accuracy of this latter work, as far as this point was concerned, has been criticized

mass of partly adsorbed chains<sup>7</sup> are located there.

In order to see the effect of the surfaces, the film is divided into slices and for each slice the average mean radius of gyration ( $R_g$ ) is derived.  $R_g$  for a chain of  $N$  segments is defined by:

$$R_g^2(z) \equiv < \frac{1}{N} \sum_{k=1}^N (\mathbf{r}_k - \mathbf{r}_{cm})^2 > \quad (2.2)$$

where  $\mathbf{r}_k$  is the coordinate vector of the  $k$ th bead,  $\mathbf{r}_{cm}$  is the coordinate vector of the center of mass of the chain and the average  $< \dots >$  is over all chains with their CM inside the particular  $z$ -slice and over the simulation time. The radius of gyration characterizes the size of the chain but does not give information about the orientation of the chain. An appropriate quantity to study the orientation is the mean square radius of gyration *tensor* defined by:

$$R_g^{ij} \equiv \frac{1}{N} \sum_{k=1}^N (\mathbf{r}_k^i - \mathbf{r}_{cm}^i) \cdot (\mathbf{r}_k^j - \mathbf{r}_{cm}^j) \quad (2.3)$$

with  $i, j$  representing three normal directions (in our case  $x, y$  and  $z$ ). The eigenvalues of this tensor, called principal components of the square radius of gyration, are in descending order denoted by  $\lambda_1, \lambda_2$  and  $\lambda_3$  and their sum is the square radius of gyration of the chain  $R_g^2 = \lambda_1 + \lambda_2 + \lambda_3$ . The eigenvalues of the  $R_g^{ij}$  tensor characterize the size and shape of the coil. In the general case, when  $\lambda_1 \neq \lambda_2 \neq \lambda_3$  the segment distribution around the CM is ellipsoidal and the eigenvalues  $\lambda_i$  give the size of its axes. The eigenvectors define the orientation of the corresponding axes of the ellipsoid and thus characterize the orientation of the chain. This implies that the eigenvector  $e_1$  which corresponds to the longest axis of the ellipsoid ( $\lambda_1$ ) points in the direction of the largest dimension of the chain [34].

In the bulk, it is obvious that although at every time instant the shape of the chain is ellipsoidal, the *time averaged* segment distribution around the CM of the coil is spherical [35]. But this is no longer valid when the isotropy of the space is disturbed, as for example in the vicinity of a solid surface, or under shear. In our simulations the time averaged radius of gyration tensor is calculated over all chains that have their CM at a certain distance away from the walls. In this way, by dividing the system into thin slices, conclusions can be derived for the time averaged size and the orientation of the chains which are located a certain distance away from the wall.

For the systems in equilibrium (i.e. no flow) the radius of gyration tensor is diagonal and its three eigenvectors are parallel to the  $x, y$  and  $z$  directions; this is a direct result of the simulation geometry. It means that time averaged the coils have an ellipsoidal shape with their longest axis parallel to the walls. If the non-zero diagonal components of the time averaged radius of gyration tensor ( $R_g^{xx}, R_g^{yy}, R_g^{zz}$ ) are presented as a function of the distance of the CM of the chain from the solid surface, the effect of the confinement can be seen (fig. 2.8). For chains with their CM near the solid surfaces, it is inevitable that  $R_g^{zz}$  is very small corresponding to a flat –“pancake” like– coil shape. Moving further away from the wall, the  $R_g^{zz}$  increases and the  $R_g^{xx}$  and  $R_g^{yy}$  components decrease and in the middle of

---

<sup>7</sup> chains with some of their segments adsorbed and some free

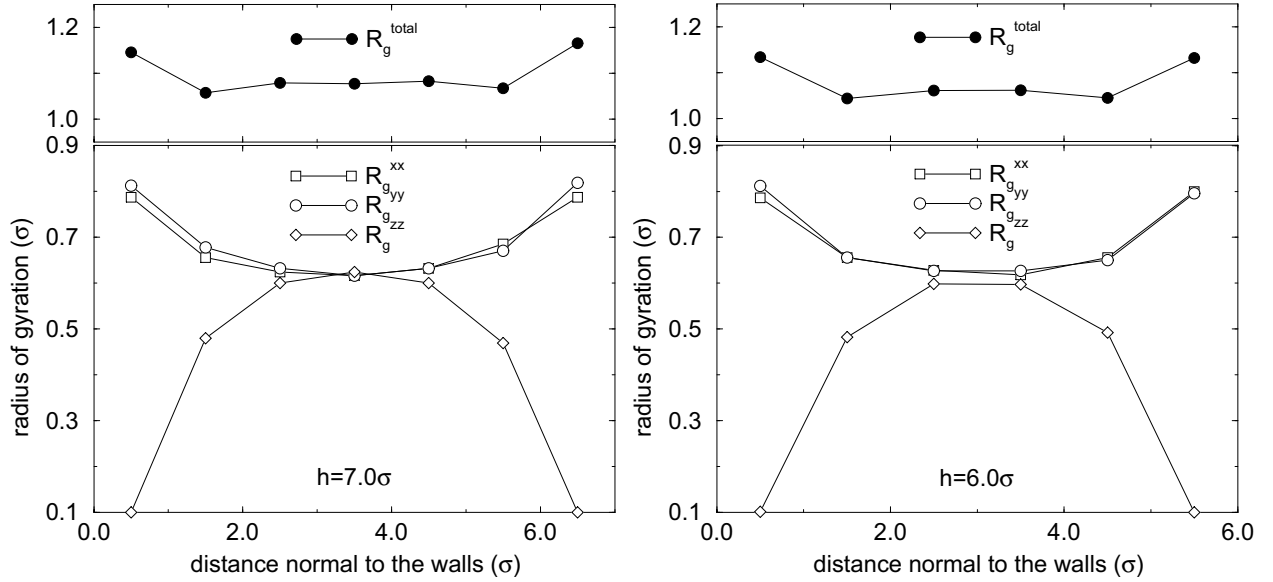


**Figure 2.8:** The Radius of gyration tensor elements parallel ( $R_g^{xx}$ ,  $R_g^{yy}$ ) and normal ( $R_g^{zz}$ ) to the surfaces are plotted versus the distance of the chain center of mass from the wall. For both film thicknesses presented the oligomers are hexamers and  $\epsilon_w = 1.0$ .

the  $h = 7$  pore the coils have an almost spherical *time averaged shape* ( $R_g^{xx} \simeq R_g^{yy} \simeq R_g^{zz}$ ). Thus as far as the radius of gyration is concerned the chains in the middle of the pore do not feel the walls, even at this very narrow confinement ( $h = 7.0\sigma$ ). On the other hand, the total radius of gyration is constant and equal to the bulk  $R_g$  throughout the film *except* for the chains with their CM inside the first layer –i.e. fully adsorbed configurations. For these chains the radius of gyration is larger than in the middle of the film, demonstrating that the chains near the walls are stretched. This dependence of  $R_g$  on distance, pronouncedly flattened near the walls and almost unperturbed after just a couple of  $R_g^{zz}$  away from the surfaces, was also observed in previous lattice [17] and off-lattice Monte Carlo [32] simulations.

For the narrower confinement ( $h = 6$ ) the effect of the two walls reaches out far enough in the pore for the time averaged radius of gyration to be anisotropic throughout the film<sup>8</sup>, even for the coils located in the middle of the system ( $R_g^{xx} \simeq R_g^{yy} > R_g^{zz}$ ). The total radius of gyration is again weakly dependent on the distance from the surfaces except for the stretched adsorbed conformations with their center of mass within  $1\sigma$  from the walls. As far as the effect of the wall interactions is concerned, it is not significant in the middle part of these pores. On the other hand, changes of  $\epsilon_w$  affect significantly the shape and size of the adsorbed chains; but as the adsorbed chains are very important to the rheological properties of the film, their static properties will be discussed in more detail in a following paragraph.

<sup>8</sup> this manifests that this wall separation is the onset of confinement for which the static properties of all chains are affected and this was one of the reasons that it was selected for most of the non equilibrium studies

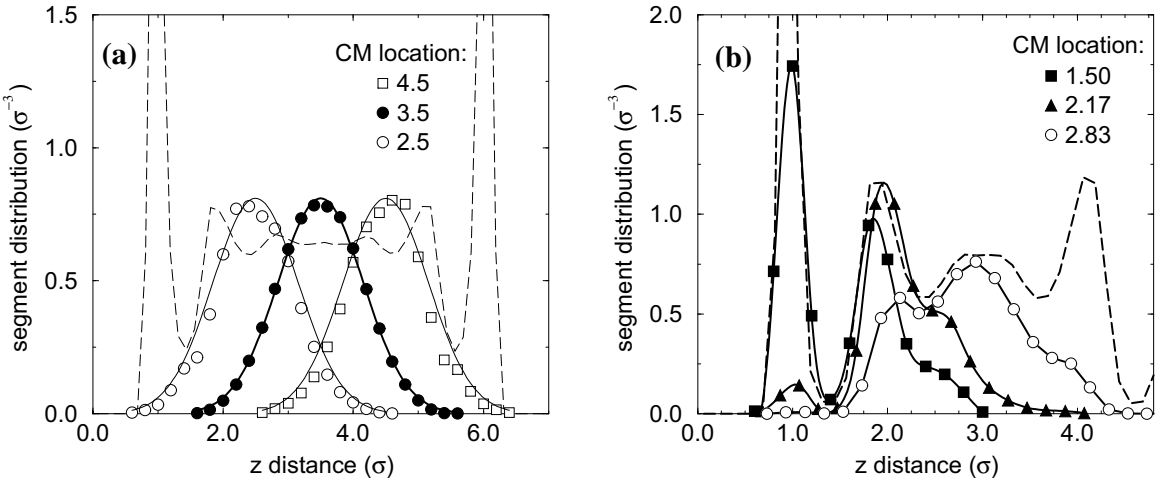


**Figure 2.9:** The spatial distribution of the segment cloud around the center of mass of the chains is presented for various CM locations across the film. (a) For wide enough films and weakly adsorbing surfaces ( $h = 7\sigma$ ,  $\epsilon_w = 1.0$ ) the chains in the middle of the pore have an almost unperturbed Gaussian distribution: the lines correspond to identical bulk oligomers. (b) For narrower confinements all the chains are distorted and especially the ones with their CM near a strongly adsorbing surface ( $h = 6\sigma$ ,  $\epsilon_w = 2.0$ ).

**Segment distribution around the center of mass.** Another way to quantify the effect of confinement on the chain shape is through the spatial distribution of the segments around the CM of the chain they belong to. In order to see the perturbation of the chain shape due to the existence of the walls we calculate the  $z$ -distribution of segments of each chain around its CM as a function of the location of its CM. A similar quantitative description for the shape of confined coils has also been used in MD simulations with flat –potential– “walls” [8] and in dynamic MC lattice simulations[17]. As before, the pore is divided in  $z$ -slices and the fraction of segments is averaged for chains with their CM inside each of these bins (figure 2.9). For bulk systems, and therefore in the middle of very wide films, the distribution of segments around the CM is approximately [33, § II.7a] Gaussian; but for chains close enough to solid walls the chain shape is distorted due to geometric constraints and energetic interactions with the confining surfaces.

In figure 2.9 the average<sup>9</sup> spatial distribution of the segmental cloud around the CM is shown. For chains with their CM located in the middle of wide enough pores the distribution remains almost bulk like; for example in fig. 2.9a chains with their CM in the middle of the pore are compared with identical bulk chains (Gaussian distribution). For chains with no segments inside the first layer the segment distribution are almost Gaussian (solid circles), whereas chains with segments inside the second layer are perturbed and become asymmetric but not strongly layered (open symbols). On the other hand, chains with segments located inside the first layer exhibit a strongly layered segment density.

<sup>9</sup> the Molecular Dynamics average: over all appropriate chains and over time

For narrow enough films (for hexamers,  $h = 6$ ) the segment distribution of all chains is distorted, independent of their CM location. Moreover, adsorbed chains (for example chains with filled symbols in figure 2.9b) have a completely “non-bulk”, strongly layered segment distribution. This is because the segments have to follow the total density of the film which is strongly inhomogeneous in the first two fluid layers. To give an example that deviates the most from the bulk distribution: for the chains with their CM located  $1.5\sigma$  away from a surface (filled squares in fig. 2.9b) their segment distribution is strongly layered and depleted of segments in the immediate vicinity of the center of mass<sup>10</sup>!

The most interesting point in the discussion of the segmental distribution of the chains is that, although is used to describe the shape of the coil, is a segmental static property. As a result, in a confined geometry it is affected only when segments are located inside the first –and *to a much lesser extent* the second– fluid layer; in these cases it exhibits the same inhomogeneities as the total film density. This is yet another proof derived from static properties that the wall-fluid interface is very narrow<sup>11</sup> ( $\sim 2$  segment diameters) and segmental properties are affected when the particles are in contact with the walls.

**Conformations of adsorbed chains:** The solid wall-oligomer fluid interface is of fundamental importance to the dynamics and the rheology of these ultra thin confined films. This interface consists of the adsorbed chains whose static properties are discussed in this paragraph. “Adsorbed” chains are those with at least one segment in contact with either of the walls, while “free” chains have all segments far from the walls. In our studies, adsorbed segments or “contacts” are defined, somehow arbitrarily, as only those segments located inside the first peak of the density profile (fig. 2.3) because those segments feel the main attractive interaction of the wall<sup>12</sup> when attraction exists ( $\epsilon_w > 0$ ). This choice is further motivated by the weak surface effect on the segment density and bond orientation (fig. 2.4 and fig. 2.5) as well as the segment dynamics inside the second layer. For chains up to decamers (10 segments per chain) and film thicknesses down to six segment diameters ( $h = 6\sigma$ ) no chains form “bridges” between the two walls, thus all adsorbed chains are in contact with a single surface.

As in the previous paragraph, chains are usually grouped according to their center of mass distance from the walls. However, recent studies [25, 9, 36] show that a more physically justified grouping is based on the number of contacts with the confining surface. Since the segment-segment potential is purely repulsive,  $\epsilon_w$  can be considered as the *excess ‘solid atom’-‘chain segment’ adhesive energy* [25] and the number of contacts multiplied by the energy parameter of the wall potential ( $\epsilon_w$ ) is the energy of adsorption of a chain [36]. The probability of a certain energy of adsorption (i.e. a certain number of contacts) per chain is defined by the distribution of these quantities over all adsorbed chains, on both surfaces, and over time (these probabilities are given in tables 2.2 and 2.3).

When the attraction of the wall increases, there is an enhancement of the inhomogeneity manifested by the increase of the first –and to a lesser extent of the second– layer

---

<sup>10</sup> it should be pointed out that some of the distances under discussion here are comparable or even smaller than the segment size  $\sigma$

<sup>11</sup> this will become very clear from the dynamic properties of the confined chains

<sup>12</sup> the Lennard-Jones potential is used

density peak (fig. 2.4). Furthermore, for the hexamers the increase of the wall affinity ( $\epsilon_w$ ) favours conformations with many contacts with the walls under equilibrium (table 2.2) driving the system to situations with one third of the adsorbed chains to be fully adsorbed on the surface. This should be attributed to the short size of the coils, as for the longer oligomers (decamers) in equilibrium –no flow– this effect is present to a lesser extent (table 2.3).

**Table 2.2:** Probability of the adsorbed hexamers to have one to six contacts with the surfaces. The wall to wall distance is  $h = 6.0\sigma$ . Probabilities are shown for different wall affinities including neutral surfaces ( $\epsilon_w = 0.0$ ). There is a definite tendency of the adsorbed chains to adopt conformations with more contacts with increasing wall attraction.

		hexamers			
$\epsilon_w$	:	0.0	1.0	2.0	3.0
1 cont.		.17	.11	.07	.07
2 cont.		.22	.17	.11	.11
3 cont.		.22	.19	.14	.13
4 cont.		.19	.18	.17	.17
5 cont.		.13	.18	.22	.22
6 cont.		.07	.16	.30	.29

$\epsilon_w$	decamers									
	number of contacts									
1	2	3	4	5	6	7	8	9	10	
0.0	.09	.15	.16	.16	.14	.11	.09	.06	.03	.01
1.0	.07	.11	.12	.12	.12	.12	.10	.10	.09	.06
2.0	.05	.06	.11	.14	.14	.11	.11	.09	.08	.09
3.0	.01	.04	.10	.16	.11	.14	.10	.11	.12	.12

**Table 2.3:** Probability of 1 to 10 contacts for the adsorbed decamers ( $\epsilon_w$  in  $\epsilon$  and  $h = 6.0\sigma$ ). The adsorption energy probabilities change with  $\epsilon_w$  as in the case of 6mers.

This tendency of the adsorbed chains to adopt conformations with more contacts as the wall attraction increases, is also affecting the chain CM distribution across the pore. In figure 2.10 the dependence of the CM density on the wall interaction is shown. For the longer oligomers (decamers), the probability of chains with their CM inside the interfacial layer –i.e. fully adsorbed chains– is almost zero for neutral surfaces and increases systematically with the wall affinity. Furthermore, for the longer oligomers (10mers) with increasing wall affinity there is a decrease in the number of partly adsorbed chains (CM located mainly inside the segment depletion zone) and for all the values of  $\epsilon_w$  used remains higher than the CM concentration in the middle of the pore. On the other hand, for the hexamers, the systematic increase of the completely adsorbed oligomers with  $\epsilon_w$  is so strong that at the same time a depletion of CM starts to be developed for strong wall attractions. The CM density is reduced in the region between the segment depletion zone and the second fluid layer (fig. 2.10) which mirrors the tendency to favour strongly<sup>13</sup>

<sup>13</sup> conformations with many surface contacts

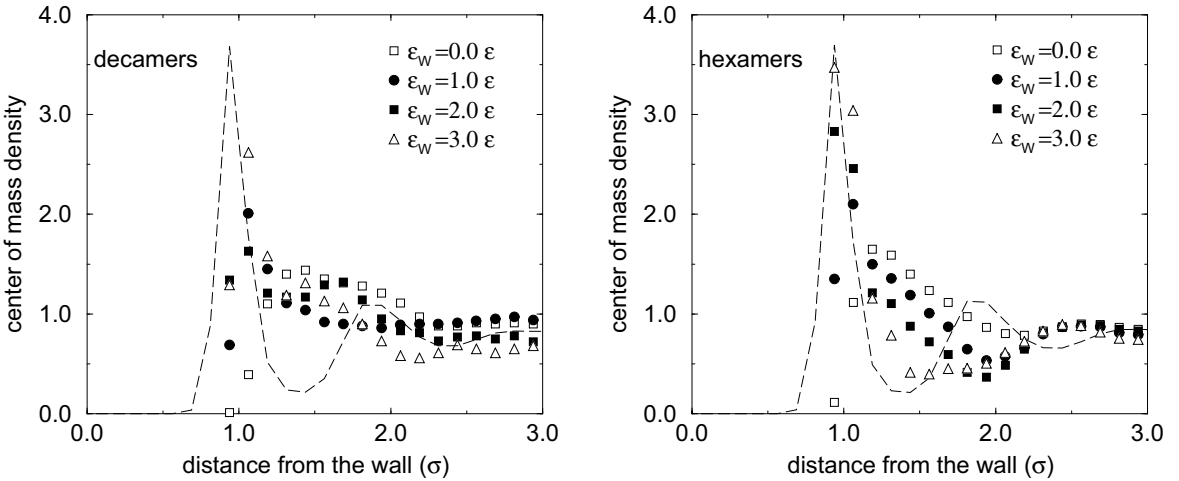


**Figure 2.10:** The CM distribution across the  $h = 6$  films for various wall affinities. This CM density is scaled by the chain length  $N$  in order to be compared with the segment density.

adsorbed chains and free chains, with a simultaneous reduction in the number of partly adsorbed oligomers.

A qualitative reasoning<sup>14</sup> for this behaviour could focus on the changes of entropy and energy near an attractive wall. In the case of an incompressible melt (random walk statistics) the average number of contacts per chain should not depend on the wall affinity the partition function is:

$$Q = \sum_{m=1}^n P(m, n) \exp(-m\epsilon_w/kT) \quad (2.4)$$

where  $P(m, n)$  is the probability of an  $n$ -mer having  $m$  contacts with the surface, which can be easily calculated from RW counting [37, 38] and does not depend on the wall energetics. From  $Q$  it can be calculated that changing the wall affinity ( $\epsilon_w$ ) only shifts the total system energy.

But in our case, the system is not completely incompressible as the increase of  $\epsilon_w$  causes a densification of the first layer (fig. 2.4 and table 2.1) i.e. there is an increase of the number of adsorbed segments. Moreover, there is a *configurational entropy loss* for an ideal chain when it is adsorbed [37]. This effect is beyond the localization of the coil. It arises from the fact that the surface provides an impenetrable obstacle which excludes many conformations for an adsorbed molecule compared with an identical one in the interior of the melt. This entropy loss scales as  $N^{1/2}$  [38, eq. 5.3]. So, for the 6mers the wall attractions in our simulation seems to be sufficient to overcome the entropy loss of multiple contact conformations to a degree that a large fraction of the adsorbed chains are

<sup>14</sup> these quantities can not be directly measured in our MD simulations

fully adsorbed. For the longer 10mers the conformational entropy loss increases, resulting in a decreased probability of fully adsorbed chain conformations.

### 2.1.3 The structure inside the first layer

The densification of the interfacial layer can only take place if the chain segments pack better inside this layer, resulting in a more structured first layer. The structure within this layer can be presented through the *in plane* (two dimensional) *radial pair correlation function*. The pair distribution function, for a system of  $N$  particles, following the canonical ensemble, is defined as [21]:

$$g^{(2)}(\mathbf{r}_1, \mathbf{r}_2) = \frac{V^2 N!}{N^2 (N-2)!} \frac{\int \int \exp(-\beta U_N) d\mathbf{r}_1 d\mathbf{r}_2}{\int_V \exp(-\beta U_N) d\mathbf{r}_1 ... d\mathbf{r}_N} \quad (2.5)$$

where  $U_N$  is the system energy and  $\mathbf{r}_1 ... \mathbf{r}_N$  are the position vectors of the  $N$  particles.  $g^{(2)}$  represents the probability of *any* particle being in  $d\mathbf{r}_1$  around  $\mathbf{r}_1$  and *any* particle being in  $d\mathbf{r}_2$  around  $\mathbf{r}_2$  irrespective of the configuration of the rest of the system. Since the Lennard-Jones potential used in this study is spherically symmetric  $g^{(2)}(\mathbf{r}_1, \mathbf{r}_2)$  depends only on the distance  $|\mathbf{r}_{12}|$  (or simply  $|\mathbf{r}| \equiv r$ ) and  $g^{(2)}(\mathbf{r}_1, \mathbf{r}_2) \equiv g^{(2)}(|\mathbf{r}_{12}|) \equiv g(r)$ . Moreover, if  $\rho$  is the average density of the system then  $\rho g(r) dr$  is the probability of observing a particle in  $dr$  given that a particle already exists at the origin of  $r$ . This means that:

$$\int_0^\infty \rho g(r) 4\pi r^2 dr = N - 1 \simeq N \quad (2.6)$$

which means that  $\rho g(r) 4\pi r^2$  is the number of particles between  $r$  and  $r + dr$  about a central particle; geometrically this defines a space between two concentric spheres. This last definition is exploited to define and calculate the in plane radial pair correlation function (pcf) in our simulations. Namely, it is defined as the probability of a particle being at a distance  $r + dr$  inside the first layer when another particle is located at the origin of  $r$  inside the first layer, this is the space between two concentric cylinders of height equal to the width of the first layer. This probability is averaged over all particles inside the two interfacial layers (upper and lower wall), over all simulation time and after excluding the bonded pairs (fig. 2.11). From the definition it becomes obvious that  $g \rightarrow 0$  as  $r \rightarrow 0$  since LJ particles become effectively “hard” as  $r \rightarrow 0$ . At the same time, since the influence of a particle diminishes as  $r$  becomes large enough,  $g \rightarrow 1$  as  $r \rightarrow \infty$ .

As far as the in-plane pcf of our confined oligomers is concerned, it reveals better and better packing of segments inside the first –adsorbed– layer with increasing  $\epsilon_w$ . This can be seen by the systematic increase of the first and second peaks and the development of well defined peaks of higher order for stronger wall attractions. For  $\epsilon_w = 0.0$  and  $\epsilon_w = 1.0$  the pcf is characteristic of an amorphous fluid, but for  $\epsilon_w = 3.0$  a splitted second peak is developed and also a third peak with a “shoulder” of half its size, which are fingerprints of hexagonal close-packing<sup>15</sup>. The explanation of this structure enhancement

---

<sup>15</sup> two kind of second neighbours in 1:1 proportion and two kind of third neighbours in 2:1 proportion

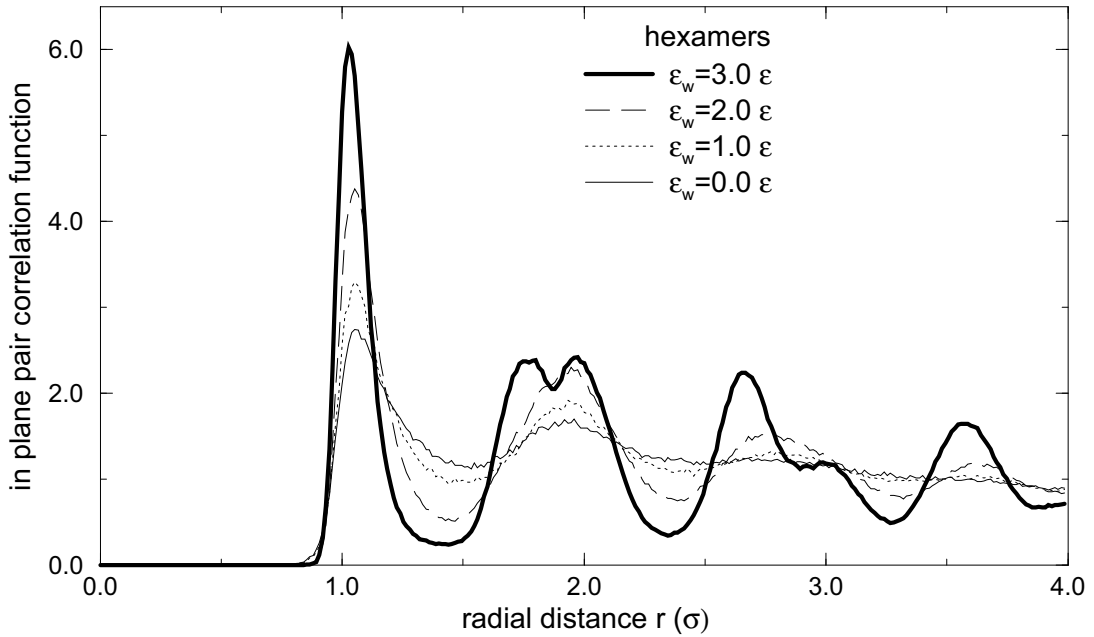


**Figure 2.11:** The in-plane radial pair correlation function of the first layer segments for various wall affinities. The in-plane structure is enhanced with increasing wall attractions ( $\epsilon_w$ ). This ordering is due to densification rather than epitaxial crystallisation

is related to the wall induced densification inside the first layer. As has been already shown there is a density increase inside the first layer which is stronger for larger values of  $\epsilon_w$  (table 2.1). Inevitably, when more particles have to be accommodated inside the first layer they must become more “organized”, more “structured” in the sense of forming a fcc-like (distorted hexagonal close-packed) in plane symmetry, which is the one that can accommodate the largest number of particles. This phenomenon is over and above a surface induced “epitaxial” ordering. In fact, the particles actually occupy the positions of least potential energy over the fcc wall creating a commensurate distorted next fcc layer (distorted both due to thermal motions and chain connectivity). But the same fcc-like pcf have been observed in the vicinity of flat –potential– walls, for oligomers similar to these [8] but also for monomers (§ 2.3). Especially, in the case of LJ monomers near a completely uncorrugated flat surface and at the same thermodynamic conditions, a very sharp –almost a first order transition– from an amorphous to a crystalline ordering with increasing the wall attraction can be observed [40].

Even beyond these examples, ordering as a result of densification is far more generic and takes place independently of the reasons causing the density increase<sup>16</sup>. From the very first simulations [39] it was shown that the pcf is driven towards more “structured”<sup>17</sup>

<sup>16</sup> in our case surface induced densification of the first (interfacial) layer

<sup>17</sup> enhancement of first peak, development of third and forth peak

forms when increasing the density, even in a bulk monomeric LJ fluid. More recent theoretical studies dealing with *pressure induced* densification of simple liquids [41] have related directly the changes in the pcf –and thus the enhancement of ordering revealed by these changes– to the density increase of the system.

## 2.2 Chain dynamics

Although the origins of the inhomogeneous density profile and of the ordering enhancement next to a surface are well understood, the nature of the confined fluids –especially in the immediate vicinity of the surfaces– requires further investigation. There are many SFA experimental studies probing the dynamics of ultra thin films of small molecules and of larger chain-like molecules often reporting striking and/or unexplained, counter-intuitive behaviour. For monomeric systems many computer simulation studies [42] provide a clear enough picture for the dynamics of confined films of small spherical molecules. On the other hand, for confined oligomers and polymers less has been done, especially towards the understanding of the dynamics of nanoscopic films [43]. The two most usual ways used in simulations to quantify the dynamics of polymeric systems are: (i) the analysis of the relaxation times of different “modes” and (ii) the study of transport properties like the self-diffusion coefficients, the mean square displacements and the viscosity. These quantities are defined from theoretical models like the Rouse and the reptation model and measured by mechanical, rheological, dielectric and scattering techniques.

**Rotational relaxation of the chains:** Altoutgh the oligomers used in my simulations are too short to exhibit genuine polymeric behaviour [7] they are characterized by very high flexibility. This fact has driven other researchers to investigate whether the Rouse modes are well defined for confined short oligomers (pentamers). While the current work was still in progress, Bitsanis and coworkers [9] published a simulation study of the dynamics of confined oligomers in equilibrium. The model used was exactly the same as the one used in the simulations reported in this thesis and unavoidably<sup>18</sup> the directions of my investigations were influenced, in more than one ways, by that study.

In reference [9] wide films ( $h = 10$ ) of pentamers are simulated, in order for two well separated solid-oligomer interfaces to be developed on each of the confining surfaces; for these systems the two first Rouse modes are defined and their relaxation times are studied. Due to the great similarity of that work and the extensive argumentation reported, in this paragraph only a brief comparative discusion will be made concerning the rotational relaxation of the chains<sup>19</sup>. It is known [4] that the time correlation function of the first Rouse mode is by definition the time correlation function of the end-to-end vector (except at very short times) and its relaxation time is the rotational relaxation time of the chains. The time correlation function of the end-to-end vector is [44]:

$$\begin{aligned} \langle \mathbf{P}(t) - \mathbf{P}(0) \rangle &= \langle (\mathbf{R}_N(t) - \mathbf{R}_0(t)) - (\mathbf{R}_N(0) - \mathbf{R}_0(0)) \rangle \\ &\propto \exp\left(-\frac{t}{\tau_r}\right), \quad t \geq \tau_r \end{aligned} \quad (2.7)$$

where  $\mathbf{P}$  is the end-to-end vector,  $N$  the number of beads in the chain,  $\mathbf{R}_i(t)$  is the position of the  $i$  bead of the chain at time  $t$  and  $\tau_r$  is the rotational relaxation time which

<sup>18</sup> there has also been some collaboration between the two research groups [8, 11, 38, 40]

<sup>19</sup> as has been discussed before although the time averaged shape of a Gaussian chain is spherical, the instanteneous shape is ellipsoidal, and thus one can speak of chain rotation even for the bulk

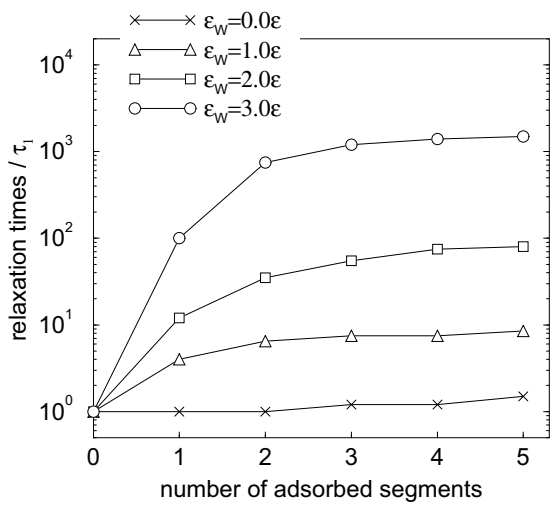


**Figure 2.12:** Relaxation times of the first Rouse mode of confined pentamers ( $h = 10$ ) as a function of the number of contacts for all the simulated wall affinities, from I. Bitsanis and C. Pan, *J. Chem. Phys.* 99, 5520 (1993). The data indicate clearly a dramatic increase of the relaxation time inside the solid-oligomer interface with increasing  $\epsilon_w$ . The origin of these “glassy” dynamics is attributed to the slowdown of segmental motions inside the adsorbed layer.

can be proven to be:

$$\tau_r = \tau_1 = \frac{\zeta N \cdot Nb^2}{k_B T \cdot 3\pi^3} = \frac{1}{D} \cdot \frac{Nb^2}{3\pi^3} \quad (2.8)$$

this means that the rotational relaxation time is by definition the relaxation time of the first Rouse mode. This quantity  $\tau_1$ , calculated for the respective bulk, will be used to scale the times throughout this section.  $D$  is the center of mass self-diffusion coefficient.

Using equation 2.7 the time correlation function of the end-to-end vector was calculated for the hexamer systems in the  $h = 6$  pores. In order to compare with reference [9] the time correlation function was calculated for the whole film (fig. 2.13a) and for the

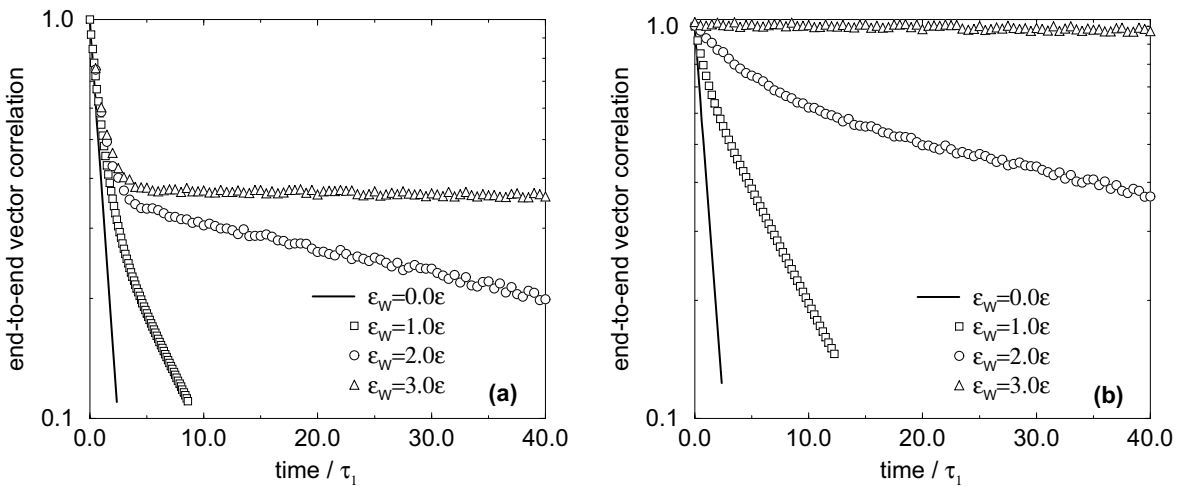


**Figure 2.13:** End-to-end vector time correlation functions for various wall attractions: (a) for the whole film ( $h = 6$ ), (b) for the adsorbed chains independently of the number of contacts.

adsorbed chains (fig. 2.13b). The obtained behaviour is in very good agreement with the findings for the wider films of pentamers; this is one more proof that the dynamics of the free chains are not affected much –remain bulklike– even in the  $h = 6$  confinements; a confinement for which the free chains are located in a layer with size comparable to the chain dimension<sup>20</sup> and thus are confined between two adsorbed, sluggish, oligomer layers. The film as a whole exhibits a multimodal relaxation. The fast, bulk-like, relaxation is due to the free chains and the slower part is due to the superposition of the slower modes of the adsorbed chains and the relaxation times involved for each mode depend on the number of adsorbed segments (fig. 2.12). For the neutral walls ( $\epsilon_w = 0$ ) the term “adsorbed chain” is rather ambiguous, since the interaction between the solid particles and the fluid segments has no attractive part, and has only the meaning of chains with segments located inside the first fluid layer. In this sense, the chains touching the neutral walls ( $\epsilon_w = 0$ ) are in an environment analogous to the one felt by free chains in the  $\epsilon_w = 2$  or  $\epsilon_w = 3$  slits or by the free pentamers inside the second layer of a very wide pore. The effect of the neutral wall is a similar extremely weak ( $\sim 1$ ) slowdown of the chain relaxations and the segment dynamics.

From our simulation data the following points can be made concerning the relaxation times of the end-to-end vector time correlation function:

- The end-to-end vector time correlation functions exhibit an exponential decay when calculated separately for the free chains and the adsorbed chains with given number of adsorbed segments and moreover there are no cross correlations. These are necessary for the rotational relaxation time to be *well defined*.
- When calculated for the whole film the end-to-end vector time correlation function exhibits a multimodal relaxation. The fast relaxation corresponds to the free chains located in the middle of the film and the slower modes to the relaxation of the adsorbed chains. This is concluded both by the relaxation times as calculated for those classes of chains separately, as well as by the ratio of the correlation function amplitudes of the fast versus the slow modes, which is very close to the ratio of the number of free versus adsorbed chains.
- For the free chains the relaxation time is the same and very close to the bulk value. This happens even for the chains located inside the second fluid layer of wide gaps [9] and the chains in much narrower confinements ( $h = 6$ ) where the space available for the free chains is comparable in size to the chain dimensions. This is also valid to a lesser extent when hexamers are confined in very narrow pores ( $h = 4$ ) where the free chains are geometrically constrained in a space just one segment diameter wide. This is quite remarkable as these chains are closely surrounded by chains with very sluggish dynamics.
- The relaxation times of the adsorbed chains are high compared to the bulk. The extent of the increase ranges from three orders of magnitude for the strongly physisorbing surfaces ( $\epsilon_w = 3$ ) to less than ten times for weakly physisorbing surfaces ( $\epsilon_w = 1$ ) and to almost a negligible degree ( $\sim 1.3$ ) for the neutral walls (fig. 2.12 and also table 2.4 & fig. 2.15).
- The relaxation time of the end-to-end vector correlation for the adsorbed chains

---

<sup>20</sup> the middle layer being approximately two segment diameters wide

depends on the number of contacts. Chains with one or two contacts have most of their segments free and thus due to their bulk like dynamics the end-to-end vector can relax pretty fast. On the other hand, for the chains with most of their segments adsorbed this process becomes very slow as the segment dynamics are very sluggish inside the solid oligomer interface (fig. 2.16). For strong wall attractions ( $\epsilon_w = 2$  or  $3$ ) the chains with more than  $3$  contacts relax with almost the same time constant. This insensitivity shows that the slowdown of the dynamics is caused by the densification inside the first layer (table 2.1) rather than the bare energetic barriers<sup>21</sup>.

It should be pointed out that although the Rouse description seems to be *a posteriori* justified [9] for these ultra confined films and for the chains in the vicinity of the surfaces, one of the most fundamental predictions of this model is that the viscosity of the systems does not depend on shear rate. This is due to the infinite extensibility assumed for the chains [45] and contradicts all experiments and simulations under shear. For this reason, and in contrast with reference [9], the second Rouse mode was not defined and studied and the term “end-to-end vector relaxation” is used instead of the “first Rouse mode”. Furthermore, the discussion of this relaxation was briefly discussed here and mostly in a comparative manner with this previous paper.

Finally, even in simulations of more realistic model oligomers (*n*-octane) their relaxation exhibits the same qualitative trends as discussed herein for our generic bead-spring model [46]. Moreover, their dynamics are affected much more dramatically near attractive surfaces due to a suppression of torsional angle transitions, which was again attributed to the elevated density inside the first layer [46]. Traces of this increase in the relaxation time of the chains have been found experimentally in SFA experiments of oligomers and polymers between mica surfaces [48, 50, 51, 52, 53, 54, 55, 56] manifested through dramatic increases in the viscosity of the films. As mica is very attractive to most of these confined systems, in most of the cases corresponds to the highest of the wall affinities used in our simulations ( $\epsilon_w \geq 3.0$ ). When mica is chemically treated to become less attractive [57] then this effect is reduced as expected from the previous discussion. Although at the time simulations had not revealed the exact nature of this decreased segment and chain mobility the reasons proposed by the experimentalists –sometimes even intuitively [56]– attributed these greater viscosities and slow dynamics to a “pinning” of the adsorbed chains on the confining surfaces.

---

<sup>21</sup> this will become even more clear in the discussion of the displacements and diffusivities of the adsorbed chains parallel to the walls (§ 2.3).

**Self diffusion of the adsorbed chains** There are many ways to define and calculate the self diffusion coefficients of an oligomer melt in Molecular Dynamics simulations [58]. The most frequently used are through the mean square displacements by the Einstein relations, through the velocity time autocorrelation function by the Green-Kubo relations and with the help of the color field method [59]. The first two methods are employed in our simulations both in the systems in equilibrium and in those under flow.

In a bulk fluid at equilibrium the diffusion is isotropic and the diffusion coefficient is a scalar quantity, the same in any direction. On the other hand, when symmetry is broken –due to confinement and/or flow– then the motions become anisotropic and a tensor has to be used to describe the self-diffusion of the particles. The general equation of diffusion in an anisotropic system is given by:

$$\frac{\partial G(\mathbf{r}, t)}{\partial t} + \mathbf{U} \cdot \nabla G(\mathbf{r}, t) = D \nabla^2 G(\mathbf{r}, t) \quad (22)$$

where  $G(\mathbf{r}, t)$  is the number density at the position  $\mathbf{r}$  in the time instant  $t$ ,  $\mathbf{U}$  is the flow field (in our NEMD systems this is  $\mathbf{U} = (\dot{\gamma}(z), 0, 0)$  with flow parallel to  $\mathbf{x}$  and the flow gradient in the  $\mathbf{z}$  direction) and  $D$  is the diffusion tensor. For our confined systems in equilibrium ( $\mathbf{U} = (0, 0, 0)$ ) the  $D$  tensor is diagonal and with  $\mathbf{x}, \mathbf{y}, \mathbf{z}$  eigenvectors, i.e. :

$$D = \begin{bmatrix} D_{xx} & 0 & 0 \\ 0 & D_{yy} & 0 \\ 0 & 0 & D_{zz} \end{bmatrix} \quad (2.10)$$

and from the Einstein relations under equilibrium  $\mathbf{U} = (0, 0, 0)$  [3]:

$$\begin{aligned} <(\mathbf{x}(t) - \mathbf{x}(0))^2> &= 2 D_{xx} t \\ <(\mathbf{y}(t) - \mathbf{y}(0))^2> &= 2 D_{yy} t \\ <(\mathbf{z}(t) - \mathbf{z}(0))^2> &= 2 D_{zz} t \end{aligned} \quad (2.11)$$

or from the velocity-velocity autocorrelation function (Green-Kubo approach)[3]:

$$\begin{aligned} <\mathbf{u}(t) \cdot \mathbf{u}(0)> &= <\mathbf{u}^2(0)> e^{-\zeta t} \\ \Rightarrow D &= \frac{1}{3} \int_0^\infty <\mathbf{u}(t) \cdot \mathbf{u}(0)> dt \\ \Rightarrow D_{ii} &= \frac{1}{3} \int_0^\infty <\mathbf{u}_i(t) \cdot \mathbf{u}_i(0)> dt \quad i : x, y, z \end{aligned} \quad (2.12)$$

Usually all of the above are defined for physical particles but in our case since we focus on the mobility of the *chains* all the above can refer to the chain center of mass. So,  $\mathbf{r}(t) = (x(t), y(t), z(t))$  is the position of the chain CM,  $D_{ii}$  the center of mass diffusion component in the  $i$  direction and  $\mathbf{U}(t) = (u_x(t), u_y(t), u_z(t))$  is the CM velocity.

---

<sup>22</sup> in the simple case of a bulk under constant strain  $(\dot{\gamma}z, 0, 0)$  this becomes:

$$\frac{\partial c}{\partial t} + \dot{\gamma} \frac{\partial c}{\partial x} = D \frac{\partial^2 c}{\partial r^2}$$

**Table 2.4:** Center of mass diffusion coefficients normal ( $D_{zz}$ ) and parallel ( $D_{yy} = D_{xx}$ ) to the walls for systems of hexamers under equilibrium (no flow) as calculated from Einstein's relations. The mobility of the “free” chains located in the middle part of the film and of “adsorbed” chains with 2, 4 and 6 surface contacts are presented. (MD units are used throughout and the width of the film is  $h = 6.0\sigma$ ).

$\epsilon_w$	equilibrium							
	$D_{zz}$				$D_{yy} = D_{xx}$			
	free	2 cont.	4 cont.	6 cont.	free	2 cont.	4 cont.	6 cont.
0.0	.0062	.0054	.0049	.0052	.0124	.0113	.0112	.0114
1.0	.0052	.0043	.0018	.00135	.0150	.0075	.0067	.0063
2.0	.0047	.0012	.0002	.00013	.0191	.0035	.0012	.0009
3.0	.0052	.0001	.00002	.000005	.0192	.0005	.0004	.0003

The aim in this paragraph is to probe the dynamics of the adsorbed chains, so in both cases the initial ( $t = 0$ ) state is an adsorbed configuration and in order to evaluate the  $D_{ii}$  of the adsorbed coils the mean square displacements and velocity autocorrelation functions are calculated for the biggest time interval that the chains remain adsorbed. Furthermore, they are averaged for many time origins throughout the simulation trajectories, for both walls and over all chains with the same number of contacts. Distinguishing the adsorbed chains according to their adsorption energy (number of contacts) is inspired by all the dependence of the other quantities presented so far and it is proven justified by the dependence of  $D$  on the number of adsorbed segments per chain (table 2.4).

There are several points one could make concerning the desorption of the adsorbed chains through the CM mobility normal to the confining surfaces; a problem which will be more analytically approached when dealing with the desorption of oligomers (chapter 5). At this point I will focus on how confinement and physisorption change the mobility and the nature of motion of the oligomer melt in the vicinity of the walls.

An observation that becomes obvious both from the diffusion coefficients (table 2.4) and the center of mass mean square displacements (fig. 2.14) is that the oligomers move faster parallel to the surfaces than normal to them. This phenomenon is observed in all simulations of confined systems, ranging from abstract chain models [9, 10] to realistic chains [60, 61] to LJ monomeric systems [29]. The differences are in most cases less than a factor of 10 and for small oligomers of the order of 2 [60, 62, 36], i.e. the CM of the adsorbed chains moves twice as fast parallel to the adsorbing surface than in the perpendicular direction. This can be explained along the same lines as the origin of the layering next to a confining surface. Namely, the geometric constraint of a solid wall results in an angular asymmetry of the number of collisions that an adsorbed segment/chain endures. As the solid particles of the walls are embodied in a crystal lattice, they do not undergo as rapid motions as the fluid particles and thus the adsorbed segments are suffering more collisions from the direction facing the surface than from the direction of

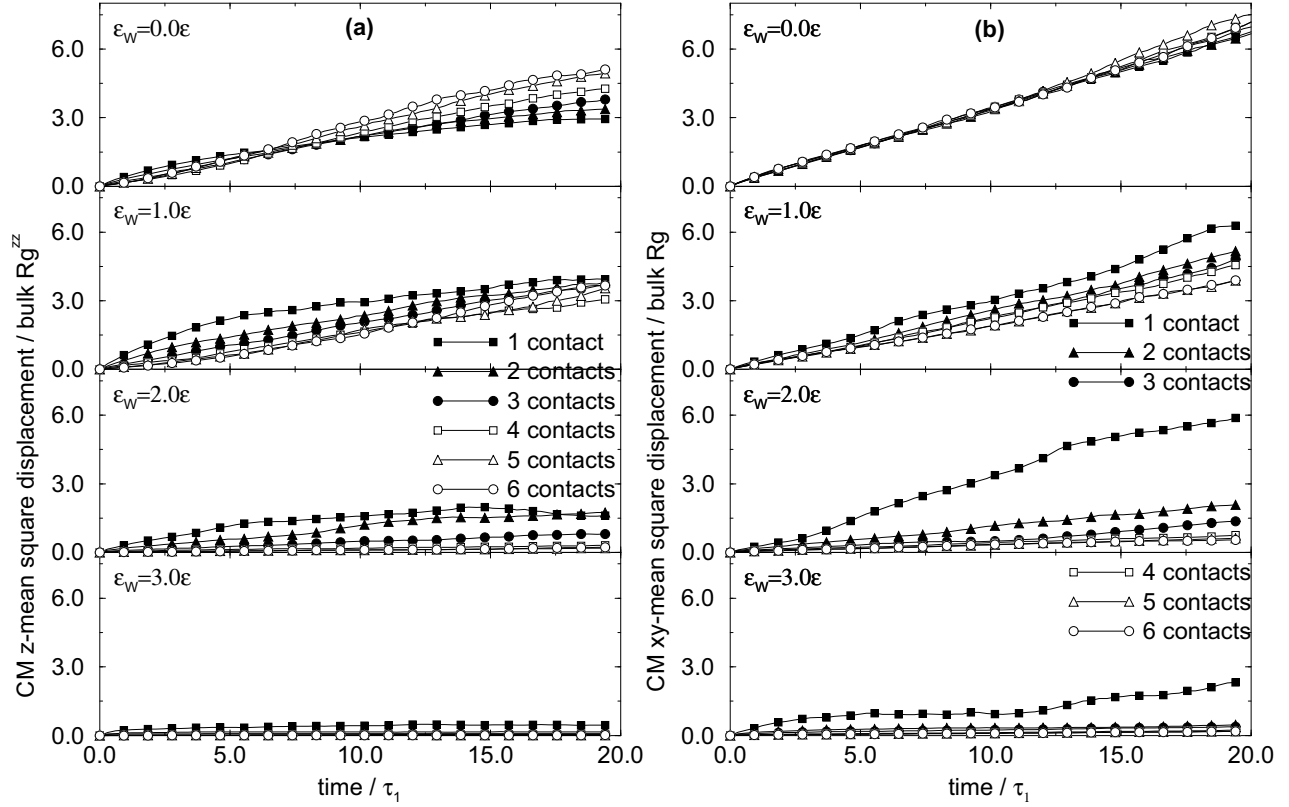


**Figure 2.14:** Center of mass mean square displacements for the adsorbed oligomers, normal (a) and parallel (b) to the confining surfaces. Time has been scaled with the bulk chain rotational relaxation time and the msd with the respective bulk radius of gyration.

the surface. In this way, an effective net force is created pushing the adsorbed segments towards the confining surface and thus suppressing their motion normal to the wall. In my simulations the particles of the wall used do not undergo any motion, which makes the above argument even stronger, but even in simulations with thermally vibrating solid particles there is a difference in the diffusivities of the adsorbed chain normal and parallel to the walls, and is of the order of 2 [62].

However, the molecular mechanism responsible for the slowdown of the chains as a function of the number of adsorbed segments per chain is different. The mobility of the adsorbed segments is naturally smaller than the free particles (table 2.4). Consequently chains with many contacts consist of many slow or even immobilized particles and thus their mobility is smaller. On the other hand, chains with fewer contacts with the walls consist of a few slow segments –contacts– connected to free, fast moving segments and thus the chain diffusivity becomes bulk-like near neutral ( $\epsilon_w = 0$ ) or weakly physisorbing surfaces ( $\epsilon_w = 1$ ).

This brings the discussion to the most interesting point of this paragraph i.e. the *dramatic slowdown* of the adsorbed chain and segment mobilities with increasing wall affinity. For example, the diffusivities for the neutral walls ( $\epsilon_w = 0$ ) do not depend markedly on the number of segments inside the first layer (table 2.4); for these surfaces

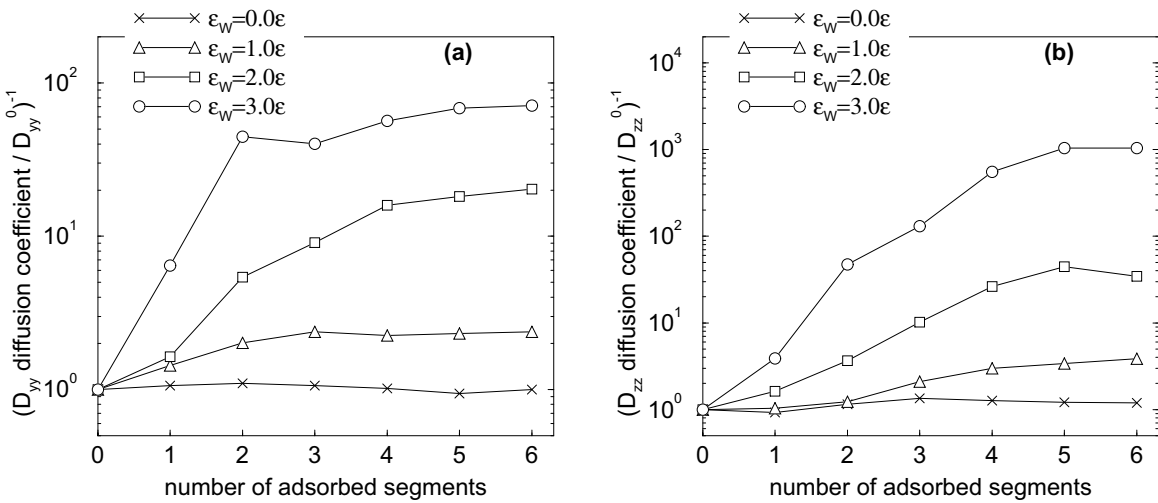


**Figure 2.15:** The magnitude of decrease of the diffusion coefficients for the adsorbed chains parallel (a) and normal (b) to the confining surfaces as a function of the number of contacts.

there is only the geometrical constraint since any attractive energetics are absent from the solid particles. As a result, even chains that are completely inside the first layer (fully adsorbed) exhibit comparable mobilities as the chains in the middle of the film –in all directions: parallel and normal to the walls. Depending on the wall affinity, the mobility of the adsorbed chains can suffer from a moderate slow down near a weakly physisorbing surface to a decrease by several orders of magnitude near a strongly adsorbing wall. For example, for the fully adsorbed hexamers (table 2.4) the diffusivities normal to the surfaces are reduced with respect to the chain mobility in the middle of the pore by a factor of less than 4 for  $\epsilon_w = 1.0$ , by almost 40 times for  $\epsilon_w = 2.0$  and by up to three orders of magnitude for  $\epsilon_w = 3.0$ . These results are in very good agreement with the decrease of the chain relaxation of pentamers in the vicinity of similar surfaces [9] and in good quantitative agreement with the reported *transport* properties in bead-spring [9] or alkane oligomer [60] systems. This dramatic decrease of the mobility normal to the walls with increasing  $\epsilon_w$  creates a sharp distinction between adsorbed chains. Near weakly physisorbing surfaces ( $\epsilon_w = 1$ ) desorption is relatively fast even for chains with many contacts, for  $\epsilon_w = 2$  chains with up to 3 contacts manage to desorb in the time of the simulation, whereas chains adsorbed on the  $\epsilon_w = 3$  are irreversibly adsorbed for the simulated time<sup>23</sup>.

Since the diffusion coefficient can be related (equation 2.8) to the longest relaxation time of the chains, an interesting comparison can be made between this slowdown of the *transport* properties of the adsorbed chains as a function of the degree of adsorption with the chain dynamics as described by the *relaxation* of the end-to-end vector. Such a comparison is achieved by plotting the inverse of the diffusion coefficient versus the

<sup>23</sup> all these will be discussed in more detail in chapter 5.

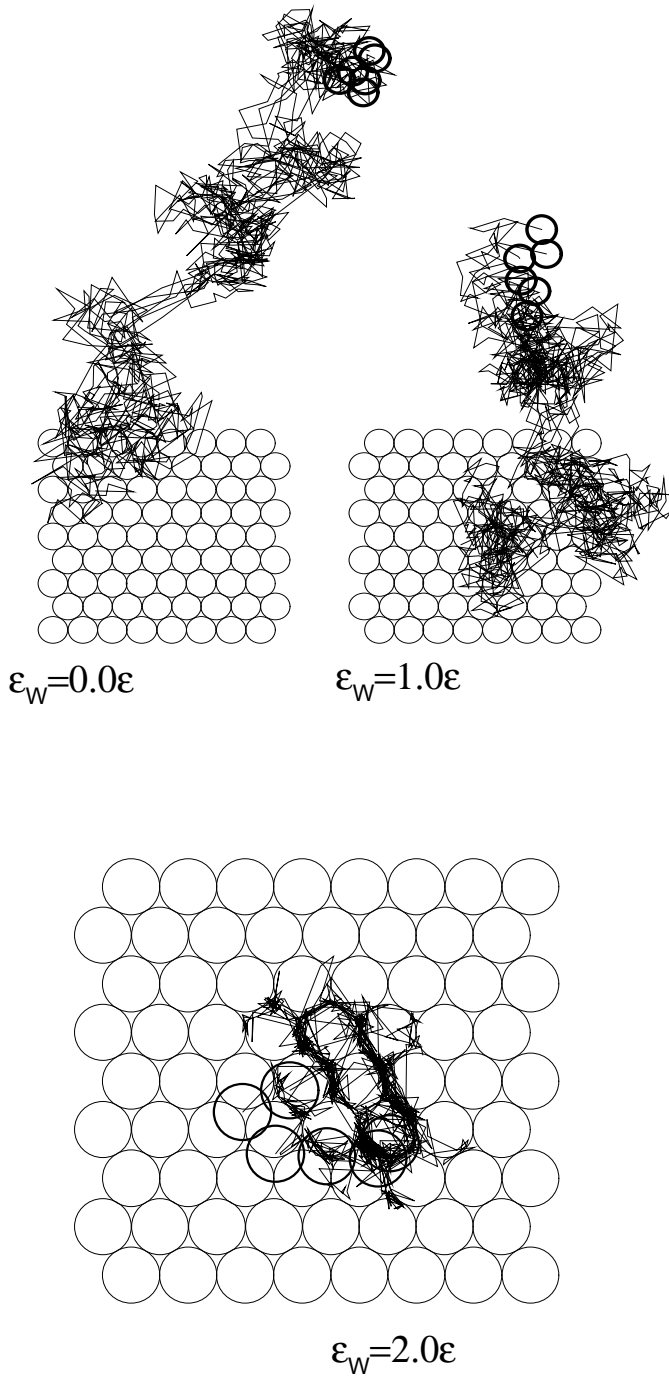


**Figure 2.16:** *In-plane trajectories for hexamers with 6 contacts with the wall throughout  $0.2 \cdot 10^6$  timesteps. The images are in scale 1:1:2.1:2.1 for increasing  $\epsilon_w$  and periodic boundary conditions are removed from the trajectories. The final conformation and the solid particles which are located inside the primary simulation cell are shown.*

**Figure 2.16:** *In plane trajectories of the typical fully adsorbed hexamers ( $\epsilon_w = 2, 3$ ).*

number of contacts (figure 2.15). Since  $\tau_r \sim 1/D$ , these graphs are comparable to the one presented in figure 2.12. The mobility of the adsorbed oligomers parallel to the

surfaces is reduced to a lesser extent by the wall energetics: for the same chains as above –fully adsorbed hexamers–  $D_{yy}$  decreases by a factor of 3, 20 and 64 for  $\epsilon_w = 1, 2$  and 3 respectively (table 2.4). But with increasing wall affinity there is also a qualitative change in this in-plane motion of the adsorbed oligomers (figure 2.16). For the neutral ( $\epsilon_w = 0$ ) and weakly attractive ( $\epsilon_w = 1$ ) surfaces the motion of the adsorbed segments is liquid-like and they move randomly inside the first layer, being able to visit *densely* all sites on top of the fcc structured wall. For the strongly physisorbing surfaces ( $\epsilon_w = 3$ ) the motion becomes solid-like and the segments vibrate around their equilibrium position or migrate to neighbouring positions with sudden jumps to stay there vibrating for a long time; the equilibrium positions are the minimum potential energy positions of the underlying fcc lattice (“epitaxial sites”). These dynamics resemble very much the motion in the glassy state. For the  $\epsilon_w = 2$  surfaces the situation is something in between, with the segments moving almost randomly inside the first layer but migrating most of their time between different positions of minimum potential energy (figure 2.16); trajectories with segments vibrating around an equilibrium position are very rare for the times simulated.

Although these in-plane trajectories bear the signature of *epitaxial vitrification* or *crystallization* the role of the wall crystalline symmetry is secondary. From studies of oligomers –and even monomers– in the vicinity of flat uncorrugated walls the same, qualitatively and quantitatively, phenomena<sup>24</sup> are observed (§ 2.3). The only difference is that for strongly physisorbing surfaces the segments do not occupy positions of minimum potential energy but rather positions dictated by the closest packing condition inside the first layer. The nature of the adsorbed segment mobility and the differentiation with  $\epsilon_w$  is caused by the increasing density (*wall induced densification*) rather than by the bare energy barriers or the crystalline symmetry of the underlying walls. This can be elegantly demonstrated through simulations with potential barriers as confining surfaces (§ 2.3). As argued previously in the paragraphs dealing with the relaxation times of the end-to-end vector and with the in-plane ordering, the decrease in chain mobility is due to the slowdown of the segmental motions, which undergo a dramatic decrease in the vicinity of strongly attractive surfaces. As shown in the previous paragraphs, this wall-induced densification causes changes to the configurational and dynamic properties of the adsorbed chains and segments such as: an enhancement in the ordering inside the first layer (fig. 2.11), an increase of the relaxation times of the chain end-to-end vector (fig. 2.12) and at the same time a qualitatively (table 2.4) and quantitative (fig. 2.16) change in the in-plane motion of the adsorbed segments. Most of the *exotic* properties and behaviour of the nanoscopically confined systems can be directly attributed to these changes inside the solid-fluid interface. Moreover, the thinner the confined films, the larger the fraction of the system which is adsorbed and the larger the deviations from the bulk-like response.

---

<sup>24</sup> enhancement of ordering, decrease of mobility, solid-like in-plane trajectories and so on

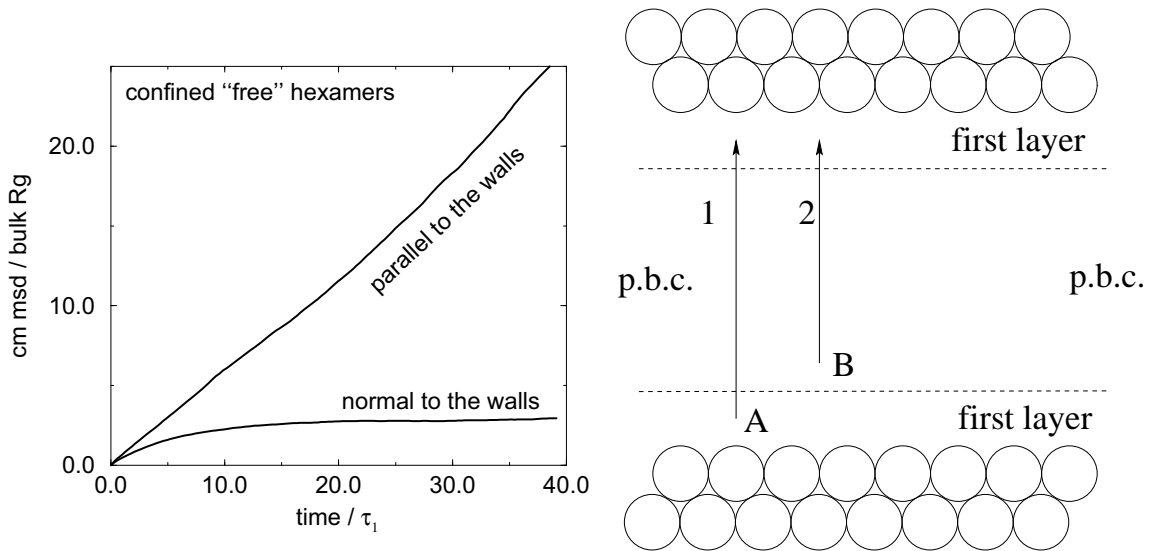


**Figure 2.17:** (a) Typical center of mass mean square displacements for free hexamers inside the  $h = 6\sigma$  pores. Both the motions normal ( $z$ -msd) and parallel ( $xy$ -msd) to the confining surfaces are shown. Time has been scaled with the bulk relaxation time of the end-to-end vector and the msd with the respective bulk radius of gyration. (b) Point A is the extreme position of an adsorbed oligomer and displacement 1 is the maximum for this pore width; similarly point B is the extreme position of a free chain and 2 is its maximum displacement.

**Self diffusion of the free chains** Although the adsorbed chains are those affected the most by confinement, in these ultra narrow geometries the mobility of the free chains is also altered in comparison with the bulk. In figure 2.17a the CM msd normal and parallel to the walls are shown for a chain that is free at the begining of time. The msd normal to the wall is proportional to time only in very small time scales. Afterwards the motion of the free chains is slowed down by the adsorbed first layer and subsequently larger displacements are prevented by the surface. In figure 2.17b the extreme position of a free chain CM is denoted by the point B and the maximum possible displacement is shown by the arrow 2. The msd parallel to the walls is proportional to time throughout the simulation, just like in the bulk, as the system extends infinitely in the  $xy$  directions due to the periodic boundary conditions.

Obviously, the  $z$ -msd of the chains will depend on how easy it is for the free chains to penetrate inside the first layer. Since the density of the first layer is dynamically constant, in order for a free chain to enter the adsorbed layer an adsorbed one has to desorb; which means that the “available space” for the free chains is determined by the desorption process. In figure 2.18a the CM msd normal to the walls is shown for various wall-fluid attractions. For the neutral and weakly physisorbing walls chains which are free at the begining of time manage to move inside the first layer, since desorption is relatively fast (table 2.4) and the exchange between adsorbed chains and free chains takes place in time scales much smaller than the simulated time (chapter 5). Near strongly physisorbing

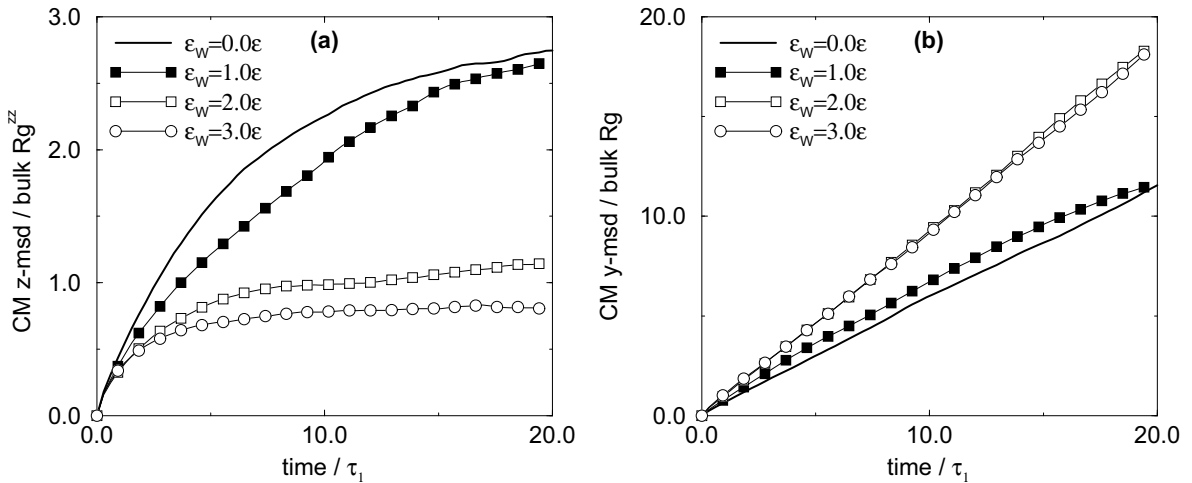


**Figure 2.18:** *Center of mass mean square displacements for the oligomers which are free at the begining of time in  $h = 6$  films normal (a) and parallel (b) to the confining surfaces.*

surfaces, however, the chains are irreversibly adsorbed for the time scale of the simulation, and the available space for the free chains to move is just the middle part of the film. For the  $h = 6\sigma$  films this layer is comparable to the radius of gyration of these oligomers in the bulk (figure 2.18a). The mobility of the “free” chains parallel to the walls is concerned it is also affected by desorption in a different way. Since periodic boundary conditions are imposed on the  $x$  and  $y$  directions, the space available for these chains to move is practically unlimited. But for the weakly attractive walls a chain that is initially free, due to the exchange between adsorbed and free chains, at some later point becomes adsorbed on a surface and its mobility is reduced and subsequently desorbs again after a small time interval. A typical chain which is initially free in the  $\epsilon_w = 0$  and  $\epsilon_w = 1$  systems visits the higher density, lower mobility, first layer several time during the simulated time (chapter 5). For the strongly physisorbing surfaces ( $\epsilon_w = 2$  or  $3$ ) since desorption is very limited the free chains remain free through out the simulated time and their mobility is comparable to that of a bulk oligomer with the same density [9] even though they are confined in an ultra narrow space between two very sluggish oligomeric layers.

## 2.3 Appendix:

### Monomers confined between uncorrugated surfaces

One of the central points of this chapter is that the origin of most of the changes taking place inside the first layer is due to the wall induced densification rather than the bare energy barriers or the corrugation of the surfaces. Important phenomena inside the solid-fluid interface like the appearance of sluggish dynamics, the enhancement of structure, the dramatic decrease of the mobilities normal to the surfaces and the qualitative change of the in-plane motion are all attributed to the enhanced density. Recent studies demonstrate beyond doubt that the dramatic increase of the relaxation times and the sluggish dynamics are actually caused by this densification [9]. On the other hand, the rest of the properties cited immediately above are fingerprints of epitaxial vitrification or crystallization. An elegant way to demonstrate the origin of both the in-plane structure and motion of the adsorbed segments is to confine the systems between two planar *uncorrugated*, flat, walls. This can be done by the use of potential barriers which can be modelled by the Lennard-Jones potential integrated over the  $xy$  plane:

$$\begin{aligned} U(z) &= \int_0^\infty dx \int_0^\infty dy \ 4\epsilon_w \left( \left( \frac{\sigma_w^2}{x^2 + y^2 + z^2} \right)^6 - \left( \frac{\sigma_w^2}{x^2 + y^2 + z^2} \right)^3 \right) \\ &= \int_0^{2\pi} d\phi \int_0^\infty \rho d\rho \ 4\epsilon_w \left( \left( \frac{\sigma_w^2}{\rho^2 + z^2} \right)^6 - \left( \frac{\sigma_w^2}{\rho^2 + z^2} \right)^3 \right) \Rightarrow \end{aligned}$$

which gives:

$$U(z) = 4\pi\epsilon_w\sigma_w^2 \left( \frac{1}{5} \left( \frac{\sigma_w}{z} \right)^{10} - \frac{1}{2} \left( \frac{\sigma_w}{z} \right)^4 \right) \quad (2.13)$$

As in our atomic walls  $\sigma_w = 1\sigma$  and in order to approximate better the double fcc corrugated walls two such potential barriers separated by the fcc  $z$  lattice spacing are used on each side of the simulation box. Moreover, to strengthen even further the point, wide films ( $h = 10\sigma$ ) of monomeric LJ fluids are simulated. The decomposition of oligomers to monomeric fluids in the vicinity of a *flat* surface will make it more difficult both for structure to be enhanced and the mobilities to decrease as, in the case of monomers, every particle is independent and is not constrained to remain a certain distance away from neighbouring particles (unlike bonded particles in an oligomer) and is far more mobile since it is not connected to other immobilized adsorbed particles. Moreover, the simulation of wide pores allows for two well separated, independent interfaces to be developed.

In current studies [40, 63] it has been found that there exists a very sharp transition inside the first layer from liquid-like to solid-like ordering with increasing  $\epsilon_w$  for both monomeric and oligomeric fluids. This transition takes place in a very narrow range of wall attractions, for a variety of confining surfaces (bcc, fcc, smooth) and independently of the correlation of the wall periodicity with the fluid particle size. The value of  $\epsilon_w$  depends only on the density of the fluid. For smooth surfaces (equation 2.13) and average number density takes place around  $\epsilon_w = 2.3\epsilon$  (figure 2.19). For  $0 \leq \epsilon_w \leq 1.7$  the radial pair

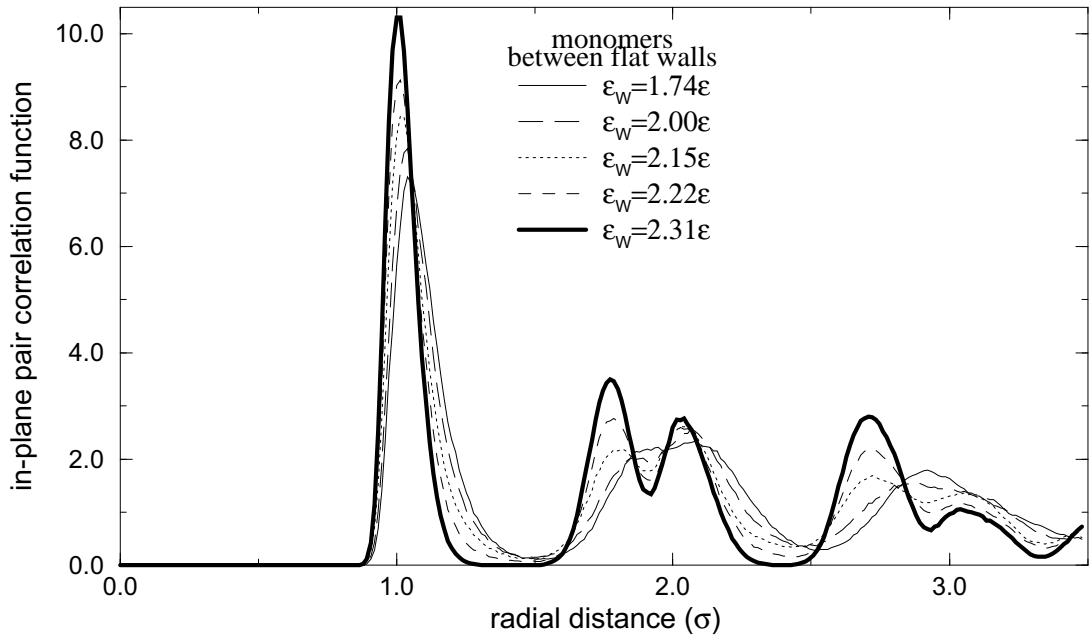


**Figure 2.19:** The in-plane radial pair correlation function of the first layer monomers for a narrow range of wall affinities. The in-plane structure is sharply enhanced with small increases of  $\epsilon_w$  around the value of  $2.0\epsilon$ . Since the confining surfaces are completely uncorrugated the high quality fcc structure that corresponds to  $\epsilon_w \geq 2.3$  is not due to epitaxial crystallisation.

correlation function (pcf) remains almost unchanged and corresponds to an amorphous liquid, whereas for systems with  $\epsilon_w \geq 2.3$  the pcf remains invariant and corresponds to a high quality fcc structure. Obviously, the observation of an adsorbed layer with crystalline fcc symmetry in the vicinity of a completely uncorrugated, structureless, surface is convincing evidence that the in-plane ordering is not due to epitaxy but rather due to better packing caused by the wall induced densification<sup>25</sup>.

**Table 2.5:** Average number densities of adsorbed monomers on smooth surfaces.

$\epsilon_w (\epsilon)$	1.00	1.74	2.00	2.15	2.22	2.31	3.45	4.62
density ( $\sigma^{-3}$ )	1.185	1.190	1.205	1.256	1.278	1.331	1.332	1.331

<sup>25</sup> one can notice that the average density inside the first layer remains the same for  $\epsilon_w \geq 2.3$  (table 2.5).

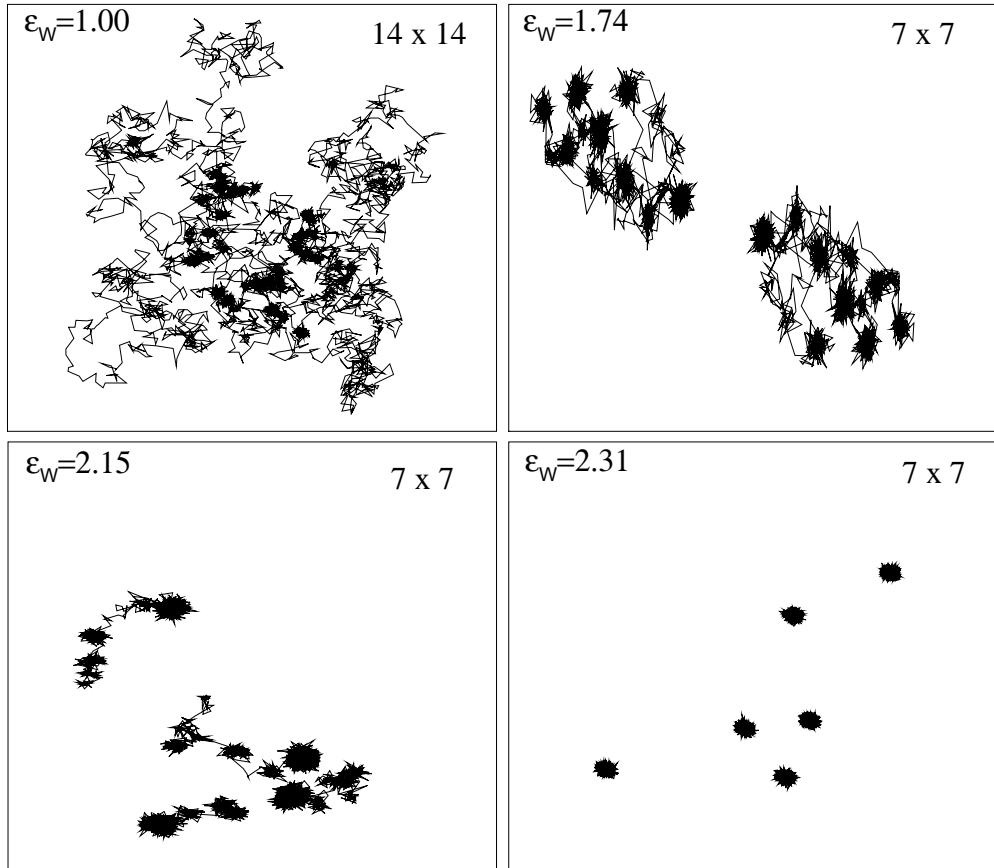


**Figure 2.20:** *In plane trajectories of adsorbed monomers on smooth surfaces. For all trajectories  $0.4 \times 10^6$  time steps are shown and the  $xy$  size is  $14\sigma \times 14\sigma$  or  $7\sigma \times 7\sigma$  as denoted. There is a qualitative change from a liquid-like ( $\epsilon_w = 1.0$ ) to more solid-like ( $\epsilon_w = 2.31$ ) type of motion.*

Furthermore, the in-plane trajectories of the adsorbed monomers on these smooth walls change qualitatively with increasing ordering inside the first layer, in the same manner as the motion of the segments of the adsorbed oligomers (§2.2). In figure 2.20, in-plane trajectories of adsorbed monomers of various systems with smooth surfaces are shown. There is a change from a random liquid-like motion near weakly attractive surfaces ( $\epsilon_w \leq 1.0$ ), to more solid-like type of motions ( $\epsilon_w = 1.75$  to  $2.15$ ) with the particles vibrating around equilibrium positions and migrating from one to another equilibrium site by sudden jumps; for even stronger adsorbing walls, diffusion is practically suspended for the time scale simulated and the adsorbed monomers are trapped, vibrating around their equilibrium positions. It should be noted that these equilibrium positions are dictated by a closest packing arrangement inside the first layer and not by any epitaxially corrugated potential as in the case of adsorbed oligomers.



## Chapter 3

### Confined films under shear (I)

In this chapter the dynamics of films in nanometer confinements subjected to shear flow are studied by Non-Equilibrium Molecular Dynamics (NEMD) in a planar Couette flow geometry. It is shown that the shape of the velocity profile which develops across the pore depends on the wall energetics. Both slippage at the wall and inside the film (interlayer slip) is observed. The location of the slippage plane is determined by the wall affinity for the oligomers, whereas flow induced structural changes inside the solid-oligomeric interface control the slip magnitude. A brief presentation of the way in which shear influences the conformations of the adsorbed chains is also given in relation with the degree of interlayer slip. A more detailed discussion of the adsorbed oligomer conformations is made in the chapter dealing with diffusion and desorption under shear (chapter 5).

Finally, inspired by shearing Surfaces Forces Apparatus (SFA) experiments an *effective viscosity* is defined and its response to increasing shear rate is studied. A number of systems with various pore sizes, wall affinities and oligomer molecules are simulated and all show strong Non-Newtonian behaviour (namely shear thinning for high flow rates). Nearly all the shear thinning takes place inside the solid-oligomer interface and the adsorbed layers are more viscous than the middle part of the films. The power law describing the shear thinning inside the solid oligomer interface is found to be determined by the wall affinity, whereas it remains insensitive to changes in the molecular architecture under the same conditions (pressure, density,  $\epsilon_w$ ). On the other hand the rheological response of the whole film is the weighted average of these two regions<sup>1</sup>, resulting in an *absence of universal response* in the shear behaviour, in agreement with recent SFA experiments on fluid lubricants.

---

<sup>1</sup> the viscous solid-oligomer interface and the bulk like middle part of the films

### 3.1 Velocity profiles across ultra thin films

Since theories predicting velocity profiles of strongly inhomogeneous systems are in an early stage of development [27, 28], one of the first questions to be addressed concerns the shape of the velocity profile in confined systems under a steady shear rate. The flow field of a confined oligomer melt can be described by the mean flow velocities of the confined oligomers after steady state flow has been established.

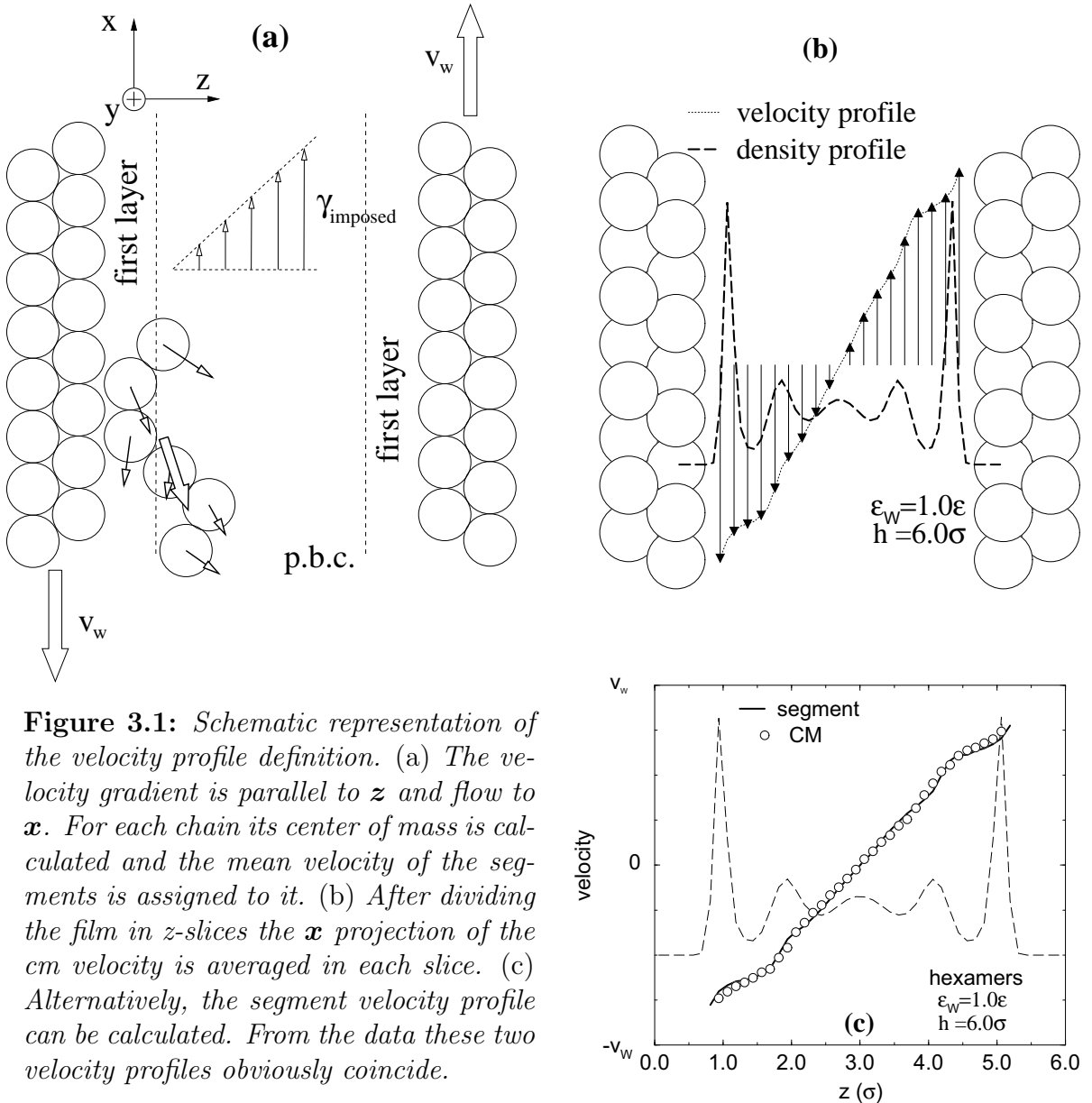


**Figure 3.1:** Schematic representation of the velocity profile definition. (a) The velocity gradient is parallel to  $z$  and flow to  $x$ . For each chain its center of mass is calculated and the mean velocity of the segments is assigned to it. (b) After dividing the film in  $z$ -slices the  $x$  projection of the cm velocity is averaged in each slice. (c) Alternatively, the segment velocity profile can be calculated. From the data these two velocity profiles obviously coincide.

The mean flow velocities of the confined oligomers are defined by:

$$\mathbf{v}^{CM}(z) = \left\langle \frac{1}{N_{ch}(z,t)} \sum_{ic=1}^{N_{ch}(z,t)} \mathbf{v}_{ic}^{CM}(z,t) \right\rangle \quad (3.1)$$

where  $\mathbf{v}^{CM}(z)$  is the average center of mass velocity of all chains with their center of mass located inside a thin slice at distance  $z$  away from the wall,  $N_{ch}(z,t)$  is the number of chains with their CM in the slice at time  $t$  and  $\mathbf{v}_{ic}^{CM}(z,t)$  is the instantaneous CM velocity of chain  $ic$ . The average is over all simulated time. In our simulation geometry flow is imposed in the  $\mathbf{x}$  direction and the velocity gradient is in the  $\mathbf{z}$  direction; this implies that the velocity profile developed by the imposed shear rate is the  $\mathbf{x}$  projection of  $\mathbf{v}^{CM}$  as a function of  $z$ , i.e.  $\mathbf{v}_x^{CM}$ . A schematic representation showing these projections is given in figure 3.1b.

Following exactly the same line of thinking the segment velocity profile can be defined as:

$$\mathbf{v}(z) = \left\langle \frac{1}{N(z,t)} \sum_{i=1}^{N(z,t)} \mathbf{v}_i(z,t) \right\rangle \quad (3.2)$$

where  $\mathbf{v}(z)$  is the average velocity of all *particles* located in a thin slice at a distance  $z$  away from the wall,  $N(z,t)$  is the number of segments in the slice at time  $t$  and  $\mathbf{v}_i(z,t)$  is the velocity of particle  $i$  at time  $t$ . These two quantities coincide (figure 3.1c) but the segmental velocity profile has better statistics than the CM velocity profile, as for a chain of length  $N$  there is only one CM for every  $N$  segments. The averaging over time is essential to distinguish the flow component in the instantaneous velocities, which is screened by the random thermal velocities. In weak flow fields this requires very demanding runs over extremely long periods, this condemns NEMD simulations to be restricted to the strong shear rates region, even for the most powerful computers available. Throughout this chapter the term *velocity profile* will refer to the time-averaged segment velocity profile at steady state flow.

Shown in figure 3.2 are the velocity profiles developed in our Couette flow geometries across pores of various widths for the weakly psysisorbing surfaces ( $\epsilon_w = 1$ ). The velocity profiles are superimposed on the corresponding density profiles and the figure borders are the positions of the walls ( $z = 0$  and  $h$ ) and the wall velocities (velocity =  $\pm v_w$ ). The velocity profiles are not linear as one would expect from the hydrodynamics of Couette flow in the bulk [64] but they do not follow the wild density variations either. In fact, they are more smooth than the velocity profiles obtained in similar geometries for monomers [65, 66, 67, 68]. For monomeric systems the density profiles are more layered in the first place (figure 2.2) and furthermore the monomers can more easily develop a non-linear, “ragged”, velocity profile [26, 27] than the oligomers; as each monomeric layer adopts a different flow velocity resulting in a “stairway”-like<sup>2</sup> velocity profile [26], due to the absence of any physical connection across  $z$  by means of chain conformations that are not completely parallel to the walls. In all cases, for the oligomers the velocity profile is linear

---

<sup>2</sup> local density approximation theories [27] predict also the same behaviour for the velocity profile

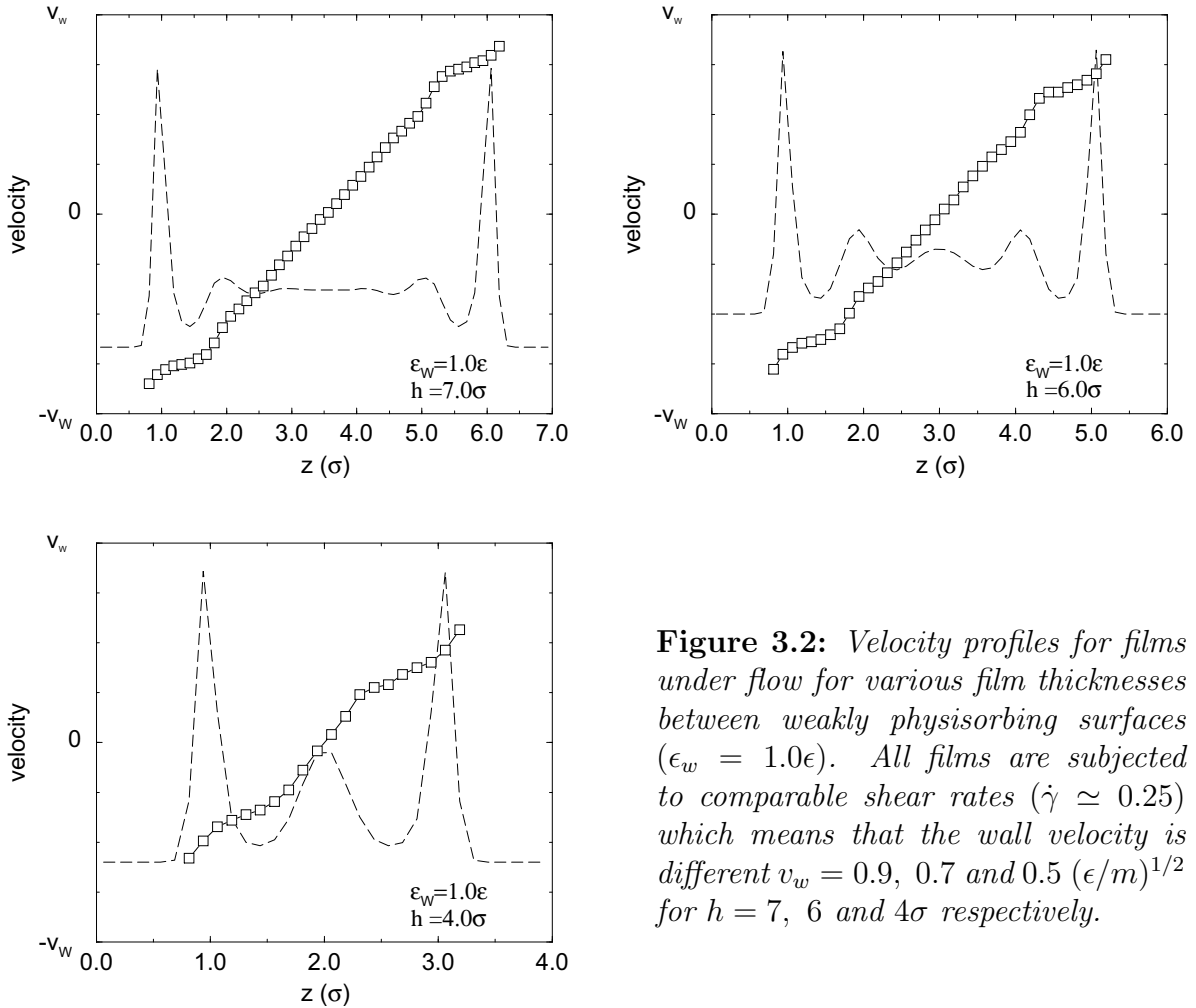


**Figure 3.2:** Velocity profiles for films under flow for various film thicknesses between weakly physisorbing surfaces ( $\epsilon_w = 1.0\epsilon$ ). All films are subjected to comparable shear rates ( $\dot{\gamma} \approx 0.25$ ) which means that the wall velocity is different  $v_w = 0.9, 0.7$  and  $0.5$  ( $\epsilon/m$ ) $^{1/2}$  for  $h = 7, 6$  and  $4\sigma$  respectively.

inside the middle part of the system where the density is almost constant (figure 3.3). In the vicinity of the surface the velocity profile changes drastically with the wall energetics. For moderately attractive walls it is almost linear inside the adsorbed layer but with a smaller slope than in the middle part of the system. This implies that in the interfacial region the effective viscosity is higher than in the middle of the film (§ 3.3). Moreover slip appears between the wall and the fluid (slip boundary conditions at the wall).

For the more attractive walls, however, this first layer locks on the wall (figure 3.3b) and much higher shear rates have to be applied to induce flow inside this interfacial area (figure 2b in [11]). At these high shear rates the low density region between the adsorbed chains and the middle of the film is characterized by an abrupt change in the velocity profile denoting the existence of slip at this location inside the film (“*interlayer slip*”) (figure 3.3b). Around the depletion zone and in the part closest to the first layer ( $z < 1.5$ ) most of the segments therein belong to adsorbed chains of the first layer. Due to the strong attraction of these walls ( $\epsilon_w = 2$ ) the adsorbed segments move with the

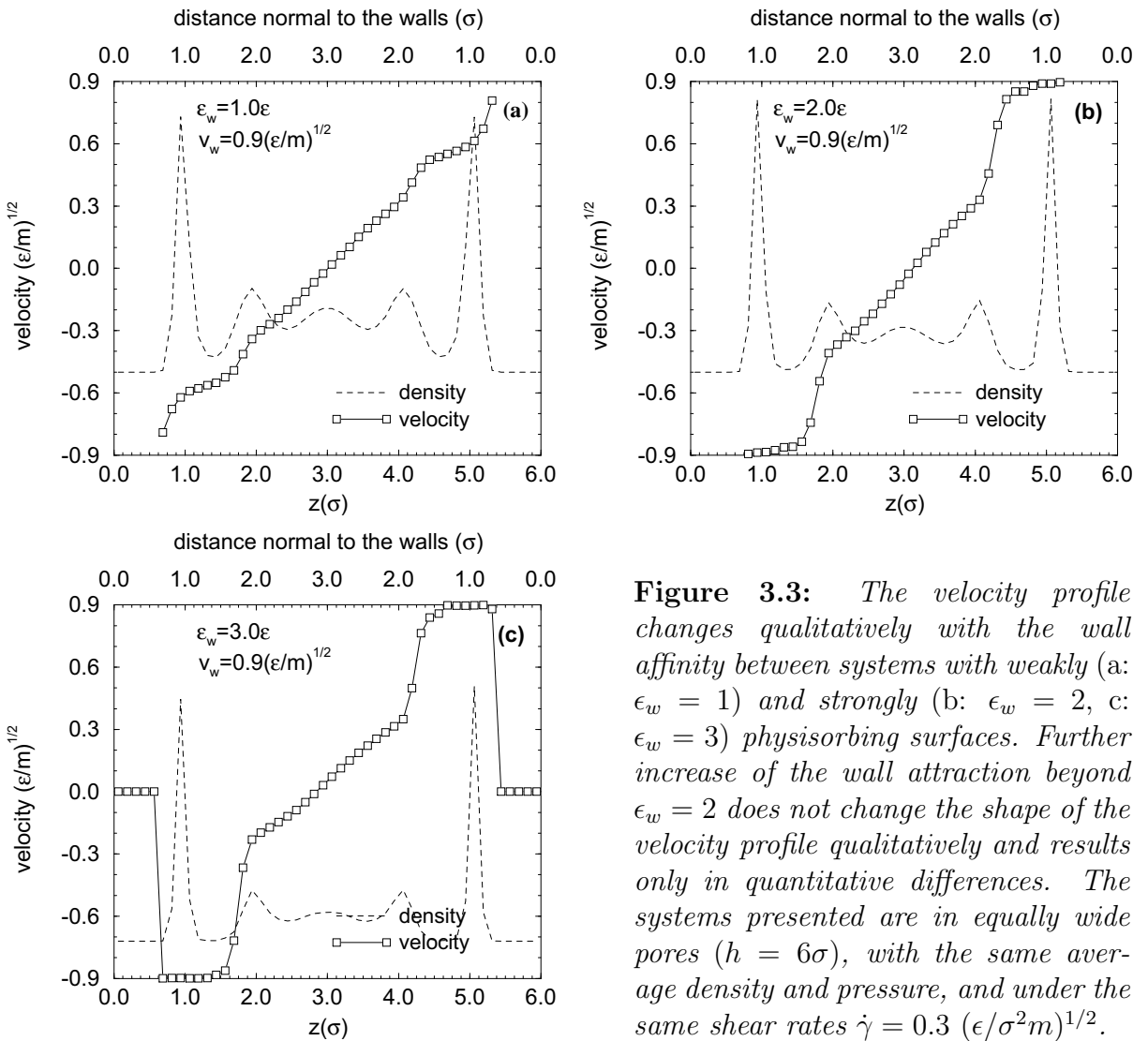


**Figure 3.3:** The velocity profile changes qualitatively with the wall affinity between systems with weakly (a:  $\epsilon_w = 1$ ) and strongly (b:  $\epsilon_w = 2$ , c:  $\epsilon_w = 3$ ) physisorbing surfaces. Further increase of the wall attraction beyond  $\epsilon_w = 2$  does not change the shape of the velocity profile qualitatively and results only in quantitative differences. The systems presented are in equally wide pores ( $h = 6\sigma$ ), with the same average density and pressure, and under the same shear rates  $\dot{\gamma} = 0.3$   $(\epsilon/\sigma^2 m)^{1/2}$ .

velocity of the wall –stick on the wall– thus developing a constant velocity profile inside the first layer (no slip boundary condition at the wall). When higher shear rates are applied these segments try to maintain the stick-type velocity profile of the first layer but are slowed down by the slower moving middle layer. In the low density area close to the middle layer (distance from the wall  $\simeq 1.8$ ) the segments belong mostly to the free chains situated in the middle of the film. This region and the first half of the second layer is where most of the slip between the interfacial layer and the rest of the film takes place:  $\sim 1.9\sigma$  away from the surface.

In all cases ( $\epsilon_w = 1, 2, 3$ ) the magnitude of slippage is increasing with higher shear rates. Moreover, for the  $\epsilon_w = 1$  surfaces the slip between the wall and the fluid increases for narrower confinements for the same imposed shear rate.

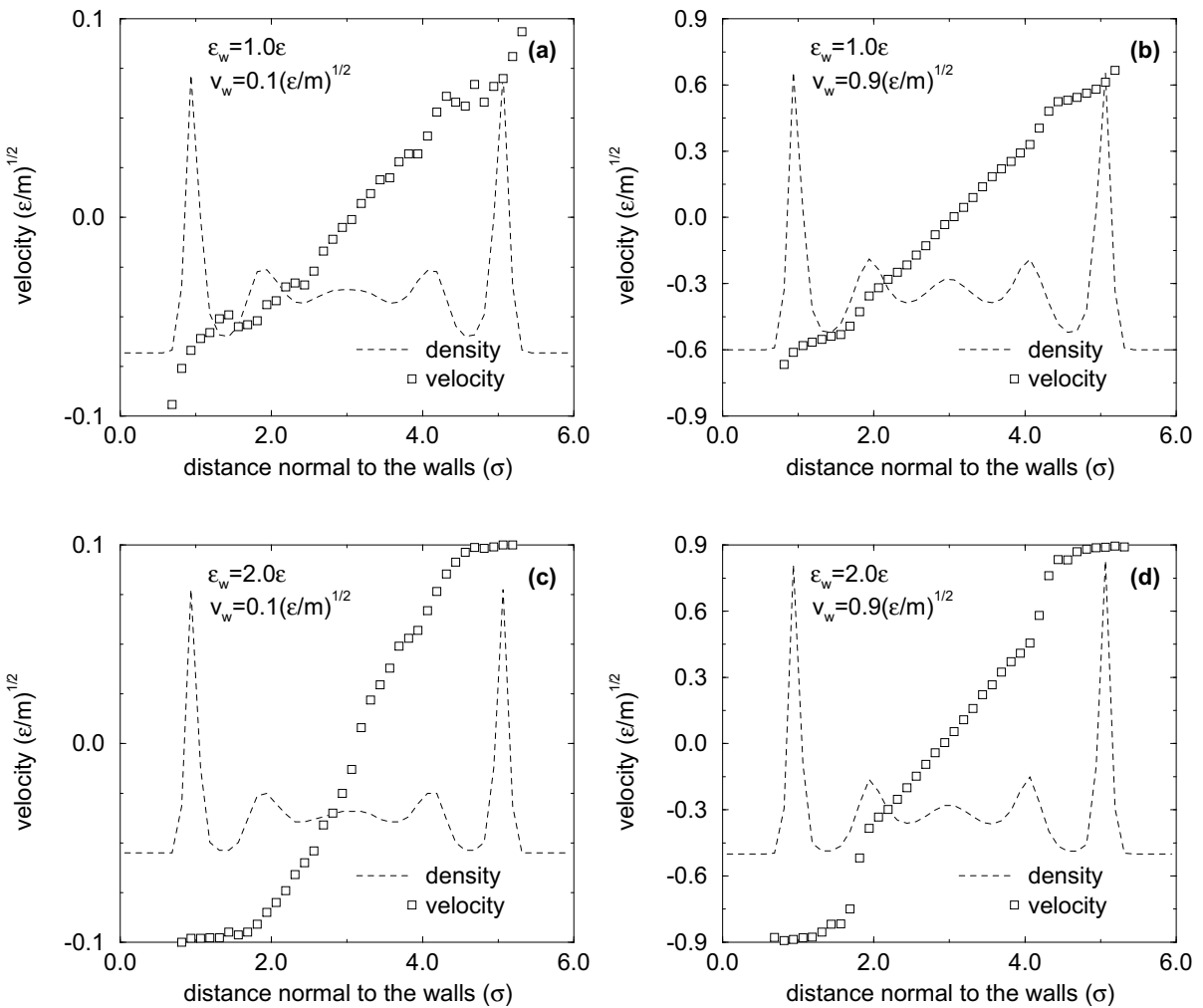
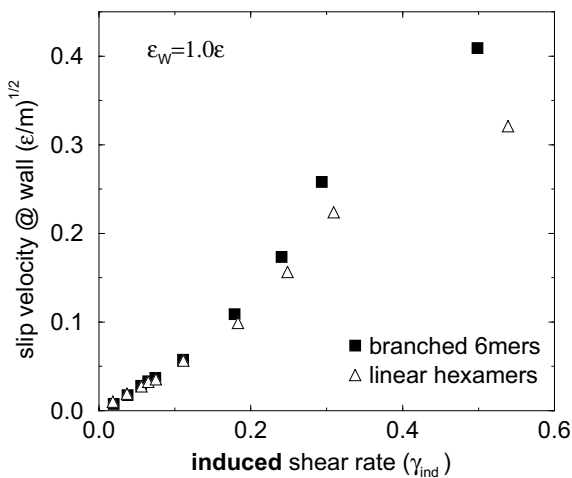


**Figure 3.4:** Velocity profiles for decamers confined in  $h = 6$  pores for weakly and strongly adsorbing walls. The effect of increasing shear rate is shown through the comparison between moderate and strong flows.

**The effect of increasing shear rate on the velocity profile:** In figure 3.4 the velocity profiles of decamers are shown for weakly (a,b:  $\epsilon_w = 1$ ) and strongly (c,d:  $\epsilon_w = 2$ ) physisorbing surfaces. A comparison between two different shear rates (fig. 3.4a,c:  $\dot{\gamma}_{imposed} = 2 \cdot v_w/h = 0.033 (\epsilon/\sigma^2 m)^{1/2}$ ) and a stronger flow (fig. 3.4b,d:  $\dot{\gamma}_{imposed} = 0.3 (\epsilon/\sigma^2 m)^{1/2}$ ).

Not surprisingly<sup>3</sup>, the velocity profiles of these longer chains are qualitatively the same as the velocity profiles of the hexamers (figure 3.3). Considering that the entanglement length for the chain model used is around 30 segments [7] the decamers are long enough to develop a typical velocity profile of unentangled chains. Further simulations with 20mers

<sup>3</sup> our model chains capture the unentangled chain behaviour for very small lengths due to their high intrinsic flexibility. Already chains with 5 segments capture the unentangled polymer response [8, 9, 11]



Definition of  $\dot{\gamma}_{ind}$ :

$\dot{\gamma}_{ind}$  is the shear rate induced in the film after slip at the wall has been taken into account:

$$\dot{\gamma}_{ind} = \frac{v(z_{min}) - v(z_{max})}{z_{max} - z_{min}} \quad (3.3)$$

where  $z_{min}$  and  $z_{max}$  are the extreme positions for which there is flow; for example in fig. 3.3a it is:

$$\dot{\gamma}_{ind} = \frac{v(5.188) - v(0.812)}{h - 2 \cdot 0.812} = 0.31 \left( \frac{\epsilon}{\sigma^2 m} \right)^{1/2}$$

**Figure 3.5:** The magnitude of slip at the wall ( $v_w - v_{fluid}$ ) as a function of the induced shear arate across the films. Films confined between ( $\epsilon_w = 1$ ) walls of a linear 6mer and a branched 6mer are shown. The definition of induced shear rate is also given above.

for a limited number of shear rates do not show any deviation from the qualitative features of the velocity profiles presented in figure 3.4. Furthermore for these flexible coils it will be shown that the velocity profile does not depend on the chain architecture. Shear flow was applied to a variety of oligomers and the velocity profile is completely insensitive to changes of the molecule type (short and long linear chains with 5, 6, 10 and 20 segments, branched and star hexamers: figure 3.10) for the same system pressures and densities (figure 4.19 and 4.20).

With an increase in the shear rate by one order of magnitude (shown in figure 3.4) the velocity profiles do not change dramatically, and this is the case for all the shear rates employed in my simulations ( $\dot{\gamma}$  extending in a range more than two orders of magnitude wide). The main differences with increasing imposed shear rate are the magnitude of the slip (figure 3.5) and the velocity profile inside the solid oligomer interface:

- (i) The slip increases almost linearly with shear rate, both in the case of wall slip ( $\epsilon_w = 1$ ) and interlayer slip ( $\epsilon_w \geq 2$ ). This becomes obvious in the velocity profiles as well: for small  $\dot{\gamma}$  there is very limited slip, as seen by the small deviation of the fluid velocity inside the first layer compared to the wall velocity ( $\epsilon_w = 1$ , figure 3.4a); for higher  $\dot{\gamma}$ , however, there is a substantial difference between the wall velocity and the velocity induced inside the first layer ( $\epsilon_w = 1$ , figure 3.4b) For stronger wall attractions and the lower shear rates used, there exists a continuous, smooth, velocity profile in the region between the adsorbed layer and the free chains for  $\epsilon_w = 2$  (figure 3.4c), i.e. for these shear rates there is no slip anywhere in the film for the strongly adsorbing walls ( $\epsilon_w \geq 2$ ). For higher  $\dot{\gamma}$  there develops a substantial difference between the velocity of the adsorbed layer ( $\simeq v_w$ ) and the velocity in the middle of the film ( $\epsilon_w = 2$ , figure 3.4d) which indicates a slip taking place *inside* the film. This behaviour is more pronounced for  $\epsilon_w = 3$  (figure 3.4c).

(ii) Although the velocity profile in the middle part of the film remains almost the same with increasing shear rate, the velocity profile inside the solid-oligomer interface changes with  $\dot{\gamma}$ . The change is constituted by an increasing slope ( $\partial u / \partial z$ ) with higher  $\dot{\gamma}$ . Especially in the case of strongly adsorbing surfaces for the lower shear rates simulated<sup>4</sup> the whole adsorbed layer locks on the wall and travels with the velocity of the wall:  $v_w$  (figure 3.4c) whereas for higher shear rates a velocity profile with a non-zero slope starts to develop inside this region (figure 3.4d). As the slope of the velocity profile represents the local shear rate, this increasing slope implies that the viscosity inside the solid oligomer interface may<sup>5</sup> decrease with increasing  $\dot{\gamma}$  (shear thinning). It will become clear later (figure 3.13) that this is the case.

An important parameter that determines the shape of the velocity profile is the *excess solid atom-fluid segment cohesive energy*:  $\epsilon_w/\epsilon$ . Representative runs have been carried out for systems where the chain segments have some cohesive energy between them (i.e. the full Lennard-Jones potential is used to model the interchain interactions instead of the shifted and truncated one, equation 1.3). As far as the flow boundary conditions at the wall are concerned, they are determined by  $\epsilon_w$  in the same manner as in our *athermal* oligomeric systems. Namely for  $\epsilon_w \leq 1$  there is slip at the wall, whereas for  $\epsilon_w \geq 2$  there is no slip at the surfaces. On the other hand the behaviour of the interlayer slip changes in a more intricate way. The molecular mechanism involved in this slip situated inside the fluid film is not a simplistic cohesion between the chains that keeps them from slipping past each other, but rather has to do with the conformations of the adsorbed chains (§ 3.2). Comparing shear rates for which the conformations of the adsorbed chains are –on average– the same, the interlayer slip and the relative velocity profiles are identical between *athermal bead-spring* and *LJ bead-spring* oligomeric systems.

Finally, when pressure is increased there are only small changes in the velocity profiles and in particular inside the solid-oligomer interface, i.e. only the velocity profile inside the first layer is affected by increased pressure. With increasing pressure there is an increase in the density throughout the film and especially inside the first layer. This makes the adsorbed layer more sluggish and “viscous” (§ 2.2) and thus reduces the slope of the velocity profile. Under different conditions flow can influence the structure and dynamics of the film in much more complicated ways. For example, extremely thin films (2 layers) of identical hexamers, confined between strongly adsorbing surfaces ( $\epsilon_w \geq 2.5\epsilon$ ) and under much higher pressures than the ones used in the present studies, exhibit strong vitrification in the vicinity of an fcc surface [10]. When shear is imposed on these films, the two layers lock on the opposite walls and slip past each other and shear can result in a shear “induced melting and reordering” of the adsorbed layers. This phenomenon is even more pronounced for monomeric systems under the same conditions [30].

---

<sup>4</sup> which actually are very high compared to the SFA experiments, but comparable with the shear rates found in high density magnetic storage devices between the head and the disk

<sup>5</sup> assuming that the corresponding stress does not decrease faster than  $\dot{\gamma}$ , which it does not (§ 3.3)

### 3.2 Molecular mechanisms of slip in the nm scale

In the previous paragraph it is pointed out that for weak wall attractions ( $\epsilon_w = 1$ ) the slip plane is located between the surfaces and the first fluid layer (figure 3.2 and 3.3a) whereas for the stronger wall affinities ( $\epsilon_w = 2$  or 3) the slip plane is located inside the film, between the adsorbed chains and the free chains (interlayer slip). In this paragraph the molecular mechanisms that cause the slip are analysed and it is shown that the location of the slip is determined by the wall energetics and the conformations of the adsorbed chains [11].

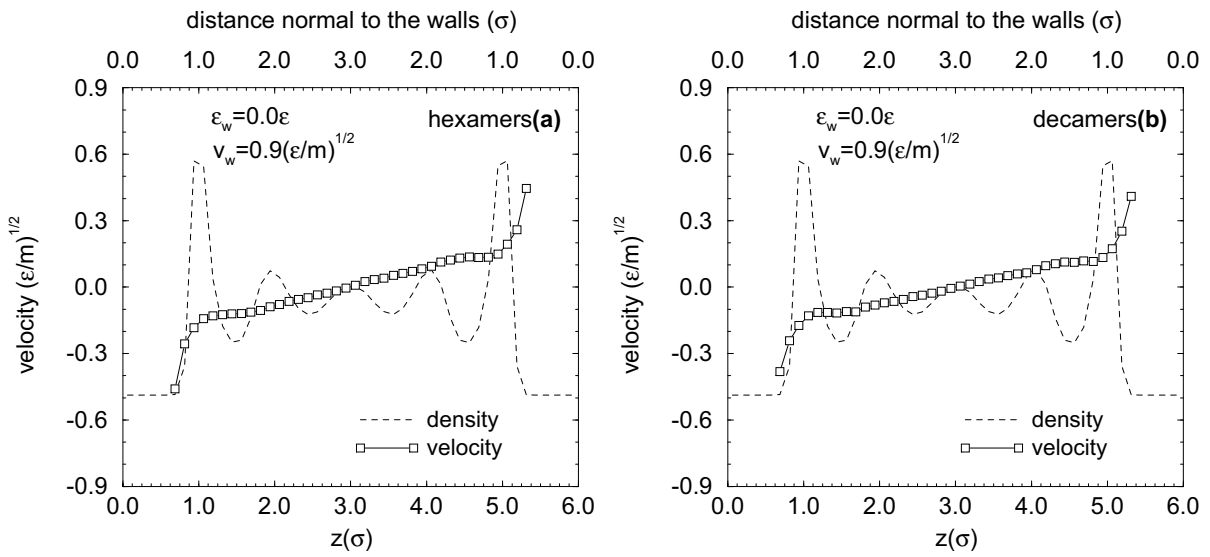


**Figure 3.6:** Velocity profile for 6mers (a) and 10mers (b) confined between nonadsorbing, neutral walls ( $\epsilon_w = 0$ ). There is very strong slip between the surface and the fluid obstructing any considerable shear flow to be developed inside the film independent of the wall velocity ( $h = 6$ ,  $v_w = 0.9$ ). Even though the chains are pretty small, the velocity profile is exactly as expected for a polymer near a nonadsorbing smooth surface (de Gennes, *Simple views on condensed matter*, 1992).

**Neutral surfaces ( $\epsilon_w = 0$ ):** The careful reader has surely noticed that no mention has been made in this paragraph of neutral walls ( $\epsilon_w = 0$ ). This is because it is impossible to induce considerable flow between *smooth* surfaces that do not possess any attraction. What really happens is that a very small velocity gradient can be induced inside the film irrespectively of how fast the neutral walls are moving and almost complete slip takes place between the walls and the fluid. This has been derived also in MD simulations of confined LJ monomers under Couette flow [67]. In the case of oligomers or polymers this effect is magnified even further by the enhanced ability of these complex fluids to resist flow in comparison with the simple LJ fluid. Since a long time now de Gennes [69] established that a polymer or an oligomer melt flowing past a smooth, nonadsorbing, surface would always slip.

**Weakly physisorbing surfaces:** After the initial theoretical studies predicting strong slip at the walls [69] Brochard and de Gennes [71, 72] extended this theory and worked out the consequences of strong slippage at a wall, explaining the dynamics of polymer wetting. From an experimental point of view, apart from pioneering experiments with a transparent extruder [73] only very recently has it been demonstrated that strong slip appears near weakly adsorbing surfaces [74]. On the other hand SFA experiments were condemned to use very attractive mica surfaces and only one study with weakly adsorbing surfaces has been published up to now, which reports slippage at the wall albeit in a very vague context [75].

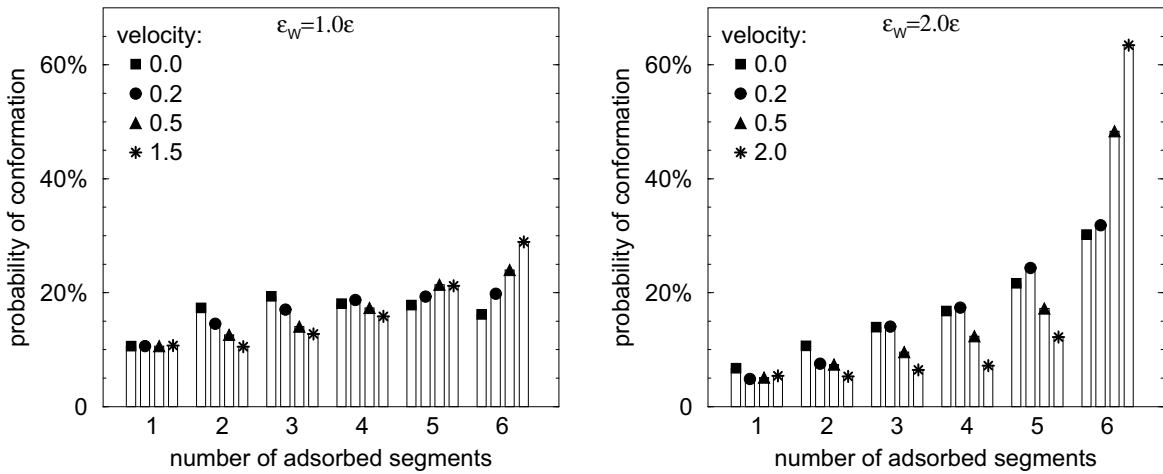
The molecular mechanism responsible for the slippage at a surface is quite well understood and intuitively expected. Slippage at the wall takes place when a smooth and weakly adsorbing surface is moving past a fluid which is characterized by some kind of *physical cohesion*. Under these circumstances<sup>6</sup> the fluid in contact with the surfaces can not follow exactly the motion of the surface but is slowed down due to its *physical connectivity* with the slower moving fluid, located further away from the walls, thus slippage appears at the wall. Even simple LJ fluids exhibit wall slip near a neutral or weakly physisorbing surface [65, 66, 67, 68]. In these systems the *connectivity* inside the fluid is due to the interparticle attraction of the LJ potential (intrinsic cohesion). In the case of long polymer melts the *connectivity*, is provided by the entanglements between adsorbed and free chains [69, 82, 83]. In our case there is no attraction in the interchain potential used (equation 1.3) and even our longer oligomers (20mers) are below the entanglement length ( $\sim 30$  monomers [7]). But there is a *physical connectivity* which arises from the existence of partly adsorbed chains, which are partially inside the first layer in contact with the surfaces (adsorbed part) and partially extending inside the middle part of the film (figure 3.9). The free tails belonging to partly adsorbed chains *bind, physically connect*, the adsorbed layers to the slower moving middle part of the film and prevent it from following exactly the motion of the surfaces –i.e. the velocity of the first layer is smaller than the wall velocity– thus giving rise to a slip between the wall and the fluid. At the same time the first layer, which is *pushed* by the moving surface through a continuous momentum transfer, does not slip past the middle part of the film since the same tails *tie* these two regions. With increasing shear rate the conformations of the adsorbed chains are expected to change (as the coils will align parallel to flow) but for the weakly adsorbing surfaces  $\epsilon_w \leq 1$  and the densities used in our simulations there is always sufficient number of partly adsorbed oligomers to ensure no interlayer slip (figure 3.9).

In chapter 2 the conformations of the adsorbed chains are depicted through the probabilities of an oligomer to have a certain number of adsorbed segments (in equilibrium: tables 2.2 and 2.3). The configurations of the adsorbed chains change radically when shear rate is imposed (figure 3.7 and tables 4.1, 4.2).

It becomes obvious from figure 3.7 that flow favours conformations with many contacts with the walls. This is expected, as the tendency for the chains in the vicinity of the walls to align parallel to them (table 2.2) is strengthened further by flow: since conformations

---

<sup>6</sup> the absence of surface roughness and surface attraction



$\epsilon_w :$	1.0 $\epsilon$				2.0 $\epsilon$				3.0 $\epsilon$			
wall velocity:	.00	.20	.50	1.5	.00	.20	.50	2.0	.00	.20	.50	2.0
1 contact	.12	.11	.11	.10	.07	.05	.05	.05	.07	.09	.02	.03
2 contacts	.17	.15	.13	.11	.10	.08	.07	.05	.11	.09	.04	.05
3 contacts	.19	.17	.14	.12	.14	.14	.10	.06	.13	.09	.08	.05
4 contacts	.18	.18	.17	.16	.17	.17	.12	.07	.17	.15	.04	.06
5 contacts	.18	.19	.21	.21	.22	.24	.17	.12	.23	.10	.15	.06
6 contacts	.16	.20	.24	.30	.30	.32	.49	.65	.29	.48	.67	.75

*A more complete set of probabilities can be found in table 4.1*

**Figure 3.7:** Probabilities of conformations with a specific number of contacts for the adsorbed hexamers confined between weakly ( $\epsilon_w = 1$ ) and strongly ( $\epsilon_w = 2$ ) physisorbing walls for several imposed wall velocities. In the table the probabilities for  $\epsilon_w = 3$  surfaces are also listed. For all systems  $h = 6\sigma$ .

with large  $z$ -size<sup>7</sup> feel a large velocity gradient across them and are unfavourable, so forces originating from the velocity gradient try to align the chains parallel to flow [45]. For the weakly adsorbing surfaces there is sufficient number of partly adsorbed chains, even for the highest shear rates that can be applied<sup>8</sup> to these systems to prevent interlayer slip (figure 3.9).

<sup>7</sup>  $z$  is the direction of the velocity gradient in the simulation geometry (figure 3.1)

<sup>8</sup> as wall slippage increases with  $\dot{\gamma}$  after a certain wall velocity ( $v_w = 2.0(\epsilon/m)^{1/2}$  for our densities) the only effect of increasing imposed shear rate is to introduce stronger slip, whereas inside the film the developed shear rate (equation 3.3) remains the same

**Strongly physisorbing surfaces:** For the more strongly physisorbing surfaces there is a change from no slip, at low shear rates, to the development of considerable interlayer slip at higher  $\dot{\gamma}$ .

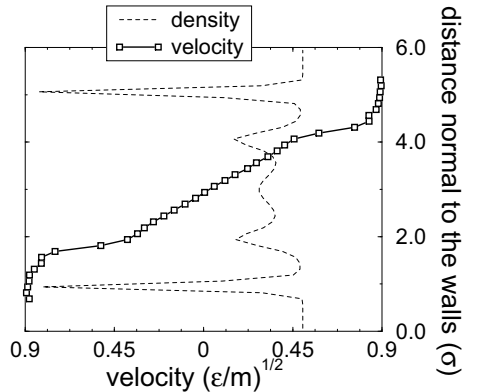
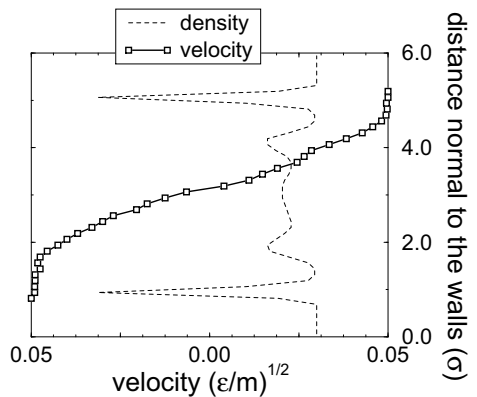
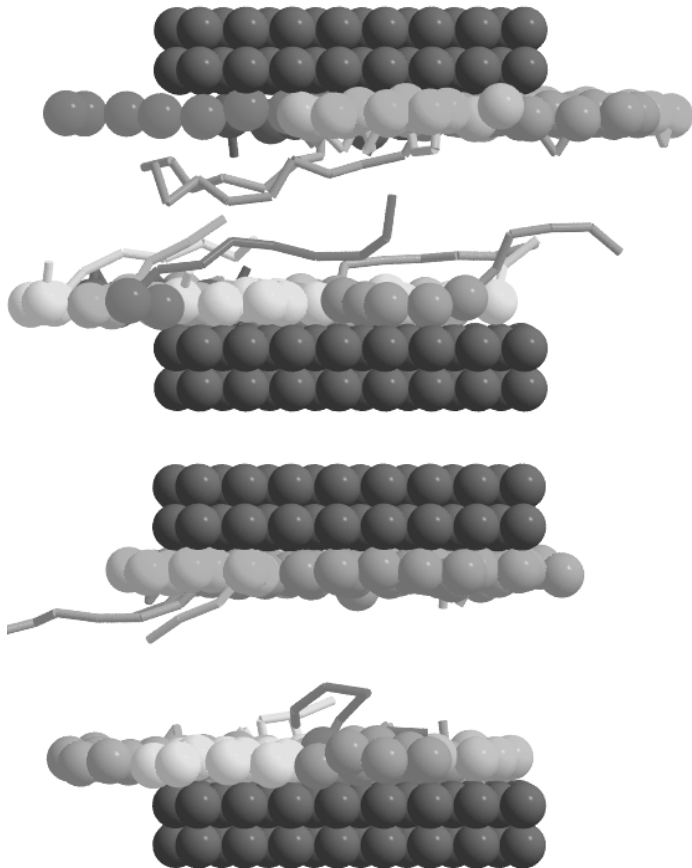
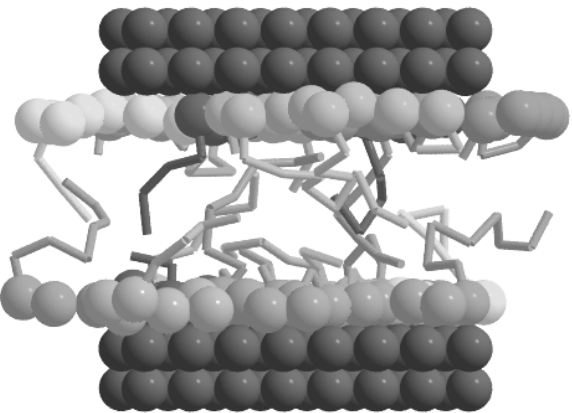
Namely, there is a qualitative change of the velocity profile and of the interlayer slip with increasing shear rate (figure 3.4c, d). Between the wall and the adsorbed layer there is no slip for the shear rates simulated, apart from extremely high shear rates<sup>9</sup>. Inside the film however (i) for small shear rates there exists still a sufficient number of partly adsorbed chains (figure 3.7) acting as *connectors* between the adsorbed layer and the middle part of the film thus hindering any interlayer slip (figure 3.8  $v_w = 0.05$ ). (ii) for the higher shear rates the adsorbed chains stretch and align parallel to the walls so strongly that nearly all the tails disappear and the *physical connectivity* provided by them is almost completely lost (figure 3.8  $v_w = 0.9$ ). This results in the appearance of a substantial interlayer slip, with the slip plane located in the region between the adsorbed chains and the middle part of the film, where the free chains are located. In these systems the adsorbed layer covers the strongly adsorbing surface and locks on it traveling with the velocity of the wall, so effectively the *wall-adsorbed layer* system behaves like a neutral wall which moves with respect to the free chains. So, this interlayer slip is completely analogous to the slip near nonadsorbing walls, as the middle part can be considered as a confined oligomer melt between two neutral ( $\epsilon_w = 0$ ) surfaces, provided by the adsorbed layers which cover the strongly adsorbing solid, screening any attraction from the underlying wall. The difference is that in this case there is some effective roughness of the surface by means of a perpetual chain exchange between adsorbed chains that desorb and free chains that take their place (chapter 5). This continuous exchange through the desorption-adsorption process sustains a weak *physical connectivity* between an effectively neutral surface and a melt of free chains, preventing complete slip from taking place, as it would do next to a neutral smooth surface (figure 3.6).

In figure 3.8 for two representative wall velocities the conformations of the adsorbed chains on strongly adsorbing surfaces ( $\epsilon_w = 2$ ) are shown. As before the free chains located in the middle are omitted for clarity and the adsorbed segments are drawn as “balls”, whereas the tails extending into the middle part of the film are represented with cylinders connecting the centers of the segments. When shear is imposed there is a definite tendency for the adsorbed chains to align parallel to the wall adopting conformations with many surface contacts. For the low shear rate shown ( $v_w = 0.05(\epsilon/m)^{1/2}$ ) there are still some partly adsorbed chains, which act as *physical connectors* between the first layer and the middle part and prevent any slippage inside the film, as it can be seen in the respective velocity profile. With increasing shear rate the adsorbed chains systematically become better aligned and less partly adsorbed coils exist (table 4.2). This results into a gradual appearance of an interlayer slip between the adsorbed layer and the free chains (the location of the slip plane can be clearly seen in the velocity profile of  $v_w = 0.9$  in figure 3.8).

---

<sup>9</sup> wall slip appears for  $v_w \sim 4(\epsilon/m)^{1/2}$  for  $\epsilon_w = 2$ , while there is no wall slip for  $v_w \leq 6(\epsilon/m)^{1/2}$  near the  $\epsilon_w = 3$  walls [11]

**Figure 3.8:** The adsorbed chain conformations (decamers,  $h = 6$ ,  $\epsilon_w = 2$ ) are shown for equilibrium and two shear rates ( $v_w = 0.05$  and  $0.9$ ). For low shear rates there exists sufficient number of partly adsorbed chains to prevent interlayer slip. For higher shear rates nearly all physical connectivity between the first layer and the middle part is lost and slippage takes place between the adsorbed layer and the free chains.



In the systems confined between the  $\epsilon_w = 3$  surfaces exactly the same phenomena are observed. But the onset of slippage shifts to lower shear rates, as the adsorbed chains exhibit an even stronger stretching next to the surface (figure 3.7). As a result for the same imposed shear rates there is stronger interlayer slip for the  $\epsilon_w = 3$  than the  $\epsilon_w = 2$  systems (figure 3.3).

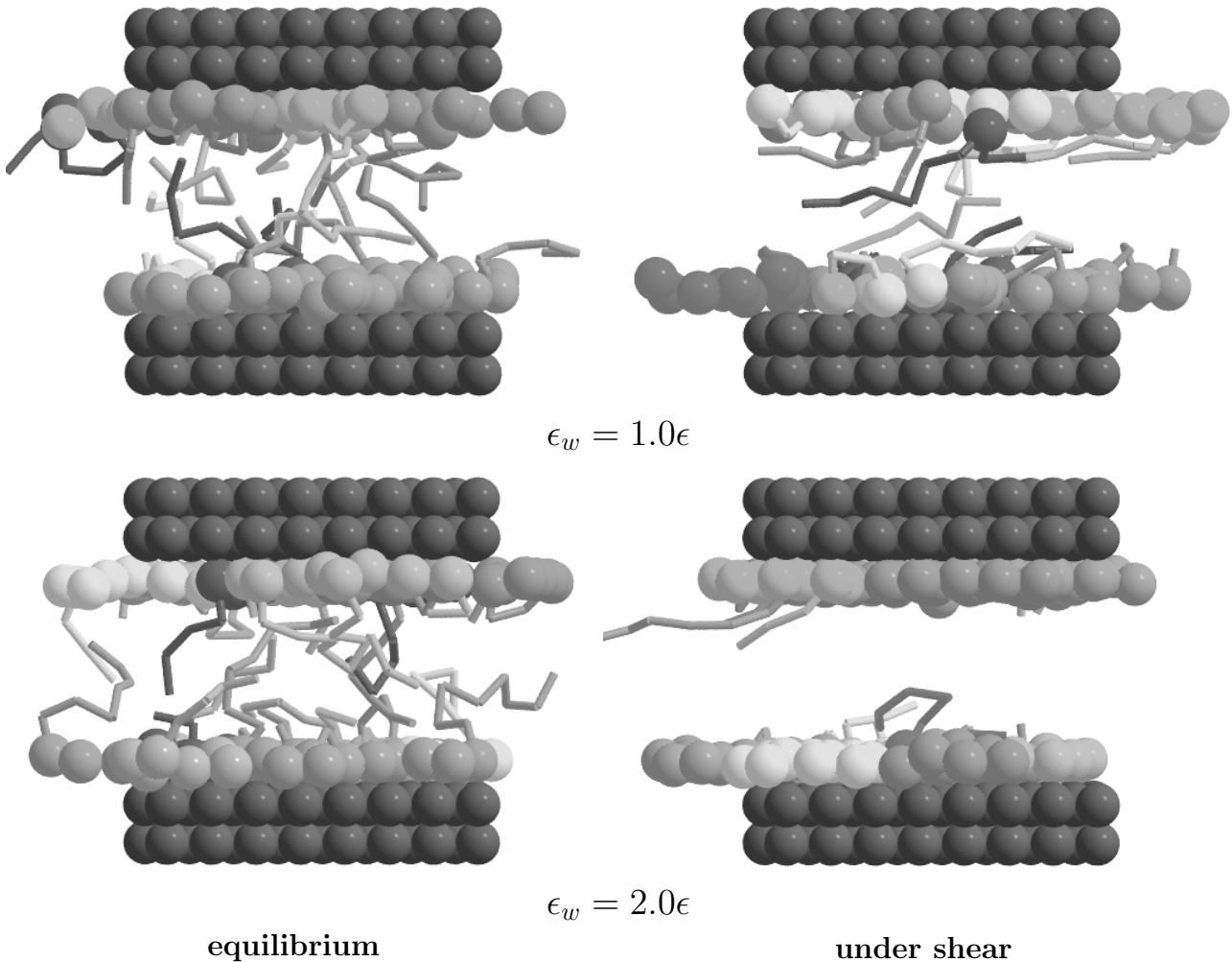


**Figure 3.9:** The adsorbed chain conformations on weakly ( $\epsilon_w = 1$ , top) and strongly ( $\epsilon_w = 2$ , bottom) physisorbing surfaces for equilibrium and  $v_w = 0.9$  (decamers,  $h = 6$ ). The free chains are omitted for clarity. The adsorbed segments are presented by balls (“beads”) and the tails belonging to partly adsorbed chains by the cylindrical bonds (“springs”). A projection of the system on the  $xz$  shear plane is shown. It is obvious that for the  $\epsilon_w = 1$  surfaces there is still a substantial number of adsorbed chains even at this high shear rate, whereas for  $\epsilon_w = 2$  there are almost no partly adsorbed chains to “tie” the adsorbed and the free part of the film. As it has been discussed in the previous pages this is the molecular mechanism of interlayer slippage.

**Comparison with SFA experiments:** In shearing SFA experiments of oligomers very often a stick-slip motion is observed [48], but this is due to the high loads exerted on these *ultra-thin* systems and the instabilities of the springs used for the lateral motion. The high normal pressures exerted on these systems of 2-3 layers of oligomers (n-hexane to tetradecane) leads to a very dense, and thus very sluggish, confined fluid, for which practically only the two adsorbed layers on the mica surfaces are probed (fig. 9 in [48]). At the same time the mica surfaces used are strongly attractive for nearly all the systems reported. This causes (§ 2.2) the development of two adsorbed layers with glassy dynamics and very high resistance to flow<sup>10</sup> which brings into play the instabilities of the springs by means of which one of the surfaces is pulled past the other (fig. 2 of [48]). More systematic SFA studies, trying to explore the effect of the wall energetics, used either evaporated metal oxides [76] or chemically attached self assembled monolayers of small molecules [75] in order to change the wall affinity of mica. Their findings suggest quantitative and qualitative differences in the sliding and the slip at the steady state in comparison with the classical mica SFA experiments [48]. These studies, and in particular Granick et al's [75], state that when strongly attractive surfaces –e.g. bare mica– are used, the “slip occurs within the film” and for moderately attractive surfaces –e.g. mica covered by OTE monolayer– the “slip is taking place at the solid wall”. These assumptions explain very nicely the experimentally obtained behaviour although they are derived in a more or less intuitive way and presented as is without any further justification<sup>11</sup>.

On the other hand, Horn et al [49] used an algorithm based on the Chan and Horn method [18] to evaluate the viscous forces in systems of confined PDMS between mica<sup>12</sup> and agreement with their SFA results was obtained only “when stick boundary conditions apply at a distance of 1.5nm from each surface” and thus “the shear plane is located inside the film”. Though the above conclusions were derived by fitting equations to experimental data, the physical justification provided for this assumption is extremely close to what the MD simulations reported herein find as well. What Horn et al proposed ([49] pg. 6772ff) is a “pinning effect” of the adsorbed chains resulting in very slow dynamics and “immobilisation” of the adsorbed chains and at the same time a physical connection in the form of “entanglements” between tails and loops of the adsorbed chains and the free chains. These thoughts are in very good agreement with the results presented in this paragraph and the proposed models of previous studies of confined PDMS [56].

**Comparison with other experiments and theory:** Although the theoretical and experimental studies referred to in this paragraph deal mainly with longer chains –sometimes even with entangled melts– they do have great similarities with my simulations as well as with the SFA experiments of oligomers and are in surprisingly good agreement as far as the molecular mechanisms of wall and interlayer slippage are concerned. There is experimental evidence that molten polymers, unlike Newtonian fluids, can slip over a surface for sufficiently high shear rates [74, 77, 78] and this is explained by theoretical approaches

<sup>10</sup> up to three orders of magnitude higher viscosities than the bulk [50]

<sup>11</sup> at the time Granick had a reprint of reference [11]

<sup>12</sup> there is very strong adhesion between PDMS and mica in our reduced units the energy of interaction would correspond to values of  $\epsilon_w$  higher than 3 [9]

[69] and stochastic simulations [80, 81] under the *crucial* conditions that there is a weak wall attraction and moreover a physical connectivity between adsorbed and free chains (either through real entanglements or by protruding tails and loops of the adsorbed chains inside the polymer melt). From a theoretical viewpoint, it has been shown by de Gennes [69] that a polymer melt flowing near a smooth, nonadsorbing, solid surface will always slip for any shear rate.

Brochard and de Gennes (BG) have recently developed a theory [82, 83] describing the response to flow of a melt near a strongly adsorbing surface. Although the theory was initially introduced for end grafted chains [82], conclusions are derived also for the case of wetting and flow near a strongly *physisorbing* surface [83]. To briefly recapitulate their conclusions, strong slip is expected near smooth nonadsorbing or weakly adsorbing surfaces. For stronger wall affinities BG expect that some chains will bind strongly to the surface creating a “fluffy carpet” and by extending into the melt they offer a link with the chemically identical melt suppressing any slippage. With increasing shear rates there is a nonslipage to slippage transition. The mechanism that they propose is that “the adsorbed chains undergo a coil stretch and disentangle from the melt”. The adsorbed chains lie on the wall and thus the surface is covered by a neutral layer of polymer which allows slip to take place. These ideas were also exploited by Bruinsma [84] who proposed a “two-fluid model” for a melt of chemically identical chains in the vicinity of a surface, with an immobilized, glassy, adsorbed layer and a bulk melt slipping over it, placing the slip plane exactly between the adsorbed layer and the free chains.

Usually experimental studies reporting slip infer it indirectly from the macroscopic behaviour. On the other hand, a method has been developed recently by Leger et al [78] that enables the direct observation of the velocity profile for extremely small distances near a surface. This method is an optical technique combining evanescent wave induced fluorescence (EWIF) and fringe pattern fluorescence recovery after photobleaching (FPFRAP) [85]. Moreover polymer melts have been studied in the vicinity of very strongly physisorbing surfaces (PDMS on silica) and weakly physisorbing surfaces (PDMS on silica covered by an OTS monolayer<sup>13</sup>) in a parallel plate Couette flow geometry. These experimental findings [78, 79] are in very good agreement with the BG theoretical predictions. They reveal the existence of an immobilized adsorbed layer near the wall. Slip is suppressed for low shear rates by means of a physical connectivity between the free bulk through the tails of the adsorbed chains extending in it. Slippage comes into play after strong enough flows are imposed, as predicted by the BG theory.

The theoretical and experimental studies reported in this paragraph deal mainly with long entangled polymer melts and only a qualitative comparison with the simulation situation should be made. The ideas used, to account for the behaviour of slippage, however, are almost identical in the two cases. Finally, it should be mentioned that the understanding and control of slip can be put to use in practical systems, such as extruders and pipe flows, where flow of polymer near a surface takes place and very often chains attach on the walls.

---

<sup>13</sup> a novel LB method was developed to created pure and mixed monolayers of aliphatic chains (octadecyltrichlorosilane: OTS) on silica with a silanation reaction [86]

### 3.3 The nature of shear thinning in nm confinements

Recent experimental studies of ultra thin films by the Surface Forces Apparatus (SFA) reveal striking behaviour in the rheological response of lubricating films when confined in dimensions comparable to the molecular size [48, 50, 51, 53, 18, 54, 55, 56]. Such films become strongly inhomogeneous [18] and their effective viscosity increases dramatically when reducing the film thickness [50]. Moreover they exhibit shear thinning for very moderate shear rates and the onset of this non-Newtonian behaviour shifts to lower shear rates in narrower confinements [54, 55]. Molecular Dynamics (MD) computer simulations have proven to be effective in interpreting this counter-intuitive behaviour of nanoscopically confined films. Equilibrium MD studies[9, 46] revealed the *origin of the “glassy” dynamics* in ultra-thin confinements. It was demonstrated that the molecular process behind the observed increase of the effective viscosity involves dramatic increases in the relaxation times inside the solid-oligomer interface, due to a decreased segmental mobility of the adsorbed oligomers. Moreover, it was shown that this segmental slowing down is caused by the densification inside the adsorbed layer, rather than by the bare adhesive energy barriers [9, 36].

On the other hand, the phenomenon of shear thinning in *nano*-confinements is not well understood. Pioneering shear-SFA studies of oligomers demonstrated that, in the non-Newtonian regime, where the effective viscosity ( $\eta_{eff}$ ) depends on the shear rate ( $\dot{\gamma}$ ), the viscosity decreases following a power law:  $\eta_{eff} \sim \dot{\gamma}^{-2/3}$ , which seemed to be a universal behaviour [54]. Subsequent Non-Equilibrium Molecular Dynamics computer simulations verified this power law, but at the same time showed the possibility of a richer response to shear [10]. Since then, a variety of shear thinning power laws have been reported in the literature and sometimes by the same researchers and for the same chemical systems: the above mentioned behaviour  $\eta_{eff} \sim \dot{\gamma}^{-0.67}$  was obtained for OMCTS and dodecane [54, 55],  $\eta_{eff} \sim \dot{\gamma}^{-0.52}$  for hexadecane [55] and  $\eta_{eff} \sim \dot{\gamma}^{-0.44}$  for poly(phenyl-methyl-siloxane) (PPMS)<sup>14</sup> [53]. In all these cases a common behaviour is observed for wide enough films: linear Newtonian-like response for small shear rates, followed by extensive, power law, shear thinning. However, quantitative divergences do exist (e.g. in the shear thinning power law) and reflect the differences in properties of the systems under investigation such as: film thickness, differences in applied pressure, isobaric or isochoric experiments and differences in the surface-fluid interactions and the chemical composition of confined fluids. In order to gain more insight in the mechanisms of shear thinning in films of nanometer thickness, we carried out Molecular Dynamics simulations of confined oligomer fluids under Couette flow [36, 11, 25].

Several different oligomer molecules were studied: linear pentamers, hexamers and decamers, a pentamer with a branched bead connected to the middle segment and a small symmetric three arm star heptamer (figure 3.10). Moreover, three different film thickness were simulated:  $h = 10\sigma$  which allows the development of a wide enough middle part and two well separated interfacial layers and  $h = 7\sigma$  or  $6\sigma$  which correspond to the

---

<sup>14</sup> all these systems where confined between mica at a separation approximately 6 molecular diameters; further discussion concernig these experimantal findings concludes this letter

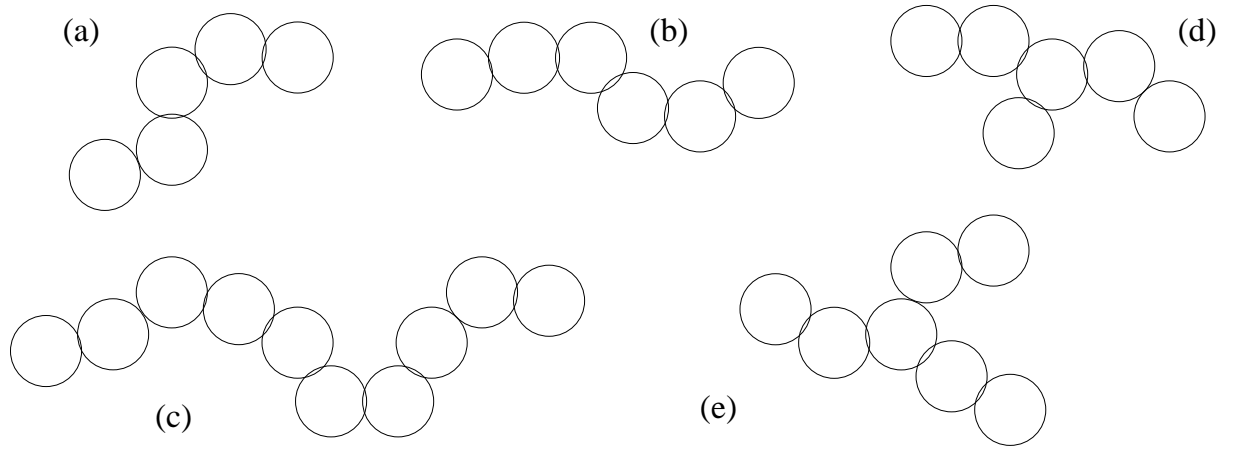


**Figure 3.10:** The molecular architectures of the oligomer molecules simulated. Linear pentamer (a), hexamer (b), decamer (c), branched hexamer (d) and symmetric three-arm star heptamer (e).

confinements for which strong deviation from bulk-like behaviour starts to appear [54, 10] and which relate to the thickness of most of the experimental systems.

In order to determine the actual shear rate that the film is subjected to, one has to take into account the flow boundary conditions at the wall and the slip. For example for  $\epsilon_w = 1.0\epsilon$  there is slip between the wall and the fluid, whereas for stronger wall affinities the slip localized inside the fluid film between the adsorbed layer and the rest of the system (fig. 3.11)[11]. When calculating the induced shear rate across the whole film the slip has to be subtracted. Moreover, a local shear rate at  $z_0$  can be defined as  $\dot{\gamma}_{local} = \left(\frac{\partial v_x}{\partial z}\right)_{z_0}$ . Although for these strongly inhomogeneous systems the definition of viscosity is very subtle, for the study of their dynamic response a quantity that is correlated with the resistance of the fluid to flow is usually defined by the mean frictional force per unit area (which is the  $xz$  stress component) divided by the induced shear rate [10]:

$$\eta_{eff} = \frac{\tau_{xz}}{\dot{\gamma}} = \frac{F_{frict}}{S \dot{\gamma}} \quad (3.4)$$

$\eta_{eff}$  has dimensions of viscosity and is named *effective* or *apparent* viscosity (this is also the way that  $\eta_{eff}$  is measured in SFA experiments [48, 50, 51, 53, 54, 55, 56]). This quantity characterizes the response of the whole film. In the same manner, taking into account that in steady state flow the stress tensor components are constant throughout the system[93], we can define a *local effective viscosity* as the stress component divided by the local shear rate. Observing now the steady state velocity profiles that are developed across these films (fig. 3.11) it becomes obvious that the local shear rate inside the adsorbed layer is smaller than in the middle and thus the fluid in the vicinity of the wall is of higher viscosity than further away from the surfaces. The existence of this “more viscous” adsorbed layer was suspected through the experiments [56] and reveals a slowdown of the chain and segment mobilities [36] and an increase of the relaxation times [9] inside the

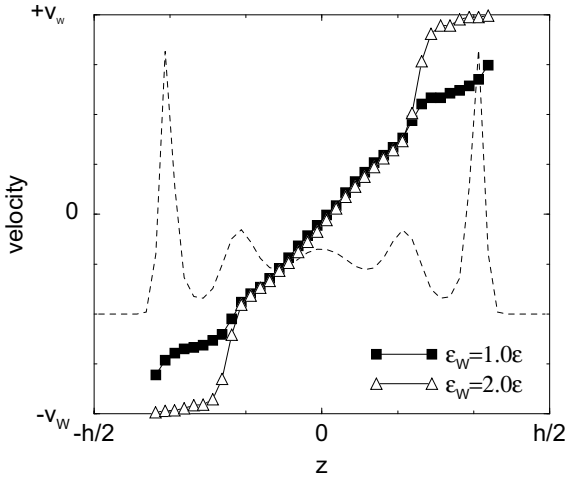


**Figure 3.11:** Density and steady state velocity profiles for a fluid oligomer lubricant confined between weakly ( $\epsilon_w = 1$ ) and strongly ( $\epsilon_w = 2$ ) adsorbing surfaces. A sufficiently high wall velocity ( $v_w$ ) is shown for slip to appear; the location of the slip is determined by  $\epsilon_w/\epsilon$ .

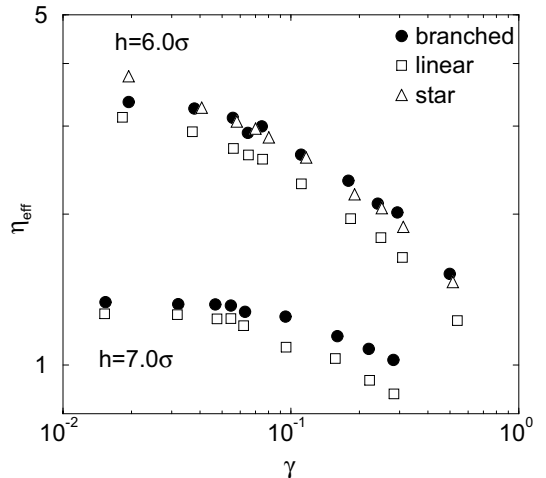


**Figure 3.12:** Total film effective viscosity versus shear rate, for different molecular architectures (linear hexamers, branched hexamers and 3arm star heptamers). Results for two pore widths are shown:  $h = 7\sigma$  (bottom sets of points) and  $h = 6\sigma$  (top sets).

solid-oligomer interface. These changes become strongly enhanced with increasing wall affinity (up to three orders of magnitude for  $\epsilon_w = 3$ ).

In figure 3.12 the dependence of the total film effective viscosity on the shear rate is shown for these two film thicknesses. In agreement with experiments a decrease in the confinement causes an increase in the effective viscosity. Moreover, the onset of the shear thinning shifts to smaller shear rates for narrower films or for longer chains. At this point it should be mentioned that the absolute value of  $\eta_{eff}$  is not very important as it depends strongly on pressure –and so on density– [10, fig. 2b], and so does the onset of shear thinning. The effect of pressure on the effective viscosity is also observed in SFA experiments: for small oligomers a strong exponential increase is reported [55], and in realistic MD simulations of alkanes [89]. For these reasons the viscosities presented in fig. 3.12 are normalized by the viscosity of a bulk with the same density as the middle part of the film. Moreover, we chose to work at such pressures that the viscosities in the middle part of the films are near their bulk value.

Keeping in mind that the strong confinement of our films results in a highly inhomogeneous system –characterized by both density oscillations and regions of different viscosity– the really interesting quantity is the local  $\eta_{eff}$ . A typical response to shear of a confined film is shown in fig. 3.13: the local effective viscosity is plotted for the adsorbed layers and the middle part of the confined film (linear hexamers,  $h = 6$ ,  $\epsilon_w = 2$ ). Although

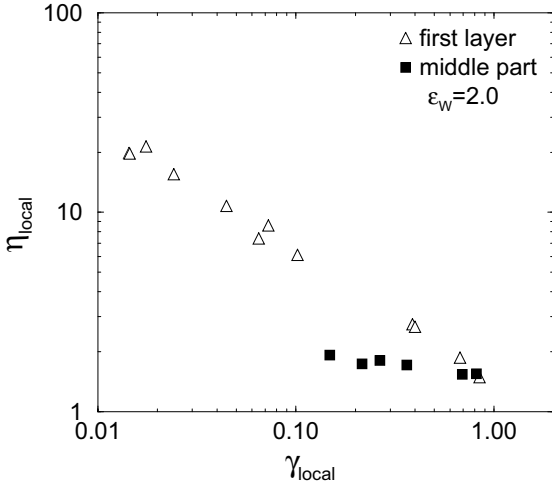


**Figure 3.13:** Typical local effective viscosity versus shear rate inside the first layer and the middle part of the film (hexamers,  $h = 6$ ,  $\epsilon_w = 2$ ). Almost all shear thinning takes place inside the solid-oligomer interface, while the middle part exhibits bulk-like behaviour, even when it's only  $2\sigma$  wide.

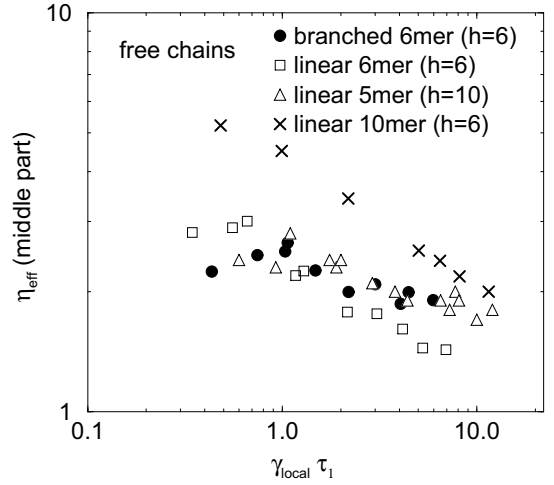


**Figure 3.14:** Local effective viscosity versus shear rate in the middle part of the films for various systems. In order to compare, all viscosities are scaled by the viscosity of a corresponding bulk system (bulk with the same density, pressure and molecular architecture).

inside the solid-oligomer interface the fluid exhibits strong shear thinning, the middle part of the film behaves almost as a Newtonian fluid, i.e. nearly all the shear thinning takes place inside the adsorbed first layer. Furthermore, as expected from the velocity profile ( $-\Delta-$  in fig. 3.11), the viscosity inside the first layer is higher than in the middle part (for the smaller shear rates almost an order of magnitude). At the same time, the viscosity in the middle part of the film is only slightly higher than the bulk value. This strong local variation of the effective viscosity was long suspected by experimentalists [56, 50] and even proposed as an explanation for their observations -both in equilibrium[56] and shearing [55]– but herein is clearly demonstrated. Finally, the response of the total film is the *average* of the response inside the first layer and in the middle of the system *weighted* by the fraction of the system in these two regions<sup>15</sup>.

For the  $h = 6\sigma$ ,  $\epsilon_w = 1\epsilon$  films, the power law decrease of this  $\eta_{eff}$  in the shear thinning region *across the whole film* is a  $\eta_{eff} \sim \dot{\gamma}^{-1/2}$ . This dependence coincides with SFA experiments of wide enough films [53, 55] and with *constant volume* NEMD simulations of flow in the bulk [88, 89, 90] and under confinement [10], but not for constant pressure MD simulations [10]. Recent NEMD studies comparing constant volume and constant pressure

<sup>15</sup> this we calculated to be valid for all the systems, and is a natural consequence of a fluid with viscosity inhomogeneities subjected to flow.

simulations [87] provide the explanation for the deviation in the exponents calculated from NPT and NVT simulations. Under the same pressure and wall affinity the effect of the molecular architecture on the response of the total film effective viscosity is minor, in agreement with previous computer simulations [89, 90, 91] and contrary to what is expected from shear thinning in the bulk[92] and from SFA experiments of much longer polymers[51].

In figure 3.14 the behaviour in the middle of the pore is presented for a variety of systems. There is only a weak shear thinning in this region for our short oligomers. The pore hosting the pentamers is wide enough ( $h = 10$ ) to guarantee that the middle part of the system is sufficiently far from the surfaces so that the oligomers are not affected from them; for the rest of the systems narrower confinements ( $h = 6$ ) were used in order to see the effects of stronger geometric constraints. The Non-Newtonian character is more pronounced for the longer coils –the decamers shear thin more than the hexamers and these more than the pentamers –and also for the linear hexamers compared to the branched ones<sup>16</sup>. This is exactly what is expected to happen in the bulk [92], i.e. the shear thinning is expected to start at lower shear rates for long linear unentangled chains than for shorter ones or for branched chains of the same size. At this point, it should be mentioned that the model oligomers of our simulations which relate [7] to the SFA systems examined to follow power law shear thinning [53, 54, 55] are the pentamers and the hexamers; the bead-spring decamers should be compared with much longer molecules than the ones reported in these experimental studies.

A quantity more relevant to the experimental findings, presented in figure 3.15, is the local effective viscosity inside the solid-oligomer interface. Most of the experiments reporting power laws for shear thinning are studying very thin films of only a few molecular diameters, which implies that they are probing mainly the effective viscosity inside the first layer. Two different approaches are shown. In figure 3.15(a) wide films of pentamers were used in order for the two interfacial regions to be well separated and a variety of wall affinities have been simulated. It becomes clear that the response of the oligomers to shear is determined by the wall affinity. For weakly adsorbing surfaces ( $\epsilon_w = 1$ ) the systems exhibit a Newtonian-like behaviour, with the viscosity being independent of  $\dot{\gamma}$ , but for stronger adsorption energies the systems shear thin throughout the range of shear rates employed in our simulations. The use of a  $\eta_{eff} \sim \dot{\gamma}_{local}^{-\alpha}$  power law to describe the shear thinning for strong enough flows seems to be justified and there is a systematic increase in the exponent with  $\epsilon_w$ . Namely,  $\alpha$  is 0.44 in the linear part for  $\epsilon_w = 1.0$  and becomes 0.53 for  $\epsilon_w = 1.5$  and 0.69 for  $\epsilon_w = 2.0$ . For the strongest wall affinity ( $\epsilon_w = 3$ ) it is very difficult for the slope of the velocity profile to be measured accurately inside the solid-oligomer interface [11] and conclusions can be drawn from strong flows only, the  $\alpha$  in this case being approximately -0.75. For our linear hexamers the same power law seems to be valid and the exponents are -0.40 for  $\epsilon_w = 1.0$  (figure 3.15b) -0.62 for  $\epsilon_w = 2.0$  (figure 3.13) and  $\sim -0.8$  for  $\epsilon_w = 3$ . In figure 3.15(b) the local  $\eta_{eff}$  in the interfacial layer

---

<sup>16</sup> if one would like to fit a power law in the linear part of the  $\log \eta - \log \dot{\gamma}$  graphs in figure 3.14, one would get -0.30 for the decamers, -0.26 for the linear hexamers, -0.16 for the pentamers and -0.19 for the branched hexamers

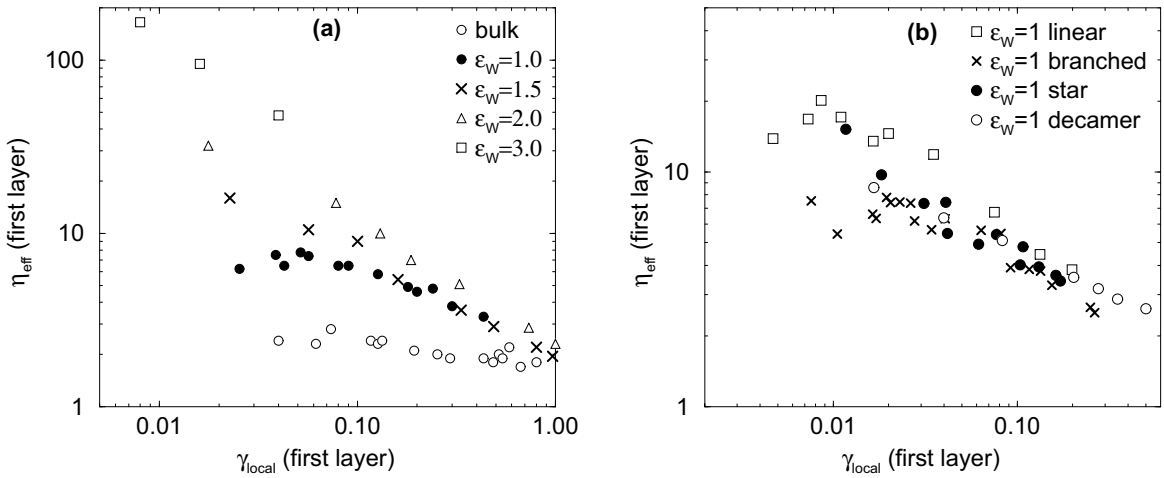


**Figure 3.15:** Local effective viscosity versus shear rate inside the solid-oligomer interface. (a) pentamers in wide enough pores ( $h = 10$ ) to allow the development of two well separated, independent interfacial layers. For higher shear rates the shear thinning can be described by a power law which depends on the wall energetics ( $\epsilon_w$ ). (b) a variety of oligomers in thin pores ( $h = 6$ ) confined between weakly physisorbing surfaces ( $\epsilon_w = 1$ ); there is a weak dependence of the shear thinning power law on the molecule architecture.

is plotted against the local shear rate for a variety of molecule confined in narrower pores ( $h = 6$ ). For these flexible model chains the power law shear thinning does not depend markedly on the molecule architecture, in contrast with the middle part. The exponents that can be derived for the fits in the linear part are -0.40 for the linear hexamers, -0.44 for the branched, -0.42 for the stars, -0.38 for the decamers and -0.44 for the pentamers (figure 3.15a). Furthermore, the effective viscosity is almost an order of magnitude higher than in the middle of the same film and increases with stronger wall attractions, but this increase is smaller than expected from previous MD studies [9, 36].

Our previous studies [11, 25, 36] revealed a strong tendency of the adsorbed chains to align and stretch against the confining surface for the shear rates employed. This behaviour clearly is a major contribution to the shear thinning observed[92]. But, beyond this molecular alignment and deformation, other effects are expected to contribute for these flexible molecules as well, such as the distortion of the neighbour shell and shear-induced changes in molecular rotation and even collective motions and shear-induced structure changes, especially inside the solid-oligomer interface. This broad distribution of relaxation times brings the various intra- and inter-molecular mechanisms into effect at different shear rates, making difficult for the development a quantitative description. Even when only the finite extensibility of the chains is taken into account, our theoretical approaches to the problem of flow next to surfaces demonstrate that different molecular mechanisms give rise to a variety of regimes with different viscosity dependence on shear rate [94].

**Table 3.1:** Power law fits ( $\eta_{eff} \sim \dot{\gamma}^{-\alpha}$ ) to the shear thinning regions for various systems. Nearly all the shear thinning takes place inside the solid-oligomer interface and the power law –describing the response of viscosity– is determined by the wall affinity, whereas is rather insensitive to the oligomer molecule architectures. In the middle of the film we only fit a power law for comparison reasons, inspired by the experimental standard procedures.

		local effective viscosities		
$\epsilon_w(\epsilon)$	$h(\sigma)$	type of oligomer	$\alpha$ middle part	$\alpha$ first layer
1.0	6	linear decamer	0.30	0.38
1.0	6	linear hexamer	0.26	0.40
1.0	6	branched 6mer	0.19	0.44
1.0	6	3arm star 7mer	0.20	0.42
1.0	7	linear hexamer	0.18	0.41
1.0	7	branched 6mer	0.12	0.43
1.0	10	linear pentamer	0.16	0.44
1.5	10	linear pentamer	0.16	0.53
2.0	10	linear pentamer	0.16	0.69
2.0	6	linear hexamer	0.13	0.62
3.0	10	linear pentamer	0.16	$\sim 0.80$
3.0	6	linear hexamer	0.14	$\sim 0.78$

Summarising, we studied with Non-Equilibrium Molecular Dynamics simulations nanoscopically confined films under shear. We observed that the viscosity inside the solid-oligomer interface is increased compared to the bulk value, due to the dramatic increase of the relaxation times [9] and the simultaneous decrease of the transport coefficients therein. Moreover, nearly all the shear thinning takes place in exactly this region and the power law –describing the response of viscosity– is determined by the wall affinity, whereas is rather insensitive to the oligomer molecular architectures. The behaviour of the whole films is the weighted average of the viscosities inside the interfacial layers and the middle part; this explains the absence of a universal law for the shear response of nanoconfined fluid lubricants. The viscosity increases reported here are not as high as in some experiments[54], but one has to take into account that the loads used in those experiments are greater than the ones used by us, and the viscosity is expected to increase dramatically with pressure [10, 55].

All this enables us to explain the experimentally obtained behaviour of the viscosity in *nm-confinements*. Since the total film response is the weighted average of the interfacial and the middle part viscosity it is expected to scale as  $\eta_{eff} \sim 1/h$  and this is what is reported for confined oligomers [95, fig. 3]. Moreover for the various shear thinning

laws reported, the  $\eta_{eff} \sim \dot{\gamma}^{-2/3}$  behaviour was obtained for small ring silicones (octa-methyl-cyclo-tetra-siloxane: OMCTS) confined between mica in *ultra*-thin films of two [54, fig. 2] or three [55, fig. 6] confined layers. It should be pointed out that the affinity between mica and siloxanes is very strong [95]. The same power law  $\eta_{eff} \sim \dot{\gamma}^{-0.67}$  was observed for short *n*-alkanes (dodecane) under high pressures (120 Pa at  $h \simeq 6\sigma$ ) [54, fig. 2] whereas for smaller pressures (6.5 Pa at  $h \simeq 6.5\sigma$ )  $\eta_{eff} \sim \dot{\gamma}^{-0.52}$  was obtained [55, fig. 3] with a simultaneous threefold decrease of viscosity. For fluids of smaller affinity for mica (PPMS) shear thinning follows  $\eta_{eff} \sim \dot{\gamma}^{-0.44}$  for  $h = 6$  and  $5\sigma$  separations, while Newtonian behaviour is observed for wide films  $h \simeq 17\sigma$  [53, fig. 5a]; when weakly adsorbing surfaces are used (OTE covered mica, which is effectively a smooth CH<sub>3</sub> surface) “*the viscosity drops below the limit for experimental measurement*” [57, pg. 3878]. Finally, non-equilibrium MD simulations of nanometric oligomer films under shear [10] under constant pressure showed that shear thinning can be described by a power law, and the -2/3 exponent fits best the response of ultra-thin films of two layers and wider films under high pressures [10, fig. 2 & 3]). The same simulations under constant volume gave a slower decrease:  $\eta_{eff} \sim \dot{\gamma}^{-1/2}$ .

## Chapter 4

### Confined films under shear (II)

Having discussed already some of the aspects of the rheology in nanometric confinements in the previous chapter, such as the shape of the velocity profile, the character of slip and its molecular origin and the nature of the Non-Newtonian behaviour of viscosity, in this chapter a more *phenomenological approach* is attempted *to the shear properties of nanoscopically confined oligomer melts*.

The way that shear flow affects the inhomogeneous density profile across a pore is discussed and a connection with the shear induced conformational changes of the adsorbed oligomers is made. The effect of shear on the structure of the adsorbed layer is also discussed, whereas the orientation of the adsorbed coils is considered from the viewpoints of chain conformations, bond orientations, radius of gyration and chain orientation. Moreover the flow induced deformation and alignment of the free coils is also discussed by analyzing the effect of shear on the radius of gyration tensor.

The molecular architecture of the oligomers is also varied –shorter and longer linear chains are used and small branches are added to the backbone. The molecules are altered in search of trends in how the rheological properties of the confined films depend on the molecular response to shear. The effect of different oligomers on the velocity profile, on the shape and orientation of chains under shear and on the conformations of the adsorbed chains is discussed.

Finally, the effect of shear on the pressure and the stress *in films of constant thickness* is discussed as a function of shear rate. This is another way of looking at the same information that the effective viscosity –as defined in the previous chapter– provides.

## 4.1 The effect of flow on the adsorbed chains and the density

It became evident, from the discussion of the previous chapter, that the most important flow induced structural change in these nanoscopically confined films of oligomers is the stretching of the adsorbed chains and their preference to become fully adsorbed on the walls. In order to probe further how this flow induced alignment affects the properties of the confined systems, a more quantitative approach to the conformations of the adsorbed coils under shear is made here. In table 4.1 the probability distribution of the adsorbed conformations is shown (for hexamers confined in  $h = 6\sigma$  pores):

**Table 4.1:** Probability of the adsorbed hexamers to have one to six contacts (cont.) with the surfaces. The wall velocity  $v_w$  is in MD units and the film thickness is  $h = 6.0\sigma$ .

	$v_w$ in units of $(\epsilon/m)^{1/2}$							
	0.0	0.1	0.2	0.3	0.5	0.9	1.5	2.0
$\epsilon_w = 1.0\epsilon$								
1 cont.	0.12	0.11	0.11	0.11	0.11	0.10	0.10	
2 cont.	0.17	0.16	0.15	0.15	0.13	0.11	0.11	
3 cont.	0.19	0.17	0.17	0.16	0.14	0.13	0.12	
4 cont.	0.18	0.17	0.18	0.17	0.17	0.17	0.16	
5 cont.	0.18	0.20	0.19	0.20	0.21	0.21	0.21	
6 cont.	0.16	0.19	0.20	0.21	0.24	0.28	0.30	
$\epsilon_w = 2.0\epsilon$								
1 cont.	0.07	0.08	0.05	0.08	0.05	0.05		0.05
2 cont.	0.10	0.09	0.08	0.10	0.07	0.06		0.05
3 cont.	0.14	0.13	0.14	0.14	0.10	0.06		0.06
4 cont.	0.17	0.19	0.17	0.15	0.12	0.08		0.07
5 cont.	0.22	0.20	0.24	0.19	0.17	0.18		0.12
6 cont.	0.30	0.31	0.32	0.34	0.49	0.57		0.65
$\epsilon_w = 3.0\epsilon$								
1 cont.	0.07	0.00	0.09	0.08	0.02	0.01		0.03
2 cont.	0.11	0.05	0.09	0.10	0.04	0.08		0.05
3 cont.	0.13	0.17	0.09	0.07	0.08	0.11		0.05
4 cont.	0.17	0.25	0.15	0.04	0.04	0.04		0.06
5 cont.	0.23	0.20	0.10	0.17	0.15	0.09		0.06
6 cont.	0.29	0.33	0.48	0.54	0.67	0.67		0.75

Although for simple liquids flow does not affect at all the density profiles of confined films, even for extremely high shear rates [26], for these oligomers the conformational changes of the adsorbed chains are expected to be reflected in changes of the density profile. In figure 4.1a the density profiles of the above systems are shown. For  $\epsilon_w = 1$  the magnitude of change in the density profiles is surprisingly small across the whole range of

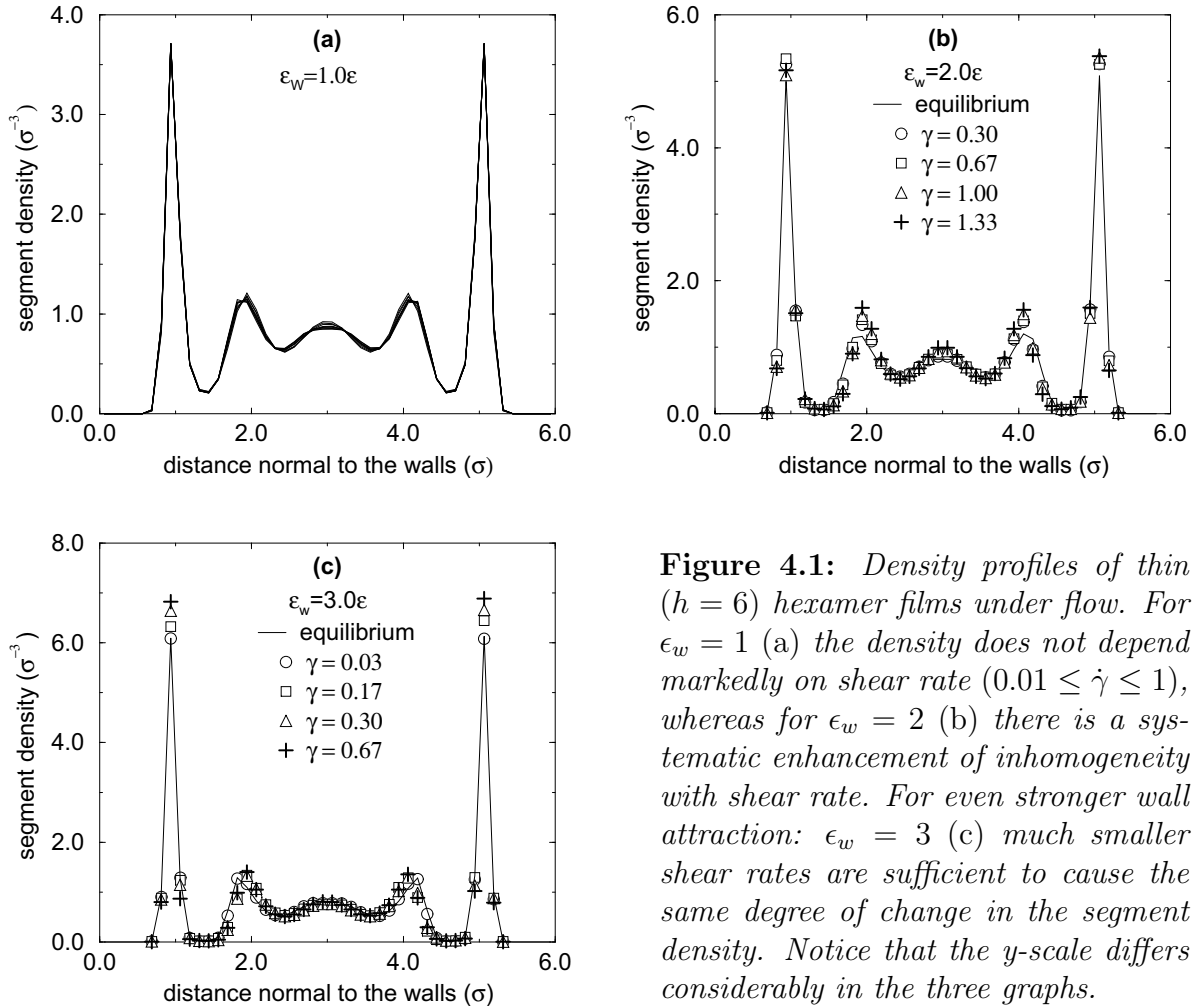


**Figure 4.1:** Density profiles of thin ( $h = 6$ ) hexamer films under flow. For  $\epsilon_w = 1$  (a) the density does not depend markedly on shear rate ( $0.01 \leq \dot{\gamma} \leq 1$ ), whereas for  $\epsilon_w = 2$  (b) there is a systematic enhancement of inhomogeneity with shear rate. For even stronger wall attraction:  $\epsilon_w = 3\epsilon$  (c) much smaller shear rates are sufficient to cause the same degree of change in the segment density. Notice that the y-scale differs considerably in the three graphs.

imposed shear rates (table 4.1:  $0.0 \leq v_w \leq 0.9(\epsilon/m)^{1/2}$ ); even though the adsorbed chain conformations change from a distribution with approximately equal probabilities for 1 to 6 contacts at equilibrium, to a distribution with 50% of the chains being almost fully adsorbed (5 or 6 contacts) for the highest shear rate ( $\dot{\gamma} = 0.5$ ). This shows that there is only a weak dependence of the density profile on shear and on the conformations of the adsorbed chains. For  $\epsilon_w \geq 2$ , however, the shear induced conformational changes are so strong that result in measurable deviations of the density with respect to the equilibrium profile (figure 4.1b, c). There is a systematic enhancement of the inhomogeneity with  $\dot{\gamma}$ , demonstrated by the increase of the density maxima in the first and second layer and the decrease of, the already extremely small, density inside the depletion zones<sup>1</sup> ( $z \simeq 1.4\sigma$  and  $z \simeq 4.6\sigma$ ). Moreover, as for the  $\epsilon_w = 3\epsilon$  surfaces the adsorbed chain conformations change more “drastically” with increasing  $\dot{\gamma}$ , smaller imposed shear rates are sufficient to

<sup>1</sup> the flow induced molecular changes responsible for the change of the second density peak are discussed in the section dealing with the shape of the chains under shear flow (§ 4.5)

**Table 4.2:** Probability of the adsorbed decamers to have one to ten contacts with the surfaces. ( $v_w$  in MD units:  $(\epsilon/m)^{1/2}$  and  $h = 6.0\sigma$ )

$v_w$ :	number of contacts									
	1	2	3	4	5	6	7	8	9	10
$\epsilon_w = 1.0\epsilon$										
0.00	.07	.11	.12	.12	.12	.12	.10	.10	.09	.06
0.05	.07	.11	.12	.12	.12	.12	.11	.10	.09	.05
0.10	.05	.11	.10	.11	.13	.13	.13	.10	.09	.06
0.20	.06	.11	.10	.10	.10	.11	.11	.12	.11	.08
0.50	.08	.08	.08	.08	.09	.10	.12	.13	.13	.11
0.70	.08	.08	.07	.07	.08	.10	.12	.14	.14	.13
0.90	.08	.08	.07	.07	.08	.09	.10	.13	.16	.15
1.50	.08	.07	.07	.07	.08	.09	.11	.12	.15	.16
$\epsilon_w = 2.0\epsilon$										
0.00	.05	.06	.11	.14	.14	.11	.11	.09	.08	.09
0.10	.03	.08	.08	.09	.08	.10	.13	.13	.13	.14
0.20	.05	.06	.06	.04	.03	.06	.09	.15	.21	.24
0.40	.04	.04	.05	.04	.04	.08	.11	.14	.20	.26
0.50	.04	.05	.05	.05	.07	.07	.10	.15	.19	.24
0.60	.04	.05	.07	.08	.04	.03	.05	.10	.17	.38
0.70	.04	.04	.03	.04	.04	.06	.07	.13	.19	.36
0.90	.04	.04	.04	.06	.04	.04	.06	.09	.16	.43
1.50	.05	.05	.04	.03	.03	.04	.04	.06	.13	.52
$\epsilon_w = 3.0\epsilon$										
0.00	.01	.04	.10	.16	.11	.14	.10	.11	.12	.12
0.10	.01	.05	.07	.08	.05	.15	.14	.09	.10	.26
0.50	.01	.01	.01	.05	.04	.22	.09	.15	.14	.28
0.90	.03	.006	.003	.06	.001	.015	.05	.03	.10	.70
1.50	.01	.005	.005	.01	.05	.08	.01	.03	.06	.74

cause the same effect on the density profile (figure 4.1c) compared with the case of  $\epsilon_w = 2$  (figure 4.1b). The conformations of the adsorbed chains at equilibrium for these rather short chains (hexamers) depend on the wall affinity (table 4.1) but this seems to be a consequence of their size being comparable to the equilibrium train size near strongly adsorbing walls ( $\sim 4.25$  segments [38]) and the compressibility of our systems.

It is obvious that under strong flow there is a competition between the frictional forces originating from the velocity gradient trying to elongate the chain and the restoring force due to the entropic loss of stretched conformations [96, 45]. Next to a surface the same idea can be exploited to study the deformation of a tethered chain [97, 98]. Our case is not so easy to be analysed theoretically since these systems are not completely incompressible. But even for incompressible melts near adsorbing surfaces the chains are expected

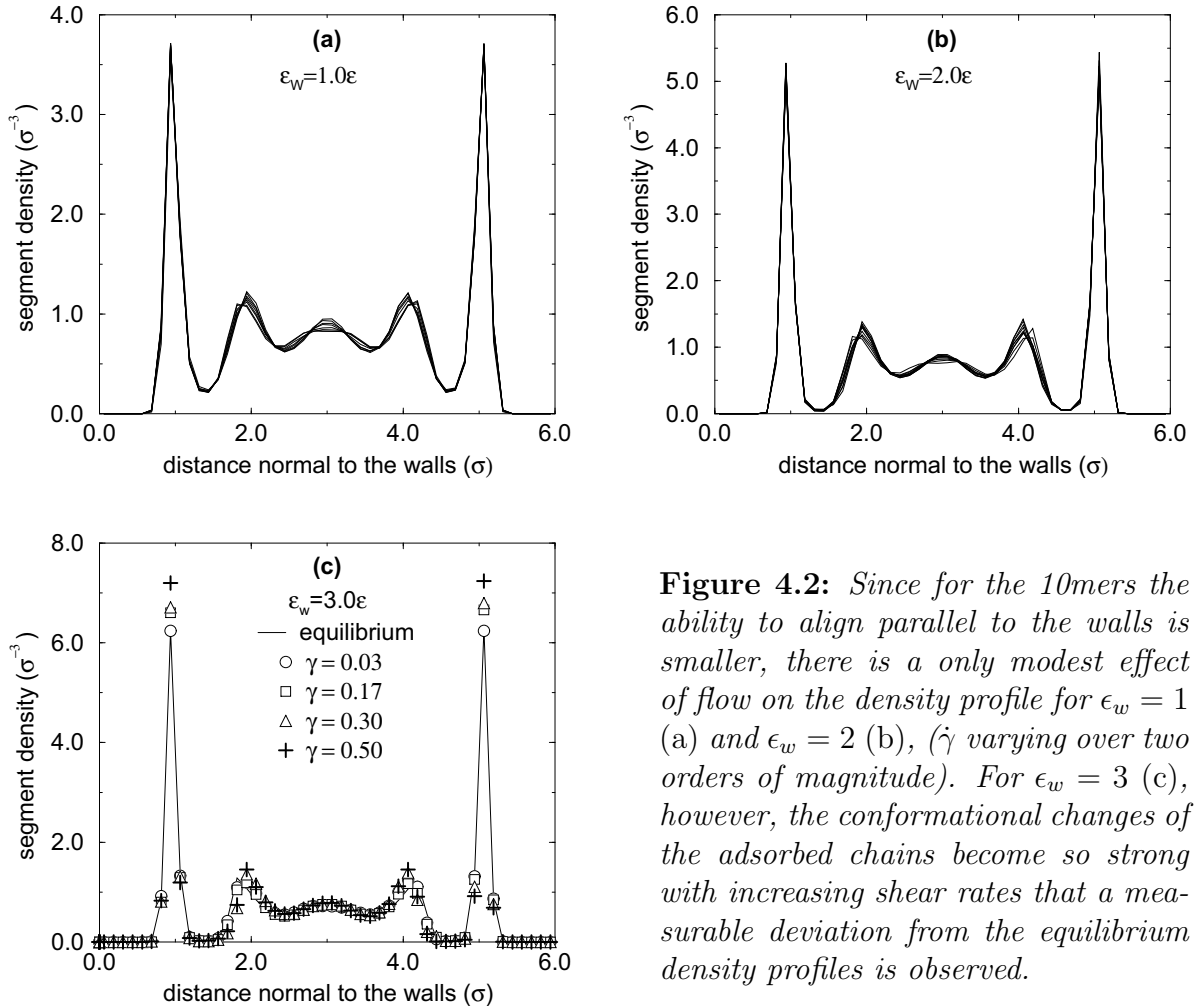


**Figure 4.2:** Since for the 10mers the ability to align parallel to the walls is smaller, there is a only modest effect of flow on the density profile for  $\epsilon_w = 1$  (a) and  $\epsilon_w = 2$  (b), ( $\dot{\gamma}$  varying over two orders of magnitude). For  $\epsilon_w = 3$  (c), however, the conformational changes of the adsorbed chains become so strong with increasing shear rates that a measurable deviation from the equilibrium density profiles is observed.

to stretch parallel to flow and under strong shear rates to prefer conformations which are strongly adsorbed [94]. The probability distribution of the adsorbed conformations for longer oligomers (decamers) is given in table 4.2. The adsorbed conformations at equilibrium do not change so much with  $\epsilon_w$  increasing from  $1\epsilon$  to  $3\epsilon$ , but under shear there is again a systematic tendency for the adsorbed chains to align parallel to flow, thus becoming more strongly adsorbed (more surface contacts). For these longer chains the entropic loss for strongly stretched conformations is greater than for the shorter hexamers and thus, for the same wall attraction, higher shear rates have to be employed to stretch the chains towards fully adsorbed conformations. For this reason the decamer population become primarily “fully” adsorbed ( $\sim 80\%$  with 9, 10 contacts) only for the  $\epsilon_w = 3$  walls and the strongest imposed  $\dot{\gamma}$ . This is also reflected in the respective density profiles that do not change markedly with flow for  $\epsilon_w = 1$  and 2, and only for the  $\epsilon_w = 3$  surfaces can a measurable deviation be observed (figure 4.2).

## 4.2 The effect of flow on the structure of the adsorbed layer

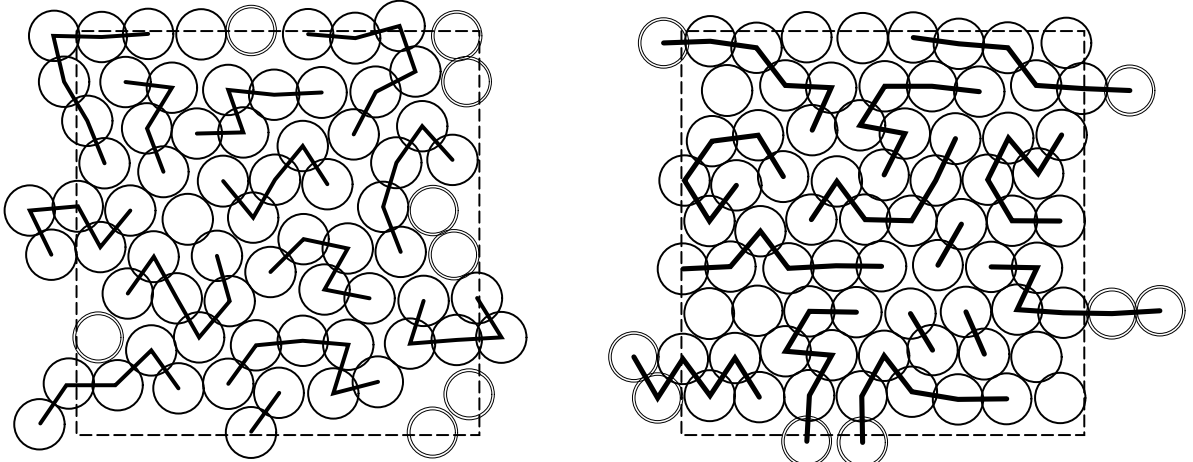


**Figure 4.3:** A snapshot of the first layer near the  $\epsilon_w = 3\epsilon$  surface, at equilibrium (left) and under shear (right:  $v_w = 0.9$ ). Clearly under flow there is an enhancement of ordering. With double circles are denoted the beads which were copied, through the periodic boundary conditions, to be connected to the rest of the chain which they belong.

For the strongly physisorbing surfaces flow causes a densification inside the, already very dense, first layer. Since the in-plane ordering is a direct result of the elevated densities next to a surface (§§ 2.1.3 & § 2.3) one would expect that there is an enhancement of the in-plane ordering. Using again the two dimensional radial pair correlation function, as defined by equation 2.6, the degree of in-plane structure<sup>2</sup> inside the solid-oligomer interface can be monitored with increasing shear rate. In figure 4.4 the radial pair correlation function (pcf) is plotted for the first layers of hexamers in the  $h = 6$  pores. For the weakly physisorbing surfaces ( $\epsilon_w = 1\epsilon$ ) the pcf does not change with flow, as expected by the constant density of the first layer under flow (figure 4.1a). For the more structured interfacial layers near the  $\epsilon_w = 2$  surfaces there is only a very weak change of the pcf reflecting the small changes of the first layer density under shear (figure 4.1b). For the adsorbed layers on the  $\epsilon_w = 3$  surfaces, however, there is an apparent enhancement of the in-plane ordering of the first layer, which was already rather structured at equilibrium (figure 4.4). The same behaviour is observed for the decamers with the pcf being insensitive to flow for  $\epsilon_w = 1$  and 2, but showing a smooth change towards a more structured first layer with increasing shear rate for  $\epsilon_w = 3$ .

<sup>2</sup> it should be noted that this is the (time) average ordering inside the first layer. Phenomena like desorption-adsorption processes or shear induced destruction of ordering do take place and disturb the structure of the first layer for short time periods [30]

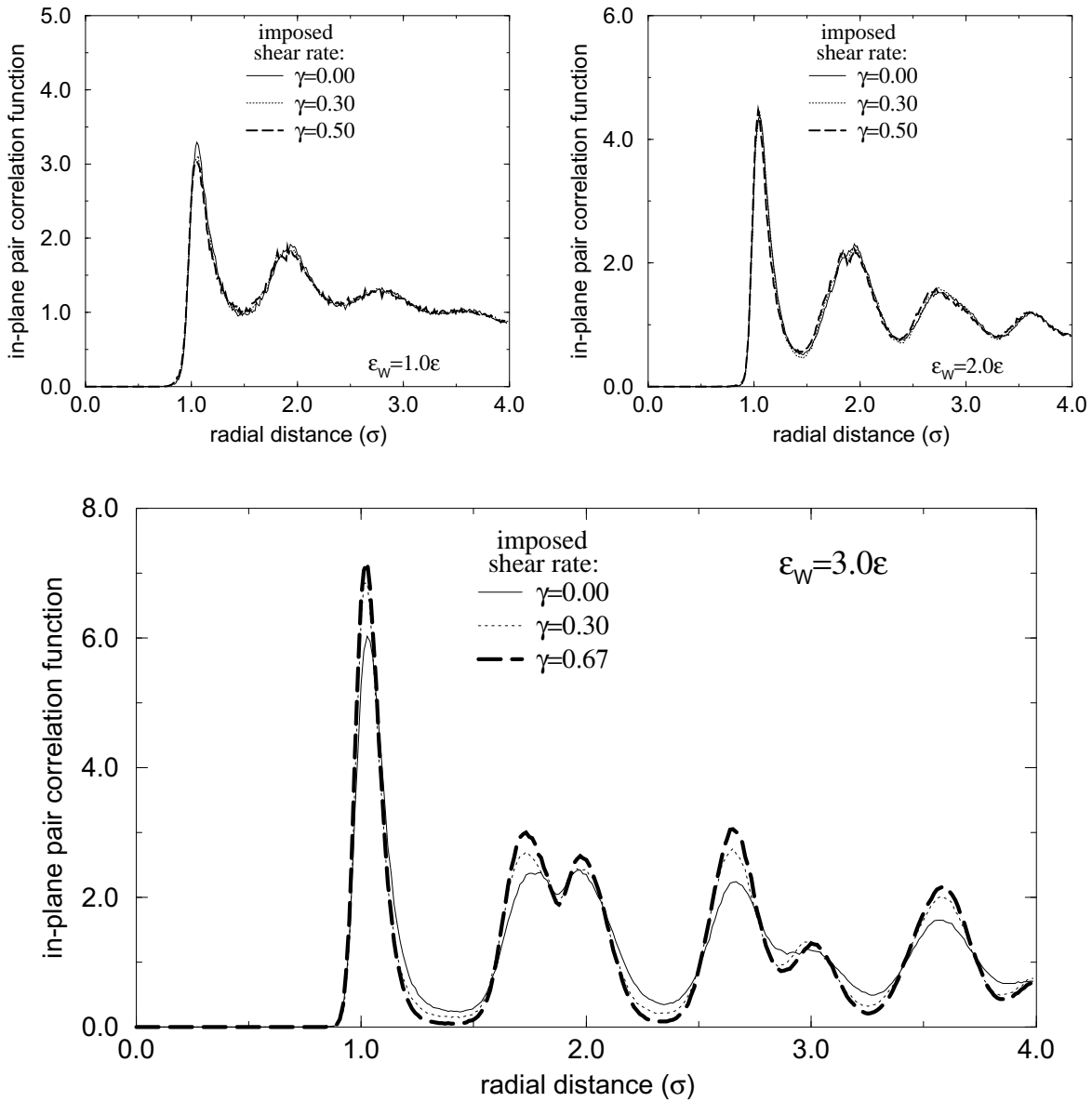


**Figure 4.4:** The ordering inside the first layer as depicted through the in-plane radial (cylindrical) pair correlation function at equilibrium and two shear rates (hexamers,  $h = 6$ ). For the  $\epsilon_w = 1$  surfaces the pcf does not change with flow, for  $\epsilon_w = 2$  there is a small effect and for  $\epsilon_w = 3$  there is a definite enhancement of ordering with increasing shear rate.

This enhancement of ordering is due to the better packing of the monomers, rather than the ordering of the oligomer chains (figure 4.3). It is well known that for certain oligomers and polymers, e.g. the n-alkanes, the *all-trans* conformations are energetically the lowest. These oligomers, when in a vicinity of a surface, tend to adopt *all-trans* con-

formations and to pack parallel to each other forming a structured monolayer<sup>3</sup>. Flow promotes further this parallel packing through the alignment of the chains inside the flow field. But even at equilibrium, the bare increase of the wall affinity is sufficient to cause a better packing of adsorbed short alkanes parallel to each other and thus an enhanced ordering in the pcf [99]. For our flexible, freely jointed, coils there are no energetics introduced through a dihedral potential and the enhanced ordering is due to better packing of the adsorbed segments. With shear there is also a very weak alignment parallel to the streamlines, which will be discussed in a following paragraph (§§ 4.5, 4.3).

---

<sup>3</sup> sometimes even crystalline ordering can be achieved near surfaces favouring epitaxy

### 4.3 Bond orientation factor

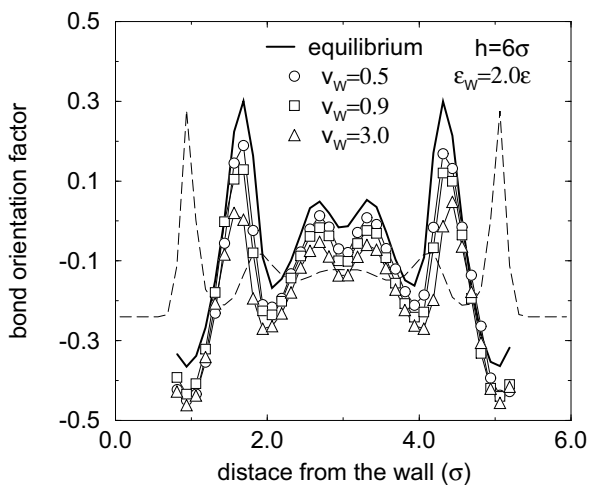
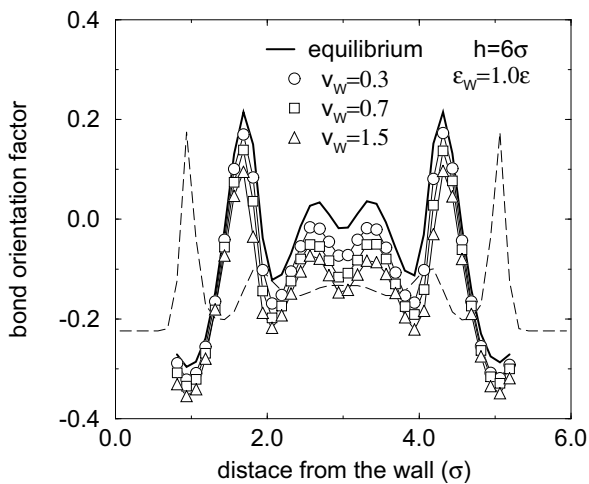
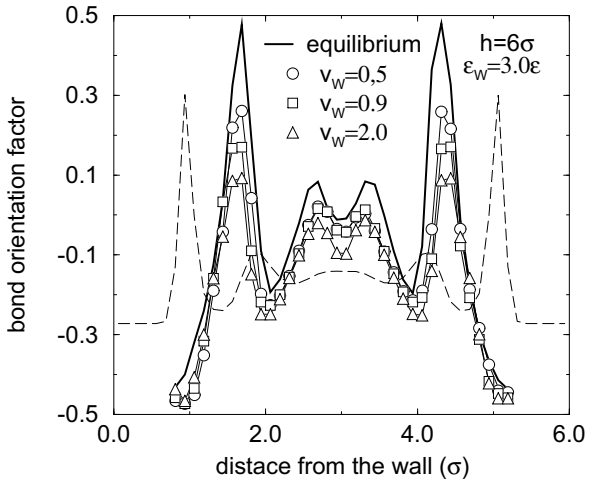


**Figure 4.5:** The bond orientation factor with respect to the normal direction to the walls ( $z$ ) for hexamer films. The bonds are parallel to the walls inside the first and second layer, due to layering and align even better with shear flow. In the middle of the film a weak orientation parallel to flow affects also the bond orientation with respect to  $z$  causing a small systematic decrease.

$$s(z) = 1.5 * \langle \cos^2 \theta \rangle - 0.5$$

$\theta$ : angle between the bond and  $z$



Although the density profile is not affected much by the shear induced conformational changes of the adsorbed chains, the bond orientation factor –as defined by equation 2.1– is expected to, since it gives the orientation of the bonds along the chain with respect to  $z$ , and thus is more sensitive to conformational changes. In figure 4.5 the orientation of the bonds with respect to the direction normal to the walls ( $z$ ) is plotted for the bonds throughout the confined film, at equilibrium and under shear. As explained before (§ 2.1.2) the physical meaning behind the numbers is:

$$s(z) = \begin{cases} -0.5 & : \text{bonds parallel to the wall} \\ 0.0 & : \text{bonds randomly oriented} \\ 1.0 & : \text{bonds normal to the solid surfaces} \end{cases}$$

and the term “bonds” denotes the ensemble average of all bonds with their middle point located inside a thin  $z$  slice, irrespectively of the chain they belong to.

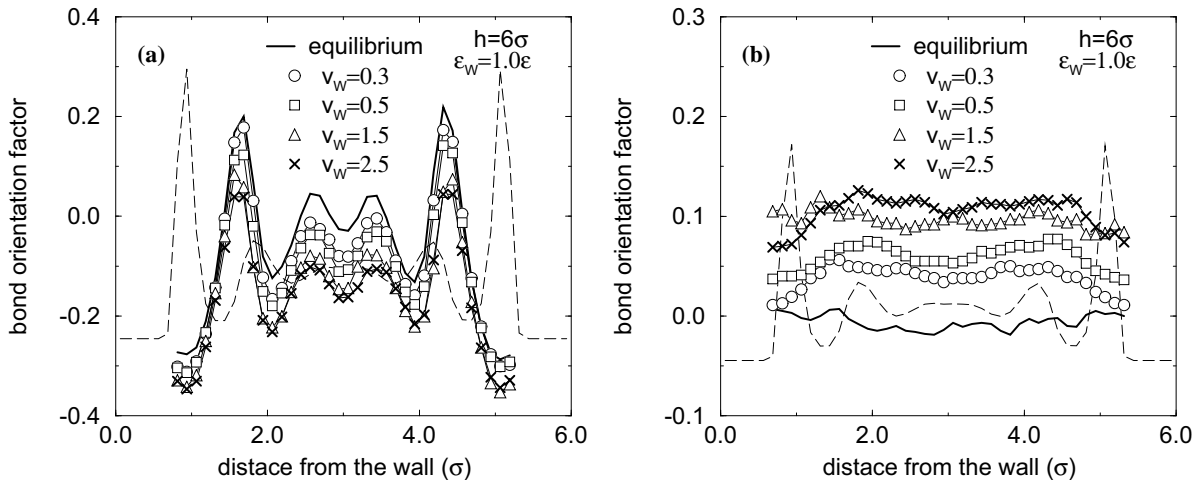


**Figure 4.6:** For a system of pentamers ( $h = 6\sigma$ ,  $\epsilon_w = 1$ ) the bond orientation factor is plotted for bonds located across the film, at equilibrium and under flow. (a) with respect to the direction normal to the walls ( $z$ ) and (b) with respect to the flow direction ( $x$ ).

As expected, the negative values inside the first layer show that the bonds connecting adsorbed segments are almost parallel to the surfaces, and with increasing  $\dot{\gamma}$  they become even more negative. This is a direct consequence of the stronger layering caused by flow, which is also manifested through the increase of the first layer density peak (figure 4.1). The stronger the inhomogeneity, the more parallel to the walls the bonds inside the first layer become, manifested by more negative values of the bond orientation factor with increasing wall affinity and higher shear rates. In addition, there is also a tendency for the bonds located inside the second layer to become parallel to the confining surfaces, especially in the case of high shear rates near strongly physisorbing surfaces. This is also a result of the strong layering inside the solid-oligomer interface. With increasing shear rate the adsorbed chains become more and more parallel to the surfaces, covering the walls and creating a smooth “monolayer” (figures 3.8 and 3.9b). Thus the chains inside the second layer are in a situation similar to that of chains near a neutral surface and start to behave in the same manner as the oligomers inside the first layer next to  $\epsilon_w = 0$  walls. This causes an increase of the second layer density and simultaneously the bonds become more parallel to the surface (figure 2.5: for  $\epsilon_w = 0$  the bond orientation factor inside the first layer is approximately -0.25).

In the middle of the film (figures 4.5, 4.6a) there is a systematic negative shift of the bond orientation factor with  $\dot{\gamma}$ , which suggests an alignment parallel to flow. Another way to quantify the orientation of the bonds parallel to the flow direction is through the bond orientation factor with respect  $x$ :  $s(z) = 1.5 * \langle \cos^2(\theta) \rangle - 0.5$ ,  $\theta$  now being the angle between the bond and  $x$ . This quantity is shown in figure 4.6b, whilst in figure 4.6a the bond orientation with respect to  $z$  for the same system is shown. At equilibrium the bonds are oriented randomly with respect to  $x$  and with increasing flow there is a systematic increase of the bond orientation factor. This indicates a possible alignment of

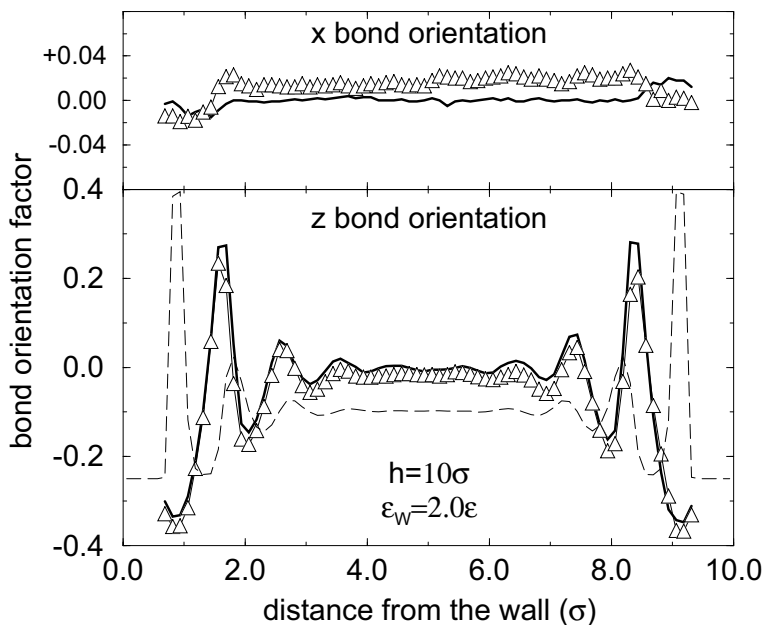


**Figure 4.7:** Bond orientation factors at equilibrium and under flow ( $v_w = 0.3$ ) for wide ( $h = 10\sigma$ ) films between strongly adsorbing surfaces ( $\epsilon_w = 2$ ). The bond orientation factor with respect to the flow direction ( $x$ ) is shown on the top and the one with respect to the normal direction to confinement ( $z$ ) is plotted in the bottom graph.

the chains parallel to the streamlines. Since the bond orientation factor is the average value over all bonds in a  $z$ -slice, a lot of the information about the chains is averaged out. Thus, although rather clear conclusions can be drawn about the layering normal to the walls from the bond orientation, it is inadequate to describe the orientation of the chains. The complementary, related information needed is usually provided through the end to end vector or the radius of gyration and through them a more illustrative discussion can be given for the shape and orientation of the chains<sup>4</sup>. Finally, something that at a first glance seems bizarre is that the bonds inside the first layer seem to order less parallel to flow than in the middle part. But this is only natural since inside the first layer the bond orientation is determined by the close-packing requirement, rather than the flow induced orientation.

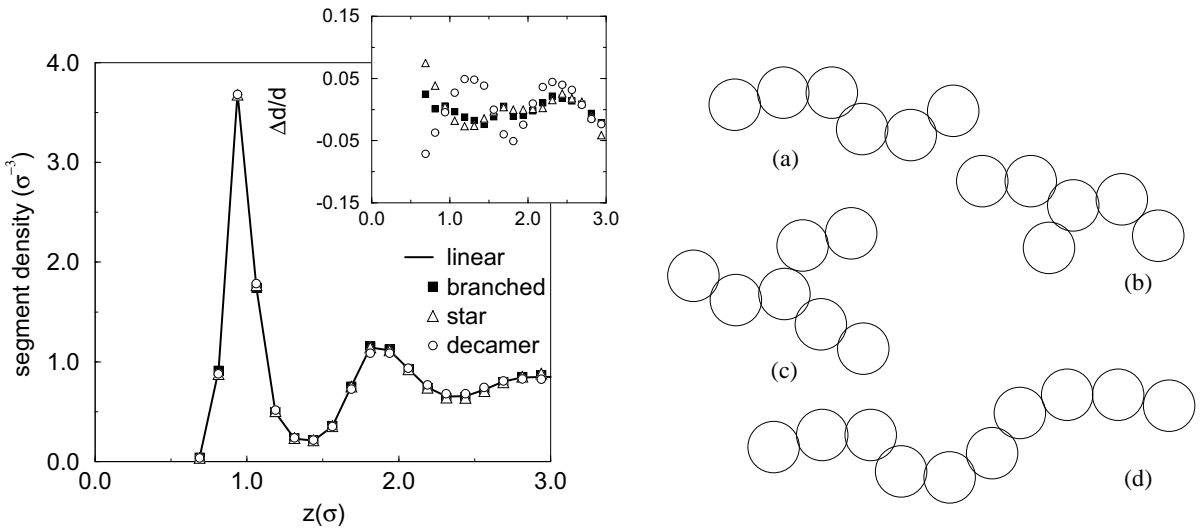
Moreover, since the bond orientation factor is very sensitive to the layering it would be interesting to see how it evolves across a wide film. In figure 4.7 the bond orientation factors are plotted for a film wide enough to develop a middle part of constant density. As expected, at equilibrium the bond orientation is completely random in the middle part of the film (both with respect to  $z$  and to  $x$ ). Near the surfaces it has exactly the same quantitative behaviour as for the thinner films and it is insensitive to the length of the oligomer as well. This is yet another point from which it is deduced that the effect of the surface is localized within one or two segment diameters (see also § 2.1.2). When flow is imposed, the same response is observed as for the thinner films; i.e. inside the first and second layer there is an enhancement in the alignment parallel to the surfaces, whereas in the middle part there is a small shift towards a more perpendicular orientation to  $z$  and more parallel to  $x$ , which are signs of chain alignment parallel to flow.

<sup>4</sup> for example the flow induced chain deformation and orientation is discussed in § 4.5

## 4.4 Changing the molecular architecture

An interesting property than can be modified in the confined films, to examine the influence on the nano-rheological behaviour, is the architecture of the oligomer molecules. Pioneering experiments on the rheology of linear and “branched” PFPE showed important rheological differences between linear chains and chains with very small branch groups [51]. In my simulations an important, though expected, difference in the rheology of linear *vs.* branched oligomers is the shear thinning in the middle part of the films discussed in § 3.3. In this chapter some further discussion will be presented on the phenomenology of confined films consisting of different molecules.

To compare confined systems of different molecules one can create films of similar thickness and by adjusting the average density<sup>5</sup> demand that the density in the middle part to the same as much as possible (figure 4.8). The reasoning behind this choice is that these systems would be in thermodynamic equilibrium with a bulk of the same temperature, pressure and density with that in the middle of the pores. The ideal situation would be if the chemical potential could be set the same in the systems of different molecules, but the calculation of the chemical potential in such dense oligomeric systems, in confinement and under shear, is extremely difficult, if possible at all [100, 101].

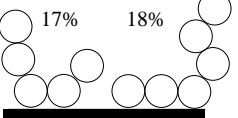
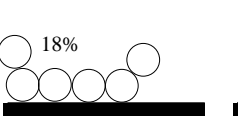
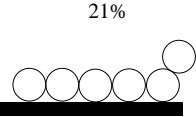
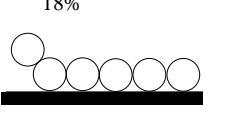
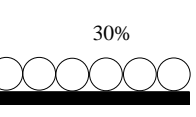
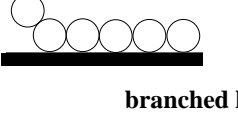
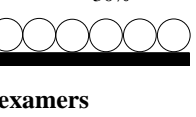
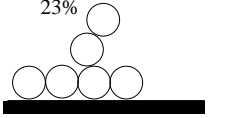
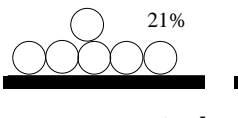
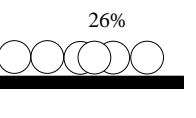
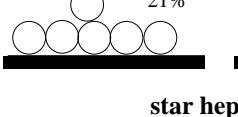
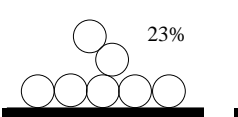
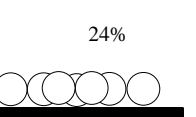
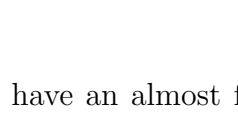
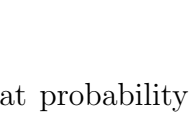


**Figure 4.8:** In order to see how the local architecture of the chain influences the rheological properties of these nanoscopically confined oligomers, small branches and tails have been connected to the 6mers resulting in a variety of molecules. By adjusting the average density (e.g. by changing slightly the wall-to-wall distance) the density profile near the wall can become almost identical for the various molecules. In the inset the relative deviation ( $\Delta d/d$ ) from the hexamer density profile is shown for the rest of the molecules.

One of the most important differences is the equilibrium conformations of the branched and the linear oligomers, even on the weakly physisorbing surfaces  $\epsilon_w = 1$  (table 4.3). In

<sup>5</sup> for example by changing slightly the film thickness  $h$

**Table 4.3:** Fraction of adsorbed chains with certain number of contacts with the  $\epsilon_w = 1$  walls, for the three different molecular architectures and various wall velocities. The imposed shear rates can be calculated from the wall velocity and  $h$ . In the inset a schematic figure of the most probable conformation at equilibrium and under shear.

$v_w$ :	.00	.05	.10	.30	.70	.90	1.50	equilibrium:	strong flow:
<b>linear hexamers (<math>h = 6.0\sigma</math>)</b>								<b>linear hexamers</b>	
1 cont.	.12	.10	.11	.10	.10	.10	.11		
2 cont.	.17	.17	.16	.15	.13	.11	.10		
3 cont.	.19	.18	.17	.16	.15	.13	.12		
4 cont.	.18	.19	.17	.18	.17	.17	.16		
5 cont.	.18	.19	.20	.20	.21	.21	.21		
6 cont.	.16	.17	.19	.21	.24	.28	.30		
<b>branched hexamers (<math>h = 6.0\sigma</math>)</b>								<b>branched hexamers</b>	
1 cont.	.14	.14	.13	.12	.11	.12	.12		
2 cont.	.15	.13	.12	.11	.09	.09	.09		
3 cont.	.13	.13	.13	.13	.10	.10	.10		
4 cont.	.23	.24	.24	.23	.20	.20	.19		
5 cont.	.21	.21	.22	.23	.25	.24	.24		
6 cont.	.14	.15	.16	.18	.25	.25	.26		
<b>star heptamers (<math>h = 5.93\sigma</math>)</b>								<b>star heptamers</b>	
1 cont.	.12	.12	.13	.11	.11	.11	.11		
2 cont.	.14	.15	.12	.11	.09	.08	.07		
3 cont.	.08	.08	.08	.08	.07	.07	.06		
4 cont.	.16	.16	.16	.15	.13	.12	.12		
5 cont.	.23	.23	.23	.23	.20	.20	.19		
6 cont.	.16	.15	.16	.18	.19	.21	.21		
7 cont.	.11	.11	.12	.14	.21	.21	.24		

contrast with the linear hexamers and decamers, which have an almost flat probability distribution for conformations with 2 to 6 contacts (tables 4.1 and 4.2), for the branched oligomers there is an apparent preference for conformations with two of the arms adsorbed and the third normal to the walls; i.e. for the branched hexamers (fig. 4.8b) the conformations with 4 or 5 contacts are predominant, whereas for the star heptamers (fig. 4.8c) the most probable conformations are those with 5 contacts (two adsorbed arms and a free one). When shear is imposed all molecules show a similar tendency towards fully adsorbed conformations (with  $\sim 50\%$  of the adsorbed chains with all, or all but one, of their segments inside the first layer, tables 4.1, 4.2 and 4.3).

## 4.5 Shape of the confined coils in shear flow

**Radii of gyration across the pore:** The influence of flow on the orientation and the shape of the coils is of vital importance for the rheological properties of the sheared fluid. Although the orientation and shape are usually studied through the end-to-end vector [92] its definition is ambiguous in the case of branched or star molecules. For this reason the radius of gyration tensor is defined<sup>6</sup> and its ensemble averaged elements are given by:

$$R_g^{ij} \equiv \left\langle \frac{1}{N} \sum_{k=1}^N (\mathbf{r}_k^i - \mathbf{r}_{cm}^i) \cdot (\mathbf{r}_k^j - \mathbf{r}_{cm}^j) \right\rangle, \quad i, j : x, y, z \quad (4.1)$$

where  $N$  is the number of segment in a chain,  $\mathbf{r}_k = (r_k^x, r_k^y, r_k^z)$  is the coordinate vector of the  $k$ th segment along the chain and  $\mathbf{r}_{cm}$  is the coordinate vector of the chain center of mass. In order to see the effect of confinement the film is divided in  $z$ -slices and the diagonal elements of the  $R_g$  are shown for the chains with their CM inside each bin.

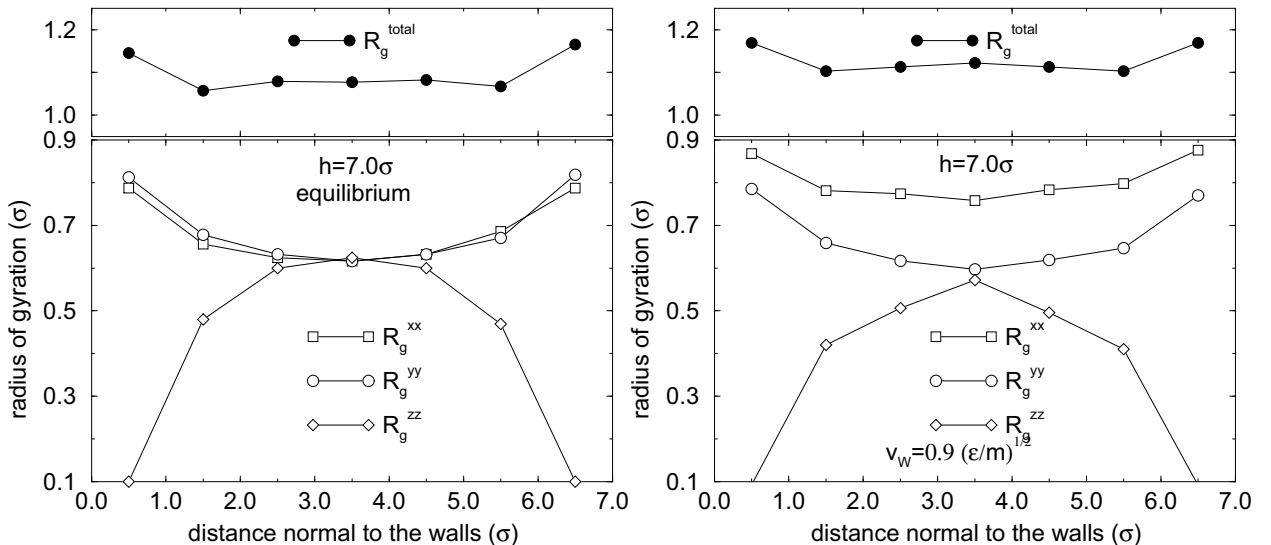


**Figure 4.9:** The  $R_g^{ii}$  elements of the  $R_g$  tensor at equilibrium (left) and under strong flow (right). Although at equilibrium the  $R_g$  tensor is, for our systems, diagonal in the Cartesian coordinates this is not the case under shear.

In figure 4.9 the  $R_g$  for hexamer films, of thickness  $h = 7$  confined between weakly adsorbing surfaces, are shown at equilibrium and under strong flow ( $v_w = 0.9(\epsilon/m)^{1/2}$ ). The total radius of gyration, which characterizes the size of the coils, is only weakly increased by flow, thus there is only a modest stretching of the hexamers across the film (near the surfaces and further away from them as well). On the other hand, the  $R_g^{ii}$  elements exhibit a greater shear induced change, especially for those chains located in the middle of the film. This shows that besides the stretching there is some kind of preferential alignment with respect to  $\mathbf{x}$ , which is the direction of flow<sup>7</sup>.

<sup>6</sup> completely analogous to the equilibrium  $R_g^{ij}$ ; for a more detailed discussion see § 2.1.2, pg. 20ff

<sup>7</sup> these points are addressed in more detail in the following paragraphs

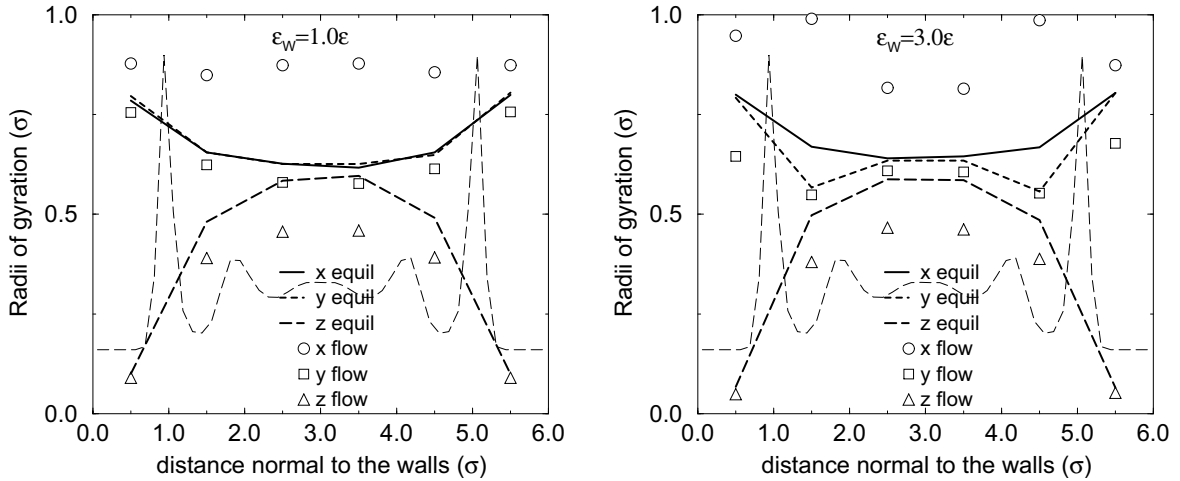


**Figure 4.10:** The  $R_g^{ii}$  elements of the radius of gyration tensor at equilibrium (lines) and under strong flow (open symbols) for weakly adsorbing ( $\epsilon_w = 1$ , left) and strongly adsorbing surfaces ( $\epsilon_w = 3$ , right). The effect of the wall energetics on the flow induced changes of  $R_g$  is minor except inside the second layer of the  $\epsilon_w = 3$  systems.

The effect of the wall affinity (figure 4.10) is minor, both on the absolute values and the flow induced changes of  $R_g^{ii}$ , throughout the film *except* for the chains located inside the second bin away from the walls. In figures 4.9 and 4.10 the  $R_g$  elements were averaged inside quite wide bins (width:  $1\sigma$ ) and the second bins from the walls are the ones containing the second density peaks, where the density profile is influenced the most by shear (figure 4.1c). The flow induced changes of  $R_g$  inside the second layer become even more clear when the bin width is reduced (figure 4.11).

Flow influences the shape of the confined chains in an expected way. Namely, for the free chains there is a stretching and a simultaneous alignment, demonstrated by an increase in their size parallel to flow ( $R_g^{xx}$ ) and a decrease in the other directions ( $R_g^{zz}$  and  $R_g^{yy}$ ). Whereas, for the adsorbed coils<sup>8</sup> there is also a slight stretching in the  $x$  direction, with a simultaneous collapse in the  $y$  direction; of course,  $R_g^{zz}$  remains unchanged inside the first bin.

A less intuitively-expected flow induced change in the shape of the coils is the one taking place inside the second density peak of systems confined between strongly physisorbing surfaces (figures 4.10b, 4.11c). This region is exactly where the density profile changes the most under shear (figures 4.1c and 4.2c) and it contains the very few chains that are weakly adsorbed (with 1 or 2 contacts) and mainly free chains that are in direct contact with the adsorbed layer. Since strong shear flows near these walls ( $\epsilon_w \geq 2$ ) force the adsorbed chains to adopt “flat”, many contact, conformations (tables 4.1, 4.2) the adsorbed layer becomes a flat oligomeric “carpet” covering completely the confining sur-

<sup>8</sup> with their CM within  $1\sigma$  from the surfaces, which are already stretched due to their proximity with the surface (equilibrium:  $R_g^{xx} \simeq R_g^{yy} \gg R_g^{zz}$ )

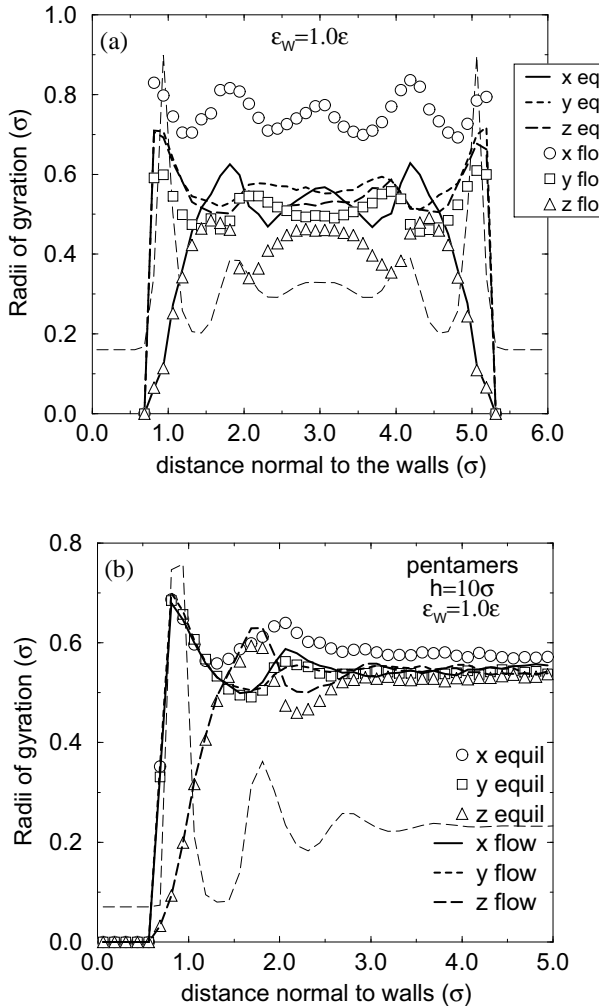
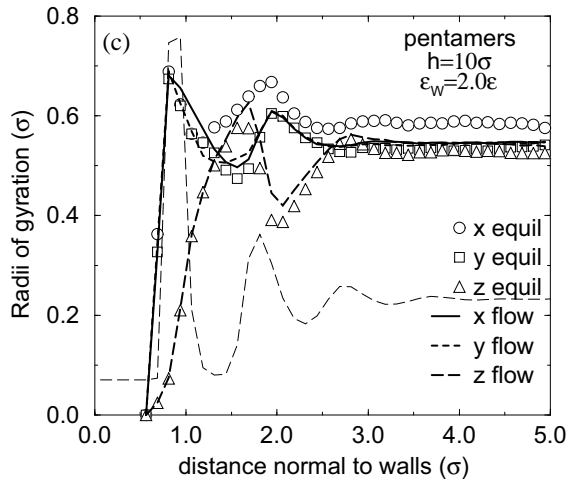


**Figure 4.11:** The  $R_g^{ii}$  tensor elements at equilibrium (lines) and under strong flow ( $v_w = 0.9$ , open symbols) for thin (a:  $h = 6\sigma$ ) and wider films (b:  $h = 10\sigma$ ). For the wider pores (b) flow affects much less the shape of the coils than in thinner pores (a). For weak wall attraction (b:  $\epsilon_w = 1$ ) the shape of the coils remains almost unperturbed throughout whereas for  $\epsilon_w = 2$  chains located inside the second density peak are influenced the most.



faces (figures 3.8, 3.9b) and thus becoming an effective neutral ( $\epsilon_w = 0$ ) surface confining the fluid in the middle of the film. In this perspective, these second density peaks are equivalent to the first layers near a neutral confining wall; and the flow induced changes taking place inside the first layers of  $\epsilon_w = 0$  or 1 systems are now observed inside the second layers of  $\epsilon_w = 2$  of 3 films. i.e. the free chains exhibit a considerable amount of alignment parallel to the wall covered by the adsorbed first layer and become even flatter with stronger imposed shear rates. This alignment parallel to flow and the simultaneous stretching give rise to an increase in the  $R_g^{xx}$  and a decrease in the  $R_g^{yy}$  and  $R_g^{zz}$ .

Although in equilibrium, owing to the simulation geometry, the  $R_g$  tensor is diagonal, under flow this is not the case. So in order to make a more quantitative approach to the shape of the coils, the  $R_g$  tensor should be diagonalized and the deformation and orientation of the chains should be studied through its eigenvalues and eigenvectors. This will be addressed in the next two paragraphs for the adsorbed and free chains.

### Radii of gyration of the adsorbed chains under shear flow:

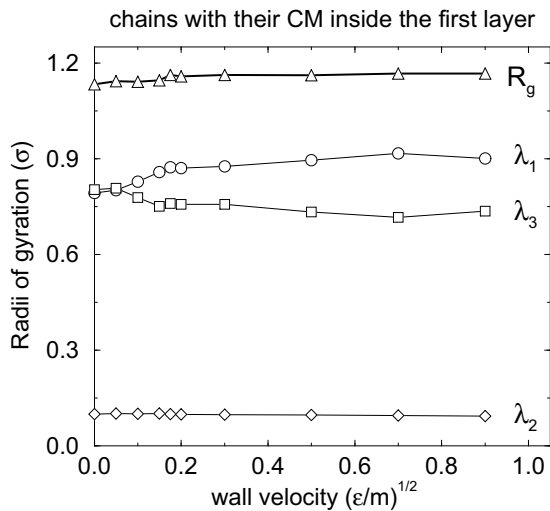


**Figure 4.12:** The eigenvalues of the  $R_g$  tensor ( $\lambda_i$ ) and the radius of gyration ( $R_g$ ) for the adsorbed chains are plotted versus the imposed shear rate (hexamers,  $h = 6$ ,  $\epsilon_w = 1$ ). For the adsorbed chains the eigenvectors are almost parallel to the Cartesian vector base, i.e.  $e_1//x$ ,  $e_2//y$  and  $e_3//z$ . The adsorbed chains exhibit only a slight stretching parallel to flow.

In this paragraph the shape of chains with their center of mass inside the first layer is studied. Although, near weakly physisorbing walls ( $\epsilon_w = 1$ ) this classification includes hexamers with three or more surface contacts (i.e. approximately 80% of all adsorbed chains), it gives a good representative picture of the shape of adsorbed chains, since chains with one or two contacts are in a dynamic, transitional, state between free chains and adsorbed chains –usually in the final stages of desorption or initial stages of adsorption<sup>9</sup>. For strongly physisorbing surfaces and systems under shear this classification includes almost the entire population of adsorbed oligomers.

Just for a quick reminder of the physical meaning of the eigenvalues and eigenvectors of the  $R_g$  tensor *as defined here*<sup>10</sup> the eigenvalues, in descending order:  $\lambda_1$ ,  $\lambda_2$  and  $\lambda_3$ , give the squared length of the axes of the ellipsoid which represents the *ensemble averaged shape of the coil* and the eigenvectors give the orientation of the *ensemble averaged respective axes* (figure 4.15). The radius of gyration is given by:  $R_g = \sqrt{\lambda_1 + \lambda_2 + \lambda_3}$ .

From the definition of the  $R_g$  tensor it is clear that it is generally not diagonal. At equilibrium, due to the simulation geometry: confinement in the  $z$  direction and isotropic  $x$  and  $y$  directions, the  $R_g$  is diagonal in the Cartesian system of reference. This is also the case for the chains with their CM inside the first layer under flow. Although now there is a double break of symmetry –by flow and confinement– the longest dimension of the coils ( $\lambda_1$ ) is always parallel to flow ( $e_1//x$ ) and their shortest dimension ( $\lambda_3$ ) is normal to confinement ( $e_3//z$ ). When  $R_g$  is plotted *vs.* shear rate only a slight stretching of the chains is observed with shear, as these chains are rather<sup>11</sup> elongated compared to the

<sup>9</sup> their conformations are studied in chapter 5 dealing with adsorption-desorption kinetics under flow

<sup>10</sup> This definition is different from the usual definition [34] of the principal components of  $R_g$  which is diagonalized at every time instant for every chain and then the  $\lambda_i$  are averaged. Here the  $R_g^{ij}$  are averaged over all chains and over time and then the  $\lambda_i$  are calculated for the *one* time averaged  $R_g$  tensor. For more details see § 2.1.2 page 20ff, [34] and references therein

<sup>11</sup> the maximum radius of gyration for a hexamer is  $R_g \simeq 1.21\sigma$  (completely stretched conformation)

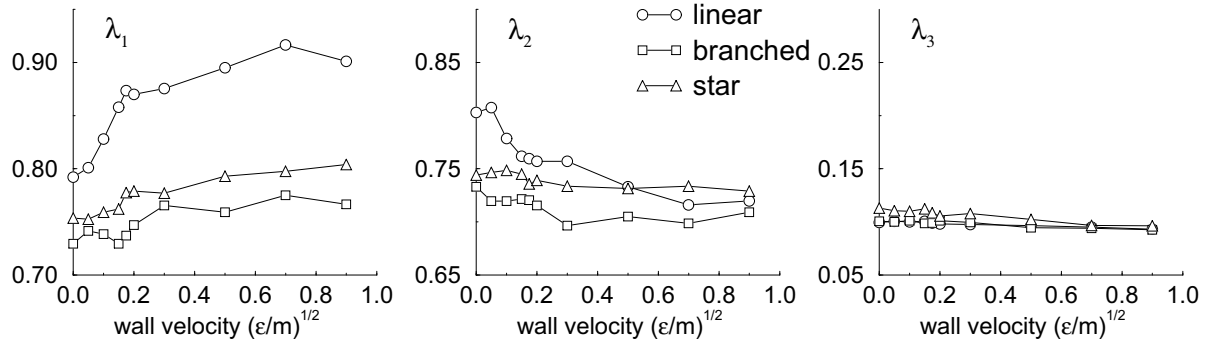


**Figure 4.13:** The principal components  $\lambda_i$  of the  $R_g$  tensor as a function of imposed shear rate for adsorbed oligomers of comparable sizes (linear hexamers, branched hexamers and star heptamers) confined between  $\epsilon_w = 1$  surfaces at a separation of  $h = 6\sigma$ .

bulk chains. From the dependence of  $\lambda_i$  on shear (figure 4.12) it is obvious that the size normal to the walls is hardly affected by flow, whereas the size parallel to flow ( $\lambda_1, \mathbf{e}_1/\|\mathbf{x}\|$ ) is moderately increased and the  $y$  size is decreased respectively. This means that the average shape of the adsorbed chains changes from a circular “pancake” at equilibrium ( $\lambda_1 \simeq \lambda_2 \gg \lambda_3$ ) to a more elongated, ellipsoidal “pancake” under shear, with its longest axis in the direction of flow ( $\lambda_1 > \lambda_2 \gg \lambda_3$ ).

The longer oligomers (decamers) exhibit the same relative stretching ( $\Delta R_g/R_g$ ) and even less alignment parallel to flow ( $\mathbf{e}_1$  deviates slightly from being parallel to  $\mathbf{x}$ ). The branched and star oligomers, which are of comparable size with the hexamers, behave in the same way as the linear hexamers (figure 4.13) but naturally, due to their more compact molecular architectures, stretch less (figure 4.13:  $\lambda_1$ ).

#### Radii of gyration of the free chains under shear flow:

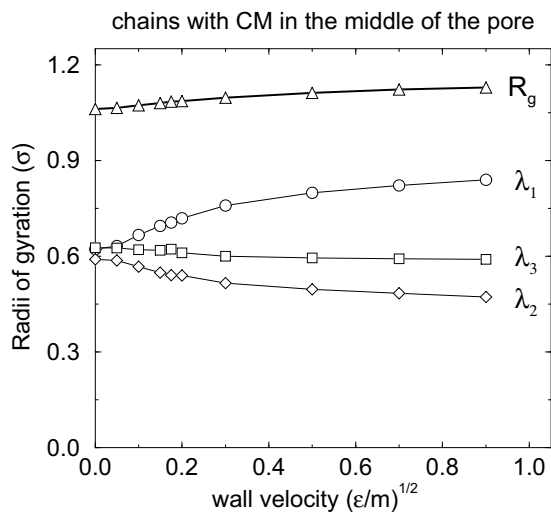


**Figure 4.14:** The principal components  $\lambda_i$  of the  $R_g$  tensor and the radius of gyration of free hexamers confined in the middle of a pore ( $h = 6\sigma$ ,  $\epsilon_w = 1\epsilon$ ). Although there is a flow induced chain elongation – $R_g$  increases– the changes of  $\lambda_i$  are greater than  $\Delta R_g$  implies, revealing the existence of a preferential orientation with respect to flow.

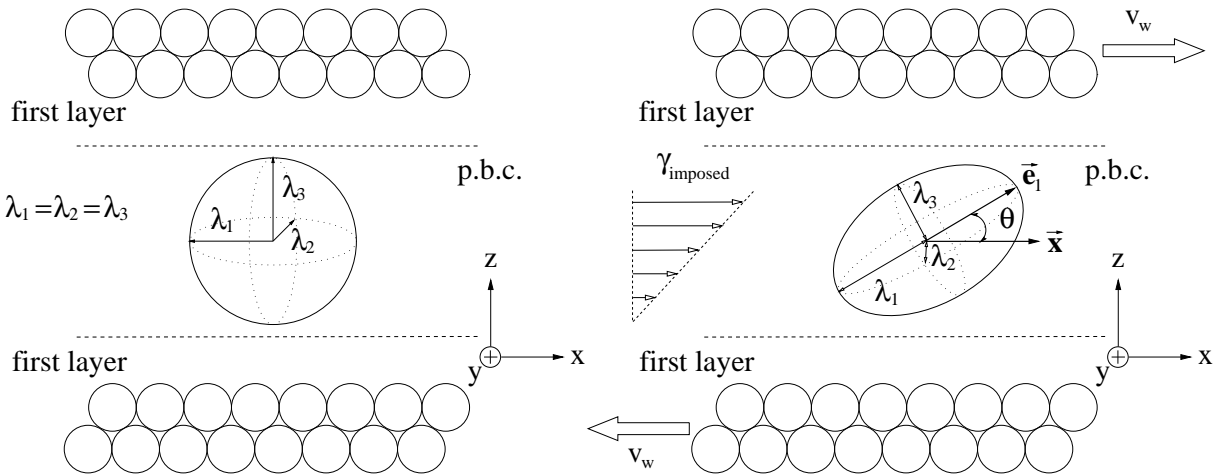


**Figure 4.15:** The time averaged shape of free coils located in the middle of  $h = 6$  pores at equilibrium (left) and under shear (right). At equilibrium the average shape is spherical, whereas under shear it becomes ellipsoidal tilted by  $\theta$  with respect to the flow direction.

Following the same approach, as for the chains located inside the first layer, the focus is now on the chains with their center of mass located in the middle of the film (in a  $z$ -bin  $1\sigma$  wide). The  $R_g$  tensor in this case is not diagonal in the Cartesian base, and after diagonalizing it for each wall velocity the principal components and the radius of gyration can be plotted as functions of imposed shear rate (figure 4.14). All the chains with their CM inside this bin are free, i.e. none of their segments is adsorbed on either wall not even in the case of decamers, and thus their behaviour can be considered as typical of chains under shear flow in  $nm$  geometric confinement and in absence of any wall energetics.

From the dependence of the radius of gyration on shear rate (figure 4.14:  $R_g$ ) the degree of flow induced stretching can be estimated. The free chains are elongated more than the adsorbed ones for the same shear rate. Moreover, from the principal components of the  $R_g$  tensor it becomes obvious that the coil elongation alone is not sufficient to explain the magnitude of change of the  $\lambda_i$ . Thus, beyond the flow induced stretching of the chains, there is also a preferential alignment related to the flow. In figure 4.15 there is a schematic representation of the average chain shape at equilibrium and under shear. At equilibrium –no flow– the chains located in the middle of the pore have a spherical shape<sup>12</sup> ( $\lambda_1 \simeq \lambda_2 \simeq \lambda_3$ ). When a velocity gradient is imposed across the film the chains elongate due to flow and the time averaged shape becomes ellipsoidal ( $\lambda_1 > \lambda_2 > \lambda_3$ ). Furthermore, there is also a preferred orientation of the coils, which can be quantified through the angle between the longest axis of the coil (its direction given by  $\vec{e}_1$ ) and the direction of flow ( $\vec{x}$  in my simulation geometry).

<sup>12</sup> it should be noted once again, that the  $\lambda_i$  give the *time averaged shape* and they are *not* the average principal components of  $R_g$ , so even though the chain is at every time instant of an ellipsoidal shape ( $\langle \lambda_1 \rangle : \langle \lambda_2 \rangle : \langle \lambda_3 \rangle$  is 14.8 : 3.06 : 1, SAW averaged over chains and time), the reorientation in time provides a spherical time averaged shape (see § 2.1.2 or [35])

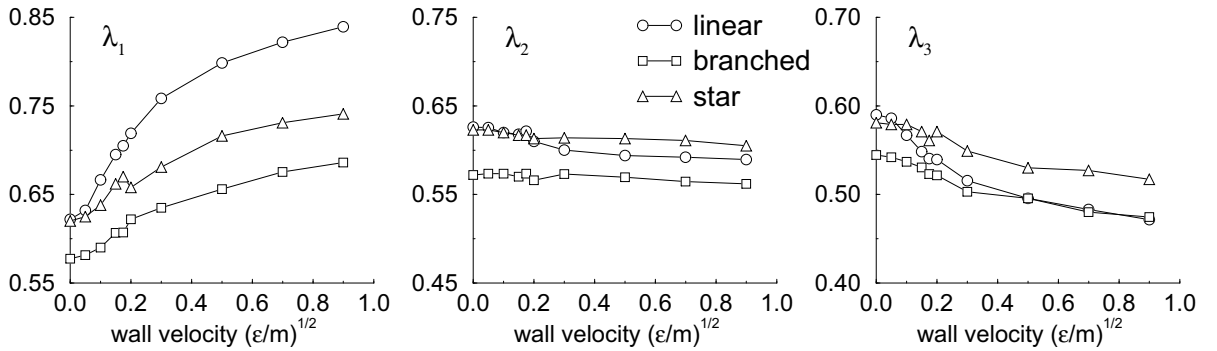


**Figure 4.16:** The principal components of the  $R_g$  tensor for free chains in  $h = 6$ .

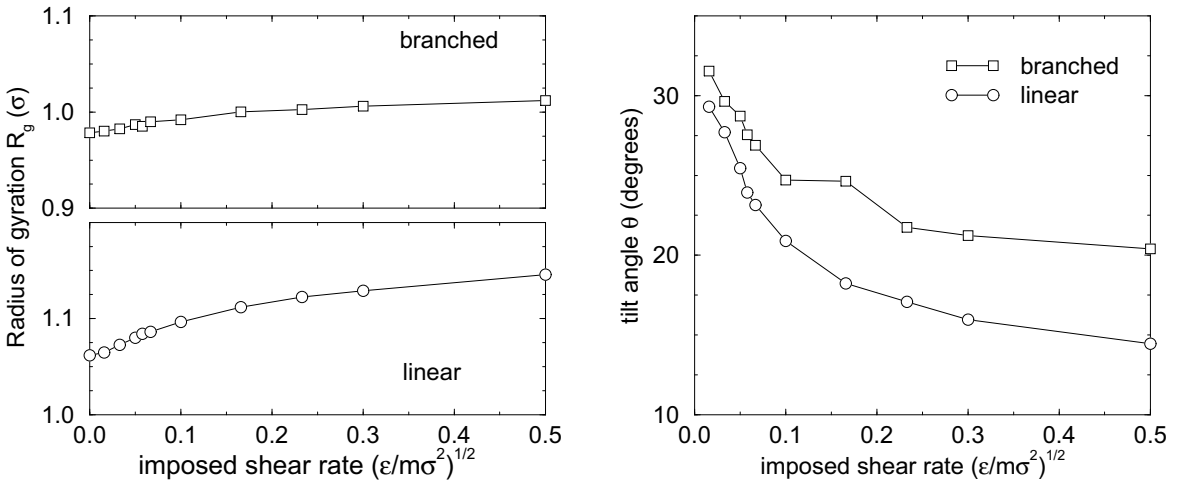


**Figure 4.17:** The flow induced deformation and orientation of linear and branched oligomers in the middle of  $h = 6$ ,  $\epsilon_w = 1$  films.

In figure 4.17 the radius of gyration and the tilt angle ( $\theta$ ) are plotted against the imposed shear rate for the  $h = 6$ ,  $\epsilon_w = 1$  films of linear and branched 6mers. As expected from the bulk rheological behaviour [92] the linear chains elongate more and they align better parallel to the flow direction than the more compact branched molecules.

This preferential alignment obviously does not mean that the coils align parallel to each other and remain at a given angle with respect to the streamlines, on the contrary the chains *do* rotate in time but on average they spend more time at this preferred tilt angle than in any other. Moreover, not all chains have the same orientation but there is a non-uniform distribution function of orientational angles.

This is a well known phenomenon in rheology and it originates from the torque created by the frictional forces acting on a chain inside a velocity gradient [102]. If the frictional forces are analyzed to a radial and a tangential part, the radial part causes the deformation (elongation) while the tangential part is responsible for the orientation (tilt angle) [102, 103]. Obviously, flow is trying to orient the chains parallel to its streamlines, so the larger the  $\theta$  the larger the torque and the faster the rotation. This orientation is opposed by the

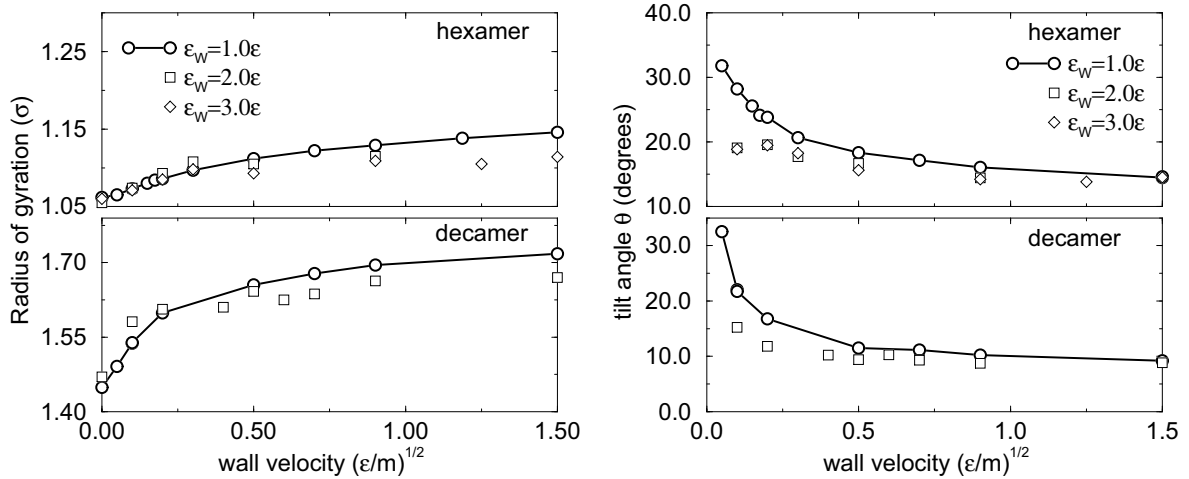


**Figure 4.18:** Although the effect of the wall energetics is minor in the flow induced deformation of the free oligomers, the orientation changes markedly for different  $\epsilon_w$ .

random thermal motions which tend to rotate the chains. A very simple derivation can show that for small shear rates the preferred angle is 45 degrees<sup>13</sup>, whereas for strong flows the velocity gradient prevails and in the limit of infinite  $\dot{\gamma}$  the chains are parallel to the direction of flow, i.e.  $\theta = 0^\circ$ . Non-Equilibrium Molecular Dynamics simulation managed to capture this 45° orientation for diatomic molecules [106] but even for small and quite rigid n-hexane the MD accessible shear rates are already so strong that a 16°-22° alignment angle is observed for the weakest flows [107]. In my case the hexamers show a tilt angle of about 30° for the smallest shear rate simulated and with increasing shear rate they align to angles 15° and 20°, for linear and branched hexamers respectively. Lower shear rates demand much more computational power to distinguish the flow velocities screened by the thermal motion and to establish a steady state flow, while for higher imposed shear rates slippage<sup>14</sup> prevents inducing a much stronger shear flow in the middle of the films.

Finally, the effect of the wall affinity on the stretching of the free oligomers in the middle of the film is minor (figure 4.18) and even for the longer decamers the deformations do not differ much for the systems confined between weakly and strongly physisorbing surfaces. On the other hand, the orientation of the free chains located in the middle of the confined films changes remarkably with  $\epsilon_w$ , especially in the lower shear rates for which the chain stretching is not affected at all. This is explained along the lines of a stronger effective confinement<sup>15</sup> in systems between strongly attractive surfaces. The adsorbed chains on strongly physisorbing surfaces become flat on the walls with high  $\dot{\gamma}$  and cover the wall, creating a stiff, impenetrable monolayer, thus reducing the available space for the free oligomers. Moreover, for the hexamers even the free chains inside the second

<sup>13</sup> for derivations see for example: for dumb-bells [102, 104] and for polymers in solutions [105, 102]

<sup>14</sup> either slippage at the wall for  $\epsilon_w \leq 1$  or interlayer slip for  $\epsilon_w \geq 2$

<sup>15</sup> see also § 2.2: pg 39ff and fig. 2.17 as well as the discussion on desorption in chapter 5

fluid layer start to become almost flat on top of the adsorbed layer, reducing even more the available space for the chains located in the middle of the film (to almost  $1\sigma$ ) and causing them to orient even more parallel to the flow direction. This alignment –parallel to the walls and the flow– of the adsorbed chains inside the first layer and the free chains inside the second layer affects the bond orientation factors both with respect to  $z$  and to  $x$  (§ 4.3).

## 4.6 Dependence of velocity profile on molecular architecture

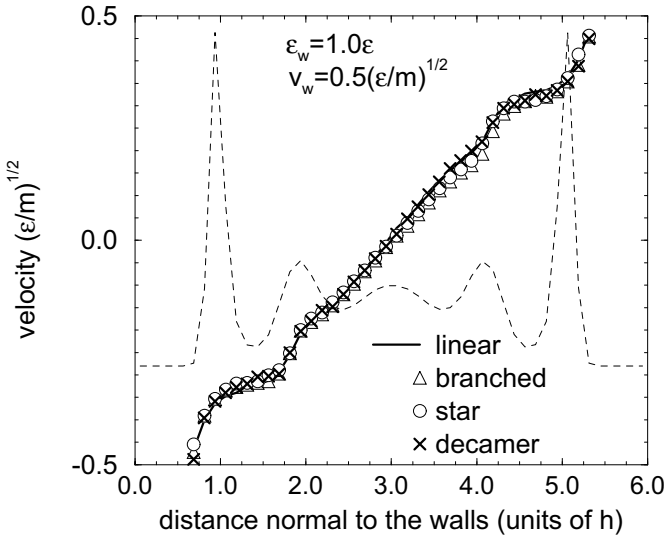
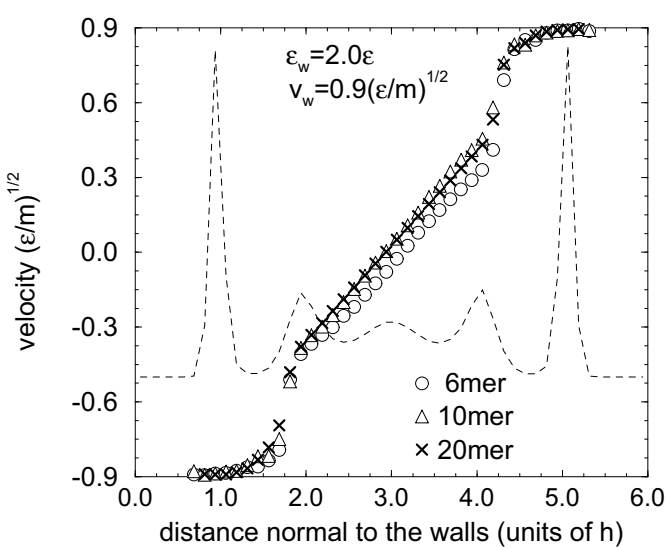


**Figure 4.19:** For the weakly physisorbing surfaces ( $\epsilon_w = 1$ ) the velocity profile is insensitive to changes of the molecular architecture, under the same densities and pressures. Various molecular architectures are shown: linear and branched hexamers, star heptamers and linear decamers, at systems with average density  $\rho = 0.89\sigma^{-3}$  and mean normal pressure  $\tau_{zz} \simeq 4\epsilon/\sigma^3$ .

When changing the molecular architecture of these flexible coils, identical density profiles can be obtained in the vicinity of the walls by changing appropriately the wall to wall distance and thus adjusting the average density (figure 4.8). Moreover, although at equilibrium there are important differences in the configurations of the adsorbed chains (table 4.3), when shear is imposed the response of the different molecules to flow is very similar, as far as the conformations of the adsorbed chains are concerned.

Since the velocity profile is determined by the local variations in the density profile [27, 28] and the behaviour of the adsorbed coils in shear flow (§§ 3.1 & 3.2) the velocity profile is not expected to differ for the different oligomer molecules, for the shear rates used in our simulations. For systems confined between weakly physisorbing walls, the velocity profile is insensitive to the molecules used (figure 4.19: linear pentamers, hexamers and decamers, branched hexamers and star heptamers) because: (i) there is always sufficient *physical connectivity* between the adsorbed layer and the middle part of the film to prevent interlayer slippage and (ii) the density profile does not change considerably with shear rate or molecular architecture.

For flow near strongly adsorbing surfaces (figure 4.20) the shape of the velocity profile also remains the same, suggesting that the important phenomena governing the develop-



Probability of adsorbed conformations  
with certain number of contacts:

10mer		20mer			
# <sup>1</sup>	% <sup>2</sup>	#	%	#	%
1	4.0	1	3.5	11	1.8
2	4.2	2	2.8	12	2.0
3	4.3	3	2.2	13	1.4
4	5.6	4	2.2	14	1.5
5	4.0	5	1.5	15	2.0
6	4.2	6	1.6	16	3.0
7	5.7	7	0.8	17	4.7
8	8.7	8	1.1	18	8.4
9	16.2	9	1.1	19	15.4
10	43.1	10	1.6	20	41.3

$$\dot{\gamma}_{imp} = 0.3 \quad \begin{matrix} ^1 \# & \text{: number of contacts} \\ ^2 \% & \text{: per cent probability} \end{matrix}$$

**Figure 4.20:** For the strongly physisorbing surfaces ( $\epsilon_w = 2$ ), although the shape of the velocity profile does not change much with the length of the chain, the onset of and the magnitude of the interlayer slip decrease weakly for greater chain lengths. Three chain lengths are shown: hexamers, decamers and eicosamers. Considering the molecular mechanism responsible for the interlayer slippage and the conformations of the adsorbed chains for this shear rate (as shown in the inlay table) these small differences are expected.

ment of the velocity profile do not depend on molecular size from hexamers to eicosamers. In figure 4.20 the velocity profiles of linear chains of various lengths are shown ( $N=6, 10$  and  $20$ : hexamers, decamers and eicosamers) and although these coils are very different in size, they develop very similar velocity profiles: There is a “locking” of the adsorbed chains onto the confining surfaces and between the adsorbed layer and the middle part of the confined film an interlayer slip appears. The location of slip does not depend on the length of the chain, as slippage appears when the shear-induced reduction of the partly adsorbed chains results in a dissociation between adsorbed layers and middle part of the system. Of course, quantitative differences do exist when changing the molecules: (a) the onset shear rate for the appearance of interlayer slip increases with  $N$ , as stronger flows are necessary to “flatten” the longer chains and (b) for the same shear rate (figure 4.20) the magnitude of interlayer slip decreases with chain length. Considering the molecular mechanism responsible for the interlayer slippage (§ 3.2) and the conformations of the adsorbed chains, which correspond to the velocity profile of figure 4.20, these small differences are expected. For the shear rate shown ( $v_w = 0.9$ ) the adsorbed hexamers and decamers adopt primarily conformations with many surface contacts ( $> 60\%$  with  $N$  or  $N-1$  contacts, tables 4.1 & 4.2). But even for the longer eicosamers this shear rate is sufficient to cause considerable alignment parallel to the walls and to favour fully adsorbed

conformations ( $\sim 57\%$  of the adsorbed coils have 19 and 20 contacts, figure 4.20: inset table). Finally, the same velocity profile is observed for branched and star molecules when sheared between  $\epsilon_w = 2$  surfaces.

## 4.7 The influence of flow on pressure

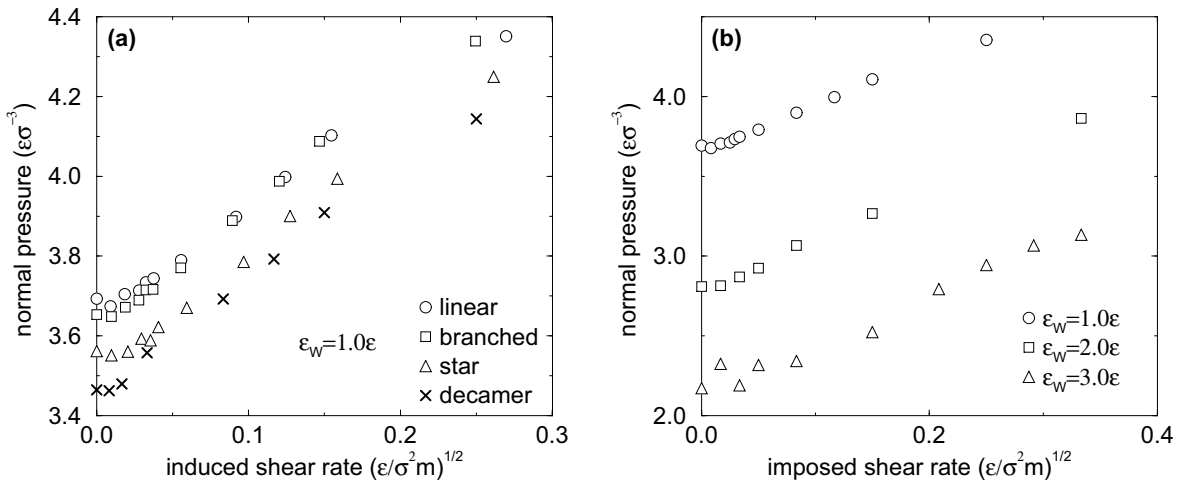


**Figure 4.21:** The normal pressure vs. shear rate: (a) The effect of molecular architecture: linear and branched 6mers and star 7mers between weakly physisorbing surfaces. (b) The effect of wall affinity: linear hexamers between various surfaces ( $\epsilon_w = 1$ , 2, and 3).

Conclusions for the normal pressure can be derived through the  $zz$  component of the stress tensor ( $\tau_{zz}$ ). This can be calculated as the ensemble average of the total force exerted by the fluid particles on the walls<sup>16</sup>:

$$P = \tau_{zz} = \frac{1}{2S} \left( \langle \sum_{j=1}^{N_{wall}} \sum_{i=1}^N \hat{z} \cdot \mathbf{F}_{ij} \rangle_{\text{lower wall}} - \langle \sum_{l=1}^{N_{wall}} \sum_{i=1}^N \hat{z} \cdot \mathbf{F}_{il} \rangle_{\text{upper wall}} \right) \quad (4.2)$$

where  $S$  is the area of the wall,  $\hat{z}$  is the unit vector in the  $z$  direction and  $\mathbf{F}_{ij}$  is the force<sup>17</sup> exerted on the wall particle  $j$  from the fluid particle  $i$ , the sums are over all pairs of the  $N_{wall}$  wall particles and the  $N$  oligomer segments. In MD simulations of confined systems at liquid densities the equilibrium normal pressure changes with the pore width, depending on whether the pore can accommodate an integer number of fluid layers. For monomeric systems the pressure changes with pore size for  $h \leq 4.5\sigma$  exhibiting maxima for pores that can accommodate an integer number of fluid layers ( $h \simeq n * \sqrt{3}/2 \sigma + 2 * z_{depl}$ ) and minima for pore widths inbetween [67]. For chain molecules, even shorter than the ones studied here, the pressure does not depend on film thickness beyond  $h \simeq 3\sigma$  due to

<sup>16</sup> this is usually the definition given in MD simulation studies for the normal pressure (e.g. [67]).

<sup>17</sup> thus  $\hat{z} \cdot \mathbf{F}_{ij}$  is the  $z$  projection of the force exerted on the wall particle

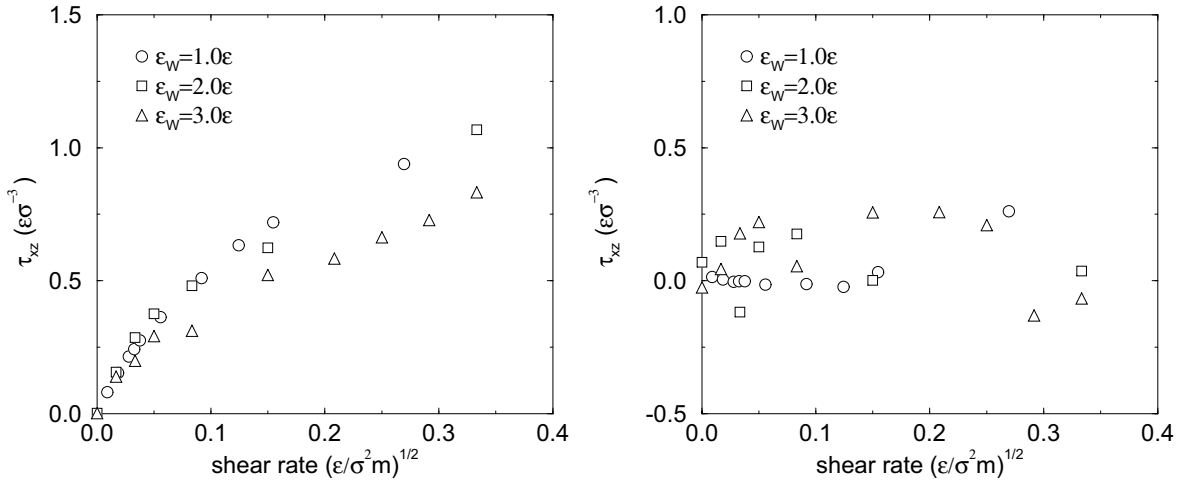


**Figure 4.22:** The influence of flow on the  $\tau_{xz}$  and  $\tau_{yz}$  elements of the stress tensor.

their intrinsically smaller tendency to form layers (§ 2.1.1) so for all the film thickness discussed herein the equilibrium pressure depends only on density [24].

In figure 4.21 the way that the normal pressures are affected by flow is shown. The influence of Couette flow on the normal pressure can provide clues about the dynamical behaviour of these  $nm$ -confined fluids. In figure 4.21a for a variety of oligomers confined between weakly physisorbing surfaces ( $\epsilon_w = 1$ ) their pressure is plotted versus the induced shear rate (eq. 3.3). The pressure shows an increase with higher shear rates, i.e. an extra force appears in the  $z$ -direction which increases with  $\dot{\gamma}$ . Changing the wall affinity does not cause any drastic differences (figure 4.21b). A similar effect – stress increasing with  $\dot{\gamma}$  – takes place also in the macroscopic shearing of Non-Newtonian fluids [104, Vol 2, Chap. 3]. This increase of pressure denotes an increasing resistance to flow with shear rate and may be a consequence of the molecular rearrangements under flow. As it has been discussed so far, the conformations of both the adsorbed and the free chains change with flow (§ 4.1, 4.5); if these rearrangements are not sufficient to compensate for flows at higher shear rates, then an excess normal force will appear as the molecules flow past each other [104, 45].

In the case of shear SFA experiments this can be viewed as an extra force that should be applied to the surfaces to keep them at constant distance while shearing an oligomer melt between them. For experiments carried out under constant load in narrow films (less than four monomer diameters wide) fixing  $\tau_{zz}$  forces the confined fluid to be squeezed out of the pore in a layer-by-layer manner [49], whereas for slightly wider films [48] the separation of the mica surfaces readjusts to attain a pressure equal to the applied load.

Finally, the other two stress tensor elements that can be calculated from the forces exerted on the walls are shown in figure 4.22. It should be mentioned that measuring the stress resistance to flow can be achieved also through the  $xz$  stress tensor element<sup>18</sup>

<sup>18</sup> in our geometry  $x$  is the flow direction and the velocity gradient is in the  $z$  direction

instead of the effective viscosity as defined by equation 3.4 (see § 3.3). The influence of flow on the  $\tau_{xz}$  element is comparable with that on the  $\tau_{zz}$  one. As expected the other off-diagonal element ( $\tau_{yz}$ ) of the stress tensor remains, within the simulation accuracy, zero at equilibrium and under shear<sup>19</sup>.

---

<sup>19</sup> this is a good criterion on the statistics of  $\tau_{ij}$  and whether the systems are at steady state flow

# Chapter 5

## Desorption kinetics under shear

The study of oligomer melts confined in ultra-thin films and subjected to shear reveals that the majority of the adsorbed oligomers adopts flat conformations on top of the walls. Although these conformations are characterized by high molecular adsorption energies, the same MD simulations show that desorption is strongly promoted by shear. The underlying mechanism is discussed. We focus on the self diffusion of oligomers near attractive surfaces and on their desorption and we study the effects of increasing energy of adsorption and shear. It is found that the mobility of the oligomers near an attractive surface is strongly decreased. Moreover, although shear forces the chains to stretch parallel to the surfaces and thus increase the energy of adsorption per chain, at the same time flow promotes desorption. The study of chain desorption kinetics reveals the molecular processes responsible for the enhancement of desorption under shear. They involve sequences of conformations starting with a desorbed tail and proceeding in a very fast, correlated, segment-by-segment manner to the desorption of the oligomers from the surfaces.

### 5.1 Effect of shear on the transverse mobility of nanoscopically confined oligomers

Recent experimental studies of ultra thin films by the Surface Forces Apparatus (SFA) reveal striking behaviour of lubricating films when confined in dimensions comparable to the molecular size. Such films become inhomogeneous [18, 49] and their effective viscosity increases dramatically when reducing the film thickness [50]. This implies that the mobility of the confined molecules decreases as the confinement becomes narrower (although characterized by liquid-like behaviour for separations down to 6 atomic diameters[49, 51, 54] ) and under further compression a solid-like behavior is observed [48]. The molecular mechanism responsible for this behaviour is the vast slowing down of molecular motions inside the adsorbed layer due to the surface induced densification [9].

The systems studied here are films of oligomers (mainly hexamers but also decamers and eicosamers) at liquid densities confined between two double layered (111) fcc surfaces. Shear is imposed by moving the walls with a constant velocity ( $v_w$ ) towards opposite directions ( $\pm \vec{x}$ ). Usually chains are grouped according to their center of mass distance from the walls. However recent studies (§ 2.2 and/or [9, 25, 36]) show that a more

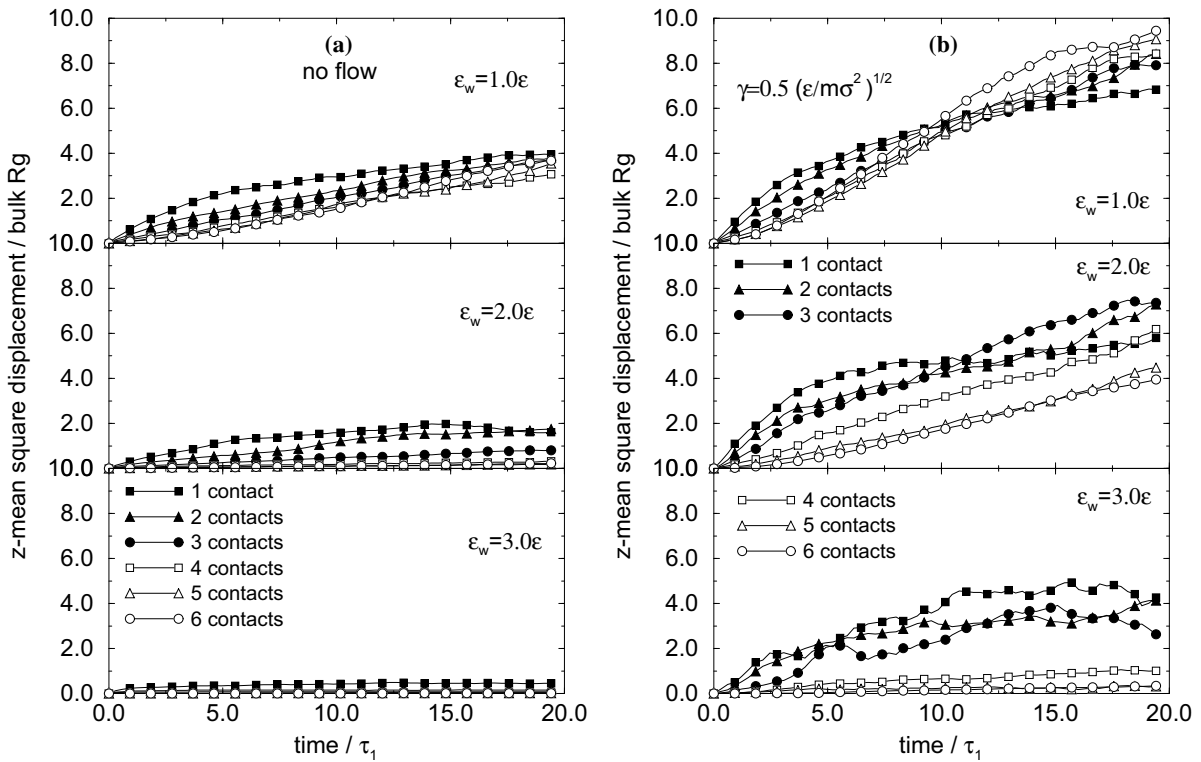


**Figure 5.1:** Center of mass mean square displacements normal to the walls ( $z\text{-msd}$ ) versus time for adsorbed chains, separated to groups with 1 to 6 contacts with the surfaces: (a) in equilibrium (no flow) and (b) under shear.

physically justified grouping is based on the number of contacts with the confining surface. “Adsorbed” chains are those with at least one segment inside the first layer (figure 2.4) of the density profile of either wall, while “free” chains have all segments outside the first layers. For chains up to decamers (10 segments per chain) and film thicknesses down to six segment diameters ( $h = 6\sigma$ ) no chains form “bridges” between the two walls, thus all adsorbed chains are in contact with a single surface. It has been found [9] that under equilibrium conditions “almost the entire population of adsorbed chains relaxes with the same time constant in a manner remarkably insensitive to the number of surface-segment contacts”. Moreover, for wall attractions  $\epsilon_w < 1.0\epsilon$  there is only a slight slowing down of the molecular motions characterizing a “weakly physisorbing” surface, whereas for  $\epsilon_w = 2.0\epsilon$  and  $3.0\epsilon$  the surfaces behave as “strongly physisorbing” by inducing an increase in the longest relaxation time of the adsorbed chains by a factor of 70 (for  $\epsilon_w = 2.0$ ) to 1500 (for  $\epsilon_w = 3.0$ ) (figure 2.12).

In this section, I will focus on the desorption of the adsorbed chains as a function of the number of surface contacts. In figure 5.1 the mean square displacement normal to the walls ( $z\text{-msd}$ ) versus the time is plotted, for adsorbed chains that have 1 to 6 contacts with the confining surfaces. The  $z\text{-msd}$  are calculated on time domains of  $64 * 10^3$  time steps and averaged over 137 time origins. In order to be directly comparable with reference [9] the  $z\text{-msd}$  are scaled with the radius of gyration in the bulk ( $R_g$ ) and time is scaled

**Table 5.1:** Fraction of the adsorbed hexamers with one to six contacts with the surfaces, for various wall affinities in  $h = 6.0\sigma$  wide pores. A more detailed table (more shear rates) can be found in the previous chapter.

$v_w :$	$\epsilon_w = 1.0\epsilon$			$\epsilon_w = 2.0\epsilon$			$\epsilon_w = 3.0\epsilon$		
	.00	.90	1.5	.00	.90	2.0	.00	.90	2.0
1 contact	.12	.10	.11	.07	.05	.05	.07	.01	.03
2 contacts	.17	.11	.10	.10	.06	.05	.11	.08	.05
3 contacts	.19	.13	.12	.14	.06	.06	.13	.11	.05
4 contacts	.18	.17	.16	.17	.08	.07	.17	.04	.06
5 contacts	.18	.21	.21	.22	.18	.12	.23	.09	.06
6 contacts	.16	.28	.30	.30	.57	.65	.29	.67	.75

by the bulk end-to-end vector relaxation time of the hexamers ( $\tau_1 = 16 \pm 2$  MD units). Under equilibrium (no flow) for weakly physisorbing surfaces ( $\epsilon_w = 1.0$ ) all chains manage to escape from the surface relatively fast. But for  $\epsilon_w = 2.0$  only those chains that have one or two contacts with the walls manage to desorb in the time scale presented. Chains with more than 3 contacts with the  $\epsilon_w = 2.0$  surface and all adsorbed chains for the case of  $\epsilon_w = 3.0$  remain adsorbed for the total time of the simulation, which is more than five times longer than the time scale presented in figure 5.1a. This is in excellent agreement with previous findings for much wider films of pentamers [9].

When shear is imposed the chains tend to adopt flatter conformations on top of the walls and this tendency is enhanced for increasing shear rates and higher  $\epsilon_w$  (tables 5.1, 4.1 and 4.2). For an imposed shear rate  $\gamma = 0.5$  ( $\epsilon/m\sigma^2)^{1/2}$ , which is much higher than the typical shear rates used in SFA experiments, ( $v_w = 0.9$  ( $\epsilon/m)^{1/2}$ ) 28% of the adsorbed chains have 6 surface contacts for  $\epsilon_w = 1.0$ , 57% for  $\epsilon_w = 2.0$  and 67% for  $\epsilon_w = 3.0$ . This implies that the average energy of adsorption per chain increases considerably for higher shear rates. In the case of strongly physisorbing surfaces more than 75% of the adsorbed chains have an adsorption energy exceeding  $10kT$  ( $\epsilon_w = 2.0$ , 5-6 contacts), whereas for  $\epsilon_w = 3.0$  more than 75% of the adsorbed chains have an adsorption energy exceeding  $15kT$  (5-6 contacts). At first sight this suggests that the desorption will be much smaller under flow, however this is not at all the case.

For a reduced shear rate  $\gamma \simeq 0.5$  the mean square displacements normal to the walls increase dramatically in comparison with the equilibrium situation (figure 5.1b). For  $\epsilon_w = 1.0$  the z-msd of all adsorbed chains (1-6 contacts) almost doubles; for  $\epsilon_w = 2.0$  even chains with 6 contacts ( $\simeq 12kT$ ) desorb relatively fast, whereas in equilibrium even chains with 2 or 3 contacts were irreversibly adsorbed. Finally for  $\epsilon_w = 3.0$  chains with less than 4 contacts still desorb in the time scales shown in figure 5.1b whereas adsorbed chains with more contacts escape from the surface in longer times than probed with our MD simulations [36].

It is known that the self diffusion in a non Newtonian fluid increases under shear. For

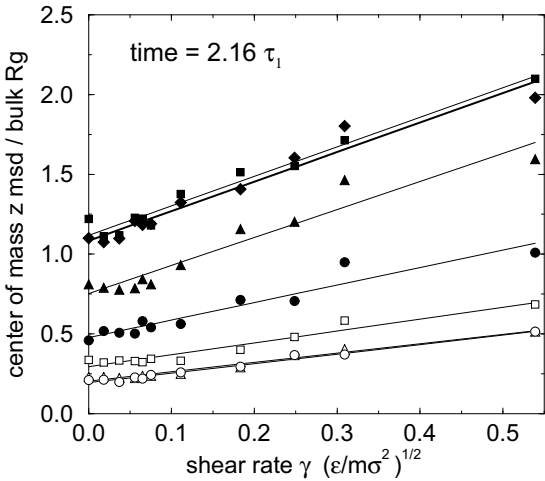


**Figure 5.2:** Center of mass mean square displacements normal to the walls ( $z$ -msd) for time  $t = 2.16\tau_1$  versus shear rate for chains with 0-6 contacts. The symbols are the same as previously.

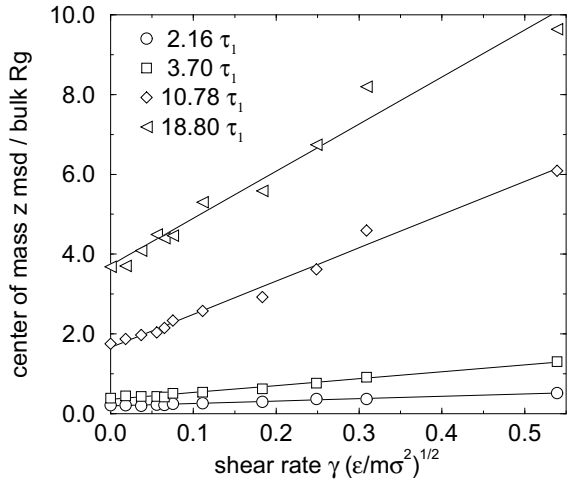


**Figure 5.3:** Center of mass mean square displacements normal to the walls ( $z$ -msd) for several times versus shear rate for chains with 6 contacts; the wall affinity is  $\epsilon_w = 1.0\epsilon$ .

example MD studies of a bulk LJ fluid at the triple point show that for the same shear rate as in figure 5.1b the diffusion coefficient parallel to the velocity gradient increases almost twofold in comparison with equilibrium [58]. This is in good agreement with our results for  $\epsilon_w = 1.0$  for short times where the msd is almost linear with time. For longer times the confinement forces the  $z$ -msd to increase more slowly as the space in the  $z$  direction that the chains can travel is restricted by the two walls. But for the stronger physisorbing surfaces self diffusion alone is not sufficient to cause such a dramatic effect as shown in figure 5.1b. The molecular mechanism behind this is believed to be the following. Adsorbed segments jump off from the wall due to diffusion. Under equilibrium the connectivity along the chain is the only variable which biases the direction of the diffusional motion, which explains why chains with some free segments (1-3 contacts) desorb fast. On the other hand, under flow when a segment diffusionaly desorbs, it feels a force due to the velocity gradient which is a driving force to peal off the rest of the adsorbed segments of the same chain. Of course, this means that the phenomenon should be enhanced by higher shear rates.

The shear rate ( $\gamma$ ) employed to obtain the result presented in figure 5.1b is extremely high in comparison with the SFA experiments, although similar shear rates can be found in magnetic storage devices. Molecular Dynamics is capable of handling shear rates of these magnitudes only [10, 58], as for smaller  $\gamma$  the flow velocities are masked by the thermal motions and averages over extremely long runs are needed. Nevertheless if the center of mass  $z$ -msd is plotted versus the shear rate an almost linear relation is found for the free and adsorbed chains (figure 5.2). This implies that if the film is subjected to a lower

shear rate the desorption will still be enhanced by flow but to a lesser extent. Moreover, concentrating on chains with 6 contacts, which exhibit the smallest slope in figure 5.2, we see in figure 5.3 that for reduced times of  $19\tau_1$  (which correspond to real time in the order of 0.6 to 15 nsec for PDMS or PI at room temperature, or for PS or PTHF at about 430K [7]) even smaller shear rates have a substantial effect on the desorption (manifested by increasing slope of line). Finally, we should point out that we focus on confined systems for which the interfacial chains are in a “glassy”, disordered state [9]. Under different conditions –temperature, pressure and wall symmetry– confinement may lead to “solidification” near the surface, manifested by the existence of domains with crystalline ordering. In these systems shear may affect the structure of these domains resulting in a destruction of their crystallinity, thus causing the melting of these “microcrystallites”.

In summary, it has been demonstrated that shear favours flat conformations of adsorbed molecules –characterized by high molecular adsorption energies. At the same time shear promotes considerably their desorption even from strongly physisorbing surfaces, on which short chains get immobilized under equilibrium conditions in the next section the molecular processes of this shear enhanced desorption and the desorption kinetics will be discussed in more detail.

## 5.2 Adsorption-desorption kinetics in nanoscopically confined oligomer films under shear.

The importance of the structural and dynamical changes taking place inside the solid-fluid interface is vital since they can determine the response of the entire film for sufficiently thin films. In this section we focus on how shear affects the mobility and desorption of oligomers near attractive surfaces. In the previous section (§ 5.1) I showed that the center of mass diffusivity normal to the walls increases with shear rate, although the average energy of adsorption per chain increases. In this section we investigate further this problem and simulate systems with longer chains –decamers– and describe the molecular mechanism responsible for this *shear enhanced desorption*.

The structure and dynamics of the adsorbed chains determine to a great extent the dynamics of these ultra-confined systems. When the attraction of the wall increases there is an enhancement of the inhomogeneity manifested by the increase of the first –and to a lesser extent of the second– layer density peak (figure 2.4). Furthermore, for the hexamers the increase of the wall affinity ( $\epsilon_w$ ) favours conformations with many contacts with the walls under equilibrium (tables 2.2 & 4.1). This should be attributed to the short size of the coils, as for the longer chains (decamers) in equilibrium –no flow– this effect is present to a much lesser extent (table 2.3 & 4.2).

Chains are again grouped according to their number of contacts with the surfaces. Since the segment-segment potential is purely repulsive,  $\epsilon_w$  can be considered as the *excess solid atom - chain segment adhesive energy* and the number of contacts multiplied by the energy parameter of the wall potential ( $\epsilon_w$ ) is the energy of adsorption of a chain. An adsorbed segment, or contact, is defined as a segment located inside the first peak of the density profile. The probability of a certain energy of adsorption (i.e. a certain number of contacts) per chain is defined by the distribution of these quantities over all adsorbed chains, on both surfaces, and over time (these probabilities are given in tables 4.1 and 4.2).

The mobility of the chains is another very important quantity and can be measured through the *center of mass diffusion coefficients*. Of course, due to confinement and flow the diffusion tensor is anisotropic (see also § 2.2 for the equilibrium case) and its two most interesting elements are the diffusion coefficient normal to the confining walls ( $D_{zz}$ ) and the diffusion coefficient parallel to the surfaces but normal to flow ( $D_{yy}$ ). The most interesting diffusion tensor elements can be determined by the slope of the respective center of mass mean square displacements [3, 25, 36, 58] and under shear (for example in a flow field  $\mathbf{u} = [\dot{\gamma}z, 0, 0]$ ) by definition  $D_{ii}$  are:

$$\begin{aligned} \langle (x(t) - x(0))^2 \rangle &= 2 D_{xx} t + \frac{2}{3} D_{zz} \dot{\gamma}^2 t^3 \\ \langle (y(t) - y(0))^2 \rangle &= 2 D_{yy} t \\ \langle (z(t) - z(0))^2 \rangle &= 2 D_{zz} t \end{aligned} \quad (5.1)$$

In our case, the flow field is pretty inhomogeneous (see § 3.11) with a complicated dependence of the local shear rate on  $z$  and at the same time  $D_{zz}$  depending on the position and

**Table 5.2:** Center of mass diffusion coefficients normal ( $D_{zz}$ ) and parallel ( $D_{yy}$ ) to the walls for systems of hexamers under shear. MD units are used throughout and the width of the film is  $h = 6.0\sigma$ .

	$D_{zz}$			$D_{yy}$		
	2 cont.	4 cont.	6 cont.	2 cont.	4 cont.	6 cont.
$\dot{\gamma}_{wall} :$						
				$\epsilon_w = 1.0\epsilon$		
.009	.0045	.0018	.0013	.0087	.0069	.0063
.017	.0047	.0019	.0013	.0092	.0074	.0069
.030	.0049	.0020	.0016	.0103	.0081	.0071
.048	.0054	.0022	.0018	.0113	.0089	.0095
.078	.0071	.0025	.0019	.0148	.0101	.0100
.099	.0072	.0028	.0024	.0152	.0125	.0132
.144	.0084	.0037	.0026	.0189	.0147	.0155
				$\epsilon_w = 2.0\epsilon$		
.007	.0019	.0002	.0001	.0036	.0011	.0009
.014	.0021	.0003	.0001	.0077	.0011	.0010
.021	.0018	.0004	.0001	.0053	.0014	.0013
.055	.0024	.0005	.0002	.0066	.0034	.0026
.087	.0069	.0007	.0003	.0129	.0041	.0044

configuration of the chain (tables 2.4 and 5.2). Thus the first of the above equations is not exact and for this reason only  $D_{yy}$  and  $D_{zz}$  are studied. In equilibrium –no flow– the mobility of chains with adsorbed segments is reduced in comparison with the *free* chains located in the middle part of the pore (table 2.4). As expected, chains with more contacts are more strongly slowed down (table 2.4 and refs. [25, 9]) and the center of mass mean square displacements and diffusion coefficients have to be calculated separately for chains with different number of contacts. Depending on the wall affinity, the mobility of the adsorbed chains can be affected from a moderate slow down near a weakly physisorbing surface up to orders of magnitude of decrease near a strongly adsorbing wall. For example, for the fully adsorbed hexamers (table 2.4) the diffusivities normal to the surfaces are reduced with respect to the chain mobility in the middle of the pore by a factor less than 4 for  $\epsilon_w = 1.0$ , by almost 40 times for  $\epsilon_w = 2.0$  and up to three orders of magnitude for  $\epsilon_w = 3.0$ . These results are in very good agreement with the decrease of the segment mobility of pentamers in the vicinity of similar surfaces reported by Bitsanis et al. [9]. As found before [60, 9], the mobility parallel to the surfaces is several times greater than the one normal to the walls and for the adsorbed chains is reduced to a lesser extent by the wall energetics; for the same chains as above –fully adsorbed hexamers–  $D_{yy}$  decreases by a factor of 3, 20 and 64 for  $\epsilon_w = 1.2$  and 3 respectively (table 2.4).

When shear is imposed there is a definite tendency for the adsorbed chains to stretch

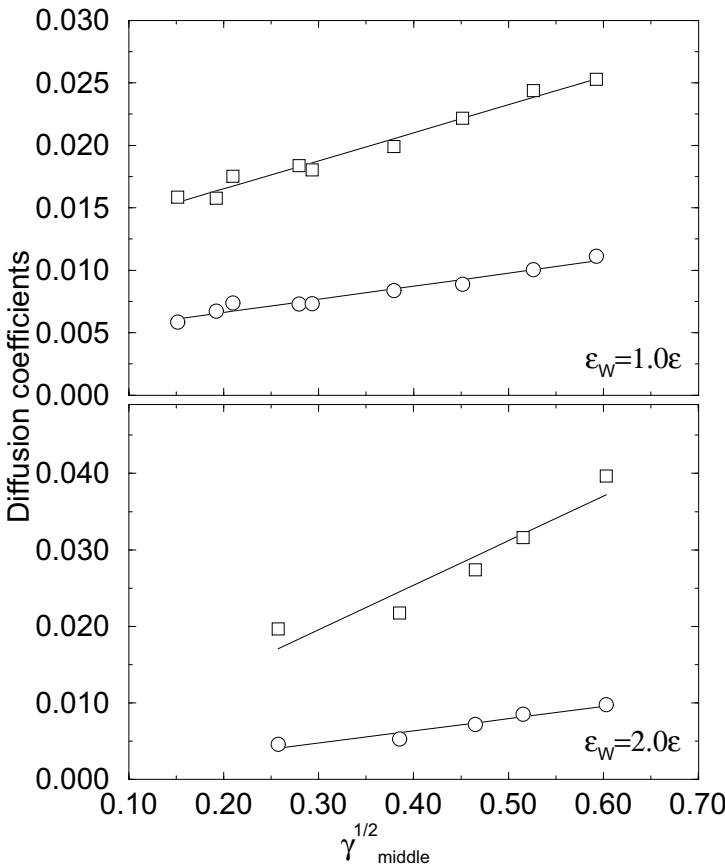


**Figure 5.4:** The center of mass diffusion coefficients of the free chains shown as a function of the square root of the local shear rate in the middle part of the pore. The diffusivities normal (circles) and parallel (squares) to the walls are presented for two different wall affinities (top:  $\epsilon_w = 1.0\epsilon$  and bottom:  $\epsilon_w = 2.0\epsilon$ ). The lines are least square fits.

along the wall, thus adopting conformations with many contacts with the surfaces. This tendency gets stronger with increasing shear rate ( $\dot{\gamma}$ ). For example the probability of a fully adsorbed chain (6 or 10 contacts with the surface) increases smoothly with  $\dot{\gamma}$  (tables 4.1 and 4.2). This preference of the adsorbed chains to adopt conformations with many contacts under flow, is observed both for the hexamers and the decamers and is much stronger for the more attractive surfaces (tables 4.1 and 4.2). This means that the average energy of adsorption per chain is increasing with shear rate. On the other hand, the center of mass diffusivity normal to the walls ( $D_{zz}$ ) also increases with shear rate (table 5.2), i.e. desorption is enhanced by the flow even though the chains are bound to the surfaces with higher adsorption energies. The effect of shear on the self diffusion of a bulk non Newtonian fluid was studied before [58] and a dependence on shear rate was found to be of the type:

$$D_{aa} = D^0 + D_{aa}^1 \dot{\gamma}^n \quad (5.2)$$

with  $n = 1/2$ . We fitted the same type of power law to our diffusivities for the free chains located in the middle of the film and we found that  $n$  is approximately  $1/2$ . So, in fig. 5.4 we plot the diffusivities normal and parallel to the walls versus the square root of the local shear rate ( $\dot{\gamma}_{middle} = \left( \frac{\partial u_x}{\partial z} \right)_{middle}$ ).

In order to get some insight in the molecular processes of chain desorption, the number of contacts of the adsorbed chains with time is monitored. For an adsorbed chain (fig.

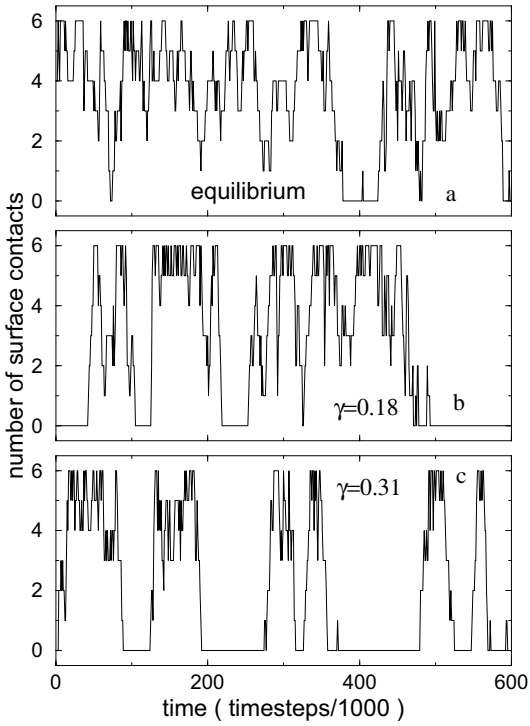


**Figure 5.5:** The evolution of number of contacts of a typical fully adsorbed hexamer with the weakly physisorbing surface ( $\epsilon_w = 1.0\epsilon$ ) in time. For systems in (a) equilibrium, (b)  $\dot{\gamma} = 0.18$  and (c)  $\dot{\gamma} = 0.31$ .

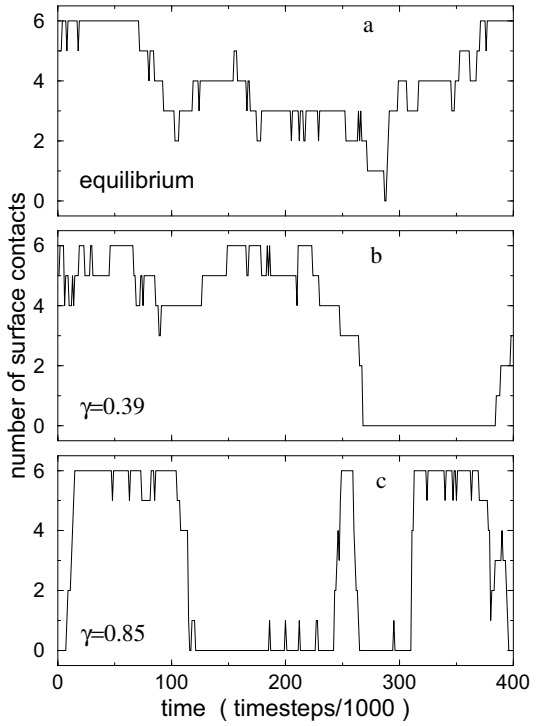


**Figure 5.6:** The same for a strongly physisorbing surface ( $\epsilon_w = 2.0\epsilon$ ): (a) equilibrium, (b)  $\dot{\gamma} = 0.39$  and (c)  $\dot{\gamma} = 0.85$ . Although under shear (b and c) most of the fully adsorbed chains desorb, for the equilibrium system (a) one of the few chains that desorbed is presented here.

5.5a, 5.6a) in equilibrium –no flow– after one of its segments diffusionaly desorbs from the surface, then either another segment desorbs and the number of contacts reduces, or one of the already free segments adsorbs. These motions are just diffusional motions biased by the attractive wall potential and the chain connectivity and the result is a struggling motion on top of the wall with a lot of segments desorbing and readsorbing diffusionaly until after some time all the segments are “free”. This kind of motion is characterized by large fluctuations of the number of adsorbed segments (contacts) as the energy barrier for desorption is comparable to the kinetic energy of the segments ( $k_B T = 1.0\epsilon$  and  $\epsilon_w = 1.0\epsilon$ ) and results in a very gradual desorption of the chain from the surface (fig. 5.5a). On average a fully adsorbed hexamer desorbs from the surface after  $120 \times 10^3$  time steps. So during the time of the simulation (i.e.  $\sim 10^6$  time steps) most fully adsorbed chains not only manage to desorb, but spend some time as “free” chains, or move to the opposite wall and adsorb there, or readsorb on the same surface. For example the chain in fig. 5.5a desorbs and then *fully* adsorbs again four times during the simulated time. For a hexamer

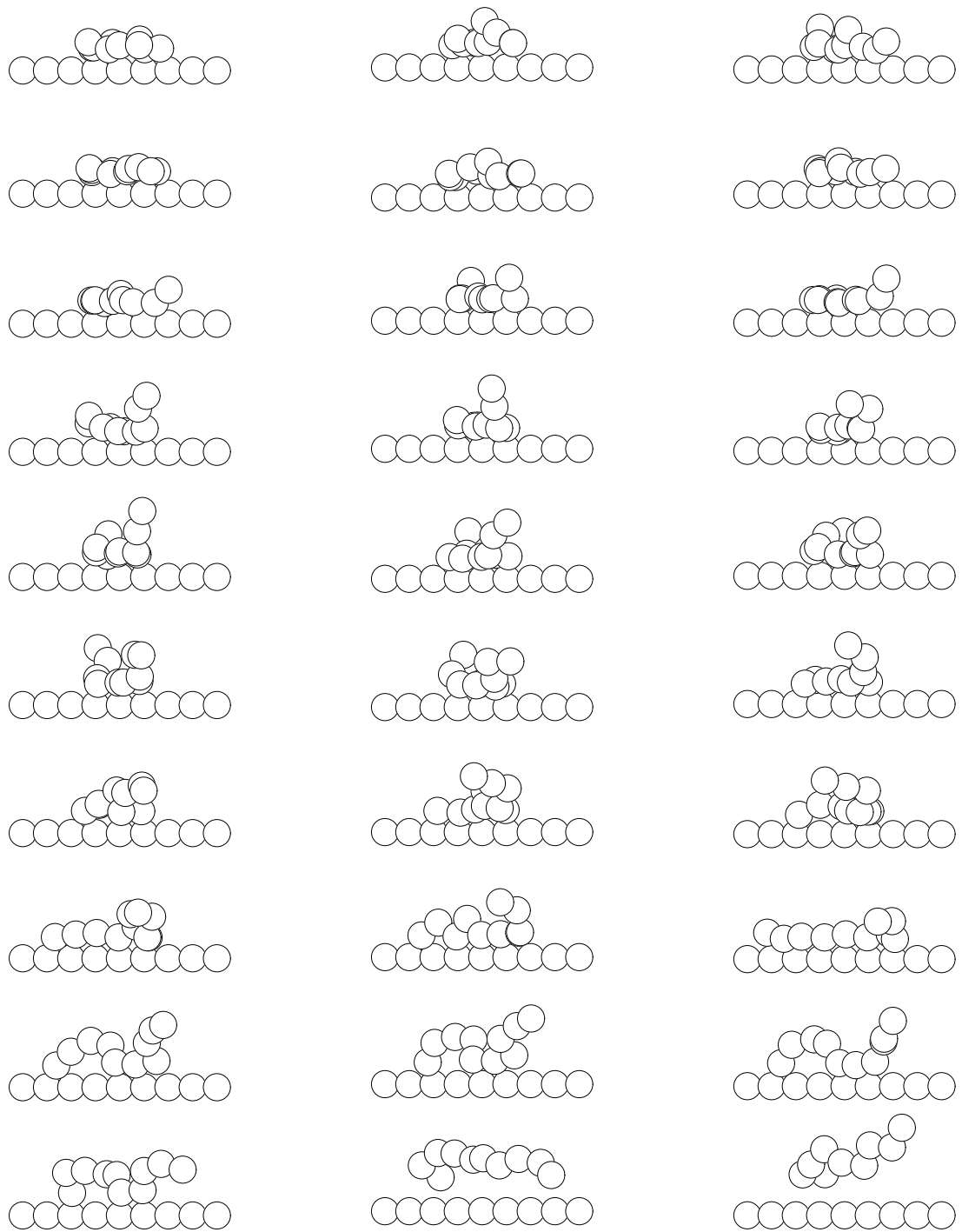


**Figure 5.7:** The ultimate stage of desorption of a typical oligomer under equilibrium. The detachment from the surface is concluded after a “struggling” motion with a lot of conformation fluctuations and after making and breaking randomly contacts with the wall.

**Table 5.3:** The fraction of fully adsorbed hexamers that desorbed in a certain time period. They are presented in desorbed chains / total number of chains observed in the specific time interval. Averages are over many time origins, so that chains with multiple desorptions are properly counted. Time is measured in thousands of time steps and the wall velocity ( $v_w$ ) and shear rate ( $\dot{\gamma}$ ) in MD units.

$v_w$	$\epsilon = 1.0\epsilon$			$\epsilon = 2.0\epsilon$				$\epsilon = 3.0\epsilon$			
	0.0	0.5	0.9	0.0	0.5	0.9	2.0	0.0	0.5	0.9	2.0
	$\dot{\gamma}$	0.0	0.18	0.31	0.0	0.22	0.39	0.85	0.0	0.22	0.39
time											
5	0/157	0/178	2/238	0/32	0/32	0/41	1/109	0/20	0/25	0/25	0/37
10	1/157	1/177	15/235	0/32	0/32	0/41	3/109	0/20	0/25	0/25	0/37
20	6/154	18/173	51/234	0/32	0/32	0/40	6/108	0/20	0/25	0/25	0/36
50	43/150	71/171	127/227	0/32	0/30	2/39	26/102	0/19	0/25	0/25	0/35
100	82/146	123/165	191/220	0/31	2/29	4/33	49/97	0/19	0/24	0/25	0/32
200	120/140	150/158	217/219	3/28	5/25	10/30	77/93	0/18	0/24	0/25	2/30
300	128/137	155/158	219/219	3/28	8/24	14/27	83/90	0/18	1/24	1/23	3/27
400	134/137	157/157	219/219	5/28	10/15	18/25	87/89	0/18	1/23	2/23	6/27
500	136/137	157/157	219/219	5/27			88/88	0/18	1/22	2/23	8/27
650	137/137			7/23				0/18	2/21	3/21	10/24
800	137/137			8/18				0/15	2/20	3/20	16/24

near a strongly physisorbing surface ( $\epsilon_w = 2$ ) in equilibrium, the picture is qualitatively the same –with segments diffusionaly desorbing and readsorbing– but the fluctuations of number of contacts with time are less frequent since now the excess adhesive energy between a solid particle and a chain segment is  $\epsilon_w = 2k_B T$  (fig. 5.6a). Furthermore, only a few (less than 20%) of the fully adsorbed chains manage to desorb in the time scale of the simulation ( $0.8 \times 10^6$  time steps). Further increase of the wall attraction ( $\epsilon_w = 3.0\epsilon$ ) results in the appearance of the same phenomena and behaviour but even more slowed down; as a result *none* of the adsorbed chains with 5 or 6 adsorbed segments desorbs for these times ( $\sim 10^6$  time steps) i.e. adsorption on these surfaces is irreversible for these configurations and for the simulated times. This picture changes qualitatively when shear is introduced, as the existence of a velocity gradient near the surface becomes a driving force for chains to stretch parallel to the flow. For partly adsorbed chains, depending on whether there is some free space on the surface adjacent to the adsorbed segments or not, the free segments can either adsorb on the surface leading to more contacts with the wall, or the adsorbed segments can be dragged away from the surface to a completely free conformation, since conformations which minimal size parallel to flow are highly favoured by the velocity gradient. But the adsorption and desorption of the chain are taking place simultaneously (in a perpetual exchange process) in such a way that the density near the surface remains dynamically constant, and defined by the wall energy parameter ( $\epsilon_w$ ) and the average fluid density of the film. So the result of shear is to make the actual processes of desorption and adsorption much faster. This can be seen in figures 5.5b and c and 5.6b

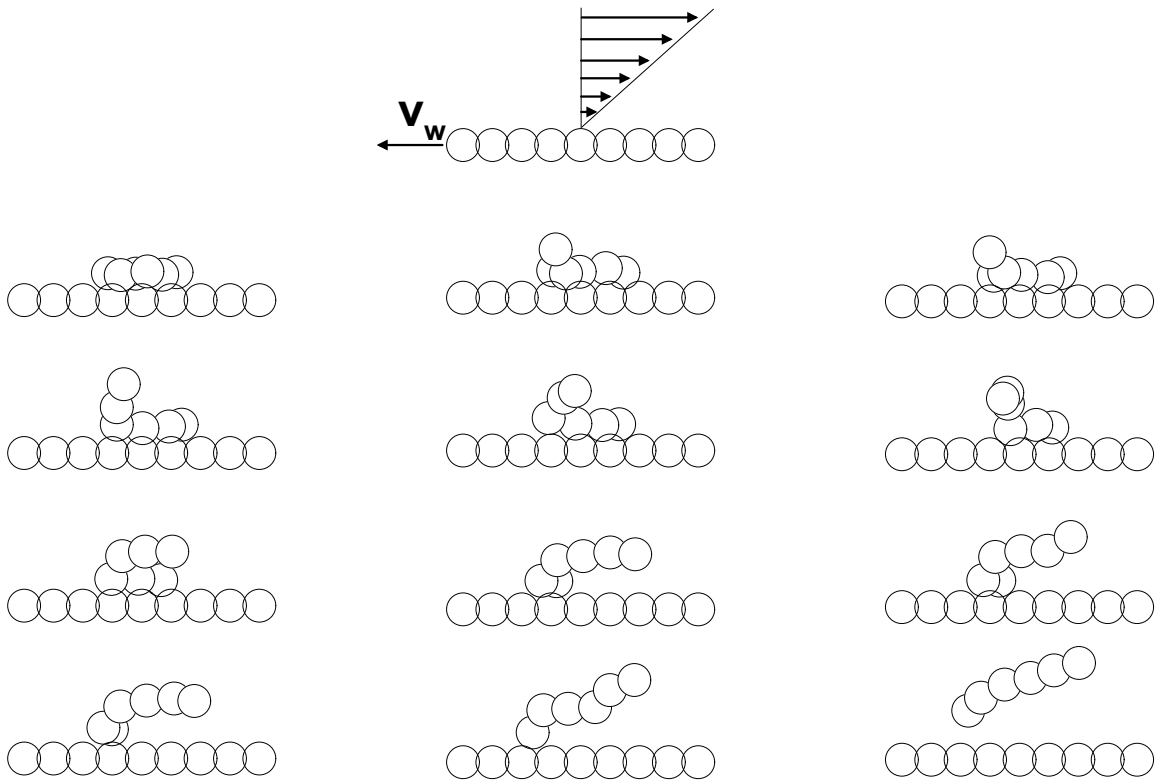


**Figure 5.8:** Successive conformations (every 1000 time steps) of a fully adsorbed hexamer desorbing from the  $\epsilon_w = 2.0$  surface under shear ( $\dot{\gamma} = 0.39$ ). A projection on the shear plane is shown, with time increasing from left to right and from top to bottom. The dragging of the front tail by the velocity gradient and the resulting segment-by-segment detachment of the chain result in a molecular mechanism promoting very rapid kinetics in the final stage of desorption.

and c, where there is a shift from a gradual, slow way of desorbing and adsorbing to a much more rapid and highly correlated desorption/adsorption denoted by a systematic change (decrease/increase) in the number of contacts. Especially for the higher shear rates (figs 5.5c and 5.6c) these processes become very sharp and sudden denoted by the almost vertical lines going from fully adsorbed to free conformations or the inverse. Moreover, it can be seen in fig. 5.5b and c, that the fluctuations in numbers of contacts become much smaller. All these result for  $\epsilon_w = 1.0\epsilon$  in a decrease of desorption time to  $55 \times 10^3$  time steps. Near the stronger physisorbing surfaces ( $\epsilon_w = 2.0$ ) the same phenomena are observed but to a smaller extent due to the greater adsorption energy barrier. Under shear a considerable fraction of the fully adsorbed chains now desorbs relatively fast. For example for a reduced imposed shear rate of  $\dot{\gamma} = 0.3$  approximately 75% of the fully adsorbed hexamers desorb in  $400 \times 10^3$  time steps from the  $\epsilon_w = 2.0$  surface, whereas for the same  $\dot{\gamma}$  and  $\epsilon_w = 3.0$  this fraction is 9% (table 5.3). This means that, although now there is a mechanism that promotes rapid desorption and adsorption, most of the chains still remain irreversibly adsorbed on the very attractive surface ( $\epsilon_w = 3.0$ ).

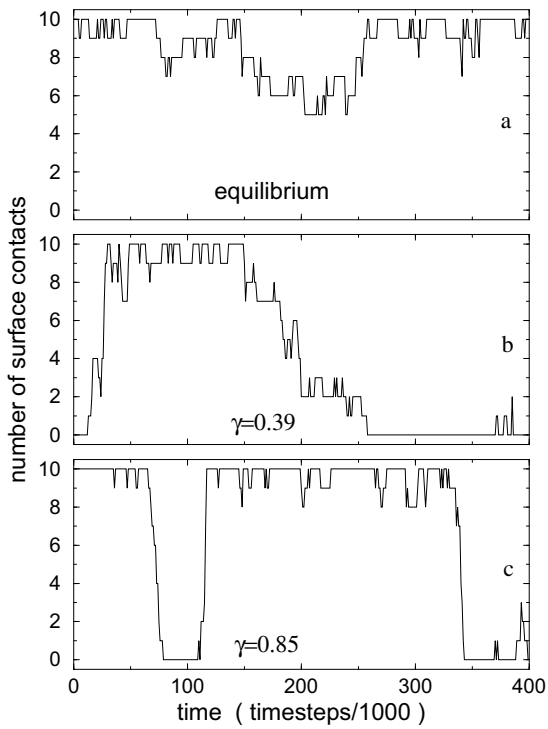


**Figure 5.9:** The number of surface contacts of a fully adsorbed decamer versus time on the  $\epsilon_w = 2.0$  surface. In equilibrium (a) although some of the adsorbed segments diffusionaly desorb the chain typically remains adsorbed for the total simulation time. Shear (b) promotes desorption and for these shear rates the time for the diffusional desorption of the front tail is comparable to the time for the final rotational stage of desorption (denoted by a systematic decrease in the number of contacts). For higher shear rates (c) the rotational part of desorption (denoted by the almost vertical lines) becomes very rapid and the desorption time is determined by the slower process of the front tail diffusional detachment.

Furthermore, in all the systems the chains that desorb abruptly follow a certain common kinetic pattern. Taking as an example a fully adsorbed hexamer, one can observe that it remains adsorbed for a long time and occasionally due to thermal motion one or two segments diffusionaly desorb, usually to be pushed towards the surface by a combination of shear and connectivity forces. But there exist instances when the diffusional desorption of a segment results in a rapid desorption of the whole chain. Analyzing our simulation trajectories it became clear that in the vast majority of such cases the end-segment of the coil on the front of the chain (fig. 5.8) is the one which diffusionaly desorbs and then due to the velocity gradient moves upwards and towards the back of the chain followed quickly by the adjacent segment; for such a conformation there is extremely small probability to readsorb, as the space on the wall below this tail is occupied by the rest of the coil. Simultaneously the existence of a tail results in an increased normal size which is unfavourable under flow. Subsequently the rest of the successive segments can only move away from the surface resulting in a very rapid desorption (fig. 5.8) in a highly correlated manner. For the strongly physisorbing surfaces, the chains that desorb also follow this very abrupt molecular mechanism, although most of the chains are irreversibly adsorbed for the simulated time scales (table 5.3). Perhaps the most interesting observation concerns the almost complete absence of readsorption of segments belonging to the free part of such a chain during the desorption of the remaining adsorbed segments for sufficiently high shear rates.

For the decamers all of the above is observed as well, slowed down a little bit due to the possibility of having even more contacts with the surfaces. Qualitatively the same

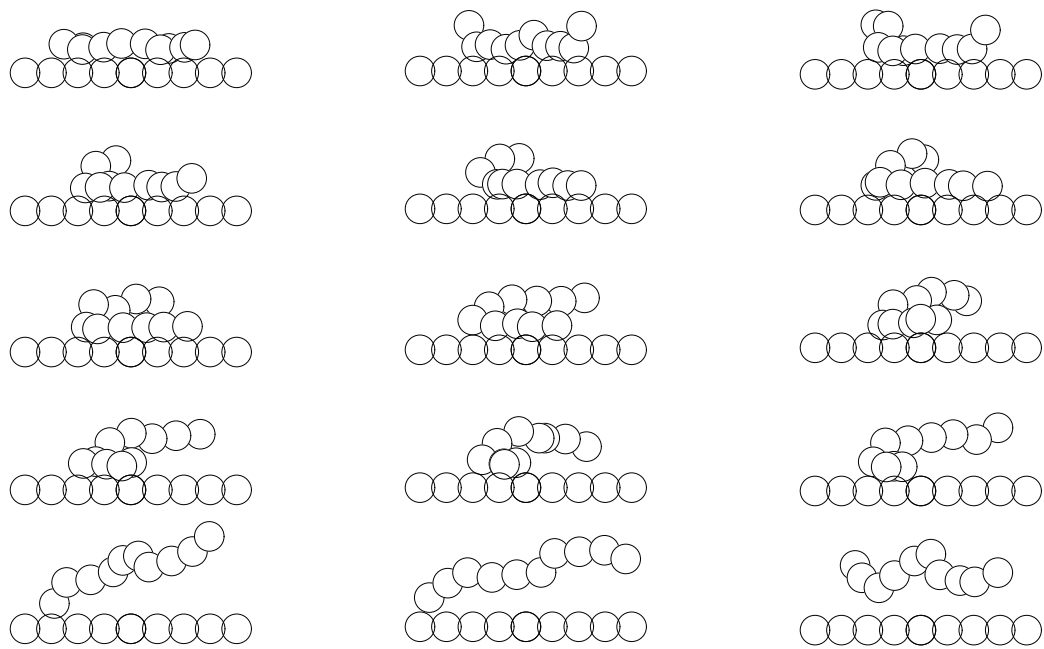


**Figure 5.10:** The most predominant molecular mechanism, for the kinetics of the final stages of desorption of the decamers under shear, involves configurations that start with a desorbed front tail and an extremely rapid, correlated, segment-by-segment desorption of the rest of the coil. Successive conformations (every 1000 time steps) with time increasing from left to right and from top to bottom ( $\epsilon_w = 2.0$ ,  $\dot{\gamma} = 0.64$ ).

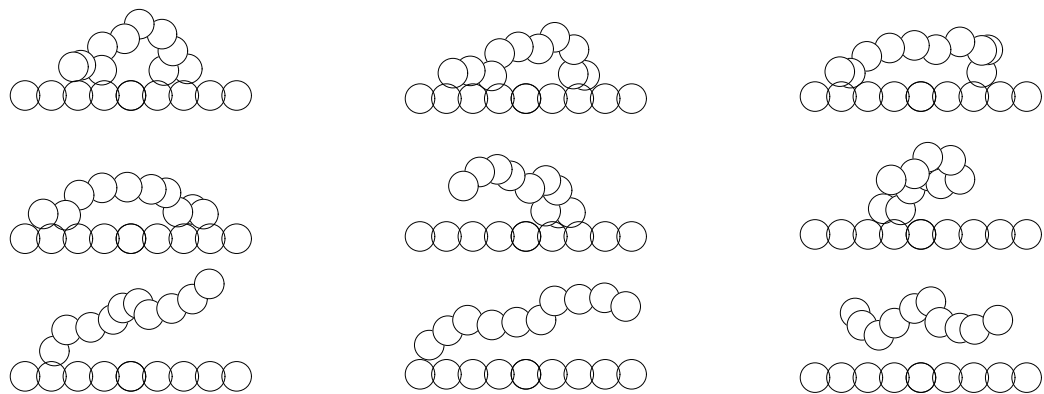


**Figure 5.11:** Although the decamer is quite short, a second mechanism of desorption can be observed as well, namely the “dragging” of a loop by the velocity gradient. For longer chains (polymers) this is expected to be the most important mechanism by which shear promotes desorption ( $\epsilon_w = 2.0$ ,  $\dot{\gamma} = 0.39$ ).

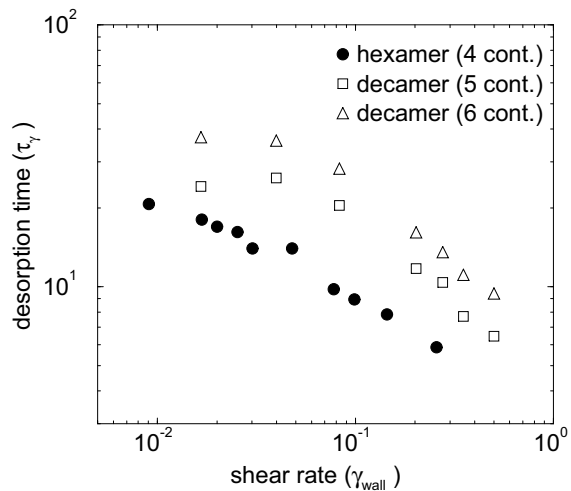


**Figure 5.12:** The desorption time versus shear rate for systems with  $\epsilon_w = 1.0$  surfaces. The desorption times that correspond to the average energy of adsorption (i.e. average number of contacts) are presented (● hexamers with 4 contacts and □ and △ decamers with 5 and 6 contacts).

behaviour is observed both in equilibrium and under shear as for the hexamers (fig. 5.9). Moreover the molecular mechanism of desorption is most of the times the same as for the shorter chains: the front end diffusionaly desorbs and the rest of the adsorbed beads follow in a segment-by-segment manner (fig. 5.10). Another characteristic example can be seen in fig. 5.11 where some of the middle segments of the chain have diffusionaly desorbed from the wall thus creating a loop. Due to the velocity gradient this kind of conformations are unfavourable and are rapidly desorbing. The ultimate desorption is again initiated by the desorption of the front segments. For the rather short chains that we simulate (ten beads per chain) this occurs very infrequently, but it is expected to be fairly typical for longer chains.

Putting together the pieces of information we get from figs 5.5, 5.6 and 5.9 with the chain kinetics from figs 5.8, 5.10 and 5.11 we can build a more complete picture of the dynamics of oligomer desorption and adsorption under shear. The total time it takes for a chain to desorb consists of two parts: *first*, conformational fluctuations of the adsorbed chain on top of the wall until a suitable conformation appears, i.e. a desorbed front tail, *and then* a very fast, correlated desorption of the complete chain takes place. Naturally, the total desorption time is determined by the slowest of the two parts: in the vicinity of strongly adsorbing surfaces and/or under high shear rates the first –diffusional– process is slower, whereas for weakly attractive walls and/or low shear rates the second –rotational– process is slower. This total desorption time can be defined, for the MD trajectories, as the time between the first instant that a chain becomes adsorbed and the moment that all of its segments are free for the first time. This desorption time is averaged over the simulation time, all desorptions observed and over all chains of the same adsorption energy. In fig. 5.12 we selected those chains with energies of adsorption (number of contacts) that correspond to the average adsorption energy in equilibrium and plotted their desorption times versus the shear rate near the wall ( $\dot{\gamma}_{wall} = \left(\frac{\partial u_x}{\partial z}\right)_{wall}$ ) taking the slip into account whenever it exists.

Furthermore, the segment-by-segment, correlated kinetic scheme of desorption shown

in figs 5.8, 5.10 and 5.11 resembles strongly conformational sequences of chains under strong rotational diffusion or turbulence. We hesitate though to use the term of enhanced rotational diffusion to describe the desorption kinetics, at this point, as there is a very peculiar behaviour near the surfaces; i.e. as observed in figs 5.5, 5.6 and 5.9 the rotational diffusion is completely halted for a long time and suddenly –with the appearance of a specific conformation– is dramatically enhanced. On the other hand, this idea can be utilized to model theoretically the desorption kinetics near an attractive surface [117, 118].

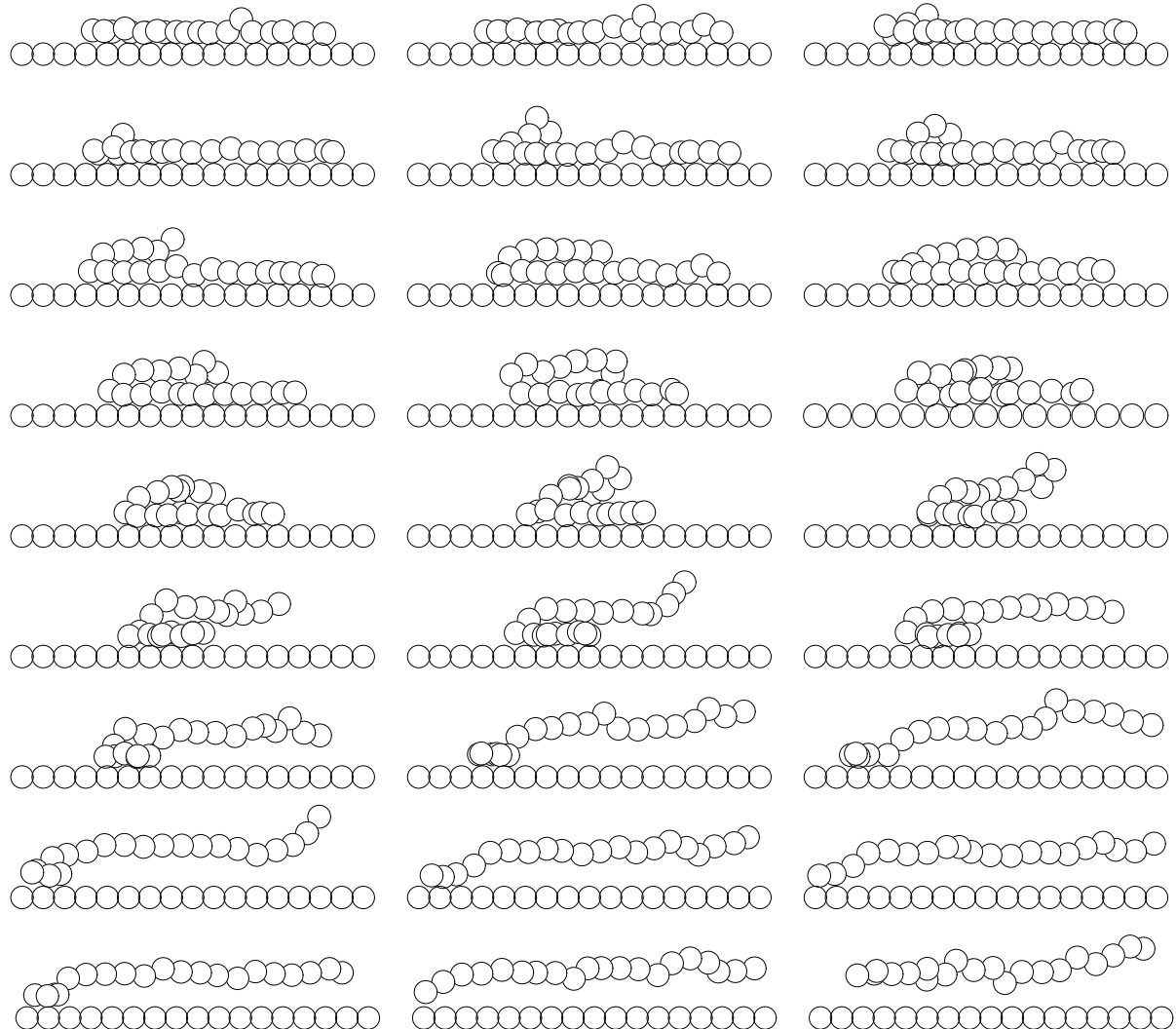


**Figure 5.13:** Even for the quite longer 20mers the conformations of the adsorbed chains become almost fully adsorbed under shear and desorption follows the common kinetics discussed herein. The ultimate stage of a typical 20mer desorbing from an  $\epsilon_w = 2$  surface under shear ( $v_w = 0.9$ ,  $h = 6$ ).

### 5.3 Conclusions

In this section we summarize our findings concerning the chain mobility near an attractive surface and the desorption dynamics of oligomer melts confined in spaces comparable to their molecular dimensions and the influence of shear. The chain mobility, which can be described through the center of mass diffusion tensor, is decreased in the vicinity of an adsorbing surface. This slowdown depends on the wall affinity and ranges from moderate next to *weakly* physisorbing surfaces (by a factor of 4 for  $\epsilon_w = 1$ ) up to three orders in magnitude near *strongly* physisorbing surfaces ( $\epsilon_w = 3$ ). These trends are in very good agreement with the decrease of the relaxation times of oligomers next to similar surfaces where they were shown to originate from the densification near the wall rather than the bare adhesive energy barriers of the surface-segment potential [9]. This reduced mobility can explain the dramatic increase of the effective viscosity in nanoscopically confined systems observed experimentally [48, 54, 47, 51, 50] especially if one takes into account that the mica surfaces used in these experiments are characterized by very strong affinities for most of the chemical systems studied [48].

As far as the desorption is concerned, in equilibrium –no flow– we find that a diffusional, gradual process in which every segment due to thermal motion can desorb from the surface and can subsequently randomly remain free or readsorb. This results in a struggling motion of the chains on the adsorbing surface. Depending on the wall attraction an oligomer desorb relatively fast ( $\epsilon_w = 1.0 \ k_B T$ ), or as the energy of adsorption becomes larger than  $k_B T$  the desorption can become limited ( $\epsilon_w = 2.0$ ), or extremely slow (for  $\epsilon_w = 3.0$  the fully adsorbed oligomers are irreversibly adsorbed on the time scale of our simulations).

When shear is introduced to a melt of oligomers there is a tendency for the chains to stretch parallel to the flow, when this melt is confined the geometrical constraint of the surface enhances this process. For the adsorbed coils this results in a systematic increase of the fraction of chains with many contacts with the surfaces, thus the average energy of adsorption per chain increases with shear. At the same time, desorption is promoted –both by the shear enhanced diffusivities normal to the walls and by the appearance of a rapid ultimate stage of chain detachment– even though the energy that binds the coils to the surfaces increases. Furthermore, the ultimate stage of desorption follows a common kinetic pattern which involves a rapid, correlated, segment-by-segment desorption of the oligomer.

It should be noted that although this molecular process of rotational desorption is very rapid, the total desorption time can be determined by the diffusional desorption of the front tail from the surface, when this is slower (fig. 5.9c). But since diffusion is also enhanced by shear both in the bulk (fig. 5.4) and in the vicinity of an attractive surface (table 5.2) the desorption time again decreases with shear rate. For example, in the case of weakly attractive surfaces ( $\epsilon_w = 1$ ) for chains with 6 contacts the decrease in desorption time is determined completely by the shear enhanced mobility (a twofold increase of the  $D_{zz}$  results in a two fold decrease of the desorption time) but for the chains with 4 contacts the shear enhanced self diffusion of the oligomers alone is insufficient to account for the

decrease of the desorption time ( $D_{zz}$  increases by a factor of 2 table 5.2 whereas the desorption time decreases by a factor of 4 fig. 5.12). In the case of strongly attractive surfaces ( $\epsilon_w = 2$ ) the latter situation becomes even more obvious. For example for the chains with 4 contacts, the diffusivity normal to the walls is enhanced by a factor less than 4 in comparison with equilibrium (table 5.2), whereas the desorption time decreases by a factor of 13.

Keeping in mind that there is a continuous exchange of chains in the surface-melt interface, all the changes described here for the desorption are simultaneously mirrored to equivalent changes in the adsorption processes. In the case of oligomers, that we study here, the predominant mechanism is due to forces acting on the tails, but as the chain length increases there exists a significant force on loops as well, which we expect to be the principal one for long polymer chains.

At this point, it should be mentioned that shear may affect the structure of certain films in much more intricate ways than the one suggested here. In particular, under different conditions -pressure, density and wall symmetry- the confinement can lead to “solidification” near the surfaces, manifested by the existence of domains with crystalline ordering [99]. In these systems shear may affect the structure of these domains resulting in a destruction of their crystallinity, thus causing the melting of these “microcrystallites”. On the other hand, the results presented in this study are more directly related to effects occurring in films with disordered (glassy or fluid) structure inside the solid-oligomer interface [9].

Finally, we comment on the correspondence between our very flexible model chains and real polymer molecules. Obviously our model is rather generic, although it has proven very effective in capturing the response of polymeric coils in a variety of systems. The lack of any intramolecular architecture –bond angles, dihedral potentials– results in a great flexibility and the best way to relate to real polymers is to compare the Kuhn segment of our model with that of a specific real polymer molecule. This leads to an “equivalence” of our segment with several real monomers [7]. Overall, we believe that the molecular mechanisms observed for our model describes the response of real chains qualitatively, but the time scales involved will depend strongly on system specific physical and chemical properties.

## Summary & Conclusions

The method of Molecular Dynamics (MD) computer simulations is employed to study ultra thin films of oligomer fluids, confined in spaces comparable to their molecular dimensions and subjected to (very) strong flows. In MD simulations the equations of motion are solved by the computer and the trajectories of the particles are calculated. As MD provides the time evolution of a physical system, relevant static and dynamic properties of sheared confined systems can be obtained from the simulations<sup>1</sup>.

### The effect of nanometer confinement

Confinement affects the properties of a fluid in very intricate ways. A fluid near a surface becomes very inhomogeneous, exhibiting large density variations by packing in layers next to the confining wall. This layered structure extends very little –five to six molecular diameters– inside the fluid<sup>2</sup> and in the case of wide films or macroscopic systems it is a very small part of the system; thus its effect is minor as the behaviour of the system is dominated by the behaviour of the *vast* bulk part of the system *away* from the surfaces. On the other hand, in very thin films (up to ten molecular diameters) these interfacial regions become a considerable portion of the whole system and affect its behaviour; the thinner the films the stronger the influence.

Inside the wall-fluid interface the properties of the oligomer chains are strongly altered. The relaxation times of the chains become longer and diffusion is hindered. These effects become *dramatic* near strongly attractive surfaces: if the wall attraction is three times stronger than the fluid cohesion the relaxation times increase more than a thousand times and the diffusion coefficients are also reduced by more than three orders of magnitude<sup>3</sup>. Furthermore, apart from these *sluggish* dynamics there is also an increasing ordering inside the interfacial layer with increasing wall affinity. These effects are consequences of the wall induced densification, rather than of the energetic barriers of the wall interactions or mechanisms of epitaxial crystallisation or vitrification. This can be elegantly demonstrated by simulations of systems confined between structureless walls. In these systems there is no wall corrugation but still the same phenomena (sluggish dynamics, enhanced in-plane ordering, “crystalline”-like in-plane motions) are observed which suggests that

<sup>1</sup> for a review: P. Cummings and D.J. Evans: Nonequilibrium Molecular Dynamics approaches to transport and non-Newtonian fluid rheology, *Ind. Eng. Chem. Res.* **31**, 1237 (1992).

<sup>2</sup> this is valid for simple –monomeric– fluids, for oligomer melts it is only two, three monomer diameters

<sup>3</sup> this difference in the wall-fluid and the fluid-fluid interaction is realistic and the flexibility of the studied model underestimates the magnitude of this wall induced effect

this behaviour originates from the geometric constraints and the need of the adsorbed segments to close-pack inside the first layer.

## The effect of flow in ultra-thin films

Confinement results in an inhomogeneity, both in the density and the dynamics across an ultra thin pore, this is reflected in the response of these systems to imposed shear. The flow induced across a nanometer wide oligomer film, when the confining surfaces are set in motion, reveals that the adsorbed chains correspond to a more viscous fluid than the free chains in the middle part of the pore. Moreover, shear thinning takes place at much smaller shear rates than in the bulk.

In addition, there is a definite correlation between the velocity profile developed across the film and the variations of the density and local viscosity across the film. Slippage takes place either between the confining wall and the fluid, for weakly physisorbing surfaces, or inside the film –interlayer slip– for systems confined by strongly physisorbing surfaces. The molecular mechanism for the latter case is related to the conformations of the adsorbed chains with respect to the physical connectivity between the adsorbed and the free part of the film.

Flow also affects the confined coils. The *adsorbed chains* which are already collapsed and stretched on the wall at equilibrium, under flow adopt conformations with many surface contacts, while there is only a slight alignment parallel to flow. This is happening because the segments prefer to be situated so as to facilitate close-packing, rather than orient parallel to the streamlines. Increasing shear rate, causes increasing density inside the solid-oligomer interface that results in a shear enhancement of in-plane ordering inside the first layer. The *free chains* located in the middle of the pores stretch by shear and align at a preferential angle with respect to the flow direction. These shear induced deformation and orientation are close to what is expected from bulk oligomeric systems. The oligomer molecule architecture is also varied in this study. Although there exist quantitative deviations in the response of different molecules, the qualitative rheological features remain the same.

Finally, shear flow affects the *adsorption-desorption process* in these nanoscopic confinements. Adsorption and desorption take place simultaneously in a perpetual exchange between adsorbed and free chains, in such a way that density remains dynamically constant. Although shear favours conformations with many contacts at the same time it enhances the mobility of the adsorbed chains thus promoting desorption. The way in which desorption is promoted is not obvious! For strongly adsorbing surfaces and under strong enough flow, adsorbed chains remain attached on the surfaces for a long time and suddenly they detach from them following a common kinetic pattern. The desorption, kinetics in the ultimate stages of desorption, involve conformations starting by a desorbed tail and then a correlated, segment-by-segment disengagement from the wall.

The *wall induced densification* and the *shear induced changes of the adsorbed chains conformation* are of immense importance to the static and rheological properties of nanoscopically confined films.

## Samenvatting

### Een computersimulatie studie Nanoreologie van korte ketenmoleculen

Dit proefschrift bevat de resultaten van een studie naar de eigenschappen van ultradunne films van oligomeervloeistoffen onder invloed van een (zeer) sterke afschuiving, verkregen met behulp van Moleculaire Dynamica (MD) computersimulaties. Bij MD simulaties worden de bewegingsvergelijkingen opgelost met de computer, die de baan van de deeltjes berekent. Met MD simulaties wordt de tijdevolutie van een fysisch systeem bepaald en hieruit kunnen de relevante statische en dynamische eigenschappen worden verkregen.

**De invloed van extreme (nanometer) ruimtelijke begrenzing bij afwezigheid van stroming:** Ruimtelijke begrenzing heeft een gecompliceerde invloed op de eigenschappen van een vloeistof. De vloeistoflaag grenzend aan een wand is zeer inhomogeen en wordt gekarakteriseerd door grote dichtheidsvariaties als gevolg van een laagsgewijze pakking vanaf de wand. Deze gelaagde structuur strekt zich slechts over een geringe afstand in de vloeistof uit -vijf tot zes moleculaire diameters- en vormt in dikke films en macroscopische systemen slechts een nagenoeg verwaarloosbaar deel van het totale systeem. In dat laatste geval zal het effect op het gedrag van het systeem minimaal zijn, en zal dit gedrag voornamelijk worden bepaald door de bulkvloeistof. In zeer dunne films, van de orde van 10 moleculaire diameters of minder, daarentegen, maken deze grenslagen een aanzienlijk deel van het hele systeem uit en deze zullen daarom het gedrag sterk beïnvloeden; naarmate de film dunner is zal de invloed groter zijn.

Binnen de wand-vloeistof grenslaag gedragen oligomeerketens zich volledig anders dan in de bulk. De relaxatietijden van de ketens nemen aanzienlijk toe en diffusie wordt belemmerd. Deze effecten worden ronduit *dramatisch* bij sterk attractieve oppervlakken: indien de aantrekking tussen de wand en de moleculen drie keer zo groot is als de vloeistofcohesie, nemen de relaxatietijden met meer dan een factor duizend toe terwijl de waarde van de diffusiecoëfficient ook met meer dan drie ordes afneemt. Behalve deze “*trage*” dynamica treedt er ordening op in deze grenslaag die toeneemt met de oppervlakteaffiniteit. Deze effecten vinden hun oorsprong in de door de oppervlakte geïnduceerde hogere dichtheid en zijn niet het resultaat van mechanismen die terug te voeren zijn op epitaxiale kristallisatie of verglazing. Dat dit zo is kan op elegante wijze worden aangetoond met behulp van simulaties van systemen die zich tussen twee structuurloze wanden bevinden. Oppervlakteribbels zijn hier afwezig maar dezelfde verschijnselen (“*trage*” dynamica, toegenomen

tweedimensionale ordening, bewegingen rondom “roosterposities”) worden waargenomen, zodat dit gedrag klaarblijkelijk door de geometrische beperking wordt opgewekt.

**De invloed van afschuifstroming in ultra-dunne films:** Ruimtelijke inperking leidt tot een inhomogeniteit zowel in de dichtheid als in de dynamica van oligomeren in een ultradunne spleet. Het stromingsprofiel dat in de film ontstaat tengevolge van de afschuiving van de twee begrenzende oppervlakken maakt duidelijk dat de laag van geadsorbeerde ketens (ketens die één of meer contacten met het oppervlak hebben) aanzienlijk meer visceus is dan de laag van vrije ketens in het midden van de spleet. Verder treedt shear-thinning op bij een veel lagere afschuifsnelheid dan in een vergelijkbaar macroscopisch systeem. Er is een duidelijke correlatie tussen het stromingsprofiel en de variatie in dichtheid en viscositeit door de film heen. Bij voldoende hoge afschuifsnelheid treedt slip op, tussen de wand en de vloeistof in het geval van zwakke vloeistof-wand attractie, en in de film tussen de geadsorbeerde laag en de daaropvolgende laag, voor sterkere vloeistof-wand attracties. Het moleculaire mechanisme in het laatste geval hangt nauw samen met de conformaties van de geadsorbeerde ketens, die bij voldoende sterke attracties en voldoende hoge afschuifsnelheden niet langer voor voldoende verbindingen tussen de geadsorbeerde en de daaropvolgende laag zorgen.

Stroming beïnvloedt de vorm en grootte van de kluwens. De geadsorbeerde ketens, die onder evenwicht al enigszins samengekrompen zijn in de richting loodrecht op de wand en gestrekt parallel aan de wand, nemen onder invloed van de afschuifstroming conformaties aan die veel oppervlaktecontacten hebben. Anderzijds vertonen deze ketens slechts een zeer geringe tendens tot richten parallel aan de stroming. De segmenten prefereren een ligging die dichte pakking bevordert in plaats van zich te oriënteren parallel aan de stroomlijnen. Toenemende afschuifsnelheid resulteert in een toenemende dichtheid in de wand-oligomeer grenslaag en een toename van de ordening in die laag. De vrije ketens in het midden van de spleet strekken zich tengevolge van de afschuiving en richten zich onder een bepaalde afschuifsnelheid-afhankelijke hoek ten opzichte van de stromingsrichting. Deze laatste, door de stroming geïnduceerde deformatie en oriëntatie is vergelijkbaar met die in macroscopische oligomeersystemen.

In deze studie is de invloed van de architectuur (lineair, vertakt, ster) van de oligomeren ook onderzocht. Maar, hoewel kwantitatieve verschillen vanzelfsprekend optreden, blijft het totaalbeeld hetzelfde.

De afschuifstroming beïnvloedt het *adsorptie-desorptie* proces, d.w.z. de uitwisseling tussen geadsorbeerde en vrije ketens, op een onverwacht spectaculaire manier. Hoewel, zoals hierboven uiteengezet, de afschuiving leidt tot conformaties van de geadsorbeerde ketens met een groot aantal contacten met het oppervlak, veelal het maximaal mogelijke, versnelt het tegelijkertijd de uitwisseling tussen geadsorbeerde en vrije ketens. Waarom desorptie door afschuiving wordt bevorderd is niet direct duidelijk, maar ook hier leveren de simulaties een verhelderende aanwijzing. In het geval van sterk adsorberende oppervlakken en hoge afschuifsnelheden blijven de geadsorbeerde ketens gedurende lange tijd op het oppervlak om vervolgens plotseling los te raken via een vast kinetisch patroon. Dit laatste stadium begint zodra een uiteinde van de keten losraakt waarna alle andere segmenten als bij een ritssluiting volgen.

## Appendix A

### Surface Forces Apparatus (SFA)

#### The experimental device

In its *standard form*<sup>1</sup> the Surface Forces Apparatus (SFA) can measure the force of interaction between two surfaces as a function of their mutual distance. The distance between the surfaces is measured by an interferometric technique (fringes of equal chromatic order) to an accuracy of about 3 Å. The force is determined simultaneously from the deflection of the horizontal leaf spring that supports the lower surface (figure A.1). The smallest force detectable is on the order of  $10^{-7}$  N.

Since surface forces act at very small distances (typically tens or hundreds of Å) the surfaces need to be atomically smooth for a well defined contact area to exist. For this reason thin foils of mica<sup>2</sup> are used as surfaces since they can provide atomically smooth surfaces with macroscopic dimensions. On the back side of the thin mica foils very thin (semitransparent) films of silver are evaporated in order to be utilized as mirrors to create the interferometer cavity. When white light is shined through the silver-mica-medium--mica-silver sandwich only discrete wavelengths are transmitted, depending on the distance between the silver layers and the refractive indices. The transmitted light is subsequently focused onto the entrance of a spectrometer where a grating disperses the light into its component wavelengths. This decomposition provides a series of sharp fringes known as fringes of equal chromatic order<sup>3 4</sup> from which the surface separation *and* the mica surface geometry can be determined.

In the polymer chemistry department of Groningen university the SFA has been modified<sup>5</sup> by mounting the lower moving part on a piezoframe, in such a way that the lower surface can also be moved parallel to the upper surface. The lateral force that develops on the upper surface is then determined by detecting the deflection of two vertical leaf springs supporting it, again by an interferometric technique<sup>6</sup>. Moreover a capacitance

<sup>1</sup> J. N. Israelachvilli and G. E. Adams *J. Chem. Soc. Faraday Trans.* **I74**, 975 (1978).

<sup>2</sup> the crystal structure of muscovite mica is philomorphic with a cleavage plane, thus crystals with extended ( $cm^2$ ) atomically flat surfaces and with  $\mu m$  width can be easily obtained when cleaved carefully

<sup>3</sup> S. Tolansky, *Multiple beam interferometry of surfaces and films*, Clarendon, London, 1949.

<sup>4</sup> S. Tolansky, *An introduction to interferometry*, Longmans Green & Co., London, 1955.

<sup>5</sup> G. F. Belder, *Ph.D. thesis*, Groningen University, 1995.

<sup>6</sup> through the interference of two reflected beams: the beam reflected from the edge of the optical fiber and the one reflected by leaf spring surface (figure A.1)

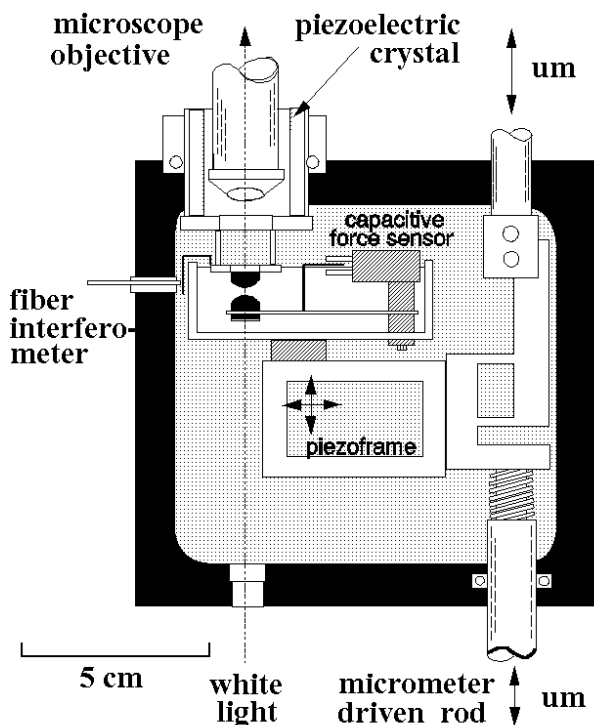


**Figure A.1:** Schematic representation of the SFA as modified in the University of Groningen (incl. shearing module and liquid cell). The distance between the surfaces is measured by an interferometric technique using white light and a spectrometer; by studying the feco (fringes of equal chromatic order) fringes the separation of the mica plates can be monitored with sub-nanometer resolution. After calibrating the leaf spring constant this distance can be translated to force providing a simultaneous measurement of force with  $10^{-7}$  Newton resolution.

force sensor has been added both to measure the distance between the mica plates and can also be utilized, as part of a feedback system, to keep<sup>7</sup> them at a given distance while shearing. Finally, a liquid cell is used in the modified apparatus. In Israelachvilli's apparatus the whole device was filled in by solvent before the injection of polymers between the two mica plates. In the device of figure A.1 only the liquid cell is filled up with solvent thus reducing dramatically the chances of contamination.

## More information

A historical review on the evolution of the SFA has been compiled by T. Lodge<sup>8</sup> whereas more info about the applications of SFA to polymer systems can be found in a review article by S. Patel<sup>9</sup> and in the references: [5, 18, 19, 20, 23, 56, 95, 108] and for nanorheological studies in: [47, 48, 50, 51, 52, 53, 54, 55, 56, 57, 76] For more details about the SFA used in the Groningen University one should refer to the Ph.D. thesis of S. Hirz (Stanford Univ., 1990) and G. F. Belder (Groningen Univ., 1995).

<sup>7</sup> the differential capacitance between the middle –moving– plate and the other two gives the deflection of the lower surface from a fixed reference point and subsequently a feedback loop can apply a suitable voltage on the capacitor plates, which drives the lower mica surface to the preset position by means of the electrostatic forces acting on the middle plate (figure A.1)

<sup>8</sup> T. Lodge, *Adv. Colloid and Interface Sci.* **19**, 27 (1983).

<sup>9</sup> S. S. Patel and M. Tirrell, *Annu. Rev. Phys. Chem.*, **40**, 597 (1989).

## Bibliography

- [1] M. P. Allen and D. J. Tildesley, *Computer simulations of liquids*, Oxford: Clarendon Press 1990.
- [2] J. P. Hansen and I. R. McDonald, *Theory of simple liquids*, Academic Press 1976.
- [3] D. A. McQuarrie, *Statistical Mechanics*, Harper and Row 1976.
- [4] M. Doi and S. F. Edwards, *The theory of polymer dynamics*, Oxford 1986.
- [5] J. Israelachvili, *Intermolecular and Surface Forces*, Academic Press 1991.
- [6] G. S. Grest and K. Kremer *Phys. Rev. A* **33**, 3628 (1986).
- [7] K. Kremer and G. Grest *J. Chem. Phys.* **92**, 5057 (1990).
- [8] I. Bitsanis and G. Hadzioannou *J. Chem. Phys.* **92**, 3827 (1990).
- [9] I. Bitsanis and C. Pan *J. Chem. Phys.* **99**, 5520 (1993).
- [10] P. A. Thompson, G. S. Grest and M. O. Robbins *Phys. Rev. Lett.* **68**, 3448 (1992).
- [11] E. Manias, G. Hadzioannou, I. Bitsanis and G. ten Brinke *Europhysics Lett.* **24**, 99 (1993).
- [12] L. Verlet *Phys. Rev. Lett.* **159**, 98 (1967).
- [13] H. J. C. Berendsen, J. P. M. Postma, W. F. van Gunsteren, A. Di Nola and J. R. Haak *J. Chem. Phys.* **81**, 3684 (1984).
- [14] M. Cieplak, E. D. Smith and M. O. Robbins *Science* **265**, 1209 (1994).
- [15] G. ten Brinke, D. Ausserre and G. Hadzioannou *J. Chem. Phys.* **89**, 4374 (1984).
- [16] D. N. Theodorou *Macromolecules* **21**, 1391, 1400, 1411, 1422 (1988).
- [17] K. F. Mansfield and D. N. Theodorou *Macromolecules* **22**, 3143 (1989).
- [18] D. Y. C. Chan and R. G. Horn *J. Chem. Phys.* **83**, 5311 (1985).
- [19] R. G. Horn and J. N. Israelachvili *J. Chem. Phys.* **75**, 1400 (1981).

- [20] H. K. Christenson *J. Chem. Phys.* **78**, 6906 (1983).
- [21] D. A. McQuarrie, *Statistical Mechanics, chapter 13*, Harper and Row 1976.
- [22] B. C. Freasier and S. Nordholm *J. Chem. Phys.* **79**, 4431 (1983).
- [23] H. K. Christenson and J. N. Israelachvili *J. Chem. Phys.* **80**, 4566 (1984).
- [24] C. Pan, *Master thesis*, U of Florida, Gainesville 1992.
- [25] E. Manias, G. Hadzioannou and G. ten Brinke *J. Chem. Phys.* **101**, 1721 (1994).
- [26] I. Bitsanis, J. J. Magda, M. Tirell and H. T. Davis *J. Chem. Phys.* **87**, 1733 (1987).
- [27] H. T. Davis, I. Bitsanis, T. Vanderlick, M. Tirell *ACS Symp. Ser.* **353**, 257 (1987).  
I. Bitsanis, T. Vanderlick, M. Tirell, H. T. Davis *J. Chem. Phys.* **89**, 3152 (1988).
- [28] L. A. Pozhar and K. E. Gubbins *J. Chem. Phys.* **94**, 1367 (1991).  
L. A. Pozhar and K. E. Gubbins *J. Chem. Phys.* **99**, 8970 (1993).
- [29] P. A. Thompson and M. O. Robbins *Phys. Rev. A* **41**, 6830 (1990).
- [30] M. J. Stevens and M. O. Robbins *Phys. Rev. E* **48**, 3778 (1993).
- [31] E.F. Casassa *Macromolecules* **17**, 601 (1984).
- [32] S. K. Kumar, M. Vacatello and D. Y. Yoon *J. Chem. Phys.* **89**, 5206 (1988).
- [33] Hiromi Yamakawa, *Modern theory of polymer solutions*, Harper & Row, NY 1971.
- [34] J. H. van Vliet and G. ten Brinke *J. Chem. Phys.* **93**, 1436 (1990).  
J. H. van Vliet, M. c. Luyten and G. ten Brinke *Macromolecules* **25**, 3802 (1992).
- [35] W. Kuhn *Kolloid-Z* **68**, 2 (1934).
- [36] E. Manias, A. Subbotin, G. Hadzioannou, G. ten Brinke *Molecular Physics* **85**, 1017 (1995).
- [37] E. A. DiMarzio *J. Chem. Phys.* **42**, 2101 (1965).
- [38] I. Bitsanis and G. ten Brinke *J. Chem. Phys.* **99**, 3100 (1993).
- [39] L. Verlet *Phys. Rev. A* **165**, 208 (1968).
- [40] R.K. Ballamudi, D.C. Koopman, E. Manias and I.A. Bitsanis *Polymer Preprints* **35(1)**, 104 (1994).
- [41] D. Gazzillo and R. G. Della Valle *J. Chem. Phys.* **99**, 6915 (1993).

- [42] S. Toxvaerd *J. Chem. Phys.* **73**, 1998 (1981).  
J. J. Magda, M. Tirell and H. T. Davis *J. Chem. Phys.* **83**, 1888 (1985).  
I. Bitsanis, J. J. Magda, M. Tirell and H. T. Davis *J. Chem. Phys.* **87**, 1733 (1987).  
M. Schoen, D. J. Diestler and J. H. Cushman *J. Chem. Phys.* **87**, 5464 (1987).  
M. Schoen, J. H. Cushman, D. J. Diestler and C. J. Rhykerd *J. Chem. Phys.* **88**, 1394 (1988).  
M. Schoen, C. J. Rhykerd and D. J. Diestler *Science* **245**, 1223 (1989).  
I. Bitsanis, S. Somers H. T. Davis and M. Tirell *J. Chem. Phys.* **93**, 3427 (1990).  
P. A. Thompson and M. O. Robbins *Phys. Rev. A* **41**, 6830 (1990).  
P. A. Thompson and M. O. Robbins *Science* **250**, 792 (1990).  
D. J. Diestler, M. Schoen, A. W. Hertzner and J. H. Cushman *J. Chem. Phys.* **95**, 5432 (1991).  
M. Lupkowski M. and F. van Swol F. *J. Chem. Phys.* **95**, 1995 (1991).  
S. Somers and H. T. Davis *J. Chem. Phys.* **96**, 5389 (1992).  
M. Schoen, D. J. Diestler and J. H. Cushman *J. Chem. Phys.* **100**, 7707 (1994).
- [43] K. F. Mansfield and D. N. Theodorou *Macromolecules* **22**, 3143 (1989).  
P. A. Thompson, G. S. Grest and M. O. Robbins *Phys. Rev. Lett.* **68**, 3448 (1992).  
E. Manias, G. Hadzioannou, I. Bitsanis, G. ten Brinke *Europhysics Lett.* **24**, 99 (1993).  
I. Bitsanis and C. Pan *J. Chem. Phys.* **99**, 5520 (1993).  
P. Daivis and D. J. Evans *J. Chem. Phys.* **100**, 541 (1994).  
D. C. Koopman, S. Gupta, R. K. Ballamudi, G. B. Westerman-Clark and I. Bitsanis *Chem. Eng. Sci.* **49**, 2907 (1994).  
E. Manias, G. Hadzioannou and G. ten Brinke *J. Chem. Phys.* **101**, 1721 (1994).  
M. Cieplak, E. D. Smith and M. O. Robbins *Science* **265**, 1209 (1994).  
P. A. Thompson, G. S. Grest and M. O. Robbins *J. Israel. Chem.* **35**, 93 (1995).
- [44] M. Doi and S. F. Edwards, *The theory of polymer dynamics*, §4.1.2, Oxford 1986.
- [45] A. Subbotin, A. Semenov, E. Manias, G. Hadzioannou and G. ten Brinke *Macromolecules* **28**, 3898 (1995).
- [46] S. Gupta, D. C. Koopman, G. B. Westermann-Clark and I. Bitsanis *J. Chem. Phys.* **100**, 8444 (1994).
- [47] J. Klein, D. Perahia and S. Warburg *Nature* **352**, 143 (1991).
- [48] M. L. Gee, P. M. McGuigan, J. N. Israelachvili and A. M. Homola *J. Chem. Phys.* **93**, 1895 (1990).
- [49] R. G. Horn, S. J. Hirz, G. Hadzioannou, C. W. Frank and J. M. Catala *J. Chem. Phys.* **90**, 6767 (1989).

- [50] S. Granick *Science* **253**, 1374 (1991).
- [51] A. M. Homola, H. Nguyen and G. Hadzioannou *J. Chem. Phys.* **94**, 2346 (1991).
- [52] S. Granick and H. Hu *Langmuir* **10**, 3857 (1994).
- [53] S. Granick, H. Hu and G. A. Carson *Langmuir* **10**, 3867 (1994).
- [54] H. Hu, G. A. Carson and S. Granick *Phys. Rev. Lett.* **66**, 2758 (1991).
- [55] G. Carson, H. Hu and S. Granick *Tribology Transactions* **35**, 405 (1992).
- [56] J. P. Montfort and G. Hadzioannou *J. Chem. Phys.* **88**, 7187 (1988).
- [57] J. Peanasky, L. Cai, S. Granick and C. Kessel *Langmuir* **10**, 3874 (1994).
- [58] P. Cummings, B. Y. Wang, K. J. Fraser and D. J. Evans *J. Chem. Phys.* **94**, 2149 (1991).
- [59] D. J. Evans, W. G. Hoover, B. H. Failor, B. Moran and A. J. C. Ladd *Phys. Rev. A* **28**, 1016 (1983).
- [60] R. G. Winkler, T. Matsuda and D. Y. Yoon *J. Chem. Phys.* **98**, 729 (1993).
- [61] T. Matsuda, G. D. Smith, R. G. Winkler and D. Y. Yoon *Macromolecules* **28**, 165 (1995).
- [62] R. G. Winkler and R. Hentschke *J. Chem. Phys.* **100**, 3930 (1994).
- [63] E. Manias, R.K. Ballamudi, D.C. Koopman and I.A. Bitsanis, *in preparation*, 1995.
- [64] S. W. Churchill, *Viscouws Flows*, Butterworth Publ. 1988.
- [65] I. Bitsanis, J. J. Magda, M. Tirell and H. T. Davis *J. Chem. Phys.* **87**, 1733 (1987).
- [66] I. Bitsanis, S. Somers H. T. Davis and M. Tirell *J. Chem. Phys.* **93**, 3427 (1990).
- [67] S. Somers and H. T. Davis *J. Chem. Phys.* **96**, 5389 (1992).
- [68] U. Heinbuch and J. Fischer *Phys. Rev. A* **40**, 1144 (1989).
- [69] P. G. de Gennes *C. R. Acad. Sci.* **228B**, 219 (1979). (also included in [70])
- [70] P. G. de Gennes, *Simple views on condensed matter*, World Scientific, Singapore 1992.
- [71] F. Brochard and P. G. de Gennes *J. de Physique Letters* **45**, L-597 (1984).
- [72] P. G. de Gennes, *Introduction to polymer dynamics*, Cambridge Univ. Press 1990.
- [73] J. Galt and B. Maxwell, *Modern Plastics*, McGraw Hill, NY 1964.

- [74] S. G. Hatzikiriakos and J. M. Dealy *J. Rheol.* **35**, 497 (1991).
- [75] G. Reiter, L. Demirel and S. Granick *Science* **263**, 1741 (1994).
- [76] S. J. Hirz, A. M. Homola, G. Hadzioannou and C. W. Frank *Langmuir* **8**, 328 (1992).
- [77] A. V. Ramamurthy *J. Rheol.* **30**, 337 (1986).
- [78] K. B. Migler, H. Hervet and L. Leger *Phys. Rev. Lett.* **70**, 287 (1993).
- [79] K. B. Migler, G. Massey, H. Hervet and L. Leger *J. Phys. Condens. Matter* **6**, A301 (1994).
- [80] S. G. Hatzikiriakos and N. Kalogerakis *Rheol. Acta* **33**, 38 (1994).
- [81] S. G. Hatzikiriakos *J. Rheol.* **39**, 61 (1995).
- [82] F. Brochard and P. G. de Gennes *Langmuir* **8**, 3033 (1992).
- [83] F. Brochard, P. G. de Gennes, H. Hervet and C. Redon *Langmuir* **10**, 1566 (1994).
- [84] R. Bruinsma *Macromolecules* **23**, 276 (1990).
- [85] J. Davoust, P. F. Devaux and L. Leger *EMBO Journal* **1**, 1233 (1982).
- [86] P. Silberzan, L. Leger, D. Ausserre and J. J. Benattar *Langmuir* **7**, 1647 (1991).
- [87] P. Daivis and D. J. Evans *J. Chem. Phys.* **100**, 541 (1994).
- [88] R. Edberg, G. P. Morriss and D. J. Evans *J. Chem. Phys.* **86**, 4555 (1986).
- [89] R. L. Rowley and J. F. Ely *Molecular Simulation* **7**, 303 (1991).
- [90] P. J. Daivis, D. J. Evans and G. P. Morriss *J. Chem. Phys.* **97**, 616 (1992).
- [91] P. Padilla and S. Toxvaerd *J. Chem. Phys.* **101**, 1490 (1994).
- [92] J. D. Ferry, *Viscoelastic Properties of Polymers* John Wiley 1980.
- [93] L. D. Landau and E. M. Lifshitz, *Fluid Mechanics*, Pergamon Press 1982.
- [94] A. Subbotin, A. Semenov, E. Manias, G. Hadzioannou and G. ten Brinke *Macromolecules* **28**, 1511, 3898, 3901 (1995).
- [95] J. van Alsten and S. Granick *Macromolecules* **23**, 4856 (1990).
- [96] P. Pincus *Macromolecules* **9**, 386 (1976).
- [97] F. Brochard *Europhysics Lett.* **23**, 105 (1993).

- [98] F. Brochard, H. Hervet and P. Pincus *Europhysics Lett.* **26**, 511 (1994).
- [99] D. C. Koopman, S. Gupta, R. K. Ballamudi, G. B. Westerman-Clark and I. Bitsanis *Chem. Eng. Sci.* **49**, 2907 (1994).
- [100] S. K. Kumar, I. Szleifer and A. Z. Panagiotopoulos *Phys. Rev. Lett.* **66**, 2935 (1991).
- [101] D. Frenkel and B. Smit *Molecular Physics* **75**, 983 (1992).
- [102] M. Bohdanecký and J. Kovar, *Viscosity of Polymer Solutions*, Elsevier, Amstrrdam 1982.
- [103] J. S. Myung and S. Sekhon *Advances in Chemical Physics* **LXVI**, 153 (1987).
- [104] R. B. Bird, R. Armstrong and C. F. Curtis, *Dynamics of Polymeric Liquids*, Wiley NY 1987.
- [105] P. Debye *J. Chem. Phys.* **14**, 636 (1946).
- [106] D. J. Evans *Molecular Physics* **42**, 1355 (1981).
- [107] J. H. R. Clarke and D. Brown *J. Chem. Phys.* **86**, 1542 (1987).
- [108] J. Israelachvili and S. J. Kott *J. Chem. Phys.* **88**, 7162 (1988).
- [109] G. S. Grest, K. Kremer and T. A. Witten *Macromolecules* **20**, 1376 (1987).
- [110] Y. Wang, K. Hill and G. Harris *J. Chem. Phys.* **100**, 3276 (1993).  
Y. Wang, K. Hill and G. Harris *Langmuir* **9**, 1983 (1993).  
Y. Wang, K. Hill and G. Harris *J. Phys. Chem.* **97**, 9013 (1993).
- [111] G. F. Belder, G. ten Brinke and G. Hadzioannou *in preparation*, 1995.
- [112] M. W. Ribasky and U. Landman *J. Chem. Phys.* **97**, 1937 (1992).
- [113] M. Schoen, D. J. Diestler and J. H. Cushman *J. Chem. Phys.* **87**, 5464 (1987).
- [114] J. van Alsten and S. Granick *Macromolecules* **22**, 3143 (1990).
- [115] P. A. Thompson and M. O. Robbins *Science* **250**, 792 (1990).
- [116] M. Lupkowski M. and F. van Swol F. *J. Chem. Phys.* **95**, 1995 (1991).
- [117] A. Subbotin, A. Semenov, G. Hadzioannou and G. ten Brinke *Macromolecules* **28**, 3901 (1995).
- [118] A. Subbotin, A. Semenov, E. Manias, G. Hadzioannou and G. ten Brinke *Macromolecules* **28**, 1511 (1995).

## Acknowledgements

Looking back in time, it is difficult to believe how much have happened the last four years that I've spent in Groningen. Having reached the point of concluding this thesis, now putting on paper the final words, I can't help thinking of all the people who made this possible and (sometimes) enjoyable. Unavoidably, much is lost from the feelings when one is trying to transform them in words, *but* engraved on the pages of a book, can and do, outlive the author and resist the march of time: from this standpoint I would like to express **my sincere thanks to:**

Professor Georges Hadzioannou for making this work possible through his unfailing support and constant guidance and advice, through the encouragement and motivation but also the freedom and the security one could feel in the lab. Moreover, for providing the opportunity to work in a multi-disciplinary scientific environment, which could give a unique perspective although sometimes one could be overwhelmed by trying to keep up with the storm of his new ideas. For all these I owe him a immeasurable dept of gratitude.

Professor Gerrit ten Brinke for his expert guidance and all the scientific instructions and education, for trying to make me reach my potential and for all the inspiring help and supervision he always offered.

Professor Yiannis Bitsanis for introducing me to the world of computer simulations and for the many enlightening discussions we so often had; I could only consider him as a third thesis advisor. Professors Herman Berendsen, Albert Pennings and especially Doros Theodorou for reading my dissertation and providing their insight and judgment.

All my colleagues in our group and the those who visited us –one way or another. Andrei Subbotin for all those long and sometimes thunderous debates, V. Koutsos, G.F. Belder and K. Andrikopoulos for the enjoyable exchange of ideas. G. Malliaras, Y. Papantoniou and F. Syntouka for being there every time I needed somebody, for their friendship and support. A. Oikonomou for the balance and the different viewpoint in difficult moments.

Last but not least, my parents Maria and Dimitris for their continuous love, encouragement and devoted support all these years that I go through one school or another; for believing in me and inspiring me to set and achieve goals in my life, for the affectionate safety that I feel knowing that they are always there for me.

Evangelos D. Manias  
Groningen, September 1995

## Published work:

Some of the work presented inside this dissertation *was* actually published:

Stick and slip behaviour of confined oligomer melts under shear. A MD study.

E. Manias, G. Hadzioannou, I. Bitsanis, G. ten Brinke

*Europhysics letters*, **24**(2), 99, 1993.

### § 5.1 in:

Effect of shear on the desorption of oligomers in nanoscopically confined films.

E. Manias, G. Hadzioannou, G. ten Brinke

*Journal of Chemical Physics*, **101**(2), 1721, 1994.

### § 5.2 in:

Adsorption-desorption kinetics in nanoscopically confined oligomer films under shear.

E. Manias, A. Subbotin, G. Hadzioannou, G. ten Brinke

*Molecular Physics*, **85**(5), 1017, 1995.

### § 3.3 in: On the nature of shear thinning in nanoscopically confined films.

E. Manias, I. Bitsanis, G. Hadzioannou, G. ten Brinke, submitted 1995.

### § 3.2 in: Inhomogeneities in sheared ultra-thin lubricating films.

E. Manias, G. Hadzioannou, G. ten Brinke, *Langmuir*, submitted 1995.

chapter 2: in preparation, to be submitted to *Macromolecules*.

chapter 3 & 4: in preparation, to be submitted to *Macromolecules*.

Other related work not presented in this thesis:

Atomic Force Microscopy and real atomic resolution. Simple computer simulations.

V. Koutsos, E. Manias, G. ten Brinke, G. Hadzioannou

*Europhysics letters*, **26**(2), 103, 1994.

Crystallization at solid-liquid interfaces.

R.K. Ballamudi, D.C. Koopman, E. Manias and I.A. Bitsanis

*Polymer Preprints*, **35**(1), 104, 1994.

Rheology of confined polymer melts under shear flow: strong adsorption limit.

A. Subbotin, A.N. Semenov, E. Manias, G. Hadzioannou, G. ten Brinke

*Macromolecules*, **28**, 1511, 1995.

Nonlinear rheology of melts under shear flow.

A. Subbotin, A.N. Semenov, E. Manias, G. Hadzioannou, G. ten Brinke

*Macromolecules*, **28**, 3898, 1995.

## Presented in conferences:

A very important influence to the directions of my research was through presenting and discussing my work in conferences, meetings and visits to universities and research centers:

Invited talks:		
Molecular confined liquids	Les Houches, FR	27 Feb. - 5 Mar. 1994
ACS Rheology Symposium	Anaheim, USA	2-7 April 1995
IBM Almaden Research Center	San Jose, USA	18 Mar. 1994
MSC biannual meeting	Vlieland, NL	25-27 Apr. 1993
SON Macromolecules	Lunteren, NL	9-10 Feb. 1994
FOM Statistical Physics	Lunteren, NL	19-20 Jan. 1995
SON Macromolecules	Lunteren, NL	13-14 Feb. 1995
Univ. of Strasbourg	Strasbourg, FR	October 1993
Univ. of Patras	Patras, GR	8 May 1995
Univ. of Crete	Heracleion, GR	17 May 1995
Contributions in other conferences:		
APS March meeting	Indianapolis, USA	March 1992
ACS National meeting	San Francisco, USA	April 1992
APS March meeting	Seattle, USA	March 1993
ACS National meeting	Denver, USA	April 1993
APS March meeting	Pittsburgh, USA	March 1994
ACS National meeting	San Diego, USA	March 1994
APS March meeting	San Jose, USA	March 1995
ACS National meeting	Anaheim, USA	April 1995
SON Macromolecules	Lunteren, NL	10-11 Feb. 1992
SON Biochemistry	Lunteren, NL	12-13 Oct. 1992
FOM Statistical Physics	Lunteren, NL	14-15 Jan. 1993
SON Macromolecules	Lunteren, NL	8-9 Feb. 1993
SON Fluids and Interfaces	Lunteren, NL	15-16 Feb. 1993
MSC biannual meeting	Vlieland, NL	25-27 Apr. 1993
FOM Condensed Matter	Bilthoven, NL	5 Nov. 1993
3 <sup>rd</sup> conference on Polymers	Thessaloniki, GR	2-3 Dec. 1993
FOM Statistical Physics	Lunteren, NL	27-28 Jan. 1994
SON Macromolecules	Lunteren, NL	9-10 Feb. 1994
SON Fluids and Interfaces	Lunteren, NL	24-25 Feb. 1994
NATO ASI "Forces in SPM"	Schluchsee, D	7-18 Mar. 1994
German Physical Society	Munster, D	21-24 Mar. 1994
FOM Statistical Physics	Lunteren, NL	19-20 Jan. 1995
SON Macromolecules	Lunteren, NL	13-14 Feb. 1995
Euroconf. on Complex Materials	Patras, GR	22-26 Sep. 1995